Impact of Gastrointestinal (GI) and Hepatic Cancer on Enzyme and Transporter Abundance Contributing to Variability in Drug Exposure

A thesis submitted to the University of Manchester for the degree of

Doctor of Philosophy

in the Faculty of Biology, Medicine and Health

2021

Areti Maria Vasilogianni

School of Health Sciences

Division of Pharmacy & Optometry

Contents

Contents 2
List of Figures 9
List of Tables 11
Abbreviations 14
Amino Acid Abbreviations 20
Abstract 21
Declaration 22
Copyright Statement 23
Dedication 24
Acknowledgements 25
Preface 26
Chapter One: The Quest to Define Cancer-Specific Systems Parameters for Pharmacokinetics Predictions 28
1.1 Abstract 29
1.2 Introduction 30
1.2.1 Drug Development in Oncology 30
1.2.2 Physiologically-based pharmacokinetic (PBPK) modelling in Oncology 31
1.3 Systems Parameters in Cancer Populations 31
1.3.1 Parameters that Decrease in Cancer Patients 32
1.3.1.1 Microsomal Protein per Gram of Liver (MPPGL) 32
1.3.1.2 Serum Albumin 32
1.3.1.3 Haematocrit 33
1.3.1.4 Reduced Hepatic Function 33
1.3.1.5 Reduced Renal Function 34
1.3.2 Parameters that Increase in Cancer Patients 34
1.3.2.1 Alpha-1 acid glycoprotein (AAG) 34
1.3.2.2 Inflammation 35
1.3.2.3 Gastrointestinal (GI) Complications 35
1.3.3 ADME Proteins Affected in Cancer 37
1.3.3.1 Drug Metabolizing Enzymes (DMEs) 37
1.3.3.2 Transporters 39
1.3.4 The Effect of Patient Demographics 40
1.4 Tyrosine Kinase Inhibitors (TKIs) for Cancer Treatment 42

1.5 Liver Cancer as a Case Example 48
1.5 Precision Dosing in Oncology 51
1.6 Conclusion 53
1.7 Expert Opinion 54
1.8 References 56
Chapter Two: Quantitative Mass Spectrometry-Based Proteomics in the Era of Model-Informed Drug Development: Applications in Translational Pharmacology and Recommendations for Best Practice 73
2.1 Abstract 74
2.2 Introduction 75
2.3 Overview of a typical quantitative proteomic experiment 76
2.4 Targeted quantitative proteomic methods 79
2.4.1 Selected/multiple reaction monitoring (SRM/MRM) 82
2.4.2 Parallel reaction monitoring (PRM) 82
2.4.3 Accurate mass and retention time (AMRT) 83
2.5. Standards for targeted proteomics 83
2.5.1 Absolute quantification (AQUA) peptide standards 87
2.5.2 Quantitative concatemers (QconCAT) 88
2.5.3 Protein standards for absolute quantification (PSAQ) 89
2.6 Global quantitative proteomic methods 90
2.6.1 Data-dependent acquisition (DDA) 92
2.6.2 Data-independent acquisition (DIA) 93
2.7 Key pharmacology applications of proteomic data 94
2.7.1 Physiology-based pharmacokinetic (PBPK) modeling and IVIVE 96
2.7.2 Quantitative systems pharmacology (QSP) models 98
2.7.3 Disease perturbation 98
2.7.4 Protein inter-correlations 99
2.7.5 Precision dosing 100
2.7.6 Ontogeny 101
2.7.7 Characterization of polymorphisms 102
2.7.8 Disease biomarker discovery 102
2.8. Recommendations for best practice in applying proteomic techniques 103
2.9. Conclusion 106
2.10 References 108
Chapter Three: Complementarity of MaxQuant and Progenesis in Identification of Drug-Metabolising Enzymes and Transporters in Human Liver 133

3.1 Abstract 134
3.2 Introduction 135
3.3 Materials and methods 139
3.3.1 Dataset 139
3.3.2 Database Fasta file 139
3.3.3 Data processing 139
3.3.4 Comparison of peptides identified by MaxQuant and Progenesis 141
3.3.4.1 Peptide score correlation between software tools 141
3.3.4.2 Numbers and sequences of peptides 141
3.3.4.3 Correlation of peptide signal intensities between software tools 141
3.3.4.4 Characteristics of identified software-specific peptides 141
3.3.4.5 Calculation of percentage identical peptides 142
3.3.5 Comparison at the protein level 142
3.3.6 Software availability and processing time 142
3.4 Results 143
3.4.1 Comparison of peptide scores between Progenesis and MaxQuant 143
3.4.2 Total number of peptides and modified peptides 144
3.4.3 Correlation between intensities in MaxQuant and Progenesis 147
3.4.5 Peptide characteristics 148
3.4.6 Multivariate analysis of peptide and protein data 149
3.4.7 Drug-metabolising enzymes and transporters 150
3.4.8 Processing time 154
3.5 Discussion 154
3.6 References 159
3.7 Supplementary Information 168
Chapter Four: Hepatic Scaling Factors for In Vitro-In Vivo Extrapolation (IVIVE) of Metabolic Drug Clearance in Patients with Colorectal Cancer with Liver Metastasis 183
4.1 Abstract 184
4.2 Introduction 185
4.3 Materials and Methods 186
4.3.1 Materials and chemicals 186
4.3.2 Liver samples 186
4.3.3 Preparation of human liver microsomal and cytosolic fractions 187
4.3.4 Measurement of total protein content in homogenates and fractions 187

4.3.5 Measurement of NADPH cytochrome P450 reductase activity 187
4.3.6 Statistical data analysis 188
4.3.7 Physiologically based pharmacokinetic (PBPK) simulations 189
4.4 Results 192
4.4.1 Protein content of liver homogenates and fractions 192
4.4.2 NADPH cytochrome P450 reductase activity in homogenates and microsomes 194
4.4.3 Corrected microsomal protein per gram of liver (MPPGL) 196
4.4.4 Effect of demographics on MPPGL values 197
4.4.5 Effect of demographics on CPPGL values 199
4.4.6 Physiologically based pharmacokinetic (PBPK) simulations 201
4.5 Discussion 204
4.6 References 208
4.7 Supplementary Information 212
Chapter Five: Changes in Abundance of Proteins Involved in Drug Pharmacokinetics and Pharmacodynamics in Colorectal Cancer Liver Metastasis Relative to Healthy Liver 220
5.1 Abstract 221
5.2 Introduction 222
5.3 Materials and Methods 223
5.3.1 Liver samples and donor characteristics 223
5.3.2 QconCATs standards 223
5.3.3 Sample preparation for proteomics 224
5.3.4 Liquid chromatography and tandem mass spectrometry (LC-MS/MS) 224
5.3.5 Analysis and annotation of proteomic data 224
5.3.6 Physiologically-based pharmacokinetic (PBPK) simulations 225
5.3.7 Data analysis 225
5.4 Results 226
5.4.1 Novel QconCAT (KinCAT) for the quantification of kinases 226
5.4.2 Abundance of CYPs and UGTs in healthy, histologically normal, and cancerous liver 227
5.4.2.1 Absolute abundance of CYP and UGT enzymes 227
5.4.2.2 Replicate of measurement of CYPs and UGTs 228
5.4.2.3 Abundance distribution of CYPs and UGTs in HP and TP 228
5.4.2.4 Fold change in the expression of CYPs and UGTs in TP and NP relative to HP 228
5.4.3 Abundance of transporters in healthy, histologically normal and cancerous liver 230
5.4.3.1 Fold changes in the expression of transporters 230

5.4.4 Differential protein abundance of non-CYP non-UGT and anti-oxidant enzymes 232
5.4.5 Assessment of changes in expression of kinases in NP and TP compared with HP 234
5.4.5.1 Expression levels of RTKs 234
5.4.5.2 Non-RTKs exclusively expressed in TP 234
5.4.5.3 Fold change in expression of RTKs between HP to NP and TP 234
5.4.5.4 RTK-related pathways affected in cancer 234
5.4.6 Abundance of markers of liver function, inflammation, desmoplasia and metastasis 235
5.4.6.1 Liver function 236
5.4.6.2 Inflammation 236
5.4.6.3 Desmoplasia 236
5.4.6.4 Metastasis markers 236
5.4.7 Physiologically-based pharmacokinetic (PBPK) simulations 237
5.5 Discussion 239
5.6 References 242
5.7 Supplementary Information 247
5.7.1 Supplementary Methods 247
5.7.2 Supplementary Results 253
5.7.3 Supplementary Tables 254
5.7.4 References 267
Chapter Six: Quantitative Proteomics of Drug-Metabolizing Enzymes and Drug Transporters in Human Colorectal Cancer Metastasis and the Surrounding Liver 269
6.1 Abstract 270
6.2 Introduction 271
6.3 Materials and Methods 273
6.3.1 Materials and chemicals 273
6.3.2 Human liver samples 273
6.3.3 Preparation of human liver microsomal fractions 273
6.3.4 Measurement of total protein content in microsomal samples 274
6.3.5 QconCATs (MetCAT and TransCAT) standards 274
6.3.6 Digestion and preparation of samples 274
6.3.7 Liquid chromatography and tandem mass spectrometry (LC-MS/MS) 276
6.3.8 Analysis and annotation of proteomic data 276
6.3.9 Statistical data analysis 276
6.3.10 Physiologically based pharmacokinetic (PBPK) simulations 277

6.4 Results 278

6.4.1 Comparison of hepatic CYP and UGT absolute abundance in healthy controls, and histologically normal and tumour HLM from cancer patients 278

6.4.2 Differences in protein expression levels of ABC and SLC transporters between tumour, normal and healthy microsomal fractions 280

6.4.3 Relative expression of CYPs and UGTs in the three sets of HLM 282

6.4.4 Relative abundance distribution of ABC and SLC transporters in healthy controls, and histologically normal and tumour HLM from cancer patients 283

6.4.5 Relative abundance of CYPs and UGTs among healthy controls, and histologically normal and tumour HLM from cancer patients 284

6.4.6 Relative abundance of ABC and SLC transporters on healthy controls, histologically normal and tumour tissues 285

6.4.7 Relative abundance of CYPs, UGTs and transporters in paired tumour and normal tissues 287

6.4.8 Normalization of the abundance of CYPs, UGTs and transporters (pmol/mg) to gram of liver 288

6.4.9 Principal component analysis (PCA) 289

6.4.10 Physiologically-based pharmacokinetic (PBPK) simulations 290

6.5 Discussion 291

6.6 References 296

6.7 Supplementary Information 301

Chapter Seven: Quantitative Proteomics of Receptor Tyrosine Kinases in Patients with Colorectal Cancer Liver Metastasis 315

7.1 Abstract 316

7.2 Introduction 317

7.3 Materials and Methods 319

7.3.1 Materials and chemicals 319

7.3.2 Liver samples 319

7.3.3 Preparation of human liver microsomal fractions 320

7.3.4 Measurement of total protein content in individual microsomal samples 320

7.3.5 QconCAT (KinCAT) standard 320

7.3.6 Digestion and preparation of samples 321

7.3.7 Liquid chromatography and tandem mass spectrometry (LC-MS/MS) 322

7.3.8 Analysis and annotation of proteomic data 322

7.3.9 Statistical data analysis 323

7.4 Results 323

7.4.1 Differential expression of RTKs in HLMs from healthy subjects, and paired histologically normal and tumour HLMs 324

7.4.2 Receptor tyrosine kinase absolute expression in healthy and CRLM 326
7.4.3 Correlations in liver RTK expression profiles 333
7.4.4 Relative abundance distribution of RTKs in healthy normal and tumour HLM 335
7.5 Discussion 336
7.6 References 340
7.7 Supplementary Information 345
Chapter Eight: Conclusions and Future Work 354
8.1 Setting the Needs for Oncology Populations 354
8.2 What this projects adds to the previous knowledge 354
8.3 Future perspectives 357

Word Count: 67,901

List of Figures

Figure 1-1 Location of clinically relevant drug transporters expressed in human hepatocytes. 39
Figure 1-2 Physiological parameters affected in cancer that lead to changes in PK metrics. 42
Figure 1-3 US FDA approved small molecule TKIs for the treatment of various cancer types. 43
Figure 1-4 Metabolic pathways involved in the metabolism of TKIs. 48
Figure 1-5 Differences in the abundance of DMEs and transporters in HCC. 50
Figure 2-1 Overview of the experimental quantitative proteomic workflow. 78
Figure 2-2 The use of proteomic data in PBPK prediction of drug exposure. 95
Figure 2-3 The characteristics and applications of absolute quantification, relative quantification and discovery proteomic approaches. 96
Figure 2-4 Decision tree for choosing suitable proteomic techniques intended for pharmacology applications. 104
Figure 3-1 Linear regression of MaxQuant and Progenesis peptide scores. 144
Figure 3-2 Linear regression of MaxQuant and Progenesis peptide signal intensities. 147
Figure 3-3 Characteristics of sample HLM76 peptides identified by the two software packages in terms of length (**A**), score (**B**) and hydrophobicity (**C**). 149
Figure 3-4 Principal components analysis (PCA) for 23 human liver samples based on percentage identical peptides (PIP) identified by Progenesis (**A**) and MaxQuant (**B**), and percentage identical proteins (PIPr) identified by Progenesis (**C**) and MaxQuant (**D**). 150
Figure 3-5 The number of samples in which CYPs and UGTs identified by each software tool. 151
Figure 3-6 The number of samples in which ABC transporters were identified by each software tool. 151
Figure 3-7 The number of samples in which solute carriers (SLCs) were identified by each software tool. 152
Figure 4-1 Total protein content (mg per gram of liver) in homogenates (HomPPGL, **A**), microsomal fractions (MPPGL before correction for losses, **B**) and cytosolic fractions (CPPGL, **C**) from histologically normal and matched tumor samples (n=16). 193
Figure 4-2 Activity of NADPH cytochrome P450 reductase in homogenates and microsomes from histologically normal (n = 16) and tumor samples (n = 11) from CRLM patients (**A**). 195
Figure 4-3 Corrected microsomal protein content (mg) per gram tissue (MPPGL) from histologically normal (n = 16) and tumor samples (n = 11). 196
Figure 4-4 Effects of liver lobe (**A**), sex (**B**), BMI (**C**) and age (**D**) on MPPGL values for histologically normal and cancer samples. 198
Figure 4-5 Effects of liver lobe (**A**), sex (**B**), BMI (**C**) and age (D) on CPPGL values for histologically normal and cancer samples. 200
Figure 4-6 Mean predicted systemic concentration over time (24 hours) after oral administration of alfentanil (**A**), midazolam (**B**), alprazolam (**C**), and desipramine (**D**). 202
Supplementary Figure 4-1 Relationship between observed (current study) and predicted MPPGL values and age (Barter et al., 2008), with 95% confidence intervals for the predicted values for Model 1. The observed MPPGL values correspond to the histologically normal samples. 219
Figure 5-1 Design and characterization of the KinCAT. 227
Figure 5-2 Protein expression of cytochrome P450 enzymes (CYPs) and UDP-glucuronosyltransferases (UGTs) in healthy (HP), histologically normal (NP) and tumorous (TP) pooled HLM samples. 229
Figure 5-3 Abundance of transporters in healthy (HP), histologically normal (NP) and tumorous (TP) pooled HLM samples. 231
Figure 5-4 Relative abundance of non-CYP non-UGT enzymes (**A**, **B**), and anti-oxidant enzymes (**C**) measured in healthy (HP), histologically normal (NP) and tumorous (TP) pooled HLM samples. 233

Figure 5-5 Abundance of kinases in healthy (HP), histologically normal (NP) and tumorous (TP) pooled HLM. 235
Figure 5-6 Relative change of markers of liver function (**A**), inflammation (**B**), desmoplasia (**C**), collagen chains (metastasis markers) (**D**), cathepsins (metastasis markers) (**E**), and other metastasis markers (**F**) in NP and TP compared with HP. 237
Figure 5-7 Mean predicted systemic concentration over time (24 hours) after oral administration of alfentanil (**A**), midazolam (**C**), and nebivolol (**E**), and clearance (Dose/AUC) of alfentanil (**B**), midazolam (**D**), and nebivolol (**E**). 238
Figure 6-1 Absolute abundance of cytochrome P450 enzymes (CYPs) (**A**) and UDP-glucuronosyltransferases (UGTs) (**B**) in healthy, histologically normal and tumorous HLM. 279
Figure 6-2 Absolute abundance of ATP-binding cassette transporters (ABCs), ATP1A1 and Cadherin-17 (CDH17) (**A**) and solute carrier transporters (SLCs) (**B**) in healthy, histologically normal and tumorous HLM. 281
Figure 6-3 Pie charts representing the relative abundance distribution of CYPs (**A, B, C**), and UGTs (**D, E, F**) in healthy, histologically normal and tumorous HLM. 282
Figure 6-4 Relative abundance distribution of ABCs (**A, B, C**), and SLCs (**D, E, F**) in healthy, histologically normal and tumorous HLM. 283
Figure 6-5 Relative abundances of CYPs, and UGTs in HLM. 285
Figure 6-6 Relative abundances of ABC and SLC transporters in HLM. 286
Figure 6-7 Relative abundance of CYPs (**A**), UGTs (**B**), ABCs (**C**), and SLCs (**D**). Relative abundances are expressed as ratios of abundance in histologically normal to matched tumour HLM for each 18 individual (n = 18). 287
Figure 6-8 Abundance of CYP2C9, CYP3A4, UGT1A9, UGT2B7, P-gp, MRP3, MCT1, and OATP2B1 in histologically normal (graphs on the top, blue bars) and tumour (graphs at the bottom, pink bars). Abundance is expressed as pmol of protein per mg of microsomal protein in the left y axis (dark blue bars for histologically normal and dark pink for tumour), and as pmol of protein per g of liver in the right y axis (light blue bars for histologically normal and light pink for tumour). 288
Figure 6-9 Principal components analysis (PCA) of peptide (**A**) and protein (**B**) similarity data, using percentage identical peptide (PIP) and percentage identical protein (PIPr) values, respectively. 290
Figure 6-10 Mean predicted systemic concentration over time after oral administration of alprazolam (**A**), crizotinib (**B**), and ibrutinib (**C**). 291
Figure 7-1 Absolute abundance of receptor tyrosine kinases (RTKs) with different levels of expression in healthy, histologically normal and tumorous HLM. 325
Figure 7-2 Absolute abundance of EGFR (**A**), INSR (**B**), VGFR3 (**C**), AXL (**D**), FGFR2 (**E**), IGF1R (**F**), EPHA2 (**G**), and PGFRB (**H**) in paired (same donor) histologically normal and tumorous HLM. 326
Figure 7-3 Absolute abundance of VGFR1 (**A**), VGFR2 (**B**), PGFRA (**C**), KIT (**D**), CSF1R (**E**), and FLT3 (**F**) 327
Figure 7-4 Absolute abundance of FGFR1 (**A**), FGFR3 (**B**), ERBB2 (**C**), NTRK2 (**D**), TIE2 (**E**), RET (**F**) and MET (**G**). 329
Figure 7-5 Absolute abundance of RTKs similarly expressed in paired histologically normal and tumorous HLM. 330
Figure 7-6 Correlation matrix of protein abundance of RTKs in healthy (green), histologically normal (blue) and tumour (purple) HLM. 334
Figure 7-7 Pie charts illustrating the relative abundance distribution of RTKs in healthy (**A**), histologically normal (**B**) and tumorous (**C**) HLM. 336

List of Tables

Table 1-1 The effects of perturbed systems parameters in cancer on PK of drugs. 36
Table 1-2 Impact of cancer on the expression of DMEs (CYPs and UGTs) in different cancer types. 38
Table 1-3 Impact of cancer on the expression of transporters. 40
Table 1-4 Small molecule TKIs approved for cancer treatment and their pathways of metabolism. .. 44
Table 2-1 The overall aims, advantages and limitations of various proteomic data acquisition methods: targeted (MRM, PRM), global data-dependent acquisition (DDA) and data-independent acquisition (DIA) techniques. 80
Table 2-2 Characteristics of standards used in targeted proteomic methods (AQUA, QconCAT and PSAQ) and their analytical performance. 85
Table 3-1 A summary of previous investigations that compared data analysis software and the outcomes compared. 138
Table 3-2 Processing parameters applied in MaxQuant and Progenesis. 140
Table 3-3 Comparison of the total number of peptides, peptides specific for each software and modified peptides as identified by MaxQuant and Progenesis. This comparison was done after removing the peptides with low scores. 145
Table 3-4 Drug-metabolising enzymes and transporters identified by the two software packages. .. 152
Supplementary Table 3-1 Detailed parameters applied with MaxQuant. 168
Supplementary Table 3-2 Range of cut-off scores in Progenesis. 171
Supplementary Table 3-3 Regression equation for the relationship between Progenesis intensities (y) and MaxQuant intensities (x) and the coefficient of determination for each individual human liver microsome (HLM) sample. 172
Supplementary Table 3-4 Comparison of the total number of peptides, peptides specific for a software and modified peptides identified by MaxQuant and Progenesis. This comparison was done before removing peptides with scores lower than 40 in MaxQuant or equivalent for Progenesis. 173
Supplementary Table 3-5 Statistical comparison between peptide characteristics for sample HLM76 in relation to peptide length, GRAVY score (hydrophobicity), isoelectric point (PI), and molecular weight of peptides detected by only one software tool MaxQuant (Max.) and Progenesis (Pro.). 174
Supplementary Table 3-6 Enzyme and transporter proteins detected in 23 human liver samples by the two software tools. 175
Supplementary Table 3-7 Median and mode scores for software-specific peptides in each sample. 180
Supplementary Table 3-8 Median and mode Gravy scores for software-specific peptides in each sample. 181
Supplementary Table 3-9 Quantification of transporters only achieved with MaxQuant. 182
Table 4-1 Mean predicted E_H, Tmax, Cmax, and $AUC_{0\text{-}inf}$ for oral alfentanil, alprazolam, midazolam, and desipramine using four different scaling methods within PBPK model. $AUC_{0\text{-}inf}$ ratios using different methods are also provided. 203
Supplementary Table 4-1 Demographic and clinical details of CRLM patients. 212
Supplementary Table 4-2 Input parameters for PBPK modelling using Simcyp v18 R1 for alfentanil (predominantly metabolized by CYP3A4), alprazolam (predominantly metabolized by CYP3A4 and CYP3A5), desipramine (predominantly metabolized by CYP2D6), and midazolam (predominantly metabolized by CYP3A4 and CYP3A5). 216
Supplementary Table 4-3 Protein content (mg/g liver tissue) in homogenates, microsomes, and cytosols from histologically normal and cancerous tissues of CRLM patients. 217
Supplementary Table 4-4 NADPH cytochrome 450 reductase activities (units/mg tissue) in homogenates and microsomes from histologically normal and tumor tissues of CRLM patients. 218

|List of Tables

Supplementary Table 5-1 Demographic and clinical details of CRLM patients provided by the MFT Biobank. 254
Supplementary Table 5-2 Demographic and clinical details of healthy subjects provided by Pfizer. 257
Supplementary Table 5-3 Re-designed TransCAT; target proteins, peptides and incorporation efficiency. 258
Supplementary Table 5-4 KinCAT; target proteins, peptides and incorporation efficiency. 260
Supplementary Table 5-5 Input parameters for PBPK modelling using Simcyp v20 R1 for alfentanil (predominantly metabolized by CYP3A4), midazolam (predominantly metabolized by CYP3A4 and CYP3A5), and nebivolol (predominantly metabolized by CYP3A4 and CYP2D6). 262
Supplementary Table 5-6 Quantification of twelve CYP and eight UGT enzymes in human HP, NP and TP liver samples. 263
Supplementary Table 5-7 Quantification of transporters in human HP, NP and TP liver samples. 264
Supplementary Table 5-8 Quantification of nineteen RTKs in human HP, NP and TP liver samples. 265
Supplementary Table 5-9 Comparison of histologically normal and tumour to healthy ratios (absolute abundance of CYPs and UGTs) between pilot study 1, and 2 (replicate study). 266
Supplementary Table 6-1 Demographic and clinical details of cancer patients provided by the MFT Biobank. 301
Supplementary Table 6-2 Demographic and clinical details of healthy subjects provided by Pfizer. 305
Supplementary Table 6-3 Expression levels (pmol mg^{-1}) of 14 CYP and 8 UGT enzymes quantified in human healthy liver controls. 307
Supplementary Table 6-4 Expression levels (pmol mg^{-1}) of 14 CYP and 8 UGT enzymes quantified in human histologically normal livers. 308
Supplementary Table 6-5 Expression levels (pmol mg^{-1}) of 14 CYP and 8 UGT enzymes quantified in human tumour livers. 309
Supplementary Table 6-6 Expression levels (pmol mg^{-1}) of 9 ABC, 14 SLC transporters, ATP1, and CDH17 quantified in human healthy liver controls. 310
Supplementary Table 6-7 Expression levels (pmol mg^{-1}) of 9 ABC, 14 SLC transporters, ATP1, and CDH17 quantified in human histologically normal livers. 311
Supplementary Table 6-8 Expression levels (pmol mg^{-1}) of 9 ABC, 14 SLC transporters, ATP1, and CDH17 quantified in human tumour livers. 312
Supplementary Table 6-9 Input parameters for PBPK modelling using Simcyp v20 R1 for alprazolam (predominantly metabolized by CYP3A4, and CYP3A5, low extraction ratio), crizotinib (predominantly metabolized by CYP3A4, intermediate extraction ratio), and ibrutinib (predominantly metabolized by CYP3A4, high extraction ratio). 313
Table 7-1 Expression levels of 21 RTKs in healthy, histologically normal and tumour livers represented by the median, the mean and standard deviation of the mean (SD), the coefficient of variation (CV), and the range (minimum to maximum value). 331
Supplementary Table 7-1 Demographic and clinical details of cancer patients provided by the MFT Biobank. 345
Supplementary Table 7-2 Demographic and clinical details of healthy subjects provided by Pfizer. 349
Supplementary Table 7-3 Targeted quantification of nineteen Receptor tyrosine kinases (RTKs) transporters in 15 human liver microsomes from healthy subjects. 351

Supplementary Table 7-4 Targeted quantification of nineteen Receptor tyrosine kinases (RTKs) transporters in 18 histologically normal (peri-carcinomateous) liver microsomes from cancer patients. 352
Supplementary Table 7-5 Targeted quantification of twenty-one Receptor tyrosine kinases (RTKs) transporters in 18 tumorous human liver microsomes from cancer patients..... 353

Abbreviations

% = Percent

ºC = Degrees Centigrade

ABC = ATP-binding Cassette Transporter Protein

ADME = Absorption, Distribution, Metabolism and Excretion

AAG = Alpha-1-acid glycoprotein

ADH = Alcohol Dehydrogenase

ALC = All Liver Cancerous

ALDH = Aldehyde Dehydrogenase

ALN = All Liver Normal

ALT = Alanine Aminotransferase

ALP = Alkaline Phosphatase

AmBic = Ammonium Bicarbonate

AMRT = Accurate Mass and Retention Time

AOX = Aldehyde Oxidase

AQUA = Absolute Quantification Standards

ASBT = Apical Sodium-dependent Bile Acid Transporter

AST = Aspartate Aminotransferase

ATP1A1 = ATPase Subunit Alpha-1

AUC = Area under the Plasma Concentration-time Curve

$AUC_{0\text{-}inf}$ = Area under the Curve from Time 0 to Infinity

AXL = Tyrosine-protein Kinase Receptor UFO

B/P = Blood to Plasma Ratio

BCA = Bicinchoninic Acid

BCRP = Breast Cancer Resistance Protein

BMI = Body Mass Index

BSA = Body Surface Area

BSA = Bovine Serum Albumin

BSEP = Bile Salt Export Pump

CAT = Catalase

CATG = Cathepsin G

CAV = Caveolin

CDH = Cadherin

cDNA = Complementary Deoxyribonucleic Acid

CES = Carboxylesterase

CL = Clearance

CLUS = Clusterin

C_{max} = Maximum Plasma Concentration

CO = Collagen Chains

COX = Cytochrome c Oxidase

CPPGL = Cytosolic Protein per Gram of Liver

CSF1R = Macrophage Colony-stimulating Factor 1 Receptor

C_{sys} = Systemic Concentration

CRC = Colorectal Cancer

CRLM = Colorectal Cancer Liver Metastasis

CTNNB1 = Catenin Beta-1

CV = Coefficient of Variation

CYP = Cytochrome P450

CYTN = Cystatin-N

Da = Dalton

DDA = Data-dependent Acquisition

DDI = Drug-drug Interaction

DIA = Data-independent Acquisition

DME = Drug Metabolising Enzyme

DSC = Desmocollin

DTT = Dithiothreitol

EDTA = Ethylenediaminetetraacetic Acid

EGFR = Epidermal Growth Factor Receptor

E_H = Hepatic Extraction Ratio

EPH2A = Ephrin Type-A Receptor 2

EPHX = Epoxide Hydrolase

ERBB2 = Erythroblastic Oncogene B2

ERK = Extracellular Signal-regulated Kinase

FA = Formic Acid

FASP = Filter Aided Sample Preparation

FcRn = Neonatal Fc Receptor

FDA = US Food and Drug Administration

FDR = False Discovery Rate

FGFR = Fibroblast Growth Factor Receptor

FLT3 = FMS-like Tyrosine Kinase

FMO = Flavin-containing Monooxygenase

f_u = Fraction Unbound

g = Gram

g = Gravity

GIST = Gastrointestinal Stromal Tumour

GIT = Gastrointestinal Tract

GPX = Glutathione Peroxidase

h = Hour

HCC = Hepatocellular Carcinoma

HEPES = 4-(2-hydroxyethyl)-1-piperazineethenesulfonic Acid

HLM = Human Liver Microsomes

HMOX = Heme-oxygenase

HomPGL = Homogenate Protein per Gram of Liver

HP = Healthy Pooled Livers

HPLC = High-performance Liquid Chromatography

IAA = Iodoacetamide

ICC = Intrahepatic Cholangiocarcinoma

IFM3 = Interferon-induced Transmembrane Protein 3

IGFR = Insulin-like Growth Factor 1 Receptor

ILF = Interleukin Enhancer-binding Factor

INSR = Insulin Receptor

ITAM = Integrin-alpha M

iTRAQ = Isobaric Tags for Relative and Absolute Quantitation

IVIVE = *In Vitro-In Vivo* Extrapolation

KCR = Creatine Kinase

kDa = Kilo Dalton

KinCAT = Concatemer of Standard Peptides from Human Receptor Tyrosine Kinases

KIT = Mast/stem Cell Growth Factor Receptor

LC = Liquid Chromatography

LC-MS = Liquid Chromatography-Mass Spectrometry

LOX5 = Arachidonate 5-lipoxygenase

MATE1 = Multidrug and Toxin Extrusion Protein 1

MCT1 = Monocarboxylate Transporter 1

MDR = Multidrug Resistance Protein

MET = Hepatocyte Growth Factor Receptor

MetCAT = Concatemer of Standard Peptides from Human Drug Metabolizing Enzymes

MGST = Microsomal Glutathione S-transferase

MIF = Macrophage Migration Inhibitory Factor

min = Minute

MK = Mitogen-activated Protein Kinase

mM = Millimolar

MM = Matrix Metalloproteinase

MPPGL = Microsomal Protein per Gram of Liver

MRM = Multiple Reaction Monitoring

mRNA = Messenger Ribonucleic Acid

MRP = Multidrug Resistance-associated Protein

MS/MS = Tandem Mass Spectrometry

MS = Mass Spectrometry

MS^E = Mass Spectrometry by Collision Energy Alternation

mTOR = Mechanistic Target of Rapamycin

MW = Molecular Weight

m/z = Mass-to-charge Ratio

n = Number Of observations

NFKB1 = Nuclear Factor NF-kappa-B

NMR = Nuclear Magnetic Resonance

NNOP = Non-naturally Occurring Peptide

NP = Histologically Normal Pooled Livers

NRTK = Non-receptor Tyrosine Kinase

NSCLC = Non-small Cell Lung Carcinoma

NTCP = Sodium-dependent Uptake Transporter

NTRK2 = Neurotrophic Tyrosine Kinase Receptor Type 2

OAT = Organic Anion Transporter Protein

OATP = Organic Anion Transporting Polypeptide

OCT = Organic Cation Transporter Protein

OST = Organic Solute Transporter

P-gp = P-glycoprotein

PBPK = Physiology-Based Pharmacokinetics

PCA = Principal Components Analysis

PD = Pharmacodynamics

PEPT1 = Peptide transporter 1

PGFR = Platelet-derived Growth Factor Receptor

pI = Isoelectric Point

PI3K = Phosphatidylinositol 3-kinase

PIP = Percentage Identical Peptides

PIPr = Percentage Identical Proteins

PK = Pharmacokinetics

pKa = Acid Dissociation Constant at Logarithmic Scale

pmol = Picomole

POR = NADPH-cytochrome P450 Reductase

ppm = Parts per Million

PRDX = Peroxiredoxin

PSAQ = Protein Standards for Absolute Quantification

PSM = Peptide-spectrum Match

PTK = Protein Tyrosine Kinase

PTM = Post-Translational Modification

Q = Quadrupole

QC = Quality Control

QconCAT = Concatemer of Standard Peptides

QSP = Quantitative Systems Pharmacology

RAC1 = Ras-related C3 Botulinum Toxin Substrate 1

RCC = Renal Cell Carcinoma

RET = Rearranged during Transfection Proto-oncogene Tyrosine-protein Kinase Receptor

RTK = Receptor Tyrosine Kinase

rpm = Revolutions per Minute

SD = Standard Deviation

SDCB1 = Syntenin-1

SILAC = Stable Isotope Labeling in Cell Culture

SLC = Solute Carrier Transporter Protein

SLCO = Solute Carrier Organic Ion Transporter Protein

SNP = Single Nucleotide Polymorphism

SOD = Superoxide Dismutase

SRM = Selected Reaction Monitoring

SULT = Sulfotransferase

SWATH = Sequential Window Acquisition of All Theoretical Fragment Mass Spectra

TENA = Tenascin (TENA)

TFA = Trifluoroacetic Acid

TIE = Angiopoietin-1 Receptor

TIMP = Metalloproteinase Inhibitor

TKI = Tyrosine Kinase Inhibitor

T_{max} = Time at which Maximum Plasma Concentration

TMT = Tandem Mass Tags

TOF = Time-of-flight

TP = Tumour Pooled Livers

TPA = Total Protein Approach

TransCAT = Concatemer of Standard Peptides from Human Transporters

UGT = Uridine 5′-diphospho-glucuronosyltransferase

V_d = Volume of Distribution

VGFR = Vascular Endothelial Growth Factor Receptor

VIME = Vimentin

v/v = Volume by Volume

w/v = Weight by Volume

Amino Acid Abbreviations

Amino Acid	Abbreviation	
	Three Letters	One Letter
Alanine	Ala	A
Arginine	Arg	R
Asparagine	Asn	N
Aspartic Acid	Asp	D
Cysteine	Cys	C
Glutamic Acid	Glu	E
Glutamine	Gln	Q
Glycine	Gly	G
Histidine	His	H
Isoleucine	Ile	I
Leucine	Leu	L
Lysine	Lys	K
Methionine	Met	M
Phenylalanine	Phe	F
Proline	Pro	P
Serine	Ser	S
Threonine	Thr	T
Tryptophan	Trp	W
Tyrosine	Tyr	Y
Valine	Val	V

Abstract
University of Manchester
Areti Maria Vasilogianni
Doctor of Philosophy
Impact of Gastrointestinal (GI) and Hepatic Cancer on Enzyme and Transporter Abundance Contributing to Variability in Drug Exposure

2021

Clinical trials in oncology recruit heterogeneous participants not often representative of the target cohort, leading to large variability in pharmacokinetics (PK). This increases the risk of toxicity and ineffective treatment. Physiologically-based pharmacokinetic (PBPK) modelling can be used as an alternative to clinical trials and inform drug labelling. These models require systems data, which are not fully characterized in cancer. In this study, scaling factors (e.g. microsomal protein per gram of liver (MPPGL)) for the *in vitro-in vivo* extrapolation of drug clearance were assessed in 16 colorectal cancer liver metastasis (CRLM) patients (paired histologically normal and cancerous livers). MPPGL was significantly lower in cancerous compared with histologically normal livers and was used to simulate plasma exposure of drugs, revealing a substantial decrease in drug exposure, when using typical scaling factors (healthy population) instead of cancer-related parameters in cancer population. Subsequently, LC-MS/MS based proteomic analysis of pooled healthy control, and histologically normal paired with cancerous liver samples from CRLM patients was carried out. Most cytochrome P450 (CYP), UDP-glucuronosyltransferase (UGT) and other drug metabolising enzymes (DMEs) were downregulated in cancer, indicating impaired drug metabolism. Similarly, most drug transporters were downregulated in CRLM, implying perturbed drug transport. A novel QconCAT standard (KinCAT) was designed to quantify receptor tyrosine kinases (RTKs). Several RTKs in addition to other pharmacodynamics protein markers were altered in CRLM. Application of perturbed CYP abundances on PBPK models demonstrated substantially higher drug exposure in cancer compared with healthy populations. These data were confirmed in individual liver samples (15 healthy, 18 cancer and paired normal). To our knowledge, this project provides the first comprehensive scaling factors for IVIVE and quantification of DMEs, transporters, RTKs and other important markers in cancer, with a focus on CRLM. The application of the experimentally-derived data on PBPK models showed the importance of using population-specific data in oncology and is a promising step towards the development of virtual cancer populations for optimal drug dosing.

Declaration

Chapter 2 has also been submitted in support of an application for another PhD qualification of University of Manchester by Eman El-Khateeb (PhD student, University of Manchester). This is a published chapter, and the first three authors share the first-authorship:

El-Khateeb, E., **Vasilogianni, A. M**., Alrubia, S., Al-Majdoub, Z. M., Couto, N., Howard, M., Barber, J., Rostami-Hodjegan, A., & Achour, B. **(2019**). Quantitative mass spectrometry-based proteomics in the era of model-informed drug development: applications in translational pharmacology and recommendations for best practice. *Pharmacol Ther* **203**:107397.

No other portion of the work referred to in the thesis has been submitted in support of an application for another degree of qualification of this or any other university or other institute of learning.

Copyright Statement

i The author of this thesis (including any appendices and/or schedules to this thesis) owns certain copyright or related rights in it (the "Copyright") and she has given the University of Manchester certain rights to use such Copyright, including for administrative purposes.

ii Copies of this thesis, either in full or in extracts and whether in hard or electronic copy, may be made **only** in accordance with the Copyright, Designs and Patents Act 1988 (as amended) and regulations issued under it or, where appropriate, in accordance with licensing agreements which the University has from time to time. This page must form part of any such copies made.

iii The ownership of certain Copyright, patents, designs, trademarks and other intellectual property (the "Intellectual Property") and any reproductions of copyright works in the thesis, for example graphs and tables ("Reproductions"), which may be described in this thesis, may not be owned by the author and may be owned by third parties. Such Intellectual Property and Reproductions cannot and must not be made available for use without the prior written permission of the owner(s) of the relevant Intellectual Property and/or Reproductions.

iv Further information on the conditions under which disclosure, publication and commercialisation of this thesis, the Copyright and any Intellectual Property and/or Reproductions described in it may take place is available at the University IP Policy (see http://documents.manchester.ac.uk/DocuInfo.aspx?DocID=24420), in any relevant Thesis restriction declarations deposited in the University Library, The University Library's regulations (see http://library.manchester.ac.uk/about/regulations/) and in The University's Policy on Presentation of Theses.

Dedication

To my Family

Acknowledgements

The funding for this PhD project came from Merck KGaA, to whom I am very grateful.

During the course of this project, I have had the great pleasure of working alongside a dedicated and enthusiastic team of researchers within the Centre for Applied Pharmacokinetics Research (CAPKR). Of these, I would like to express my foremost appreciation to my supervisors, Professor Amin Rostami-Hodjegan, Dr Jill Barber, and Dr Sheila Annie Peters (Merck KGaA) for their invaluable insights, expertise, and support. Thank you for the opportunity to complete a PhD at the University of Manchester. I am grateful to Dr Zubida Al-Majdoub, Dr Brahim Achour, and Dr Daniel Scotcher for their support and guidance throughout my PhD on many different aspects of the project, from method optimisation to data analysis and modelling, and everything in-between. I also thank Dr Adam Darwich for supervising me in the beginning of my PhD, and Dr Narciso Couto for sharing his knowledge on LC-MS proteomics with me.

I would like to thank Jay Brown (CMFT Biobank), who provided the human liver tissue samples from cancer patients that were vital for the completion of the project.

Thank you to the team in the Biological Mass Spectrometry Core Research Facility, University of Manchester; Stacey Warwood, Emma-Jayne Keevill, Jullian Selley, and David Knight, for the use of vital equipment and software.

Thank you to my colleagues and friends Eman El-Khateeb and Sarah Alrubia for all our discussions and pleasant time spent together throughout this project.

Last but not least, I thank my family for their immense love, encouragement and support!

Preface

The work in this thesis is presented in the journal format. This format was chosen as it allows the preparation of chapters in a format that is appropriate for publications in peer-reviewed journals. The thesis consists of seven separate but linked chapters that have been or will be submitted to journals. In this case, this format is ideal for maximizing the publications of the work generated during this PhD project. The thesis contains seven research papers of which the thesis author is also the lead author. A declaration at the start of each chapter highlights the contribution of each author. The structure of the thesis is outlined below.

Recruiting appropriate populations in clinical trials in oncology is very challenging. The heterogeneity of cancer patients results in a high variability in drug pharmacokinetics (PK), and dedicated studies beyond the intended population are usually limited. The high rate of patients not responding well to the treatment and the high cost of cancer therapy are also limiting factors. Model-informed precision dosing can reduce these limitations via *in vitro-in vivo* extrapolation (IVIVE) techniques and physiologically-based pharmacokinetic (PBPK) modelling, which is now gaining wider regulatory acceptance in oncology. IVIVE-PBPK strategies require the incorporation of drug data and population-specific systems parameters for the accurate prediction of the fate of drugs in patient populations. Some systems parameters have been studied, but there are still many unknown areas for several types of cancer that have to be defined. This project aims to fill in these gaps with a focus on colorectal cancer liver metastasis (CRLM).

The first step was to comprehensively review the systems parameters that differ in cancer patients affecting the pharmacokinetics (PK) of drugs, and the parameters that have not been studied sufficiently. The aim for this was to identify the gaps that should be filled in throughout this project and set the research aims. Among the less studied parameters, scaling factors specific for CRLM population have not been defined, and their characterization is important for IVIVE of drug clearance. Perturbations in them can significantly affect drug clearance. Additionally, drug-metabolizing enzymes (DMEs) and transporters have not been fully investigated in cancer, and perturbed expression of them can result in significantly altered PK. LC-MS proteomics can facilitate the elucidation of the expression of DMEs and transporters. Therefore, the next step was to comprehensively review the available LC-MS proteomics methods and their applications in translational pharmacology. This review assisted with the selection of the appropriate quantitative proteomic method for the purpose of this PhD. The final step before the experimental work was to compare two widely-used software packages

for proteomic analysis, in order to decide which is the most appropriate for the analysis of data derived from the samples used in this PhD.

The steps described above were crucial for defining the research aims that needed to be achieved during this PhD. More specifically, the aims of the project were to:

- Determine for the first time scaling factors specific for colorectal cancer liver metastasis (CRLM) population for in vitro-in vivo extrapolation (IVIVE) of drug clearance and apply them in PBPK simulations of various metabolically cleared drugs. This is very important for proving the necessity of population-specific scaling for model-informed precision dosing in oncology and is substantial for accurate predictions of drug PK.
- Quantify for the first time with the aid of LC-MS proteomics the absolute abundance of DMEs and transporters in patients with liver cancer, with a focus on CRLM and assess the disease impact on these proteins. DMEs and transporters are crucial for the absorption, disposition and metabolism of drugs and any significant decrease or increase in their abundance due to cancer could substantially affect the drug exposure.
- Apply for the first time the experimentally-measured scaling factors and abundance data of DMEs on PBPK models to assess their contribution to drug exposure in CRLM patients.
- Define for the first time the absolute abundance of receptor tyrosine kinases (RTKs) in patients with liver cancer, with a focus on CRLM. RTKs are very important clinical markers for the diagnosis and treatment of cancer and several RTK inhibitors are widely used for cancer therapy. However, their absolute abundance has not been assessed in human tissues. This study aims to quantify 21 RTKs for the first time in human liver microsomes from CRLM patients, with the aid of the QconCAT technology. For this purpose, a novel QconCAT standard (‘KinCAT’) was designed and applied for the first time.
- Investigate changes in the expression of other proteins affected in CRLM. This study aims to quantify for the first time a wide range of pharmacodynamics markers that may be affected in CRLM and could be viewed as potential diagnostic and therapeutic biomarkers.

Overall, this project aims to define for the first time systems parameters specific for CRLM population and assess their potential impact on the exposure of several drugs, by creating virtual cancer populations.

Chapter One: The Quest to Define Cancer-Specific Systems Parameters for Pharmacokinetics Predictions

Declaration

Areti-Maria Vasilogianni, Brahim Achour, Zubida M. Al-Majdoub, Sheila Annie Peters, Jill Barber, and Amin Rostami-Hodjegan

I carried out the literature search, collation of data and wrote the manuscript. Dr Brahim Achour and Dr Zubida M. Al-Majdoub suggested edits to the manuscript. Dr Sheila Annie Peters, Dr Jill Barber and Prof. Amin Rostami-Hodjegan provided guidance. I retained final editorial control.

1.1 Abstract

Introduction: Clinical trials in oncology routinely recruit heterogeneous populations, often not representative of the target cohort, leading to large variability in pharmacokinetics (PK). To address enrolment challenges in clinical trials, PBPK models can be used as an alternative to clinical studies to inform dosing guidance for clinical practice. These modelling tools require cancer-specific system data, which are scarce with many unknowns that need to be addressed.

Areas covered: This review explores the system parameters that affect PK in cancer and highlights important gaps in data that have not been addressed sufficiently, with liver cancer as a case example. Changes in drug-metabolizing enzymes (DMEs) and transporters have not been fully investigated in cancer. Impaired expression of these proteins in cancer can have a significant impact on the patients' capacity for drug elimination. The importance of changes in DMEs, especially CYP3A, for the effectiveness of anti-cancer tyrosine kinase inhibitors (TKIs) is also reviewed. Finally, the review highlights the use of PBPK modelling for precision dosing in oncology.

Expert opinion: PBPK modelling is useful tool for appropriate dosing in cancer populations, which are excluded from oncology clinical trials. There is still a lack of fully characterised systems parameters in cancer cohorts, which are required in PBPK models. Generation of such data and application of cancer models in clinical practice should be encouraged.

1.2 Introduction

Cancer is a leading cause of mortality globally, with rising incidence as life expectancy continues to increase (Heron, 2013; Sung et al., 2021). The most prevalent cancer types are breast, lung and colorectal cancers, while the most lethal are lung, colorectal and liver cancers (Sung et al., 2021). It is important to understand that cancer is not a unique disease, as it has multifaceted genetic and epigenetic components, resulting from the dysregulation of cell proliferation and apoptosis (Zhang et al., 2009). Surgical resection is the ideal option for treatment, resulting in improved survival in patients with solid tumours. However, this is not always feasible for many patient cohorts for various reasons, including instability of overall health, comorbidities, site of tumour and number of lesions. Other methods are sometimes more applicable, such as chemotherapy, immunotherapy, radioembolization, and radiofrequency ablation aiming to reduce the tumorous tissue (Chen et al., 2014; Mitchell et al., 2019).

1.2.1 Drug Development in Oncology

Drug discovery and development is expensive and time-consuming with high attrition rates (Zhang and Tang, 2018). The causes of attrition vary, with the most important being clinical safety, efficacy, non-clinical toxicology, pharmacokinetics (PK), and commercial viability (Waring et al., 2015). A field where the drug development is very challenging is oncology (DiMasi and Grabowski, 2007), with attrition rates very high across all tumour sites. Failure of anti-cancer agents seems to happen more frequently in the most expensive later phases of development (phases 2 and 3), suggesting that improvement in predictions during the early-phases are needed to increase the success rates in development of anti-cancer agents (Nixon et al., 2017).

While most drugs are initially tested in healthy volunteers, this is not the case in clinical trials of anti-cancer agents. Healthy subjects do not participate in these studies for ethical reasons, as the anti-cancer agents may be cytotoxic or mutagenic (Faucette et al., 2017). To recruit a sufficient number of volunteers, heterogeneous cancer populations with various comorbidities are enrolled in Phase 1 first-in-human studies and in initial dose-escalation studies of anticancer agents (Pasqualetti et al., 2010; Venkatakrishnan et al., 2010). An example of the devastating effects of anticancer agents in healthy subjects is the case of TGN1412 (monoclonal antibody against a human lymphocytic antigen), which resulted in systemic organ failure when tested in healthy subjects in a first-in-man trial in London in March 2006 (Kenter and Cohen, 2006). These studies usually recruit advanced and/or metastatic solid tumour patients who cannot be

treated with existing therapies (Senderowicz, 2010), and the dose of new anti-cancer drugs is escalated in these patients up to the maximum tolerated dose (Williams & Pazdur, 2006).

There are significant challenges in oncology drug development, including the recruitment of appropriate patient populations, especially when advanced tumour patients are critically ill, safety issues when testing highly toxic anti-cancer drugs, and the overall cost (DiMasi and Grabowski, 2007; Gutierrez et al., 2009; Bates et al., 2015). Treatment of cancer patients is also hindered by the tendency of anti-cancer drugs to be poorly tolerated, as the toxic effects are not only targeted at cancer cells (Guan, 2015). In addition, since these drugs are rarely tested in their intended target population, appropriate dosage guidance is required. Alternative approaches, such as simulations using physiologically-based pharmacokinetic (PBPK) models, can be applied for predicting changes in drug exposure and guiding dose adjustment in cancer (Darwich et al., 2017).

1.2.2 Physiologically-based pharmacokinetic (PBPK) modelling in Oncology

Model-informed precision dosing (MIDD), which relies on PBPK modelling and simulation has recently been proposed to address the challenges in the area of oncology, and is now gaining wider regulatory acceptance (Darwich et al., 2017), with PBPK simulations having higher regulatory acceptance in the development of anti-cancer drugs than other types of drugs (Yoshida et al., 2017). PBPK models in combination with *in vitro–in vivo* extrapolation (IVIVE) techniques are used to predict absorption, distribution, metabolism, and excretion (ADME) of drugs. This approach requires the incorporation of systems parameters (from the patients) and drug data to predict PK profiles (Rostami-Hodjegan, 2012). Despite the recent success in the application of PBPK models, there are still many gaps in systems parameters in oncology. For example, expression data of metabolic enzymes and transporters in these special patient populations are scarce, and different types of cancer tend to affect expression levels differently (Sharma et al., 2020). Therefore, population-specific systems parameters are important to be defined in different types of cancer to improve the performance of PBPK models and provide more accurate predictions of drug PK in cancer patients.

1.3 Systems Parameters in Cancer Populations

Systems parameters including serum albumin, and alpha-1 acid glycoprotein were reviewed in the past, compared between cancer and healthy populations and their impact on PK of drugs in

cancer populations was assessed (Cheeti et al., 2013). Changes in systems parameters in cancer patients may have a significant impact on PK of drugs (anti-cancer agents and other drugs), and it is important to shed light to parameters have not been investigated yet. Reviewing, updating and defining which parameters need to be assessed in the future is useful for the improvement of PBPK models in cancer populations. Figure 1-2 depicts systems parameters that are known to be different in cancer leading to altered PK. Table 1-1 presents changes in parameters in cancer and their effects on the PK of several drugs as examples.

1.3.1 Parameters that Decrease in Cancer Patients

1.3.1.1 Microsomal Protein per Gram of Liver (MPPGL)

Microsomal protein per gram of liver (MPPGL) is a scaling factor that is used for IVIVE of hepatic drug clearance, and reflects the hepatic metabolic capacity. MPPGL is age-dependant in healthy donors (Barter et al., 2008), while data on MPPGL and its covariates in cancer patients are limited. Investigation of MPPGL in hepatocellular carcinoma (HCC) showed a significant decrease of MPPGL in cancer compared with histologically normal liver tissues, which led to significantly reduced hepatic clearance (CL_H) of most cytochrome P450 (CYP) substrates (Zhang et al., 2015; Gao et al., 2016). MPPGL values have not been defined in other types of hepatic cancer, such as colorectal cancer liver metastasis (CRLM), where hepatic lesions also affect liver function and metabolic capacity. Disease-specific model parameterization requires definition of the level of change in these types of liver cancer, which should improve model performance.

1.3.1.2 Serum Albumin

Albumin is the most abundant protein in the blood, with an average concentration of about 40 mg/mL in healthy people (Larsen et al., 2016). A positive correlation between albumin levels and plasma protein binding was observed for voriconazole in adult intensive care unit patients (Vanstraelen et al., 2014) and pazopanib in cancer patients (Imbs et al., 2016), indicating higher levels of free drug with decreased albumin concentrations. Lower albumin levels lead to increased unbound drug fraction (f_u), which is the proportion of systemic drug levels available for distribution and clearance (CL) from the body. This results in faster clearance and lower drug exposure (Ulldemolins et al., 2011). Additionally, the level of serum albumin is

responsible for variability in central volume of distribution (Blair et al., 2006). Cancer patients are generally characterized by hypoalbuminemia (Cheeti et al., 2013), which has been suggested as a negative prognostic factor for the survival of patients with gastrointestinal (GI) (Nazha, 2015) and breast carcinomas (Fijii et al., 2020). Low serum albumin has also been associated with aggressive HCC (Carr and Guerra, 2017). In patients with advanced solid tumours, higher CL of raltitrexed (highly plasma protein bound anti-cancer drug) was observed in patients with lower levels of albumin. On the other hand, hypoalbuminemia was reported to lead to longer time to clear methotrexate in patients with non-solid tumours, such as leukaemia or lymphoma (Reiss et al., 2016).

1.3.1.3 Haematocrit

Anaemia is a characteristic symptom in many cancer patients, resulting in lower haematocrit levels (Knight et al., 2004). In addition to its impact on the patient's general health, lower haematocrit can impact drug PK. Lower haematocrit levels were correlated with lower CL of amikacin in patients who received high-dose cancer chemotherapy (cisplatin, etoposide, and cyclophosphamide) (Davis et al., 1991). Varying haematocrit levels are known to affect the disposition of drugs that have a high affinity for binding to red blood cells (Størset et al., 2014). For example, everolimus is highly bound to erythrocytes, and a decrease in haematocrit in cancer patients reduced whole-blood exposure to this drug by half, albeit with no impact on its PK (van Erp et al., 2016).

1.3.1.4 Reduced Hepatic Function

Liver impairment is a common comorbidity in liver cancer patients, which can dramatically affect drug absorption, distribution and metabolism due to impaired liver function (Zhao et al., 2020). For example, the degree of hepatic impairment was reported to affect the exposure of everolimus (measured as the area under the plasma concentration-time curve, AUC); dose adjustment was recommended for patients with mild and moderate impairment, while its use in patients with severe hepatic impairment was not recommended (Peveling-Oberhag et al., 2013). Plasma exposure (AUC and Cmax) of crizotinib was also affected in patients with a variety of advanced cancer (hepatocellular carcinoma, colorectal, pancreatic, lung, bladder cancer etc.) depending on the degree of hepatic impairment, requiring dose adjustment for patients with moderate and severe hepatic impairment (El-Khoueiry et al., 2018). Afatinib is

another drug with higher plasma concentration in advanced non-small cell lung cancer (NSCLC) patients with hepatic impairment (Nakao et al., 2019). However, hepatic impairment does not affect carfilzomib PK (AUC and Cmax) in patients with advanced malignancies, possibly because of its extrahepatic metabolism (Brown et al., 2017). Further, osimertinib plasma concentration (C_{max}) in patients with malignant solid tumors was lower for patients with mild or moderate hepatic impairment compared with those with normal hepatic function, but no dose adjustment was required (Grande et al., 2019).

1.3.1.5 Reduced Renal Function

Renal insufficiency (RI) is as a common characteristic of oncology patients, with chronic kidney disease (CKD) affecting a large proportion of patients with solid tumours (Launay-Vacher et al., 2007). The impact of varying grades of RI on PK of orteronel (predominantly renally cleared drug) led to increased AUC and reduced renal CL with the severity of RI (Suri et al., 2015). On the contrary, lower exposure to sunitinib was observed in patients with RI compared with those with normal renal function, potentially due to lower GI absorption of sunitinib in RI patients (Khosravan et al., 2010). General dosing guidance suggests that most anti-cancer drugs can be used at the same dose in cancer patients with mild or moderate RI, but data on severe impairment are very limited, and this gap in clinical guidance should be addressed by future studies (Silvestris et al., 2019).

1.3.2 Parameters that Increase in Cancer Patients

1.3.2.1 Alpha-1 acid glycoprotein (AAG)

Alpha-1 acid glycoprotein (AAG) is a serum protein that is reported to increase in several cancer types (Israili and Dayton, 2001), which can affect drug binding in plasma. Higher AAG concentration results in lower levels of free drug in plasma, and therefore less drug available for elimination. This decreases the volume of distribution and CL of drugs. Apomine (apomorphine) is highly bound to AAG and its apparent CL and V_d in patients with solid tumours are reported to be lower relative to healthy subjects (Bonate et al., 2004). Lower clearance was also reported in cancer patients for other drugs with high affinity to AAG, including tipifarnib, imatinib and saquinavir (Perez-Ruixo et al., 2006; Widmer et al., 2006; Cheeti et al., 2013). This trend was confirmed with imatinib in gastrointestinal stromal tumours

(GIST) (Haouala et al., 2013) and with erlotinib and docetaxel in NSCLC (Lu et al., 2006; Kenmotsu et al., 2017).

1.3.2.2 Inflammation

Inflammation is a common feature of cancer (Shinko et al., 2017). It affects the production of cytokines and increases oxidative stress, which may lead to perturbations in proteins involved in drug metabolism and disposition (Shinko et al., 2017; Schwenger et al., 2018). Reduced abundance of cytochrome P450 (CYP) enzymes in cancer models was shown to better predict PK of anti-cancer drugs (Schwenger et al., 2018). Induced inflammation in mice was reported to increase the C_{max} and AUC of irinotecan (Chityala et al., 2020). Cachectic cancer patients had increased plasma concentration of oxycodone, possibly due to suppressed CYP3A. This decrease was associated with elevated levels of the inflammation marker interleukin 6 (IL-6) in cachexia (Sato et al., 2016).

1.3.2.3 Gastrointestinal (GI) Complications

GI complications, such as constipation, diarrhoea and vomiting, are frequent in cancer patients, who are subjected to chemotherapy or radiation therapy. They can affect any part of the GI tract (GIT), and can sometimes be life-threatening (Davila and Bresalier, 2008). Constipation leads to inadequate absorption of orally administered drugs (Mancini and Bruera, 1998), and this may affect the efficacy of the drug. Diarrhoea affects drug absorption in two different ways. In the case of drugs with low bioavailability, such as ganciclovir and saquinavir, damage to the intestinal mucosa causes higher intestinal permeability and increased absorption of drugs, leading to higher AUC and lower CL/F (oral clearance). In the case of drugs with high intestinal absorption (e.g. stavudine and didanosine), diarrhoea provokes higher elimination from the GIT and lower fraction of drug absorbed, resulting in lower bioavailability (Trobec et al., 2013). Achlorhydria is another GIT complication in cancer patients, where hydrochloric acid production in the stomach is impaired. In leukaemia patients treated with dasatinib, administration of gastric acid suppressants (e.g. famotidine, nizatidine and lansoprazole) resulted in decreased AUC and plasma concentration of dasatinib (Takahashi et al., 2012). Oral bioavailability of certain anti-cancer drugs is dependent on stomach pH; for example, reduced bioavailability was reported for erlotinib when co-administered with proton pump inhibitors

(PPIs), while reducing gastric pH in patients with NSCLC increased AUC of erlotinib administered with esomeprazole (van Leeuwen et al., 2016).

Table 1-1 The effects of perturbed systems parameters in cancer on PK of drugs.

Systems Parameters	Change in Cancer	Drug	PK in Cancer	References
MPPGL	↓		↓ CL_H	(Zhang et al., 2015; Gao et al., 2016)
Albumin	↓	Voriconazole	↑ f_u	(Vanstraelen et al., 2014)
		Pazopanib	↑ f_u	(Imbs et al., 2016)
		Raltitrexed	↑ CL, ↑V_d	(Blair et al., 2006)
		Methotrexate	longer time to clear	(Reiss et al., 2016)
Haematocrit	↓	Amikacin	↓ CL	(Davis et al., 1991)
		Everolimus	↓ blood exposure	(van Erp et al., 2016)
AAG	↑	Apomine	↓ CL, ↓ V_d	(Bonate et al., 2004)
		Tipifarnib	↓ CL	(Perez-Ruixo et al., 2006)
		Imatnib	↓ CL	(Widmer et al., 2006; Haouala et al., 2013)
		Saquinavir	↓ CL	(Cheeti et al., 2013)
		Erlotinib	↓ CL	(Lu et al., 2006)
		Docetaxel	↓ CL	(Kenmotsu et al., 2017)
Hepatic function	↓	Everolimus	↑ AUC	(Peveling-Oberhag et al., 2013)
		Crizotinib	↑ AUC, ↑ C_{max}	(El-Khoueiry et al., 2018)
		Afatinib	↑ plasma concentration	(Nakao et al., 2019)
		Carfilzomib	None	(Brown et al., 2017)
		Osimertinib	↓ Cmax	(Grande et al., 2019)
Renal function	↓	Orteronel	↑ AUC	(Suri et al., 2015)
		Sunitinib	↓ AUC	(Khosravan et al., 2010)
GIT complications	↑			
• **Constipation**			↓ drug absorption	(Mancini and Bruera, 1998)
• **Diarrhoea**		Ganciclovir, Saquinavir	↑ absorption, ↑ AUC, ↓ CL/F	(Trobec et al., 2013)
		Stavudine, Didanosine	↑ GIT elimination, ↓ absorption, ↓ bioavailability	(Trobec et al., 2013)
• **Achlorhydria**		Dasatinib	↓ AUC, ↓ plasma concentration	(Takahashi et al., 2012)
		Erlotinib	↓ bioavailability	(van Leeuwen et al., 2016)
Inflammation	↑	Oxycodone	↑ plasma exposure	(Sato et al., 2016)

AUC, area under the plasma concentration-time curve; CL, clearance; CL/F, oral clearance; CL_H, hepatic clearance; C_{max}, maximum plasma concentration; f_u, fraction unbound; V_d, volume of distribution

1.3.3 ADME Proteins Affected in Cancer

1.3.3.1 Drug Metabolizing Enzymes (DMEs)

CYP enzymes are responsible for the metabolism of the majority of clinically used drugs in all therapeutic areas, including oncology, with CYP3A4/5 being the most clinically relevant pathway, followed by CYP2D6 (Zanger and Schwab, 2013). CYPs and UDP-glucurosyltransferases (UGTs) contribute to the metabolism of more 90% of drugs that are dependent on hepatic clearance (CL_H) for elimination from the body (Rowland et al., 2013). Reports on changes in CYP expression in breast cancer are inconsistent, indicating either a decrease in CYP1A1, 2E1, and 3A4 abundance in tumours with immunoblotting (El-Rayes et al., 2003) or an increase of CYP3A4 with immunohistochemistry (Kapucuoglu et al., 2003). Higher expression of CYP1B1 was observed with Western blotting in colorectal adenocarcinomas relative to histologically normal human large bowel samples (Gibson et al., 2003). In addition, immunoblotting data suggested that a set of CYP enzymes (CYP1B1, CYP2D6, CYP2S1, CYP2U1, CYP3A5, and CYP51) are upregulated in colorectal cancer compared with histologically normal control (Kumarakulasingham, 2005). In the same type of cancer, Western blotting also revealed higher expression of CYP2W1 (Karlgren et al., 2006), which correlated with the stage of disease (Travica et al., 2013). Expression of UGT1A isoforms was found to be downregulated in colon cancer compared with normal colon tissues using immunohistochemistry (Giuliani et al., 2005). More recently, CYP3A4, CYP2D6, CYP2C8,CYP2C9, CYP1A2, CYP2A6, CYP2E1, UGT1A1, UGT1A4 and UGT2B7 were shown to be downregulated, while UGT1A6 and UGT1A9 were unchanged, in HCC tumours compared with normal livers analysed by liquid chromatography in conjunction with mass spectrometry (LC-MS) (Yan, Gao, et al., 2015; Yan, Lu, et al., 2015). Western blot data also demonstrated lower expression of UGT1A1, UGT1A9, UGT1A4 and UGT2B7 in liver cancer tissue compared with adjacent normal tissue from HCC patients (Lu et al., 2015). In NSCLC, immunohistochemistry data showed increased CYP3A4 and decreased CYP3A5 levels in cancerous lung tissue (Qixing et al., 2017). In ovarian cancer, liver expression of CYP1B1, CYP2A/2B, CYP2F1, CYP2R1, CYP2U1, CYP3A5, CYP3A7, CYP3A43, CYP4Z1, CYP26A1, and CYP51, quantified by immunohistochemistry, was significantly increased compared with normal tissue (Downie et al., 2005). In renal cell carcinoma (RCC), data from immunohistochemistry, immunoblotting and reverse transcriptase polymerase chain reaction (RT-PCR) indicated similar expression of CYP3A in both tumorous and normal kidney tissue

(Murray et al., 1999). Other immunohistochemistry data showed that CYP4A11 levels were significantly lower in clear cell renal cell carcinoma (ccRCC) than normal renal tissue (Kim et al., 2020). Table 1-2 summarizes literature findings on the expression of DMEs in cancer.

Table 1-2 Impact of cancer on the expression of DMEs (CYPs and UGTs) in different cancer types.

Cancer Type	Impact on DMEs	Method	References
Breast cancer	↓ CYP1A1, 2E1, 3A4	Immunoblotting	(El-Rayes et al., 2003)
	↑ CYP3A4	Immunohistochemistry	(Kapucuoglu et al., 2003)
Colorectal adenocarcinoma	↑ CYP1B1	Western blot	(Gibson et al., 2003)
Colorectal cancer	↑ CYP1B1, CYP2D6, CYP2S1, CYP2U1, CYP3A5, CYP51	Immunohistochemistry	(Kumarakulasingham, 2005)
Colon cancer	↑ CYP2W1	Western blot	(Karlgren et al., 2006)
	↓ UGT1A	Immunohistochemistry	(Giuliani et al., 2005)
HCC	↓ CYP3A4, CYP2D6, CYP2C8,CYP2C9, CYP1A2, CYP2A6, CYP2E1	LC-MS	(Yan, Gao, et al., 2015; Yan, Lu, et al., 2015)
	↓ UGT1A1, UGT1A4, UGT2B7. No change in UGT1A6, UGT1A9	LC-MS	(Yan, Gao, et al., 2015; Yan, Lu, et al., 2015)
	↓ UGT1A	Western blot	(Lu et al., 2015)
NSCLC	↑ CYP3A4, ↓CYP3A5	Immunohistochemistry	(Qixing et al., 2017)
Ovarian cancer	↑ CYP1B1, CYP2A/2B, CYP2F1, CYP2R1, CYP2U1, CYP3A5, CYP3A7, CYP3A43, CYP4Z1, CYP26A1, CYP51	Immunohistochemistry	(Downie et al., 2005)
RCC	No change in CYP3A	Immunohistochemistry, Immunoblotting, RT PCR	(Murray et al., 1999)
ccRCC	↓ CYP4A11	Immunohistochemistry	(Kim et al., 2020)

HCC, hepatocellular carcinoma; NSCLC, non-small cell lung cancer, RCC, renal cell cancer; ccRCC, clear cell RCC

1.3.3.2 Transporters

Drug transporters have a key role in disposition of drugs, drug-drug interactions (DDIs) (Liang et al., 2020), and possibly in resistance to anti-cancer agents (Akhdar et al., 2012). Figure 1-1 shows the location of important drug transporters in hepatocytes. Literature evidence suggests that the expression of transporters is affected in different types of cancer.

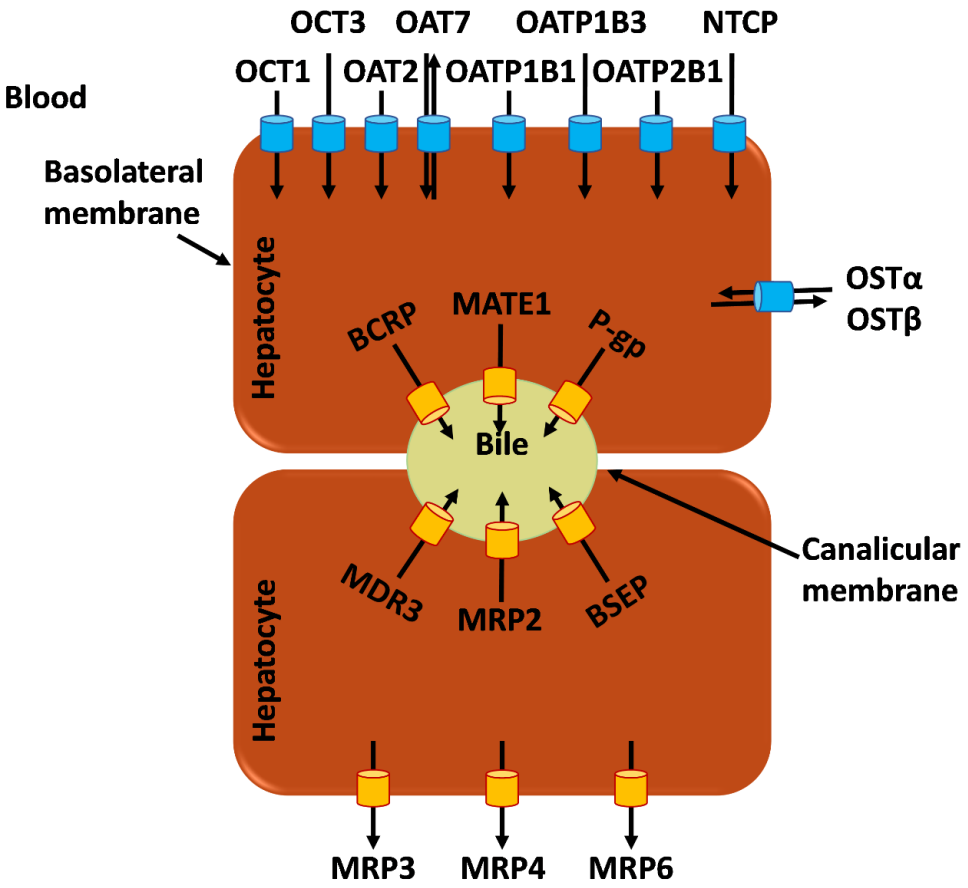

Figure 1-1 Location of clinically relevant drug transporters expressed in human hepatocytes. Uptake transporters located on the basolateral membrane include members of the SLC superfamily, such as OCT1, OCT3, OAT2, OAT7, OATP1B1, OATP1B3, OATP2B1, and NTCP. Efflux transporters located on the basolateral membrane include members of the ABC superfamily, such as MRP3, MRP4, and MRP6. Efflux transporters are also located in the canalicular membrane and include BCRP, BSEP, MATE 1, MDR3, MRP2, and P-gp.

In HCC patients, LC-MS proteomics data showed that levels of OATP1B1, OATP1B3, OATP2B1, OCT1, BSEP, BCRP, MRP2, MRP3, P-gp, and NTCP were lower in cancerous livers, while MATE1 expression was unchanged (Billington et al., 2019). The decrease in OATP1B3 is in agreement with Western blotting data (Vavricka et al., 2004), while RT-PCR confirmed downregulation of MRP2 in HCC (Bonin et al., 2002). Changes in mRNA expression of transporters, measured by RT-PCR, were also observed in colon cancer, indicating a reduction in OATP1A2 expression in cancer tissue, while OATP1B1 expression was increased and OATP1B3 was unchanged (Ballestero et al., 2006). Similarly, increased MRP2 expression was reported in colon cancer (Hinoshita et al., 2000). Northern blot data showed that BCRP expression decreased in colon cancer tissue compared with matched normal colon (Gupta et al., 2006). Finally, immunohistochemistry showed that P-gp protein levels were lower in colorectal cancer tissue relative to matched normal tissue (De Iudicibus et al., 2008). A summary of these data is provided in Table 1-3.

Table 1-3 Impact of cancer on the expression of transporters.

Cancer Type	Impact on Transporter	Method	References
HCC	↓ OATP1B1, OATP1B3, OATP2B1, OCT1, BSEP, BCRP, MRP2, MRP3, NTCP, P-gp	LC-MS	(Billington et al., 2019)
	No change in MATE1	LC-MS	(Billington et al., 2019)
	↓ OATP1B3	Western blotting	(Vavricka et al., 2004)
	↓ MRP2	RT-PCR	(Bonin et al., 2002)
Colon cancer	↓ OATP1A2	RT-PCR	(Ballestero et al., 2006)
	↑ OATP1B1	RT-PCR	(Ballestero et al., 2006)
	No change in OATP1B3	RT-PCR	(Ballestero et al., 2006)
	↑ MRP2	RT-PCR	(Hinoshita et al., 2000)
	↓ BCRP	Northern blotting	(Gupta et al., 2006)
	↓ P-gp	Immunohistochemistry	(De Iudicibus et al., 2008)

1.3.4 The Effect of Patient Demographics

Demographics may also play an important role in defining PK of drugs used in cancer patients. For example, sex may affect the PK due to the differences in anatomical and physiological parameters between male and female patients, such as body composition, body fat content, enzymatic activity, plasma volume, cardiac output, plasma proteins, and pregnancy (Soldin and Mattison, 2009). These differences were reported to affect several anti-cancer drugs, including paclitaxel, fluorouracil, doxorubicin, imatinib, sunitinib, bevacizumab, and rituximab, with

men demonstrating higher elimination capacity and lower susceptibility to toxicity than women (Özdemir et al., 2018). Age is another covariate with potential impact on PK due to ontogeny (developmental) changes and differences in older patients compared with adults; differences include organ function, body composition, co-morbidities, and co-medications (He et al., 2011). In paediatric populations, the growth and maturation are key contributors to changes in metabolic capacity, with the ontogeny of DMEs being a significant contributor to difference in drug clearance and exposure across the population and in comparison with populations of adults (Kearns et al., 2003; Duan et al., 2019; Matlock et al., 2019). Several studies have assessed the impact of age after maturity on PK, but older age itself was not sufficient for PK predictions, requiring physiological parameters for each individual patients (Crombag et al., 2016). Some examples showing decreased clearance of drugs with increasing age are docetaxel (Launay-Iliadis et al., 1995), etoposide, cisplatin (Miller et al., 1997), paclitaxel (Smorenburg et al., 2003; Lichtman et al., 2006) and omeprazole (Ishizawa et al., 2005).

Body mass index (BMI) is another factor contributing to PK changes. A study in cabozantinib in patients with progressive, metastatic medullary thyroid carcinoma showed decreased CL/F with increasing BMI, but no dose adjustment was recommended (Miles et al., 2016). Additionally, larger BMI resulted in smaller absorption rate constant (K_a) of heparanase endoglycosidase inhibitor PI-88 injected subcutaneously into the abdominal fat showing that more adipose tissue leads to slower drug absorption (Hudachek et al., 2010). Body surface area (BSA) may also contribute to PK changes. Studies in docetaxel (Launay-Iliadis et al., 1995), paclitaxel (Miller et al., 2004) and heparanase endoglycosidase inhibitor, PI-88 (Hudachek et al., 2010), showed increased CL with higher BSA. This may be useful when dosing patients with obesity or cachexia.

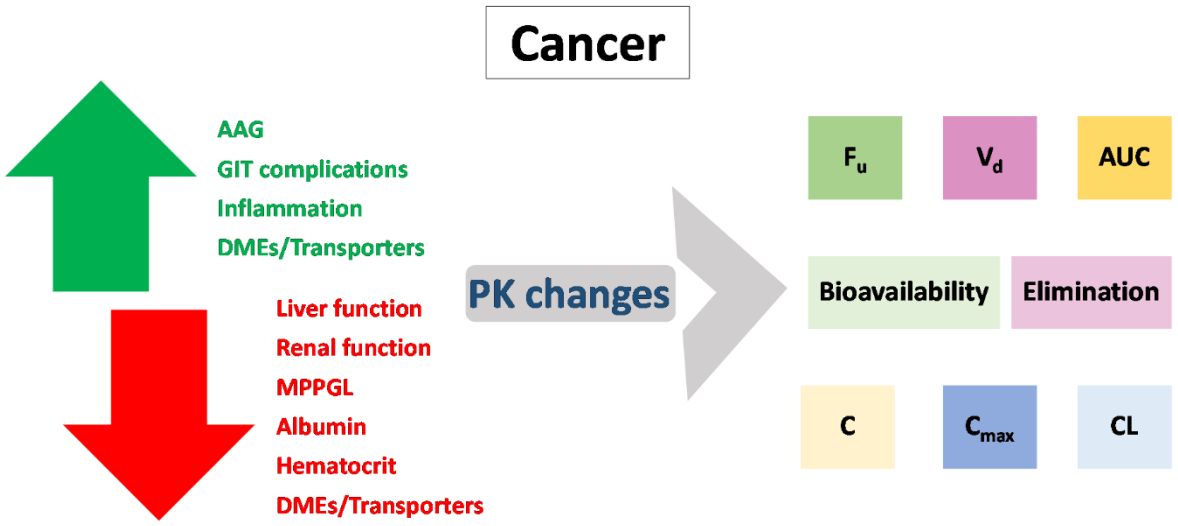

Figure 1-2 Physiological parameters affected in cancer that lead to changes in PK metrics.

1.4 Tyrosine Kinase Inhibitors (TKIs) for Cancer Treatment

Protein tyrosine kinases (PTKs) catalyse the transfer of phosphate groups from ATP to tyrosine residues on proteins, and this reaction triggers regulation of cell growth, differentiation, and death (Wang and Cole, 2014). PTKs can be divided into receptor PTK (RTK) and non-receptor PTK (NRTK). NRTK are cytoplasmic and lack extracellular ligand-binding domain. Of the 518 identified human kinase genes, 90 are members of the PTK family, which includes 58 RTK and 32 NRTK genes (Jiao et al., 2018). Many proto-oncogene and oncogene products have PTK activity and their mutations or altered expression affect cell proliferation and cause tumorigenesis, metastasis, and resistance to chemotherapeutic agents, highlighting the need for developing drugs that target PTKs in all cancer types (Paul and Mukhopadhyay, 2004; Smyth and Collins, 2009; Bhullar et al., 2018; Jiao et al., 2018).

Kinase inhibitors are widely used in oncology, with most of the FDA approved anti-cancer new molecular entities in the period 2011-2017 being small molecule kinase inhibitors (Faucette et al., 2017). Tyrosine kinase inhibitors (TKIs) are small molecule inhibitors that target cancer cells by binding to intracellular tyrosine kinases (Hojjat-Farsangi, 2014). TKIs are ATP competitors for the ATP binding site of tyrosine kinases, reducing the level of tyrosine kinase-mediated phosphorylation and inhibiting tumour cell proliferation. This leads to inhibition of cell repair, cell division and angiogenesis, as well as inducing apoptosis. This class of molecules has several advantages, including high selectivity, uncommon severe adverse

reactions, and oral administration (Wang and Cole, 2014; Jiao et al., 2018). Although TKIs are a promising therapeutic class, high heterogeneity and prevalent mutation of kinases cause resistance to TKIs, which is a key challenge to effective treatment. This raises the need for better understanding of underlying resistance mechanisms and focused investigation of suitable predictive biomarkers to facilitate more targeted therapy (Chen et al., 2019; García-Aranda and Redondo, 2019). Currently, there are 43 small molecule receptor and non-receptor TKIs approved by the US FDA for the treatment of a wide range of cancer types, such as liver, GIT, breast, lung, pancreas cancers (Figure 1-3).

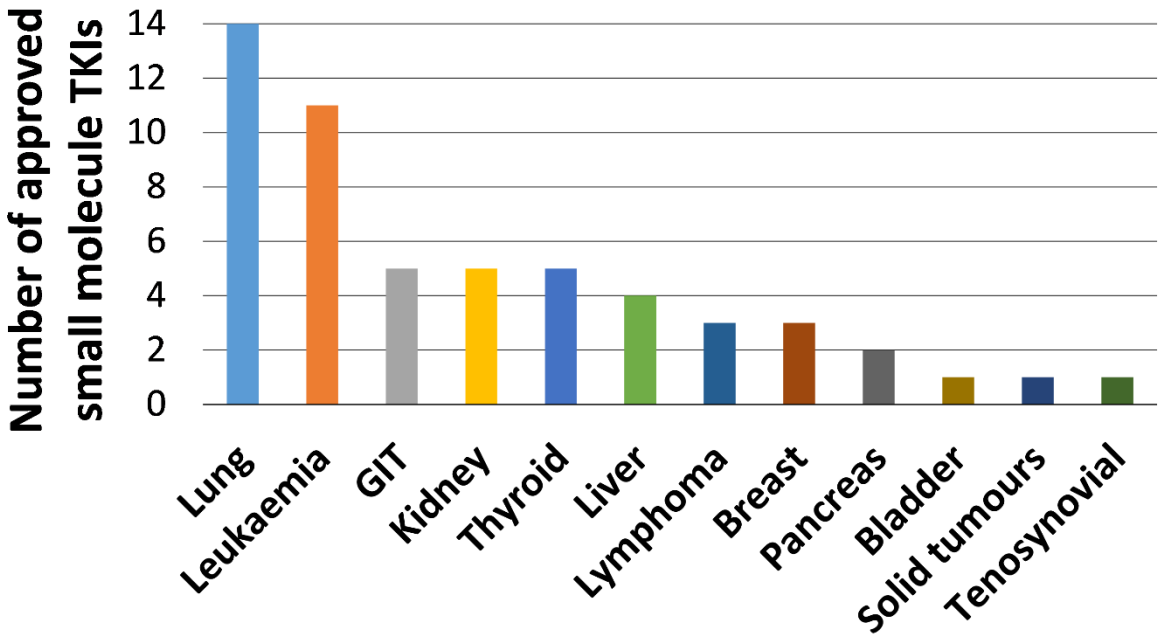

Figure 1-3 US FDA approved small molecule TKIs for the treatment of various cancer types. Drugs used for more than one cancer type: 2 drugs used for both lymphoma and leukaemia, 1 for thyroid, kidney, and liver cancer, 1 for lung and pancreas cancer, 1 for leukaemia and gastrointestinal (GIT) cancer, 1 for liver and GIT cancer, 1 for lung and thyroid cancer, 1 for liver, kidney and thyroid cancer, and 1 for GIT, kidney and pancreas cancer.

The main pathway of metabolism for small molecule TKIs is predominantly CYP3A, particularly CYP3A4 (Table 1-4). Other DMEs contribute, to a lower extent, to the metabolism of TKIs, and these include mainly CYP2D6, CYP2C8, CYP2C9, CYP2C19, and UGT1A1. Data describing the major and minor contributors to the metabolism of TKIs were collated from several publications (Shibata and Chiba, 2015; Teo et al., 2015; Giri et al., 2015; Lamb, 2019; Podoll et al., 2019; Dhillon, 2020a; b; Poggesi et al., 2020; Syed, 2020; Topletz-Erickson et al., 2020; Glaenzel et al., 2020; Hoy, 2020; Markham, 2020a; b; Talpaz and Kiladjian, 2021; Meneses-Lorente et al., 2021) and are presented in Table 1-4.

Table 1-4 Small molecule TKIs approved for cancer treatment and their pathways of metabolism.

Drug	**Year of approval**	**Kinase family**	**Targeted diseases**	**Metabolism**	
				Major contributors	**Minor contributors**
Acalabrutinib	2017	NRTK	Mantle cell lymphoma, CLL, small lymphocytic lymphomas	CYP3A	
Afatinib	2013	RTK	NSCLC	Negligible	
Alectinib	2015	RTK	ALK-positive NSCLC	CYP3A4	
Avapritinib	2020	RTK	GIST	CYP3A4	CYP2C9
Axitinib	2012	RTK	Advanced RCC	CYP3A4/5	CYP1A2/2C19, UGT1A1
Bosutinib	2012	NRTK	CML	CYP3A4	
Brigatinib	2017	RTK	ALK-positive NSCLC	CYP2C8/3A4	
Cabozantinib	2012	RTK	Advanced medullary thyroid cancer, RCC, HCC	CYP3A4	CYP2C9
Capmatinib	2020	RTK	NSCLC	CYP3A4	

Ceritinib	2014	RTK	ALK-positive NSCLC resistant to crizotinib	CYP3A4	
Crizotinib	2011	RTK	ALK or ROS1-postive NSCLC	CYP3A4/3A5	
Dacomitinib	2018	RTK	EGFR-mutant NSCLC	CYP2D6	CYP3A4
Dasatinib	2006	NRTK	CML	CYP3A4	FMO-3, UGT
Entrectinib	2019	RTK	Solid tumours with NTRK fusion proteins, ROS1-positive NSCLC	CYP3A	
Erdafitinib	2019	RTK	Urothelial bladder cancers	CYP2C9/3A4	
Erlotinib	2004	RTK	NSCLC, pancreatic cancer	CYP3A4	CYP1A2/1A1
Fedratinib	2019	NRTK	Myelofibrosis	CYP3A4/2C19, FMO3	
Gefitinib	2003	RTK	NSCLC	CYP3A4/2D6	
Gilteritinib	2018	RTK	AML	CYP3A4	
Ibrutinib	2013	NRTK	CLL, mantle cell lymphoma, marginal zone lymphoma	CYP3A4	CYP2D6
Imatinib	2001	NRTK	Philadelphia chromosome-positive CML or ALL, aggressive systemic mastocytosis, chronic eosinophilic leukaemia, dermatofibrosarcoma protuberans, hypereosinophilic syndrome, GIST,	CYP3A4	CYP1A2/2D6/2C9/ 2C19

			myelodysplastic/myeloproliferative disease		
Lapatinib	2007	RTK	HER2-positive breast cancer	CYP3A4/3A5	CYP2C19/2C8
Larotrectinib	2018	RTK	Solid tumours with NTRK fusion proteins	CYP3A4	
Lenvatinib	2015	RTK	Differentiated thyroid cancer	CYP3A4, AO	
Lorlatinib	2018	RTK	ALK-positive NSCLC	CYP3A4, UGT1A4	CYP2C8/2C19/3A5, UGT1A3
Midostaurin	2017	RTK	AML, mastocytosis, mast cell leukaemia	CYP3A4	
Neratinib	2017	RTK	HER2-positive breast cancer	CYP3A4	
Nilotinib	2007	NRTK	Philadelphia chromosome-positive CML	CYP3A4	CYP2C8
Osimertinib	2015	RTK	NSCLC	CYP3A4/3A5	
Pazopanib	2009	RTK	RCC, soft tissue sarcomas	CYP3A4	CYP1A2/2C8
Pemigatinib	2020	RTK	Cholangiocarcinoma with FGFR2 fusions or rearrangements	CYP3A4	
Pexidartinib	2019	RTK	Tenosynovial giant cell tumours	CYP3A4, UGT1A4	
Ponatinib	2012	NRTK	Philadelphia chromosome-positive CML or ALL	CYP3A4	CYP2C8/2D6/3A5
Pralsetinib	2020	RTK	RET-fusion protein NSCLC	CYP3A4	CYP2D6/1A2

Regorafenib	2012	RTK	CRC, HCC	CYP3A4	UGT1A9
Ripretinib	2020	RTK	GIST	CYP3A4	CYP2C8,CYP2D6
Ruxolitinib	2011	NRTK	Myelofibrosis, polycythaemia vera	CYP3A4/2C9	
Selpercatinib	2020	RTK	NSCLC, thydroid cancer	CYP3A4	
Sorafenib	2005	RTK	HCC, RCC, thyroid cancer (differentiated)	CYP3A4	UGT1A9
Sunitinib	2006	RTK	GIST, RCC, pancreatic neuroendocrine tumours	CYP3A4	
Tucatinib	2020	RTK	HER2-positive breast cancer	CYP2C8	CYP3A
Vandetanib	2011	RTK	Medullary thyroid cancer	CYP3A4	FMO-1, FMO-3
Zanubrutinib	2019	NRTK	Mantle cell lymphoma	CYP3A	

ALL, acute lymphoblastic leukaemia; ALM, acute myelogenous leukaemia; CLL, chronic lymphocytic leukaemia; CML, chronic myelogenous leukaemia; CRC, colorectal cancer; GIST, gastrointestinal stromal tumour; HCC; hepatocellular carcinoma; NRTK, non-receptor protein-tyrosine kinase; NSCLC, non-small cell lung carcinoma; RCC, renal cell carcinoma; RTK, receptor protein-tyrosine kinase.

Analysis of metabolic data related to TKIs approved by the US FDA for the treatment of cancer indicated that 93% of TKIs are predominantly metabolized by CYP3A4/5 (major contributor to metabolism), while only 2.3% of TKIs are mainly metabolized by CYP2C8, 2.3% by CYP2D6 and 2.3% are not metabolized by DMEs (Figure 1-4A). Focusing on TKIs metabolised mainly by CYP3A4, 87% of these TKIs have only CYP3A4/5 as the major contributor, while 5% are predominantly metabolized by CYP3A and CYP2C9, 2.5% by CYP3A and CYP2C8, 2.5% by CYP3A, CYP2C19 and FMO3, and 2.5% by CYP3A and UGT1A4 (Figure 1-4B). These data show the importance of CYP enzymes, especially CYP3A4, in the metabolism of TKIs.

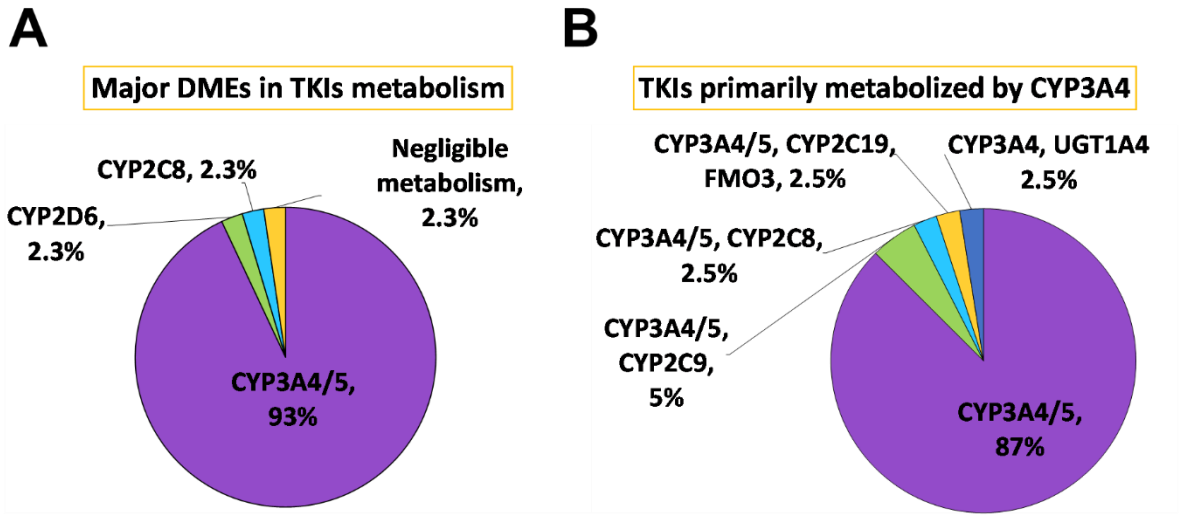

Figure 1-4 Metabolic pathways involved in the metabolism of TKIs. **(A)** Major DMEs contributing to the metabolism of TKIs, **(B)** TKIs metabolized by CYP3A4.

1.5 Liver Cancer as a Case Example

Primary liver cancer is the sixth most common and the third most lethal cancer type (Sung et al., 2021), with its prevalent forms being HCC and intrahepatic cholangiocarcinoma (ICC) (Bray et al., 2018). Colorectal cancer (CRC) is the third most common and the second most lethal type of cancer (Bray et al., 2018). It mainly metastasizes to the liver and, less frequently, to the lungs, distant lymph nodes, and peritoneum (Holch et al., 2017). Approximately one fourth of the patients have liver metastases at the initial diagnosis of primary cancer, and half have liver metastases during the course of the disease (Maher et al., 2017). Metastasis is the main cause of mortality (Siegel et al., 2018) and can affect hepatic function through lesions that occupy space in liver tissue and lead to abnormal liver function tests (Jiang et al., 2018). Although surgical resection of liver cancer (primary or secondary) is the ideal option for treatment and long-term survival, this is not always possible and other methods are used, including chemotherapy, immunotherapy, radioembolization, and radiofrequency ablation with the aim to control tumour growth (Chen et al., 2014; Mitchell et al., 2019).

Liver is the main organ of drug metabolism, and the presence of tumour lesions can affect the PK of drugs in cancer patients. It is crucial to know the PK parameters affected in patients with liver cancer. For example, knowing the disease impact on the abundance of DMEs and transporters would inform predicting changes in metabolism and disposition in these patients. Defining changes in DMEs and transporters in both tumorous and histologically normal peri-

carcinomatous livers is important. Both sections of tissue may be important for drug metabolism and disposition in cancer patients, as the DMEs, especially CYPs and UGTs, in the tumour itself are responsible for activation of anti-cancer prodrugs and their subsequent metabolism in tissue (Michael and Doherty, 2005). Drug transporters are also very critical for drug disposition and anti-cancer drug resistance, which occurs when efflux transporters (particularly P-gp and MRPs) are upregulated and uptake transporters (such as OATPs) are suppressed (Akhdar et al., 2012).

The absolute abundance levels of several CYP and some UGT enzymes in histologically normal and tumorous liver tissue from HCC patients has previously been reported (Yan, Gao, et al., 2015; Yan, Lu, et al., 2015). Based on these data (Yan, Gao, et al., 2015), the relative difference in abundance of DMEs in tumour with reference to levels in histologically normal tissue was assessed, as shown in Figure 1-5. The figure shows that CYPs decrease by approximately 20% in cancer tissue (Figure 1-5A). CYP3A4, the most important contributor to the metabolism of TKIs and most other drugs, decreased by 18%. UGTs are also perturbed in liver cancer. The data suggest that people with liver cancer may have impaired hepatic metabolism, and hence, altered PK of drugs used for their treatment. If CYP3A4 is decreased by 18%, the metabolic capacity of the liver against CYP3A4 substrates may decrease by up to 18% in advanced cancer, where most of the liver is cancerous. This may result in lower clearance and potentially higher toxicity. Other non-CYP non-UGT DMEs are perturbed in HCC. Expression of sulfotransferases (SULT) 1A1, 1B1, 1E1, 2A1 is lower, whereas that of SULT1A3 increased in cancer relative to normal liver tissue, analyzed by LC-MS (Xie et al., 2017). Alcohol dehydrogenases (ADH), aldehyde dehydrogenase (ALDH), and flavin-containing monooxygenases (FMOs) were downregulated (Hu et al., 2014). Along with enzyme expression, MPPGL is another parameter that decreases in HCC (mean 28.85 mg/g tissue) compared with histologically normal livers (mean 39.60 mg/g tissue) (Zhang et al., 2015; Gao et al., 2016). This can lead to further reduction in the metabolic capacity of cancer patients.

The case of drug transporters reflected significant changes in both histologically normal and tumorous tissue compared with healthy livers, analyzed with LC-MS proteomics (Billington et al., 2019). The most significant changes were the increase of NTCP levels by almost 2 fold in normal livers and the decrease of OCT1 abundance by 88% in cancerous livers (Figure 1-5B). These perturbed abundances of transporters may lead to differences in drug exposure and distribution.

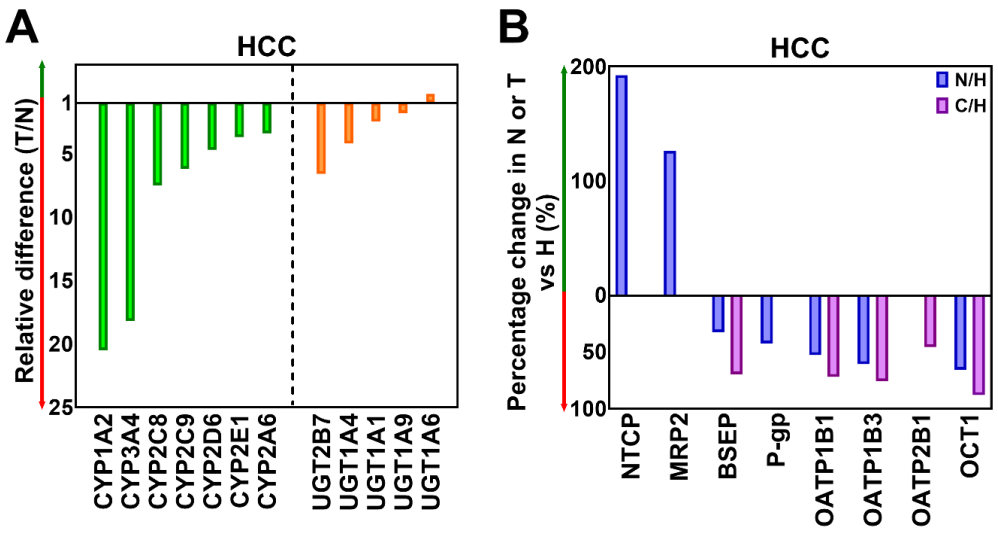

Figure 1-5 Differences in the abundance of DMEs and transporters in HCC. Changes in DMES between histologically normal and cancerous livers (**A**) and in transporters between normal tissue and tumours compared with healthy livers (**B**). Data are extracted from previous publications (Yan, Gao, et al., 2015; Billington et al., 2018).

In contrast to primary liver cancer, to our knowledge, there are no reports of quantitative data on the expression of CYP and UGT enzymes in liver tissue from CRLM patients. One previous study (Lane et al., 2004) investigated the impact of liver metastasis on the qualitative expression profile of CYPs, but did not provide any quantitative data. There are however, limited data showing downregulation of microsomal glutathione S-transferases (MGST) in CRLM tissue compared with normal liver, analyzed using immunoblotting (Mulder et al., 1994). Downregulation of aldehyde oxidase 1 (AOX1) and ADH4 and upregulation of SULT1B1 were also reported based on LC-MS data (van Huizen et al., 2019). Considering the altered expression of these DMEs, the suppressed CYPs and UGTs in primary liver cancer and the inflammatory cancerous environment, DMEs may also be affected in the livers of CRLM patients, which may lead to perturbed PK. MPPGL is another parameter not yet assessed in CRLM. Therefore, we believe that it is important to assess these factors in order to be able to accurately predict PK profiles in CRLM patients. Similar to DMEs, studies on transporters are quite limited in CRLM. Available mRNA data, such as those of OATPs, may not correlate well with proteins abundance (Wlcek et al., 2011). Absolute quantification using LC-MS are focused on comparison of several transporters between healthy livers and histologically normal livers from CRLM patients, with no measurements in tumorous livers (Kurzawski et al., 2019). Such proteomic data showed similar expression of MRP1, MRP2, MRP3, MRP4, BCRP, BSEP, MCT1, OCT1, OCT3, OAT2, OATP1B1, OATP1B3, and OATP2B1 between normal

and healthy tissue, but significantly higher levels of NTCP and significantly lower levels of P-gp in normal livers. These data confirm the assumption that the expression of some transporters may differ even in normal liver tissue from CRLM patients due to cancerous environment, and therefore, we should expect further changes in tumorous liver tissue. Additional studies are required for the elucidation of the impact of metastatic cancer on hepatic transporters.

1.5 Precision Dosing in Oncology

Precision medicine takes into consideration the specific characteristics of a patient, including genotype, phenotype, comorbidities and co-medications, in order to define the optimal treatment and the best dosage regimen for maximum efficacy and minimum toxicity (Marsousi et al., 2017). Its application can be achieved using the knowledge of the mechanisms of the disease, its progressive stages, and the inter-individual variability that contributes to response to drugs (Schwaederle et al., 2016).

Traditionally, BSA of the treated patient is the parameter used to decide the dosing of anti-cancer agents, especially in the first cylce of treatment, assuming that higher BSA contributes to higher elimination rate. Under this hypothesis, higher doses should be administered to patients with higher BSA. Nevertheless, for most cytotoxic drugs, BSA does not correlate well with plasma drug exposure in adults (White-Koning et al., 2018). The risks presented by this approach are greater in specific patient populations (e.g. hepatic impairment), where suboptimal dosing may cause toxicity and limited efficacy of the treatment. MIPD platforms can assist with these issues and guide dose optimization for patients in a stratified manner, by using simulations and incorporating systems data from specific cancer cohorts into PBPK models (Darwich et al., 2017).

Several PBPK platforms have been developed for cancer populations. A cancer PBPK model is built by incorporation of demographic data and system parameters that are known to differ in cancer patients (e.g. albumin, AAG, expression of enzymes and transporters), followed by investigating the parameters that may affect PK of drugs in cancer patients (Cheeti et al., 2013). PBPK models can be used for different applications; this can be illustrated by the previous use of such a model to optimize dosing of docetaxel in a paediatric cancer population (Thai et al., 2015). The impact of changes in CYP enzymes was assessed in another PBPK model, which demonstrated better performance when reducing CYPs in an oncology population for various

compounds (Schwenger et al., 2018). Application of PK modelling in precision dosing of anticancer compounds has been sufficiently reviewed (Darwich et al., 2017).

The success of models significantly depends on the availability of systems data specific for the target population. Abundance data of ADME proteins are a very important parameter because of the impact changes in expression of these proteins can have on PK of drugs. A recent review covered the impact of disease on expression of DMEs and transporters in various cancer types (Sharma et al., 2020). However, such data are not available for every cancer type and are sometimes limited to mRNA or semi-quantitative protein data (immunohistochemistry). A systematic literature search highlighted existing gaps in modelling PK in liver cancer. In CRLM for example, there is a lack of population-specific scaling factors for IVIVE. For predicting hepatic drug clearance, different *in vitro* systems can be used, including recombinantly expressed enzymes, hepatocytes, liver microsomes and cytosol. The scalars related to liver microsomes and cytosol are MPPGL and cytosolic protein per gram of liver (CPPGL) (Barter et al., 2007), data related both of which are lacking in CRLM. Proteomic data on ADME proteins are also not available, and this impedes accurate PK predictions. Advances in LC-MS proteomics have contributed a huge amount of quantitative data in various tissues with wide applications in systems pharmacology, which could address the lack of abundance data in cancer (Prasad et al., 2017, 2019; El-Khateeb et al., 2019). This approach, along with recently developed liquid biopsy technology (Rowland et al., 2019; Achour et al., 2020), are very promising in the quest towards creating realistic 'virtual twins' to achieve precision dosing in the clinic. 'Virtual twins' are *in silico* models that represent individual patients, generated by the incorporation of system parameters specific for each patient in order to simulate personalized drug response (Patel et al., 2018).

Novel *in vitro* systems that can further advance IVIVE and application of precision dosing are organ-on-chip tools. Although the use of these systems is beyond the scope of this review, it is worth mentioning that integration of cancer cultures with microfluidic devices can mimic the tumour microenvironment, enabling studies of disease progression and drug response, which can offer better understanding of cancer behaviour *in vivo* (Sun et al., 2019). Past applications include studying the microenvironment of lung cancer and testing chemotherapeutic drugs (Xu et al., 2013), modelling of cancer metastasis (Caballero et al., 2017), and assessing exposure of CRC cells to dynamic anti-cancer drug concentrations (Komen et al., 2020).

PBPK modelling can also be applied to biologics, which are protein or peptide drugs with complex pharmacokinetics. Biologics, particularly monoclonal antibodies, are a new treatment option for cancer, and this area is witnessing an increase in the use of PBPK models to study their disposition. Information on the interaction between the Fc-based antibody drugs and the neonatal Fc receptor (FcRn) is required for such models; FcRn plays an important role in the distribution of antibodies and prolonging their half-lives in the body (Wong and Chow, 2017). Despite advances in PBPK modelling applied in biologics, there are still many unknowns to be addressed (Kamath, 2016). Recently, a generic PBPK model was developed to simulate the distribution and clearance of biologics by incorporating systems data, including those related to FcRn; the model provided useful predictions of tissue concentration profiles (Niederalt et al., 2018). An application in cancer is a minimal PBPK model developed to predict the impact of the perturbation of the FcRn-mediated recycling pathway on drug–disease interactions. The model quantified the interaction among M-protein, the characteristic paraprotein of multiple myeloma (competitor for FcRn-mediated Immunoglobulin G recycling), and the anti-CD38 antibody daratumumab indicated for multiple myeloma treatment (Abdallah and Zhu, 2020).

1.6 Conclusion

Cancer is a leading cause of death, with a large burden on healthcare systems. Clinical trials in oncology face difficulty in recruitment of patients, due to serious ethical and toxicity issues. This leads to large heterogeneity in enrolled cohorts with variable PK. A promising avenue for addressing such heterogeneity is the use of PBPK models, which can provide predictions of PK in cancer patients. Such models need population-specific systems parameters, some of which are available for several types of cancer, allowing impact of such parameters on PK of drugs to be assessed. Such assessment suggests that differences in systems parameters in cancer patients, compared with healthy subjects, result in altered PK (including changes in CL and drug exposure). However, there are still gaps in parametrization of cancer PBPK models, which require further studies, particularly the lack of data on abundance of ADME proteins in liver from CRLM patients. Of particular interest are CYP and UGT enzymes, which are very important for the metabolism of TKIs and other anti-cancer drugs, with changes in their expression leading to perturbed PK. LC-MS proteomics provides reliable quantitative measurements, which are used to update ADME protein data in PBPK models, including those for cancer populations. Scaling factors specific for cancer populations are also lacking due to limited availability of high quality tissue samples. Incorporation of appropriate systems

parameters in PBPK models can facilitate precision dosing in oncology, with the main aims of preventing toxicity and achieving optimal efficacy.

1.7 Expert Opinion

Cancer patients are a heterogeneous population with many physiological differences. Key parameters that lead to variation in cancer include perturbations in plasma proteins and haematocrit, effects of comorbidities and changes in abundance and activity of DMEs and transporters. These covariates, along with patient demographics, have a clear impact on the PK of drugs in cancer patients. Changes in these parameters lead to altered drug clearance, exposure, plasma concentrations, absorption, distribution and elimination in cancer patients. Cancer is not one disease, with each type of cancer displaying a range of phenotypes, with differences in the highlighted parameters.

Oncology clinical trials do not routinely recruit patients from the target population, and data on sub-populations are not generally available before a drug is marketed. Therefore, there is no specific guidance on dosage adjustments for such patients. Including more sub-populations in clinical trials with less strict criteria could provide more information on a wider range of true patient populations and assist with precision dosing in special populations that are generally excluded from clinical trials (Tyson et al., 2020). An alternative approach to addressing challenges in recruiting special populations in oncology is the utilization of PBPK modelling. PBPK has gained wider acceptance by regulatory agencies in oncology, relative to other areas of drug development, due to the highlighted difficulties in oncology clinical trials. It is important to mention that PBPK tools are not widely used by clinicians and more action should be taken to bring this approach to healthcare, for example through collaboration between clinicians, modellers, pharmaceutical companies, and regulatory bodies, as well as appropriate training.

Although PBPK models can potentially improve the drug dosage adjustment in cancer populations by reducing toxicity issues and increasing effective treatment, there are still limitations in its applicability. For instance, there are still critical gaps in systems data in cancer, which are vital for developing robust models and providing accurate PK predictions in cancer populations. There is a need to investigate the expression levels of drug metabolising enzymes and transporters, and assess the disease impact in order to establish systems parameters. This is particularly important for cancer types affecting the main elimination organs (liver, intestine,

and kidney). It is critical to assess systems parameters specific for each cancer type and stage of cancer, as heterogeneity among cancer types and stages affect system parameters differently. Generating the required system data will require access to high quality samples and application of state-of-the-art methodology, such as LC-MS proteomics for measuring changes in the expression of DMEs and transporters. LC-MS proteomics could also provide quantitative measurements of important pharmacology proteins markers targeted by anti-cancer drugs (for example, receptor tyrosine kinases) that are not studied extensively. Incorporation of such data into models could provide better predictions of not only PK but also pharmacodynamics (PD) (e.g. level of receptor binding), and exposure-response relationships. Recent advances, particularly liquid biopsy technology as a minimally invasive alternative to tissue biopsies together with 'virtual twin' models, should take PBPK modelling a step closer towards individualization of precision dosing in cancer patients.

1.8 References

Abdallah HM, and Zhu AZX (2020) A Minimal Physiologically-Based Pharmacokinetic Model Demonstrates Role of the Neonatal Fc Receptor (FcRn) Competition in Drug–Disease Interactions With Antibody Therapy. *Clin Pharmacol Ther* **107**:423–434.

Achour B, Al-Majdoub ZM, Grybos-Gajniak A, Lea K, Kilford P, Zhang M, Knight D, Barber J, Schageman J, and Rostami-Hodjegan A (2020) Liquid Biopsy Enables Quantification of the Abundance and Interindividual Variability of Hepatic Enzymes and Transporters. *Clin Pharmacol Ther* **109**:222-232.

Akhdar H, Legendre C, Aninat C, and More F (2012) Anticancer Drug Metabolism: Chemotherapy Resistance and New Therapeutic Approaches, in *Topics on Drug Metabolism* p 6, InTech.

Ballestero MR, Monte MJ, Briz O, Jimenez F, Martin FG-S, and Marin JJG (2006) Expression of transporters potentially involved in the targeting of cytostatic bile acid derivatives to colon cancer and polyps. *Biochem Pharmacol* **72**:729–738.

Barter Z, Bayliss M, Beaune P, Boobis A, Carlile D, Edwards R, Brian Houston J, Lake B, Lipscomb J, Pelkonen O, Tucke G, and Rostami-Hodjegan A (2007) Scaling Factors for the Extrapolation of In Vivo Metabolic Drug Clearance From In Vitro Data: Reaching a Consensus on Values of Human Micro-somal Protein and Hepatocellularity Per Gram of Liver. *Curr Drug Metab* **8**:33–45.

Barter ZE, Chowdry JE, Harlow JR, Snawder JE, Lipscomb JC, and Rostami-Hodjegan A (2008) Covariation of human microsomal protein per gram of liver with age: Absence of influence of operator and sample storage may justify interlaboratory data pooling. *Drug Metab Dispos* **36**:2405–2409.

Bates SE, Berry DA, Balasubramaniam S, Bailey S, LoRusso PM, and Rubin EH (2015) Advancing Clinical Trials to Streamline Drug Development. *Clin Cancer Res* **21**:4527–4535.

Bhullar KS, Lagarón NO, McGowan EM, Parmar I, Jha A, Hubbard BP, and Rupasinghe HPV (2018) Kinase-targeted cancer therapies: progress, challenges and future directions. *Mol Cancer* **17**:48.

Billington S, Ray AS, Salphati L, Xiao G, Chu X, Humphreys WG, Liao M, Lee CA, Mathias

A, Hop CECA, Rowbottom C, Evers R, Lai Y, Kelly EJ, Prasad B, and Unadkat JD (2018) Transporter Expression in Noncancerous and Cancerous Liver Tissue from Donors with Hepatocellular Carcinoma and Chronic Hepatitis C Infection Quantified by LC-MS/MS Proteomics. *Drug Metab Dispos* **46**:189–196.

Billington S, Salphati L, Hop CECA, Chu X, Evers R, Burdette D, Rowbottom C, Lai Y, Xiao G, Humphreys WG, Nguyen TB, Prasad B, and Unadkat JD (2019) Interindividual and Regional Variability in Drug Transporter Abundance at the Human Blood–Brain Barrier Measured by Quantitative Targeted Proteomics. *Clin Pharmacol Ther* **106**:228–237.

Blair EYL, Rivory LP, Clarke SJ, and Mclachlan AJ (2006) Population pharmacokinetics of raltitrexed in patients with advanced solid tumours. *Br J Clin Pharmacol* **57**:416-426.

Bonate PL, Floret S, and Bentzen C (2004) Population pharmacokinetics of APOMINE???: A meta-analysis in cancer patients and healthy males. *Br J Clin Pharmacol* **58**:142–155.

Bonin S, Pascolo L, Crocé LS, Stanta G, and Tiribelli C (2002) Gene expression of ABC proteins in hepatocellular carcinoma, perineoplastic tissue, and liver diseases. *Mol Med* **8**:318–325.

Bray F, Ferlay J, Soerjomataram I, Siegel RL, Torre LA, and Jemal A (2018) Global cancer statistics 2018: GLOBOCAN estimates of incidence and mortality worldwide for 36 cancers in 185 countries. *CA Cancer J Clin* **68**:394–424.

Brown J, Plummer R, Bauer TM, Anthony S, Sarantopoulos J, De Vos F, White M, Schupp M, Ou Y, and Vaishampayan U (2017) Pharmacokinetics of carfilzomib in patients with advanced malignancies and varying degrees of hepatic impairment: an open-label, single-arm, phase 1 study. *Exp Hematol Oncol* **6**:27.

Caballero D, Kaushik S, Correlo VM, Oliveira JM, Reis RL, and Kundu SC (2017) Organ-on-chip models of cancer metastasis for future personalized medicine: From chip to the patient. *Biomaterials* **149**:98–115.

Carr BI, and Guerra V (2017) Serum Albumin Levels in Relation to Tumor Parameters in Hepatocellular Carcinoma Patients. *Int J Biol Markers* **32**:391–396.

Cheeti S, Budha NR, Rajan S, Dresser MJ, and Jin JY (2013) A physiologically based pharmacokinetic (PBPK) approach to evaluate pharmacokinetics in patients with cancer. *Biopharm Drug Dispos* **34**:141–154.

Chen S, Cao Q, Wen W, and Wang H (2019) Targeted therapy for hepatocellular carcinoma: Challenges and opportunities. *Cancer Lett* **460**:1–9.

Chen X, Liu H-PL, Li M, and Qiao L (2014) Advances in non-surgical management of primary liver cancer. *World J Gastroenterol* **20**:16630.

Chityala PK, Wu L, Chow DS-L, and Ghose R (2020) Effects of inflammation on irinotecan pharmacokinetics and development of a best-fit PK model. *Chem Biol Interact* **316**:108933.

Crombag M-R, Joerger M, Thürlimann B, Schellens J, Beijnen J, and Huitema A (2016) Pharmacokinetics of Selected Anticancer Drugs in Elderly Cancer Patients: Focus on Breast Cancer. *Cancers (Basel)* **8**:6.

Darwich AS, Ogungbenro K, Hatley OJ, and Rostami-Hodjegan A (2017) Role of pharmacokinetic modeling and simulation in precision dosing of anticancer drugs. *Transl Cancer Res* **6**:S1512–S1529.

Davila M, and Bresalier RS (2008) Gastrointestinal complications of oncologic therapy. *Nat Clin Pract Gastroenterol Hepatol* **5**:682–696.

Davis RL, Lehmann D, Stidley CA, and Neidhart J (1991) Amikacin pharmacokinetics in patients receiving high-dose cancer chemotherapy. *Antimicrob Agents Chemother* **35**:944–947.

De Iudicibus S, De Pellegrin A, Stocco G, Bartoli F, Bussani R, and Decorti G (2008) ABCB1 gene polymorphisms and expression of P-glycoprotein and long-term prognosis in colorectal cancer. *Anticancer Res* **28**:3921–8.

Dhillon S (2020a) Avapritinib: First Approval. *Drugs* **80**:433–439.

Dhillon S (2020b) Ripretinib: First Approval. *Drugs* **80**:1133–1138.

DiMasi JA, and Grabowski HG (2007) Economics of New Oncology Drug Development. *J Clin Oncol* **25**:209–216.

Downie D, McFadyen MCE, Rooney PH, Cruickshank ME, Parkin DE, Miller ID, Telfer C, Melvin WT, and Murray GI (2005) Profiling Cytochrome P 450 Expression in Ovarian Cancer: Identification of Prognostic Markers. *Clin Cancer Res* **11**:7369–7375.

Duan P, Wu F, Moore JN, Fisher J, Crentsil V, Gonzalez D, Zhang L, Burckart GJ, and Wang

J (2019) Assessing <scp>CYP</scp> 2C19 Ontogeny in Neonates and Infants Using Physiologically Based Pharmacokinetic Models: Impact of Enzyme Maturation Versus Inhibition. *CPT Pharmacometrics Syst Pharmacol* **8**:158–166.

El-Khateeb E, Vasilogianni A-M, Alrubia S, Al-Majdoub ZM, Couto N, Howard M, Barber J, Rostami-Hodjegan A, and Achour B (2019) Quantitative mass spectrometry-based proteomics in the era of model-informed drug development: Applications in translational pharmacology and recommendations for best practice. *Pharmacol Ther* **203**:107397.

El-Khoueiry AB, Sarantopoulos J, O'Bryant CL, Ciombor KK, Xu H, O'Gorman M, Chakrabarti J, Usari T, and El-Rayes BF (2018) Evaluation of hepatic impairment on pharmacokinetics and safety of crizotinib in patients with advanced cancer. *Cancer Chemother Pharmacol* **81**:659–670.

El-Rayes BF, Ali S, Heilbrun LK, Lababidi S, Bouwman D, Visscher D, and Philip PA (2003) Cytochrome p450 and glutathione transferase expression in human breast cancer. *Clin Cancer Res* **9**:1705–9.

Faucette S, Wagh S, Trivedi A, Venkatakrishnan K, and Gupta N (2017) Reverse Translation of US Food and Drug Administration Reviews of Oncology New Molecular Entities Approved in 2011-2017: Lessons Learned for Anticancer Drug Development. *Clin Transl Sci* 1–24.

Fijii T, Tokuda S, Nakazawa Y, Kurozumi S, Obayashi S, Yajima R, and Shirabe K (2020) Implications of Low Serum Albumin as a Prognostic Factor of Long-term Outcomes in Patients With Breast Cancer. *In Vivo* **34**:2033–2036.

Gao J, Zhou J, He XP, Zhang YF, Gao N, Tian X, Fang Y, Wen Q, Jia LJ, Jin H, and Qiao HL (2016) Changes in cytochrome P450s-mediated drug clearance in patients with hepatocellular carcinoma in vitro and in vivo: A bottom-up approach. *Oncotarget* **7**:28612–28623.

García-Aranda M, and Redondo M (2019) Targeting Receptor Kinases in Colorectal Cancer. *Cancers (Basel)* **11**:433.

Gibson P, Gill JH, Khan PA, Seargent JM, Martin SW, Batman PA, Griffith J, Bradley C, Double JA, Bibby MC, and Loadman PM (2003) Cytochrome P450 1B1 (CYP1B1) is overexpressed in human colon adenocarcinomas relative to normal colon: implications for

drug development. *Mol Cancer Ther* **2**:527–34.

Giri N, Masters JC, Plotka A, Liang Y, Boutros T, Pardo P, O'Connell J, and Bello C (2015) Investigation of the impact of hepatic impairment on the pharmacokinetics of dacomitinib. *Invest New Drugs* **33**:931–941.

Giuliani L, Ciotti M, Stoppacciaro A, Pasquini A, Silvestri I, De Matteis A, Frati L, and Aglianò A-M (2005) UDP-glucuronosyltransferases 1A expression in human urinary bladder and colon cancer by immunohistochemistry. *Oncol Rep* **13**:185–91.

Glaenzel U, Jin Y, Hansen R, Schroer K, Rahmanzadeh G, Pfaar U, Jaap van Lier J, Borell H, Meissner A, Camenisch G, and Zhao S (2020) Absorption, Distribution, Metabolism, and Excretion of Capmatinib (INC280) in Healthy Male Volunteers and In Vitro Aldehyde Oxidase Phenotyping of the Major Metabolite. *Drug Metab Dispos* **48**:873–885.

Grande E, Harvey RD, You B, Batlle JF, Galbraith H, Sarantopoulos J, Ramalingam SS, Mann H, So K, Johnson M, and Vishwanathan K (2019) Pharmacokinetic Study of Osimertinib in Cancer Patients with Mild or Moderate Hepatic Impairment. *J Pharmacol Exp Ther* **369**:291–299.

Guan X (2015) Cancer metastases: challenges and opportunities. *Acta Pharm Sin B* **5**:402–418.

Gupta N, Martin PM, Miyauchi S, Ananth S, Herdman A V., Martindale RG, Podolsky R, and Ganapathy V (2006) Down-regulation of BCRP/ABCG2 in colorectal and cervical cancer. *Biochem Biophys Res Commun* **343**:571–577.

Gutierrez ME, Kummar S, and Giaccone G (2009) Next generation oncology drug development: opportunities and challenges. *Nat Rev Clin Oncol* **6**:259–265.

Haouala A, Widmer N, Guidi M, Montemurro M, Leyvraz S, Buclin T, Eap CB, Decosterd LA, and Csajka C (2013) Prediction of free imatinib concentrations based on total plasma concentrations in patients with gastrointestinal stromal tumours. *Br J Clin Pharmacol* **75**:1007–1018.

He X, Clarke SJ, and McLachlan AJ (2011) Clinical Pharmacology of Chemotherapy Agents in Older People with Cancer. *Curr Gerontol Geriatr Res* **2011**:1–6.

Heron M (2013) Deaths: leading causes for 2010. *Natl Vital Stat Rep* **62**:1–96.

Hinoshita E, Uchiumi T, Taguchi K, Kinukawa N, Tsuneyoshi M, Maehara Y, Sugimachi K,

and Kuwano M (2000) Increased Expression of an ATP-binding Cassette Superfamily Transporter, Multidrug Resistance Protein 2, in Human Colorectal Carcinomas. *Clin Cancer Res* **6**:2401–2407.

Hojjat-Farsangi M (2014) Small-Molecule Inhibitors of the Receptor Tyrosine Kinases: Promising Tools for Targeted Cancer Therapies. *Int J Mol Sci* **15**:13768–13801.

Holch JW, Demmer M, Lamersdorf C, Michl M, Schulz C, von Einem JC, Modest DP, and Heinemann V (2017) Pattern and Dynamics of Distant Metastases in Metastatic Colorectal Cancer. *Visc Med* **33**:70–75.

Hoy SM (2020) Pemigatinib: First Approval. *Drugs* **80**:923–929.

Hu H, Ding X, Yang Y, Zhang H, Li H, Tong S, An X, Zhong Q, Liu X, Ma L, Liu Q, Liu B, Lu Z, Zhang D, Hu P, and Ren H (2014) Changes in glucose-6-phosphate dehydrogenase expression results in altered behavior of HBV-associated liver cancer cells. *Am J Physiol Liver Physiol* **307**:G611–G622.

Hudachek SF, Eckhardt S, Hicks B, and Gustafson D (2010) Population pharmacokinetic model of PI88, a heparanase inhibitor. *Cancer Chemother Pharmacol* **65**:743–753.

Imbs D-C, Paludetto M-N, Négrier S, Powell H, Lafont T, White-Koning M, Chatelut E, and Thomas F (2016) Determination of unbound fraction of pazopanib in vitro and in cancer patients reveals albumin as the main binding site. *Invest New Drugs* **34**:41–48.

Ishizawa Y, Yasui-Furukori N, Takahata T, Sasaki M, and Tateishi T (2005) The effect of aging on the relationship between the cytochrome P450 2C19 genotype and omeprazole pharmacokinetics. *Clin Pharmacokinet* **44**:1179–1189.

Israili ZH, and Dayton PG (2001) Human alpha-1-glycoprotein and its interactions with drugs. *Drug Metab Rev* **33**:161–235.

Jiang Z, Li C, Zhao Z, Liu Z, Guan X, Yang M, Li X, Yuan D, Qiu S, and Wang X (2018) Abnormal Liver Function Induced by Space-Occupying Lesions Is Associated with Unfavorable Oncologic Outcome in Patients with Colorectal Cancer Liver Metastases. *Biomed Res Int* **2018**:1–7.

Jiao Q, Bi L, Ren Y, Song S, Wang Q, and Wang Y (2018) Advances in studies of tyrosine kinase inhibitors and their acquired resistance. *Mol Cancer* **17**:36.

Kamath A V. (2016) Translational pharmacokinetics and pharmacodynamics of monoclonal antibodies. *Drug Discov Today Technol* **21**–**22**:75–83.

Kapucuoglu N, Coban T, Raunio H, Pelkonen O, Edwards RJ, Boobis AR, and Iscan M (2003) Expression of CYP3A4 in human breast tumour and non-tumour tissues. *Cancer Lett* **202**:17–23.

Karlgren M, Gomez A, Stark K, Svärd J, Rodriguez-Antona C, Oliw E, Bernal ML, Ramón Y Cajal S, Johansson I, and Ingelman-Sundberg M (2006) Tumor-specific expression of the novel cytochrome P450 enzyme, CYP2W1. *Biochem Biophys Res Commun* **341**:451–458.

Kearns GL, Abdel-Rahman SM, Alander SW, Blowey DL, Leeder JS, and Kauffman RE (2003) Developmental Pharmacology — Drug Disposition, Action, and Therapy in Infants and Children. *N Engl J Med* **349**:1157–1167.

Kenmotsu H, Imamura CK, Ono A, Omori S, Nakashima K, Wakuda K, Taira T, Naito T, Murakami H, Takahashi T, and Tanigawara Y (2017) The effects of advanced age and serum α 1 -acid glycoprotein on docetaxel unbound exposure and dose-limiting toxicity in cancer patients. *Br J Clin Pharmacol* **83**:2416–2425.

Kenter M, and Cohen A (2006) Establishing risk of human experimentation with drugs: lessons from TGN1412. *Lancet* **368**:1387–1391.

Khosravan R, Toh M, Garrett M, La Fargue J, Ni G, Marbury TC, Swan SK, Lunde NM, and Bello CL (2010) Pharmacokinetics and Safety of Sunitinib Malate in Subjects With Impaired Renal Function. *J Clin Pharmacol* **50**:472–481.

Kim S, Kim JM, Lee HJ, Lim JS, Seong I-O, and Kim K-H (2020) Alteration of CYP4A11 expression in renal cell carcinoma: diagnostic and prognostic implications. *J Cancer* **11**:1478–1485.

Knight K, Wade S, and Balducci L (2004) Prevalence and outcomes of anemia in cancer: a systematic review of the literature. *Am J Med* **116**:11–26.

Komen J, Westerbeek EY, Kolkman RW, Roesthuis J, Lievens C, van den Berg A, and van der Meer AD (2020) Controlled pharmacokinetic anti-cancer drug concentration profiles lead to growth inhibition of colorectal cancer cells in a microfluidic device. *Lab Chip* **20**:3167–3178.

Kumarakulasingham M (2005) Cytochrome P450 Profile of Colorectal Cancer: Identification

of Markers of Prognosis. *Clin Cancer Res* **11**:3758–3765.

Kurzawski M, Szeląg-Pieniek S, Łapczuk-Romańska J, Wrzesiński M, Sieńko J, Oswald S, and Droździk M (2019) The reference liver – ABC and SLC drug transporters in healthy donor and metastatic livers. *Pharmacol Reports* **71**:738–745.

Lamb YN (2019) Pexidartinib: First Approval. *Drugs* **79**:1805–1812.

Lane CS, Nisar S, Griffiths WJ, Fuller BJ, Davidson BR, Hewes J, Welham KJ, and Patterson LH (2004) Identification of cytochrome P450 enzymes in human colorectal metastases and the surrounding liver: a proteomic approach. *Eur J Cancer* **40**:2127–2134.

Larsen MT, Kuhlmann M, Hvam ML, and Howard KA (2016) Albumin-based drug delivery: harnessing nature to cure disease. *Mol Cell Ther* **4**:3.

Launay-Iliadis MC, Bruno R, Cosson V, Vergniol JC, Oulid-Aissa D, Marty M, Clavel M, Aapro M, Le Bail N, and Iliadis A (1995) Population pharmacokinetics of docetaxel during phase I studies using nonlinear mixed-effect modeling and nonparametric maximum-likelihood estimation. *Cancer Chemother Pharmacol* **37**:47–54.

Launay-Vacher V, Oudard S, Janus N, Gligorov J, Pourrat X, Rixe O, Morere JF, Beuzeboc P, and Deray G (2007) Prevalence of renal insufficiency in cancer patients and implications for anticancer drug management: The renal insufficiency and anticancer medications (IRMA) study. *Cancer* **110**:1376–1384.

Liang X, Staiger KM, Riddle E, Hao J, and Lai Y (2020) Role of transporters in drug disposition and drug-drug interactions, in *Identification and Quantification of Drugs, Metabolites, Drug Metabolizing Enzymes, and Transporters* pp 311-337.

Lichtman SM, Hollis D, Miller AA, Rosner GL, Rhoades CA, Lester EP, Millard F, Byrd J, Cullinan SA, Rosen DM, Parise RA, Ratain MJ, and Egorin MJ (2006) Prospective Evaluation of the Relationship of Patient Age and Paclitaxel Clinical Pharmacology: Cancer and Leukemia Group B (CALGB 9762). *J Clin Oncol* **24**:1846–1851.

Lu JF, Eppler SM, Wolf J, Hamilton M, Rakhit A, Bruno R, and Lum BL (2006) Clinical pharmacokinetics of erlotinib in patients with solid tumors and exposure-safety relationship in patients with non-small cell lung cancer. *Clin Pharmacol Ther* **80**:136–145.

Lu L, Zhou J, Shi J, Peng X, Qi X, Wang Y, Li F, Zhou F-Y, Liu L, and Liu Z-Q (2015) Drug-

Metabolizing Activity, Protein and Gene Expression of UDP-Glucuronosyltransferases Are Significantly Altered in Hepatocellular Carcinoma Patients. *PLoS One* **10**:e0127524.

Maher B, Ryan E, Little M, Boardman P, and Stedman B (2017) The management of colorectal liver metastases. *Clin Radiol* **72**:617–625.

Mancini I, and Bruera E (1998) Constipation in advanced cancer patients. *Support Care Cancer* **6**:356–364.

Markham A (2020a) Pralsetinib: First Approval. *Drugs* **80**:1865–1870.

Markham A (2020b) Selpercatinib: First Approval. *Drugs* **80**:1119–1124.

Marsousi N, Desmeules JA, Rudaz S, and Daali Y (2017) Usefulness of PBPK Modeling in Incorporation of Clinical Conditions in Personalized Medicine. *J Pharm Sci* **106**:2380–2391.

Matlock MK, Tambe A, Elliott-Higgins J, Hines RN, Miller GP, and Swamidass SJ (2019) A Time-Embedding Network Models the Ontogeny of 23 Hepatic Drug Metabolizing Enzymes. *Chem Res Toxicol* **32**:1707–1721.

Meneses-Lorente G, Bentley D, Guerini E, Kowalski K, Chow-Maneval E, Yu L, Brink A, Djebli N, Mercier F, Buchheit V, and Phipps A (2021) Characterization of the pharmacokinetics of entrectinib and its active M5 metabolite in healthy volunteers and patients with solid tumors. *Invest New Drugs*, doi: 10.1007/s10637-020-01047-5.

Michael M, and Doherty MM (2005) Tumoral drug metabolism: Overview and its implications for cancer therapy. *J Clin Oncol* **23**:205–229.

Miles D, Jumbe NL, Lacy S, and Nguyen L (2016) Population Pharmacokinetic Model of Cabozantinib in Patients with Medullary Thyroid Carcinoma and Its Application to an Exposure-Response Analysis. *Clin Pharmacokinet* **55**:93–105.

Miller A, Rosner L, Green R, Ratain J, and Hoffis R (1997) Pharmacology i . v . Cisplatin Cancer : (CALGB of 21-Day in Patients Oral with Etoposide Group Given B Study in Combination Small with A Cancer and Leukemia. **3**:719–725.

Miller AA, Rosner GL, Egorin MJ, Hollis D, Lichtman SM, and Ratain MJ (2004) Prospective Evaluation of Body Surface Area as a Determinant of Paclitaxel Pharmacokinetics and Pharmacodynamics in Women with Solid Tumors. *Clin Cancer Res* **10**:8325–8331.

Mitchell D, Puckett Y, and Nguyen QN (2019) Literature Review of Current Management of Colorectal Liver Metastasis. *Cureus* **11**:e3940.

Murray GI, McFadyen MCE, Mitchell RT, Cheung Y-L, Kerr AC, and Melvin WT (1999) Cytochrome P450 CYP3A in human renal cell cancer. *Br J Cancer* **79**:1836–1842.

Nakao K, Kobuchi S, Marutani S, Iwazaki A, Tamiya A, Isa S, Okishio K, Kanazu M, Tamiya M, Hirashima T, Imai K, Sakaeda T, and Atagi S (2019) Population pharmacokinetics of afatinib and exposure-safety relationships in Japanese patients with EGFR mutation-positive non-small cell lung cancer. *Sci Rep* **9**:18202.

Nazha B (2015) Hypoalbuminemia in colorectal cancer prognosis: Nutritional marker or inflammatory surrogate? *World J Gastrointest Surg* **7**:370.

Niederalt C, Kuepfer L, Solodenko J, Eissing T, Siegmund H-U, Block M, Willmann S, and Lippert J (2018) A generic whole body physiologically based pharmacokinetic model for therapeutic proteins in PK-Sim. *J Pharmacokinet Pharmacodyn* **45**:235–257.

Nixon NA, Khan OF, Imam H, Tang PA, Monzon J, Li H, Sun G, Ezeife D, Parimi S, Dowden S, and Tam VC (2017) Drug development for breast, colorectal, and non-small cell lung cancers from 1979 to 2014. *Cancer* **123**:4672–4679.

Özdemir BC, Csajka C, Dotto G-P, and Wagner AD (2018) Sex Differences in Efficacy and Toxicity of Systemic Treatments: An Undervalued Issue in the Era of Precision Oncology. *J Clin Oncol* **36**:2680–2683.

Pasqualetti G, Gori G, Blandizzi C, and Del Tacca M (2010) Healthy volunteers and early phases of clinical experimentation. Eur J Clin Pharmacol **66**:647–653.

Patel N, Wiśniowska B, Jamei M, and Polak S (2018) Real Patient and its Virtual Twin: Application of Quantitative Systems Toxicology Modelling in the Cardiac Safety Assessment of Citalopram. *AAPS J* **20**:6.

Paul MK, and Mukhopadhyay AK (2004) Tyrosine kinase – Role and significance in Cancer. *Int J Med Sci* **1**:101–115.

Perez-Ruixo JJ, Piotrovskij V, Zhang S, Hayes S, Porre P De, and Zannikos P (2006) Population pharmacokinetics of tipifarnib in healthy subjects and adult cancer patients. *Br J Clin Pharmacol* **62**:81–96.

Peveling-Oberhag J, Zeuzem S, Yong WP, Kunz T, Paquet T, Bouillaud E, Urva S, Anak O, Sellami D, and Kobalava Z (2013) Effects of Hepatic Impairment on the Pharmacokinetics of Everolimus: A Single-Dose, Open-Label, Parallel-Group Study. *Clin Ther* **35**:215–225.

Podoll T, Pearson PG, Evarts J, Ingallinera T, Bibikova E, Sun H, Gohdes M, Cardinal K, Sanghvi M, and Slatter JG (2019) Bioavailability, Biotransformation, and Excretion of the Covalent Bruton Tyrosine Kinase Inhibitor Acalabrutinib in Rats, Dogs, and Humans. *Drug Metab Dispos* **47**:145–154.

Poggesi I, Li LY, Jiao J, Hellemans P, Rasschaert F, de Zwart L, Snoeys J, De Meulder M, Mamidi RNVS, and Ouellet D (2020) Effect of Fluconazole and Itraconazole on the Pharmacokinetics of Erdafitinib in Healthy Adults: A Randomized, Open-Label, Drug–Drug Interaction Study. *Eur J Drug Metab Pharmacokinet* **45**:101–111.

Prasad B, Achour B, Artursson P, Hop CECA, Lai Y, Smith PC, Barber J, Wisniewski JR, Spellman D, Uchida Y, Zientek MA, Unadkat JD, and Rostami-Hodjegan A (2019) Toward a Consensus on Applying Quantitative Liquid Chromatography-Tandem Mass Spectrometry Proteomics in Translational Pharmacology Research: A White Paper. *Clin Pharmacol Ther* **106**:525–543.

Prasad B, Vrana M, Mehrotra A, Johnson K, and Bhatt DK (2017) The Promises of Quantitative Proteomics in Precision Medicine. *J Pharm Sci* **106**:738–744.

Qixing M, Juqing X, Yajing W, Gaochao D, Wenjie X, Run S, Anpeng W, Lin X, Feng J, and Jun W (2017) The expression levels of CYP3A4 and CYP3A5 serve as potential prognostic biomarkers in lung adenocarcinoma. *Tumor Biol* **39**:101042831769834.

Reiss SN, Buie LW, Adel N, Goldman DA, Devlin SM, and Douer D (2016) Hypoalbuminemia is significantly associated with increased clearance time of high dose methotrexate in patients being treated for lymphoma or leukemia. *Ann Hematol* **95**:2009–2015.

Rostami-Hodjegan A (2012) Physiologically Based Pharmacokinetics Joined With In Vitro–In Vivo Extrapolation of ADME: A Marriage Under the Arch of Systems Pharmacology. *Clin Pharmacol Ther* **92**:50–61.

Rowland A, Miners JO, and Mackenzie PI (2013) The UDP-glucuronosyltransferases: Their role in drug metabolism and detoxification. *Int J Biochem Cell Biol* **45**:1121–1132.

Rowland A, Ruanglertboon W, van Dyk M, Wijayakumara D, Wood LS, Meech R, Mackenzie

PI, Rodrigues AD, Marshall J-C, and Sorich MJ (2019) Plasma extracellular nanovesicle (exosome)-derived biomarkers for drug metabolism pathways: a novel approach to characterize variability in drug exposure. *Br J Clin Pharmacol* **85**:216–226.

Sato H, Naito T, Ishida T, and Kawakami J (2016) Relationships between oxycodone pharmacokinetics, central symptoms, and serum interleukin-6 in cachectic cancer patients. *Eur J Clin Pharmacol* **72**:1463–1470.

Schwaederle M, Zhao M, Lee JJ, Lazar V, Leyland-Jones B, Schilsky RL, Mendelsohn J, and Kurzrock R (2016) Association of Biomarker-Based Treatment Strategies With Response Rates and Progression-Free Survival in Refractory Malignant Neoplasms. *JAMA Oncol* **2**:1452.

Schwenger E, Reddy VP, Moorthy G, Sharma P, Tomkinson H, Masson E, and Vishwanathan K (2018) Harnessing Meta-analysis to Refine an Oncology Patient Population for Physiology-Based Pharmacokinetic Modeling of Drugs. *Clin Pharmacol Ther* **103**:271–280.

Senderowicz AM (2010) Information Needed to Conduct First-in-Human Oncology Trials in the United States: A View from a Former FDA Medical Reviewer. *Clin Cancer Res* **16**:1719–1725.

Sharma S, Suresh Ahire D, and Prasad B (2020) Utility of Quantitative Proteomics for Enhancing the Predictive Ability of Physiologically Based Pharmacokinetic Models Across Disease States. *J Clin Pharmacol* **60**:S17–S35.

Shibata Y, and Chiba M (2015) The Role of Extrahepatic Metabolism in the Pharmacokinetics of the Targeted Covalent Inhibitors Afatinib, Ibrutinib, and Neratinib. *Drug Metab Dispos* **43**:375–384.

Shinko D, Diakos CI, Clarke SJ, and Charles KA (2017) Cancer-Related Systemic Inflammation: The Challenges and Therapeutic Opportunities for Personalized Medicine. *Clin Pharmacol Ther* **102**:599–610.

Siegel RL, Miller KD, and Jemal A (2018) Cancer statistics, 2018. *CA Cancer J Clin* **68**:7–30.

Silvestris N, Argentiero A, Cosmai L, Porta C, Gesualdo L, Brunori G, Brunetti O, Rampino T, Secondino S, Rizzo G, and Pedrazzoli P (2019) Management of targeted therapies in cancer patients with chronic kidney disease, or on haemodialysis: An Associazione

Italiana di Oncologia Medica (AIOM)/Societa' Italiana di Nefrologia (SIN) multidisciplinary consensus position paper. *Crit Rev Oncol Hematol* **140**:39–51.

Smorenburg C., ten Tije A., Verweij J, Bontenbal M, Mross K, van Zomeren D., Seynaeve C, and Sparreboom A (2003) Altered clearance of unbound paclitaxel in elderly patients with metastatic breast cancer. *Eur J Cancer* **39**:196–202.

Smyth LA, and Collins I (2009) Measuring and interpreting the selectivity of protein kinase inhibitors. *J Chem Biol* **2**:131–151.

Soldin OP, and Mattison DR (2009) Sex Differences in Pharmacokinetics and Pharmacodynamics. *Clin Pharmacokinet* **48**:143–157.

Størset E, Holford N, Hennig S, Bergmann TK, Bergan S, Bremer S, Åsberg A, Midtvedt K, and Staatz CE (2014) Improved prediction of tacrolimus concentrations early after kidney transplantation using theory-based pharmacokinetic modelling. *Br J Clin Pharmacol* **78**:509–523.

Sun W, Luo Z, Lee J, Kim H-J, Lee K, Tebon P, Feng Y, Dokmeci MR, Sengupta S, and Khademhosseini A (2019) Organ-on-a-Chip for Cancer and Immune Organs Modeling. *Adv Healthc Mater* **8**:1801363.

Sung H, Ferlay J, Siegel RL, Laversanne M, Soerjomataram I, Jemal A, and Bray F (2021) Global cancer statistics 2020: GLOBOCAN estimates of incidence and mortality worldwide for 36 cancers in 185 countries. *CA Cancer J Clin* caac.21660.

Suri A, Chapel S, Lu C, and Venkatakrishnan K (2015) Physiologically based and population PK modeling in optimizing drug development: A predict-learn-confirm analysis. *Clin Pharmacol Ther* **98**:336–344.

Syed YY (2020) Zanubrutinib: First Approval. *Drugs* **80**:91–97.

Takahashi N, Miura M, Niioka T, and Sawada K (2012) Influence of H2-receptor antagonists and proton pump inhibitors on dasatinib pharmacokinetics in Japanese leukemia patients. *Cancer Chemother Pharmacol* **69**:999–1004.

Talpaz M, and Kiladjian J-J (2021) Fedratinib, a newly approved treatment for patients with myeloproliferative neoplasm-associated myelofibrosis. *Leukemia* **35**:1–17.

Teo YL, Ho HK, and Chan A (2015) Metabolism-related pharmacokinetic drug-drug

interactions with tyrosine kinase inhibitors: Current understanding, challenges and recommendations. *Br J Clin Pharmacol* **79**:241–253.

Thai HT, Mazuir F, Cartot-Cotton S, and Veyrat-Follet C (2015) Optimizing pharmacokinetic bridging studies in paediatric oncology using physiologically-based pharmacokinetic modelling: Application to docetaxel. *Br J Clin Pharmacol* **80**:534–547.

Topletz-Erickson AR, Lee A, Sun H, Mayor J, Walker L, and Endres CJ (2020) Abstract 3016: Tucatinib inhibits CYP3A, CYP2C8 and P-gp-mediated elimination and is impacted by CYP2C8 inhibition in healthy volunteers, in *Experimental and Molecular Therapeutics* pp 3016–3016.

Travica S, Pors K, Loadman PM, Shnyder SD, Johansson I, Alandas MN, Sheldrake HM, Mkrtchian S, Patterson LH, and Ingelman-Sundberg M (2013) Colon Cancer-Specific Cytochrome P450 2W1 Converts Duocarmycin Analogues into Potent Tumor Cytotoxins. *Clin Cancer Res* **19**:2952–2961.

Trobec K, Kerec Kos M, von Haehling S, Springer J, Anker SD, and Lainscak M (2013) Pharmacokinetics of Drugs in Cachectic Patients: A Systematic Review. *PLoS One* **8**:e79603.

Tyson RJ, Park CC, Powell JR, Patterson JH, Weiner D, Watkins PB, and Gonzalez D (2020) Precision Dosing Priority Criteria: Drug, Disease, and Patient Population Variables. *Front Pharmacol* **11**:420.

Ulldemolins M, Roberts JA, Rello J, Paterson DL, and Lipman J (2011) The effects of hypoalbuminaemia on optimizing antibacterial dosing in critically ill patients. *Clin Pharmacokinet* **50**:99–110.

van Erp NP, van Herpen CM, de Wit D, Willemsen A, Burger DM, Huitema ADR, Kapiteijn E, and ter Heine R (2016) A Semi-Physiological Population Model to Quantify the Effect of Hematocrit on Everolimus Pharmacokinetics and Pharmacodynamics in Cancer Patients. *Clin Pharmacokinet* **55**:1447–1456.

van Huizen NA, Coebergh van den Braak RRJ, Doukas M, Dekker LJM, IJzermans JNM, and Luider TM (2019) Up-regulation of collagen proteins in colorectal liver metastasis compared with normal liver tissue. *J Biol Chem* **294**:281–289.

van Leeuwen RWF, Peric R, Hussaarts KGAM, Kienhuis E, IJzerman NS, de Bruijn P, van der

Leest C, Codrington H, Kloover JS, van der Holt B, Aerts JG, van Gelder T, and Mathijssen RHJ (2016) Influence of the Acidic Beverage Cola on the Absorption of Erlotinib in Patients With Non–Small-Cell Lung Cancer. *J Clin Oncol* **34**:1309–1314.

Vanstraelen K, Wauters J, Vercammen I, de Loor H, Maertens J, Lagrou K, Annaert P, and Spriet I (2014) Impact of Hypoalbuminemia on Voriconazole Pharmacokinetics in Critically Ill Adult Patients. *Antimicrob Agents Chemother* **58**:6782–6789.

Vavricka SR, Jung D, Fried M, Grützner U, Meier PJ, and Kullak-Ublick GA (2004) The human organic anion transporting polypeptide 8 (SLCO1B3) gene is transcriptionally repressed by hepatocyte nuclear factor 3beta in hepatocellular carcinoma. *J Hepatol* **40**:212–8.

Venkatakrishnan K, Pickard MD, and von Moltke LL (2010) A Quantitative Framework and Strategies for Management and Evaluation of Metabolic Drug-Drug Interactions in Oncology Drug Development. *Clin Pharmacokinet* **49**:703–727.

Wang Z, and Cole PA (2014) Catalytic Mechanisms and Regulation of Protein Kinases. *Methods Enzymol* **548**:1-21.

Waring MJ, Arrowsmith J, Leach AR, Leeson PD, Mandrell S, Owen RM, Pairaudeau G, Pennie WD, Pickett SD, Wang J, Wallace O, and Weir A (2015) An analysis of the attrition of drug candidates from four major pharmaceutical companies. *Nat Rev Drug Discov* **14**:475–486.

White-Koning M, Osborne C, Paci A, Boddy A V., Chatelut E, and Veal GJ (2018) Investigating the potential impact of dose banding for systemic anti-cancer therapy in the paediatric setting based on pharmacokinetic evidence. *Eur J Cancer* **91**:56–67.

Widmer N, Decosterd LA, Csajka C, Leyvraz S, Duchosal MA, Rosselet A, Rochat B, Eap CB, Henry H, Biollaz J, and Buclin T (2006) Population pharmacokinetics of imatinib and the role of α1-acid glycoprotein. *Br J Clin Pharmacol* **62**:97–112.

Williams G, and Pazdur R (2006) Regulatory considerations in clinical trials of novel anticancer drugs, in *Novel Anticancer Agents* pp 263–284.

Wong H, and Chow TW (2017) Physiologically Based Pharmacokinetic Modeling of Therapeutic Proteins. *J Pharm Sci* **106**:2270–2275.

Xie C, Yan T, Chen J, Li X, Zou J, Zhu L, Lu L, Wang Y, Zhou F, Liu Z, and Hu M (2017)

LC-MS/MS quantification of sulfotransferases is better than conventional immunogenic methods in determining human liver SULT activities: implication in precision medicine. *Sci Rep* **7**:3858.

Xu Z, Gao Y, Hao Y, Li E, Wang Y, Zhang J, Wang W, Gao Z, and Wang Q (2013) Application of a microfluidic chip-based 3D co-culture to test drug sensitivity for individualized treatment of lung cancer. *Biomaterials* **34**:4109–4117.

Yan T, Gao S, Peng X, Shi J, Xie C, Li Q, Lu L, Wang Y, Zhou F, Liu Z, and Hu M (2015) Significantly Decreased and More Variable Expression of Major CYPs and UGTs in Liver Microsomes Prepared from HBV-Positive Human Hepatocellular Carcinoma and Matched Pericarcinomatous Tissues Determined Using an Isotope Label-free UPLC-MS/MS Method. *Pharm Res* **32**:1141–1157.

Yan T, Lu L, Xie C, Chen J, Peng X, Zhu L, Wang Y, Li Q, Shi J, Zhou F, Hu M, and Liu Z (2015) Severely Impaired and Dysregulated Cytochrome P450 Expression and Activities in Hepatocellular Carcinoma: Implications for Personalized Treatment in Patients. *Mol Cancer Ther* **14**:2874–2886.

Yoshida K, Budha N, and Jin JY (2017) Impact of physiologically based pharmacokinetic models on regulatory reviews and product labels: Frequent utilization in the field of oncology. *Clin Pharmacol Ther* **101**:597–602.

Zanger UM, and Schwab M (2013) Cytochrome P450 enzymes in drug metabolism: Regulation of gene expression, enzyme activities, and impact of genetic variation. *Pharmacol Ther* **138**:103–141.

Zhang DY, Ye F, Gao L, Liu X, Zhao X, Che Y, Wang H, Wang L, Wu J, Song D, Liu W, Xu H, Jiang B, Zhang W, Wang J, and Lee P (2009) Proteomics, pathway array and signaling network-based medicine in cancer. *Cell Div* **4**:20.

Zhang H, Gao N, Tian X, Liu T, Fang Y, Zhou J, Wen Q, Xu B, Qi B, Gao J, Li H, Jia L, and Qiao H (2015) Content and activity of human liver microsomal protein and prediction of individual hepatic clearance in vivo. *Sci Rep* **5**:1–12.

Zhang Z, and Tang W (2018) Drug metabolism in drug discovery and development. *Acta Pharm Sin B* **8**:721-732.

Zhao D, Chen J, Long X, and Wang J (2020) Dose adjustment for tyrosine kinase inhibitors in

non-small cell lung cancer patients with hepatic or renal function impairment (Review). *Oncol Rep* **45**:413–426.

Chapter Two: Quantitative Mass Spectrometry-Based Proteomics in the Era of Model-Informed Drug Development: Applications in Translational Pharmacology and Recommendations for Best Practice

Declaration

This chapter constitutes a published article.

El-Khateeb, E., **Vasilogianni, A. M**., Alrubia, S., Al-Majdoub, Z. M., Couto, N., Howard, M., Barber, J., Rostami-Hodjegan, A., & Achour, B. **(2019**). Quantitative mass spectrometry-based proteomics in the era of model-informed drug development: applications in translational pharmacology and recommendations for best practice. *Pharmacol Ther* **203**:107397.

The literature search and the manuscript writing were equally divided among the first three authors who share the first-authorship. Dr Zubida M. Al-Majdoub, Dr Narciso Couto, Dr Martyn Howard, Dr Jill Barber, Prof Amin Rostami-Hodjegan suggested edits to the manuscript. Dr Brahim Achour outlined the structure of the review, edited the manuscript, and retained editorial control through the journal's invitation.

2.1 Abstract

Quantitative translation of the fate and action of a drug in the body is facilitated by models that allow extrapolation of *in vitro* measurements (such as the rate of metabolism, active transport across membranes, inhibition of enzymes and receptor occupancy) to *in vivo* consequences (intensity and duration of drug effects). These models use various physiological parameters, including data that describe the expression levels of pharmacologically relevant enzymes, transporters and receptors in tissues and *in vitro* systems. Immunoquantification approaches have traditionally been used to determine protein expression levels, generally providing relative quantification data with compromised selectivity and reproducibility. More recently, the development of several quantitative proteomic techniques, fuelled by advances in state-of-the-art mass spectrometry, has led to generating a wealth of qualitative and quantitative data. These data are currently used for various quantitative systems pharmacology applications, with the ultimate goal of conducting virtual clinical trials to inform clinical studies, especially when assessments are difficult to conduct on patients. In this review, we explore available quantitative proteomic methods, discuss their main applications in translational pharmacology and offer recommendations for selecting and implementing proteomic techniques.

2.2 Introduction

Translational pharmacology requires extrapolation of *in vitro* observations to predict the outcome of therapy *in vivo* using various scaling factors measured in tissues and relevant *in vitro* systems (Rostami-Hodjegan, 2012). When extrapolating measurements made *in vitro* (e.g. Km, Vmax, Jmax), functional data may be used as scalars when selective probes are available, for example in the case of several cytochrome P450 (CYP) (Walsky and Obach, 2004) and uridine 5′-diphospho-glucuronosyltransferase (UGT) enzymes (Walsky et al., 2012; Achour, Dantonio, et al., 2017). However, owing to a lack of specific substrates for many enzymes and for the majority of transporters and receptors, the use of abundance data remains the preferred approach for *in vitro-in vivo* extrapolation (IVIVE), facilitated by analytical methods that can quantify the levels of individual proteins in heterogeneous biological matrices. Over the past two decades, quantitative proteomics based on liquid chromatography in conjunction with mass spectrometry (LC-MS) has replaced traditional immunoquantitative methods, such as Western blotting and enzyme-linked immunosorbent assays (ELISA) (Aebersold et al., 2013), mainly because traditional techniques require purified protein standards and specific antibodies for each target, which are not always available.

Pharmacologically active enzymes and transporters tend to have high sequence homology and most of these proteins are found at very low amounts within the membranes of tissues and cellular systems (Vildhede et al., 2015). Highly selective and sensitive mass spectrometry techniques are therefore ideal for implementation in pharmacology applications (Al Feteisi, Achour, Rostami-hodjegan, et al., 2015; Heikkinen et al., 2015). LC-MS analysis offers various other advantages including reproducibility, high throughput and the ability to multiplex measurements. This allows simultaneous detection and quantification of dilute amounts of a large number of proteins (hundreds to thousands) in complex biological systems (Ong and Mann, 2005). Quantitative proteomic techniques have therefore been implemented by different laboratories worldwide for various pharmacology applications, leading to improved extrapolation of drug pharmacokinetics (Doki et al., 2018; Kumar et al., 2018) and better understanding of the effects of various factors, including age (van Groen et al., 2018; Ladumor et al., 2019), ethnicity (Kawakami et al., 2011; Peng et al., 2015; Ladumor et al., 2019), and genetics (Peng et al., 2015; Weiß et al., 2018; Bhatt et al., 2019) on the expression of enzymes and transporters.

The typical aim of a proteomic experiment is to characterize the entire set of proteins expressed in a particular system (global proteomics) or to target a specified set of proteins for

quantification (targeted proteomics) (Gillet et al., 2016). These two types of proteomic analysis require specific considerations for robust analysis to be achieved (Prasad et al., 2019). In this review, we explore state-of-the-art mass spectrometry-based proteomic methods, both global and targeted, used for the characterization of drug metabolizing and transporting proteins as well as drug targets, and discuss their advantages, limitations, caveats for implementation and their main applications in translational pharmacokinetics (PK) and pharmacodynamics (PD).

2.3 Overview of a typical quantitative proteomic experiment

The quantitative proteomic workflow can be customized for the type of biological sample and the target proteins to be quantified; however, routinely applied bottom-up methods tend to follow generally similar steps (Figure 2-1A). A biological sample (tissues, cell lines or biofluids) is processed by cell lysis or homogenization, often followed by enrichment of specific fractions (e.g. microsomes, cytosol, S9, plasma membrane, mitochondrial fraction) (Figure 2-1B) prior to protein solubilization and digestion (Drozdzik et al., 2014; Harwood et al., 2014; Wiśniewski, Wegler, et al., 2016). The variable array of available samples requires consideration of the effects of the type of sample and subsequent processing on end-point protein abundance (Bhatt and Prasad, 2018).

Whole cell lysates or tissue homogenates can be used for the quantification of various pharmacologically relevant proteins (Wegler et al., 2017). When enriched systems are required, the localization of the target protein is critical to the decision of which fraction to use (Wiśniewski, Wegler, et al., 2016). Cytosolic proteins (e.g. alcohol/aldehyde dehydrogenases, sulfotransferases) are best quantified in cytosol or S9 fractions (Prasad et al., 2018). Membrane-bound reticular proteins (e.g. CYPs and UGTs) are enriched in microsomal membrane fractions (Chen et al., 2016). Enzymes localized in the reticular lumen (e.g. carboxylesterases) can be quantified in microsomes; however, a proportion of these proteins is expected to be lost into the cytosol during sample processing and therefore these proteins are quantified more accurately in S9 fractions (consisting of microsomes and cytosol) provided the target proteins are sufficiently abundant (Prasad et al., 2018; Wang et al., 2019). Transporters and PD-relevant targets, such as receptors, protein phosphatases and kinases, can be found in the plasma membrane (Ohtsuki et al., 2012; Batth et al., 2018), and therefore cell membrane-enriched fractions can be used for these applications. Detailed sub-cellular location information can be found in various databases, including Gene Ontology (www.geneontology.org) and UniProt (www.uniprot.org).

Bottom-up proteomic techniques rely on quantitative analysis of unique (proteotypic) peptides used as surrogates for target proteins (Gillet et al., 2016). Sample proteins are digested using specific proteases, typically trypsin or lysyl endopeptidase (LysC), independently or in combination (Wiśniewski and Mann, 2012; Achour and Barber, 2013). Other proteases, such as chymotrypsin, can be used for specific applications, such as increased depth and reproducibility of analysis (Wiśniewski et al., 2019). Sample digestion can be done in gel, in solution or using filter-aided sample preparation (FASP) (Fallon et al., 2008; Langenfeld et al., 2009; Wiśniewski et al., 2009). Complementary data is expected to be generated when several protein preparation workflows are used (Choksawangkarn et al., 2012; Al Feteisi et al., 2018). After digestion, peptides are desalted, enriched, separated by liquid chromatography (LC) and analyzed using mass spectrometry (MS). Additional separation prior to mass spectrometry can be performed using ion mobility (Distler et al., 2014; Achour, Al Feteisi, et al., 2017). Multiple quantitative MS and data acquisition approaches can be used (Figure 2-1C), depending on the aim of the experiment and the availability of instrumentation (Smith et al., 2019). Targeted and global methodologies are routinely used to identify and quantify expression levels of pharmacologically-relevant proteins. Standards are added at different stages of the proteomic workflow (Figure 2-1A). Data acquisition is followed by data analysis and interpretation, often facilitated by vendor or open-source software. Assessment of the performance of various software packages used for targeted and global proteomics was previously reported (Cox and Mann, 2008; Röst et al., 2014; Välikangas et al., 2017)

Several quality control (QC) steps are required at certain stages of the experiment. Assessment of the quality of sample processing during homogenization and fractionation is required to ensure maximum recovery of protein, normally using colorimetric/fluorometric protein assays. Assessment of the digestion efficiency is done before LC-MS analysis; this is achieved by evaluating time-dependent release of peptides in targeted experiments or by monitoring the rate of missed cleavage in global experiments. Finally, the reliability of the proteomic quantification technique depends on the performance of the LC-MS system, which can be assessed using internal standards and well-characterized QC samples (Bhatt and Prasad, 2018; Prasad et al., 2019).

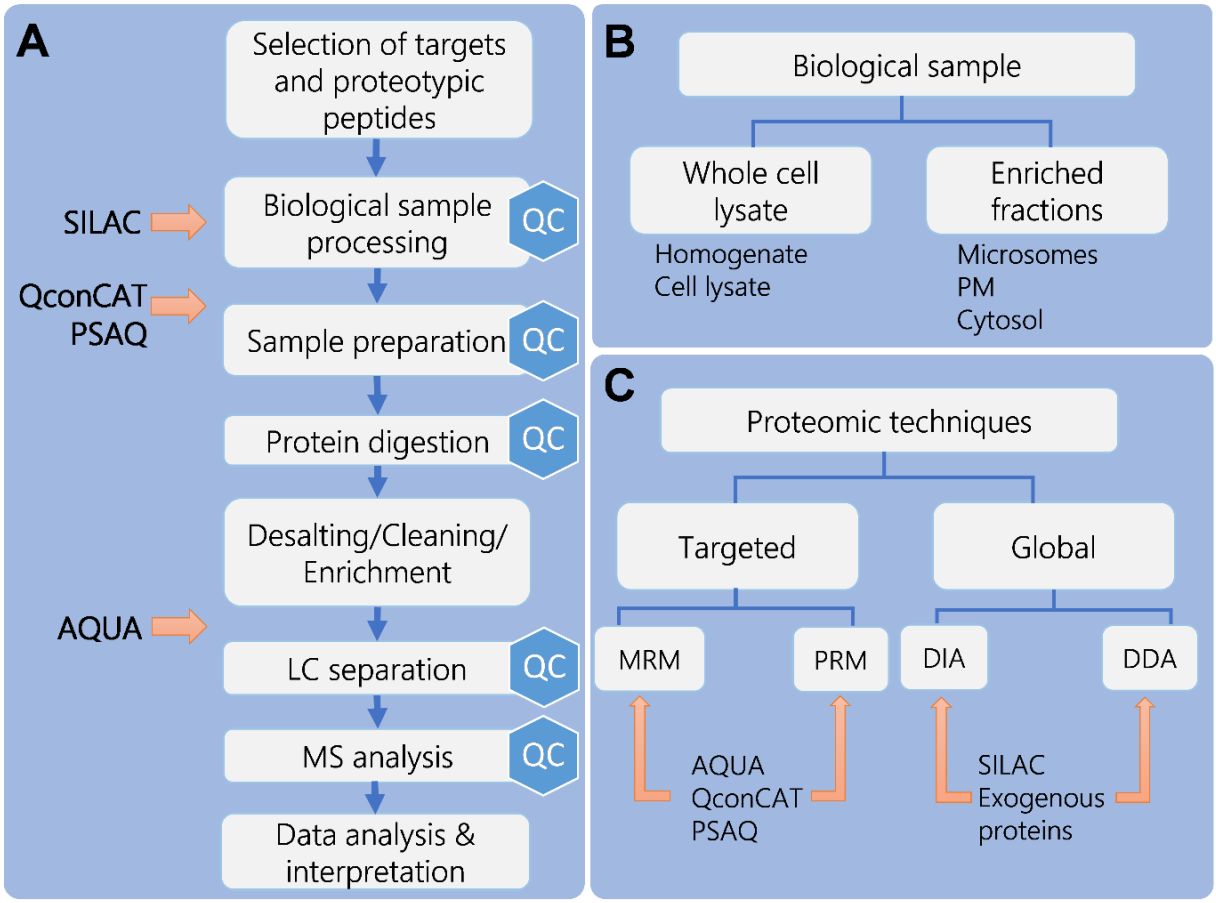

Figure 2-1 Overview of the experimental quantitative proteomic workflow. **A.** Basic proteomic strategy starting from selection of targets and sample preparation, followed by LC-MS analysis, and finally data analysis/interpretation. Protein digestion relies on proteases, such as trypsin and lysyl endopeptidase (LysC), and can be done in solution, in gel or using filter-aided sample preparation (FASP). Standards are added at different stages of sample preparation. SILAC mixtures represent isotopically labeled proteomes; QconCAT and PSAQ protein standards are added to samples prior to protein digestion; AQUA peptide standards are added before LC-MS analysis. Several quality control (QC) steps are required throughout the workflow. **B.** The two main types of samples used to generate proteomic data, whole cell lysates (cell and tissue homogenates) and enriched fractions (e.g. microsomes, plasma membrane, cytosol, mitochondrial fractions or S9 fractions). **C.** The main types of proteomic techniques (targeted and global) and data acquisition methods (MRM/PRM for targeted proteomics and DDA/DIA for global proteomics). Red arrows show the steps where standards are introduced. Abbreviations: AQUA, absolute quantification peptide standards; DDA, data-dependent acquisition; DIA, data-independent acquisition; MRM; multiple reaction monitoring; QC, quality control; QconCAT, quantitative concatemers; PM, plasma membrane; PRM, parallel reaction monitoring; PSAQ, protein standards for absolute quantification; SILAC, stable isotope labeling by amino acids in cell culture.

2.4 Targeted quantitative proteomic methods

Targeted methods are in many ways superior to global methods for the quantification of specific proteins of interest that are known to be expressed in a particular system. The use of targeted proteomics with enriched fractions (e.g. plasma membrane, microsomes) offers highly reproducible measurements of proteins expressed at low levels. The workflow of quantification using these methods starts with identifying the target proteins of interest, followed by selection of proteotypic peptides used as surrogates to quantify the selected targets. These methods require stable isotope labeled (SIL) internal standards for absolute quantification. Generally, MS platforms used for targeted techniques include triple quadrupole (QqQ), quadrupole/time-of-flight (Q-TOF) and hybrid Orbitrap mass spectrometers. Table 2-1 summarizes the advantages and limitations of targeted proteomic methods. The types of targeted acquisition methods are discussed below.

Table 2-1 The overall aims, advantages and limitations of various proteomic data acquisition methods: targeted (MRM, PRM), global data-dependent acquisition (DDA) and data-independent acquisition (DIA) techniques.

Method	Advantages	Disadvantages
Targeted techniques (MRM, PRM) Aim: Robust quantification of a selected set of proteins, known to be expressed in a particular system	• High sensitivity and reproducibility • Simple data analysis • Allows relative and absolute quantification; SIL standards address matrix effects • High resolution instruments are not required for MRM • High selectivity with PRM	• Limited resolution and selectivity with MRM • Limited number of target proteins (10-50 targets per single analysis) • Requirement of prior knowledge of target proteins • Requirement for synthesis of internal standards • Targeted methods cannot be used for discovery of novel targets or pathways
Global data-dependent acquisition (DDA) techniques Aim: discovery proteomics and proteome-wide quantification	• Simple method setup • High proteome coverage • Internal SIL standards are not needed • Allows relative and absolute quantification (with spiked standards or TPA approach) • PTMs can be characterized using global data	• Bias toward highly expressed proteins and compromised reproducibility for low abundance proteins • Sensitive to changes in LC-MS conditions due to longer runs required • Absolute quantification is relatively less reliable than targeted methods

	• Data can provide guidance for targeted quantification	• Requirement of instrument with high-end specifications • Selectivity and sensitivity are compromised
Global data-independent acquisition (DIA) techniques Aim: discovery proteomics and proteome-wide quantification. In the case of sequential window methods (SWATH), the aim can also be set to the quantification of a limited number of target proteins	• Moderate/high precision of peptide quantification. • Wide breadth of peptide identification and quantification leading to high target coverage (typically higher than DDA) • Amenable to discovery and quantitative applications • Provides rich data for targeted methods, including peptide information, fragment information, PTMs and potentially SNPs	• Complex and convoluted data • SWATH requires multiple steps to compile spectral libraries, with many parameters to optimize • Requirement of instrument with high-end specifications • Requirement for specialist software and high computational power for analysis

PTM, post-translational modifications; SNP, single-nucleotide polymorphism; TPA, total protein approach.

2.4.1 Selected/multiple reaction monitoring (SRM/MRM)

Selected or multiple reaction monitoring (SRM/MRM) is the most commonly used targeted proteomic method in biological and pharmacological research (Kitteringham et al., 2009; Gillette and Carr, 2013). In MRM, a peptide and a selected set of its fragment ions (transitions) are monitored by mass filtering on a triple quadrupole instrument (Carr et al., 2014). The technique is routinely used with internal SIL standards, and heavy (standard) and light (analyte) ions are analyzed simultaneously. This technique offers several advantages including multiplexed analysis, high throughput, reproducibility, sensitivity and wide dynamic range (Aebersold et al., 2013; Carr et al., 2014). The sensitivity achieved by this method makes it ideal when samples are small, e.g. biopsies (Vrana et al., 2017). The limitations of targeted techniques include the requirement for extensive method development and the selection of suitable targets. Low abundance analyte proteins are not accurately quantifiable and interference can occur due to the use of pre-defined mass filters and low resolution mass analyzers (Kitteringham et al., 2009; Gillette and Carr, 2013).

Several applications of this technique have been reported including determination of inter-individual variability in drug-metabolizing enzymes and transporters (Gröer et al., 2014; Kumar et al., 2015; Margaillan et al., 2015), prediction of variability in clearance (Vildhede et al., 2016) and drug-drug interactions (DDIs) (Doki et al., 2018), determination of inter-species differences of transporter expression at the blood-brain barrier (Hoshi et al., 2013; Al Feteisi et al., 2018), characterization of various hepatocyte-based in vitro systems (Schaefer et al., 2012; Kumar et al., 2019), region-specific transporter expression in the brain (Billington et al., 2019), kidney (B. Prasad et al., 2016) and intestine (Drozdzik et al., 2014), region-specific enzyme expression in the kidney (Knights et al., 2016), quantification of biomarkers in biological fluids, such as plasma and urine (Abbatiello et al., 2015) and assessment of the effects of disease on different organs (Billington et al., 2018; Prasad et al., 2018; Al-Majdoub et al., 2019).

2.4.2 Parallel reaction monitoring (PRM)

Parallel reaction monitoring (PRM) is a recently introduced targeted method with higher specificity than MRM (Gallien et al., 2013; Schiffmann et al., 2014) because of the use of high-end mass spectrometers, such as Orbitrap (Gallien et al., 2012; Peterson et al., 2012) and quadrupole/time-of-flight (Schilling et al., 2015) platforms, offering high resolution and high mass accuracy. The principle of PRM is based on simultaneous monitoring of all (precursor

ion/fragment ion) transitions of a targeted peptide arising from both standard and sample, in parallel at the MS and tandem MS (MS/MS) levels. By contrast, the MRM approach monitors only pre-defined fragments. The combination of full scan mode, high resolution and high mass accuracy makes PRM a very attractive method, especially for the analysis of complex biological matrices. PRM requires less time for method development and is less prone to interference than MRM owing to the availability of a higher number of quantifiable fragments (Gallien et al., 2014; Ronsein et al., 2015). Because of the large number of monitored transitions, the sensitivity of PRM is sometimes reduced relative to MRM, and the requirement of high resolving power makes the technique less widely applicable (Gallien et al., 2014). Comparable performance by MRM and PRM has recently been demonstrated (Ronsein et al., 2015; Nakamura et al., 2016). Reported applications of PRM-MS include plasma biomarker analysis (Kim et al., 2015), quantification of enzyme variants (Shi et al., 2018), and characterization of liver, kidney and intestine pools (Nakamura et al., 2016).

2.4.3 Accurate mass and retention time (AMRT)

Quantification (relative or absolute) based on accurate mass and retention time (AMRT) is a simple and rapid method (Silva et al., 2005). This method is less widely used than MRM and PRM techniques and relies on measurement of precursor ion intensity of analyte and standard peptides at a predefined mass (*m/z* ratio) and retention time. Confirmation of the peptides identities is carried out after fragmentation at the MS/MS level. This method can be used in conjunction with global proteomic methods to quantify selected targets in proteome-wide analyses. Because AMRT relies on the parent ion intensity in the MS scan, its efficiency is dependent on reproducible peptide separation (by LC) and the use of high resolution mass analyzers (MS). In addition, only a limited number of moderate to high abundance proteins can be quantified. This technique was applied to measuring protein abundance in human serum (Silva et al., 2005) and assessment of disease perturbations in the expression of transporters at the blood-brain barrier (Al-Majdoub et al., 2019).

2.5. Standards for targeted proteomics

Absolute quantification is typically achieved by targeted techniques that use SIL peptides or proteins as standards or calibrants (Calderón-Celis et al., 2018). These standards represent heavy versions of the surrogate peptides selected to quantify the target proteins. Standards are synthesized chemically or biologically and incorporate a heavy isotope (^{13}C, ^{15}N), which allows distinction between analyte (light) and standard (heavy) by mass spectrometry. The types of

standards routinely used in targeted quantitative proteomics include absolute quantification (AQUA) peptides, quantitative concatemers (QconCAT) and protein standards for absolute quantification (PSAQ). A summary of the characteristics of these standards is shown in Table 2-2.

Table 2-2 Characteristics of standards used in targeted proteomic methods (AQUA, QconCAT and PSAQ) and their analytical performance.

	AQUA	**QconCAT**	**PSAQ**
Description	Chemically synthesized isotope labelled peptides	Biologically synthesized sequence of isotope labelled peptides	Intact isotopically labelled recombinant protein
Commercial availability	Available	Available	Available
Digestion evaluation	Necessary	Necessary	Not Necessary but desirable
Number of target proteins	One for each standard	Up to 50 per standard protein	One for each standard
Cost	Low, depending on the number of targets	Moderate	High
Considerations for synthesis	Subject to stability issues during the chemical synthesis	Subject to failure of expression	Subject to failure of expression
Addition in the experimental workflow	Post-digestion	Before solubilization and digestion	Before solubilization and digestion
Compatible proteomic techniques	MRM PRM	MRM PRM AMRT	MRM PRM

Performance of targeted methods	Highly reproducible Multiplexed	Highly reproducible Multiplexed Ideal for stoichiometric analysis	Highly reproducible Accurate
SNP and stoichiometric analysis	Possible; requires QC	Yes	No
Analysis of PTMs	Yes	No	No

AMRT, accurate mass and retention time mass spectrometry; MRM, multiple reaction monitoring; PRM, parallel reaction monitoring; PTM, post-translational modifications; QC, quality control; SNP, single-nucleotide polymorphism.

The selection of standard peptide sequences is a critical step and follows previously reported criteria (Kamiie et al., 2008). These criteria can also be applied to select surrogate peptides in global proteomic methods (Prasad et al., 2019). Generally accepted requirements include:

- **Proteotypic sequence:** unique to the protein of interest with distinct mass (*m/z*) and fragmentation pattern (MS/MS); isobaric and isomeric sequences are avoided.
- **Cleavable by proteases used in quantitative proteomics:** the sequence should not be mapped to transmembrane domains; absence of closely occurring cleavage sites in the target protein sequence (e.g. arginine (R) and lysine (K) in the case of trypsin).
- **Detectable by LC-MS:** optimal hydrophobicity (LC) and ionizability (MS); absence of known single nucleotide polymorphism (SNP) and post-translational modification (PTM); optimal length (7-25 amino acids depending on the MS platform).
- **Stable:** not susceptible to chemical modification during storage and handling including oxidation of methionine (M) and deamidation of asparagine/glutamine (N/Q).

These general selection criteria can be customized for different biological applications. For example, peptides with known PTMs and SNPs are targeted if the biological question requires such stoichiometric analysis. Allele-specific protein quantification was demonstrated recently for the assessment of significant genetic variations in CYP and UGT enzymes (Russell et al., 2013; Shi et al., 2018).

2.5.1 Absolute quantification (AQUA) peptide standards

SIL peptides or AQUA standards are chemically synthesized isotope labeled standard peptides with sequences specific to the target proteins. High quality and high purity peptides are available commercially in isotopically labeled form, making them easily accessible for large scale studies (Kirkpatrick et al., 2005; Kettenbach et al., 2011). A known amount of the AQUA peptide is introduced into the sample at a late stage of sample preparation, usually after protein digestion. AQUA standards can be applied with MRM or PRM techniques, making these targeted techniques very useful when screening a specific protein in a large number of samples as a clinical test or when the quantification of a small set of proteins is desirable (Smith et al., 2019). AQUA can also be applied to the elucidation of PTMs, such as phosphorylation (Kettenbach et al., 2011). However, synthesis and quantification of standards for large scale studies is expensive and time-consuming (Al Feteisi, Achour, Barber, et al., 2015). The need to store peptides can be limiting as they tend to precipitate during long-term storage and lead to inconsistent quantification (Mirzaei et al., 2008). AQUA peptides are normally added to the

sample directly before LC-MS analysis and the accuracy of quantification by the AQUA method can therefore be affected by analyte peptide loss during sample preparation (Havliš and Shevchenko, 2004). We recommend addition of standards to the samples before pre-fractionation and desalting so that equal loss of standard and analyte peptides is incurred from the mixture.

The AQUA-MRM approach is the most widely used quantification method in pharmacokinetic research and has been used to quantify various enzymes and transporters in different human tissues. Quantified enzymes include CYP and UGT enzymes in liver (Ohtsuki et al., 2012; Sato et al., 2012, 2014; Fallon et al., 2013; Cieślak et al., 2016; Prasad et al., 2018; Weiß et al., 2018; Hansen et al., 2019), intestine (Harbourt et al., 2012; Gröer et al., 2014; Sato et al., 2014; Drozdzik et al., 2018) and Kidney (Harbourt et al., 2012; Sato et al., 2014; Knights et al., 2016). In brain, the AQUA-MRM workflow was used to quantify CYPs, glutathione S-transferases (GSTs) and catechol O-methyltransferase (COMT) (Shawahna et al., 2011). Non-CYP and non-UGT drug-metabolizing enzymes quantified by this method include liver flavin-containing monooxygenases (FMOs), sulfotransferases (SULTs), aldehyde oxidase 1 and alcohol and aldehyde dehydrogenases (Fu et al., 2013; Chen et al., 2016; Bhatt et al., 2017; Yoshitake et al., 2017). In additions, drug transporters were successfully quantified using this quantitative strategy in various tissues, including liver (Prasad et al., 2013; Wegler et al., 2017), intestine (Gröer et al., 2013; Drozdzik et al., 2014), kidney (B. Prasad et al., 2016), brain (Shawahna et al., 2011; Uchida et al., 2011; Billington et al., 2019) and lung (Fallon et al., 2018).

2.5.2 Quantitative concatemers (QconCAT)

QconCAT is a concatenated set of peptides expressed recombinantly from an artificial gene. The host organism is usually *E. coli* grown in culture media, supplemented with labeled amino acids, usually $^{13}C_6$-lysine and $^{13}C_6$-arginine. QconCATs are available commercially but can also be expressed in-house at relatively reasonable costs (Russell et al., 2013). The QconCAT protein is added to the sample at a known concentration (estimated using an unlabeled peptide corresponding to a standard peptide within the QconCAT) prior to digestion and can be used with several targeted techniques (MRM, PRM, AMRT). A single QconCAT can be designed to quantify several proteins (up to 50), making it amenable to multiplexing and achieving higher coverage of protein targets. QconCAT ensures a strict 1:1 stoichiometry making it particularly advantageous in determining polymorphisms (Russell et al., 2013; Shi et al., 2018)

and establishing protein-protein inter-correlations (Achour, Russell, *et al.*, 2014). The development of QconCAT constructs is time-consuming and most worthwhile when a significant number of proteins (10-50) are to be quantified in a large number of samples. The QconCAT-MRM workflow has been successfully used to quantify hepatic drug-metabolizing enzymes (Achour, Russell, et al., 2014; Wang et al., 2015; Shi et al., 2018; Wang et al., 2019) as well as transporters in liver (Wegler et al., 2017), intestine (Harwood et al., 2015; Matthew D. Harwood, Achour, et al., 2016) and brain microvessels (Al Feteisi et al., 2018; Al-Majdoub et al., 2019).

Complete cleavage of peptides in the digestion process is, of course, essential, and there has been some interest in the use of 'flanking' sequences to make the environment of the peptides more analyte-like so that incomplete digestion will better resemble digestion efficiency of the target proteins (Kito et al., 2007; Cheung et al., 2015). Although this idea is attractive in theory, the claim of comparable digestion efficiency between standard and analyte proteins is yet to be tested. We have preferred to optimize the digestion process so that there is complete release of peptides from the QconCAT and as far as possible of the target proteins (Al-Majdoub et al., 2014; Achour et al., 2015).

There is always the possibility of expression failure of a QconCAT, and this has been addressed in several ways (Russell et al., 2013; Achour et al., 2015). Experience indicates that smaller QconCATs are generally expressed more efficiently than larger constructs and ideally QconCATs should be below 100 kDa in size (Brownridge et al., 2011). The use of a small, insoluble tag, such as a ribosomal construct (Al-Majdoub et al., 2014) can force a QconCAT to express in insoluble form in inclusion bodies, from which it may be readily isolated (Russell et al, 2013). More radically, to address the issue of low yield and expression failure of larger QconCATs, multiplexed efficient expression of recombinant QconCATs (MEERCAT) was recently introduced to serve as standard for large scale protein quantification. The QconCATs are expressed in cell-free medium, with advantages such as expression efficiency, cost-effectiveness and ability to monitor the number of expressed QconCATs (Takemori et al., 2017).

2.5.3 Protein standards for absolute quantification (PSAQ)

A PSAQ standard is similar in concept to a QconCAT, but consists of an intact isotopically labeled recombinant protein added at a known concentration to the sample under investigation early in the sample preparation workflow. When a PSAQ standard is employed to quantify an

unmodified protein, it can control for solubilization efficiency, digestion and LC-MS conditions; digestion discrepancies are avoided as PSAQ conserves the native context of the target peptides (Chen et al., 2017). This approach is particularly advantageous when quantifying low abundance, soluble targets in clinical samples (Dupuis et al., 2008; Adrait et al., 2012). However, PSAQ is only applicable to a small number of proteins; the development of such standards is prohibitively expensive and requires rigorous quality control (Al Feteisi, Achour, Barber, et al., 2015). This technique is not useful for assessing PTMs, identifying inter-correlations or multiplexed quantification of a large number of targets (Smith et al., 2019). The application of PSAQ in the quantification of drug-metabolizing enzymes and drug transporters in human tissue is yet to be reported. In biomarker research, this method was successfully used to quantify enzymes useful as indicators of cardiovascular disease (Huillet et al., 2012) and acute kidney injury (Gilquin et al., 2017) in biological fluids.

2.6 Global quantitative proteomic methods

Global untargeted proteomic approaches are routinely used for assessment of protein expression profiles, biomarker discovery, and identification and quantification of a large number of target proteins. Global approaches offer a wide dynamic range and broad proteome coverage while targeted approaches offer higher precision and accuracy. Proteome-wide quantification by global methods is routinely performed either by stable isotope labeling of sample proteins or peptides, e.g. stable isotope labeling by amino acids in cell culture (SILAC) and isobaric tags for relative and absolute quantitation (iTRAQ) (Ong et al., 2002; Wiese et al., 2007), or by label-free analysis of the entire identifiable proteome (Silva et al., 2006; Vildhede et al., 2015).

In metabolic labeling methods, such as SILAC, samples are labeled with amino acids (e.g. arginine, lysine or leucine) carrying a stable isotope label (^{13}C, ^{15}N) and pooled before further sample processing, thus minimizing bias due to handling. The ratios of light to heavy peptide signals at defined retention times are used to relatively quantify protein expression differences between control and treatment conditions. Recent developments in labeling technology increased the ability of SILAC to multiplex from 2 samples to 6 samples (Merrill et al., 2014). SILAC is best suited for induction studies, elucidation of drug effects on protein expression (Zhang et al., 2017; Kurokawa et al., 2019), and analysis of post-translational modifications, such as relative quantification of phosphorylated proteins and identification of novel phosphorylation sites (Ibarrola et al., 2003). In addition, SILAC has been used to prepare

labeled standard mixtures for targeted proteomics (Geiger et al., 2010). These labeled standards are added to analyte samples before protein digestion (Figure 2-1A), demonstrating similar performance to AQUA standards (Prasad and Unadkat, 2014). Metabolic labeling of whole animals, such as rodents, represents a recent extension of SILAC, with various applications in pharmacology research, such as the direct quantification of liver drug-metabolizing enzymes (MacLeod et al., 2015).

Chemical labeling methods, such as iTRAQ and tandem mass tags (TMT), are used at the peptide level after proteolytic digestion of sample proteins. Chemical tags react with amine groups and unique reporter ions are released upon fragmentation in MS/MS analysis (Ross et al., 2004). Unlike SILAC, chemical labeling can be used to analyze up to 8 samples and 11 samples in the same pool using iTRAQ and TMT reagents, respectively. Chemical labeling methods in conjunction with global proteomics demonstrated comparable performance to targeted AQUA-MRM methodology (Vildhede et al., 2018). Applications of chemical labeling include quantification of hepatic drug-metabolizing enzymes and drug transporters (Vildhede et al., 2018), characterization of plasma proteins in acute renal rejection (Freue et al., 2010), biomarker identification for breast cancer (Meiqun et al., 2011), eye disease (Linghu et al., 2017) and gum disease (Tsuchida et al., 2013), and relative quantification of proteins in Alzheimer's disease (Morales et al., 2017). It is worth noting that proteome-wide labeling methods (SILAC/iTRAQ/TMT) are more aligned with applications that require relative quantification.

In label-free methods, normalization of measurements uses either unlabeled exogenous protein references or the total protein approach (TPA). Exogenous proteins include various protein standards distinct from the target proteome; for example, quantification of human enzymes can employ bovine serum albumin or yeast alcohol dehydrogenase at known concentrations (Silva et al., 2006). The TPA method uses the total intensity of peptide peaks belonging to a certain protein relative to the total intensity of all quantifiable peptides in the proteome (Wiśniewski et al., 2012). Both methods have previously been used to quantify human liver enzymes and transporters (Vildhede et al., 2015; Achour, Al Feteisi, et al., 2017; Couto et al., 2019).

Global proteomic techniques are generally carried out using Q-TOF or Orbitrap instruments. To correct for changes in MS conditions over long analyses, sophisticated correction and chromatographic alignment procedures are used to compensate for retention time shifts and to avoid mismatching peptide peaks across runs (Ludwig et al., 2018). Data acquisition methods

used in global proteomics include data-dependent acquisition (DDA) and data-independent acquisition (DIA). DDA represents the standard shotgun approach widely used for whole-proteome analysis (Geromanos et al., 2009). On the other hand, the more recent DIA approach can generate more depth of analysis and broader proteome coverage, especially when window acquisition approaches, such as sequential window acquisition of all theoretical fragment mass spectra (SWATH), are used (Hu et al., 2016; Smith et al., 2019). A summary of the advantages and limitations of global proteomic methods is presented in Table 2-1.

2.6.1 Data-dependent acquisition (DDA)

In DDA, the initial scan of peptide peaks is used for the selection of peptides for fragmentation depending on their ion intensity, with the most abundant ions being selected preferentially. The main advantages of DDA are its flexibility and broad proteome coverage compared with targeted methods. DDA proteomics can identify thousands of proteins and provide reliable relative quantification across samples (Hu et al., 2016). DDA can also be used for absolute quantification using suitable exogenous protein standards (Silva et al., 2006). However, this method is less precise in comparison with targeted quantitative methods as low abundance peptides are not detected reproducibly, leading to bias toward high abundance proteins (Michalski et al., 2011; Hu et al., 2016; Wegler et al., 2017). The performance of this method declines as sample complexity increases (Geromanos et al., 2009; Bilbao et al., 2015).

Q-TOF or Orbitrap mass analyzers are normally used and data are interpreted using software packages, such as MaxQuant, Progenesis or Peaks. DDA data analysis can be performed either by spectral counting or by ion abundance/intensity (Ishihama et al., 2005; Silva et al., 2006), with ion intensity preferred owing to its higher accuracy and reproducibility (Distler et al., 2014; Prasad et al., 2019). Importantly, to ensure robust quantification, consistency in sample preparation and stability of LC-MS conditions are required. DDA shotgun methodology was successfully used for the quantification of transporters and receptors at the blood-brain barrier (Al-Majdoub et al., 2019) and for profiling various enzymes and transporters in liver tissue (Vildhede et al., 2015, 2018; Wegler et al., 2017; Couto et al., 2019; Wiśniewski et al., 2019) and hepatocyte-based in vitro systems (Vildhede et al., 2015; Wiśniewski, Vildhede, et al., 2016).

2.6.2 Data-independent acquisition (DIA)

DIA was proposed to address the limitations of DDA in relation to limited depth of analysis and biased quantification. In DIA, all precursor ions within a selected mass range are fragmented and analyzed (Hu et al., 2016). Theoretically, this method identifies all detectable peptides within the selected mass range and is therefore less biased towards high abundance proteins. However, the generated data tend to be highly complex and specialized software is required for data deconvolution post-acquisition (Ludwig et al., 2018). DIA combines the advantage of broad proteome coverage offered by DDA methods and highly reproducible quantification, typically achieved by targeted techniques (Gillet et al., 2016; Hu et al., 2016). The most widely used DIA approaches include MS^E (Silva et al., 2006; Distler et al., 2014) and SWATH (Gillet et al., 2012). MS^E is a collision energy alternation method that uses a range of collision energies over a m/z window, leading to high- and low-energy fragmentation (Distler et al., 2014). The deconvoluted spectra are searched against a protein database for identification, while quantification can be done using an unlabeled standard protein. The applications of MS^E include relative and absolute label-free quantification of proteins (Bilbao et al., 2015). For example, this method was successfully used for quantitative profiling of various drug-metabolizing enzymes in human liver (Achour, Al Feteisi, et al., 2017).

In methods that use fragmentation windows, such as SWATH-MS, instead of fragmenting the entire set of precursor ions in a particular scan, small m/z windows can be selected for fragmentation and acquisition (Gillet et al., 2012). This potentially reduces the complexity of data and theoretically improves analytical depth and coverage. SWATH is widely applied using Q-TOF and Orbitrap mass analyzers, and data are processed by sophisticated pipelines, such as the open-source, cross-platform software OpenSWATH (Röst et al., 2014). The main advantages of SWATH are its compatibility with the analysis of low abundance sub-proteomes and PTMs, such as acetylation and glycosylation (Keller et al., 2016), and its high reproducibility and consistency owing to peptide-centric scoring analysis (Ludwig et al., 2018). SWATH is therefore particularly applicable when wide proteome coverage, high consistency and accurate quantification are required. Post-acquisition interrogation of selected data yields high quality quantification of target proteins comparable to targeted MRM analyses (Gillet et al., 2012). SWATH has only recently been introduced and therefore it has not been widely used in pharmacology research; reported applications include profiling of hepatic drug-metabolizing enzymes (Jamwal et al., 2017) and quantification of enzymes and transporters in pooled liver, intestine and kidney microsomes (Nakamura et al., 2016). Importantly, the utility of SWATH

has recently been demonstrated in digital biobanking of tissue proteomic maps in health and disease (Guo et al., 2015).

2.7 Key pharmacology applications of proteomic data

The interaction between various intrinsic and extrinsic factors that affect patient populations can result in variability in the expression levels of PK-relevant proteins and PD targets, leading to variations in drug exposure and response profiles (Figure 2-2A). Proteomic methods are used to assess the effects of these factors, including age (B Prasad et al., 2016; Boberg et al., 2017; van Groen et al., 2018; Bhatt et al., 2019), disease (Margaillan et al., 2015; Wang et al., 2016; Billington et al., 2018; Prasad et al., 2018; Al-Majdoub et al., 2019), ethnicity (Kawakami et al., 2011; Peng et al., 2015) and genetics (Prasad et al., 2013; Peng et al., 2015; Bhatt et al., 2019), individually or in combination, on protein expression profiles. Changes in abundance associated with perturbed systems relative to control are then used to predict effects on the fate of drugs (Figure 2-2B) (Bi et al., 2013; Vildhede et al., 2014, 2018; Wang et al., 2016; Ishida et al., 2018; Prasad et al., 2018).

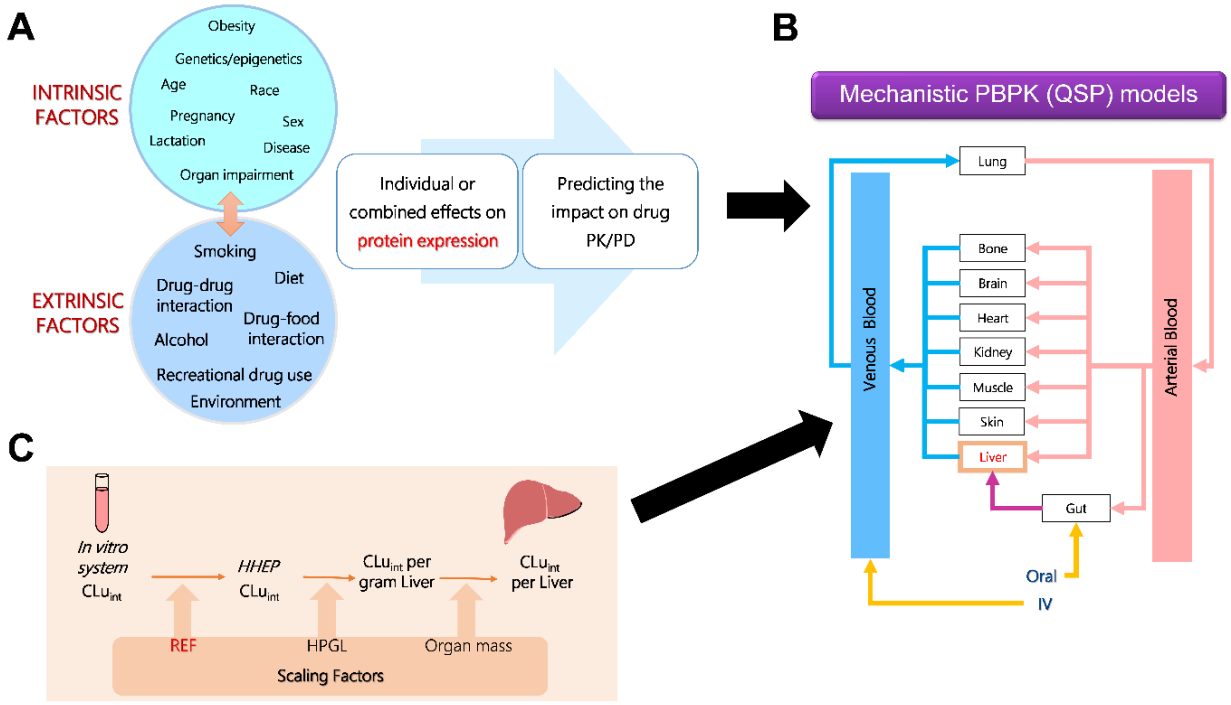

Figure 2-2 The use of proteomic data in PBPK prediction of drug exposure. **A.** Several intrinsic and extrinsic factors can affect the abundance of proteins which in turn can affect drug PK and PD. **B.** Effects of intrinsic and extrinsic factors can be simulated using QSP (PBPK) models that incorporate physiological parameters (e.g. abundance) and drug data. **C.** The process of extrapolation from in vitro measurements in hepatocytes to the prediction of clearance in human liver; the process of IVIVE is used in combination with PBPK (or QSP) models (**B**) to predict drug PK (or PD) in a population of interest. Scaling factors used in IVIVE from hepatocytes are REF = Abundance in tissue/Abundance in the in vitro system, HPGL and liver mass. Abbreviations: CLu_{int}, intrinsic clearance of unbound drug; HHEP, human hepatocytes; HPGL, hepatocytes per gram liver; IV, intra-venous administration; PBPK, physiology-based pharmacokinetics; PD, pharmacodynamics; PK, pharmacokinetics; QSP, quantitative systems pharmacology; REF, relative expression factor measured using abundance data.

Ideally, measurement of the effects on abundance and activity of functional proteins should be carried out and used to achieve robust predictions; however, specific substrates and optimized functional assays are still lacking for enzymes and transporters, with the exception of several CYP and UGT enzymes (Walsky and Obach, 2004; Walsky et al., 2012; den Braver-Sewradj et al., 2017). Abundance is commonly used as a surrogate for activity; correlation between protein abundance and activity was demonstrated for various hepatic and renal drug-metabolizing enzymes, such as CYPs, UGTs, carboxylesterase 1, aldehyde oxidase 1, flavin-containing monooxygenases and sulfotransferases (Venkatakrishnan et al., 2000; Ohtsuki et al., 2012; Fu et al., 2013; Margaillan et al., 2015; Chen et al., 2016; Knights et al., 2016; Achour, Dantonio, et al., 2017; Xie et al., 2017; Wang et al., 2019). This was also demonstrated for certain transporters, such as P-gp and BCRP (Kumar et al., 2015; Harwood, Neuhoff, et al., 2016). In vitro measurements are therefore routinely extrapolated to in vivo activity (IVIVE)

using scaling factors that rely on abundance measurements (Figure 2-2C) (Barter et al., 2007; Matthew D. Harwood, Achour, et al., 2016). In addition to scaling, measuring the abundance of pharmacologically relevant proteins also allows evaluation of the sources of variability in activity rates; inter-individual variation is driven by variability in the level of expression, alterations in intrinsic protein activity, or a combination of these factors (Zhang et al., 2016). Below is a brief account of the main pharmacology applications of proteomic data. Each application requires a different level of proteomic analysis (absolute quantification, relative quantification or discovery/identification) as illustrated in Figure 2-3.

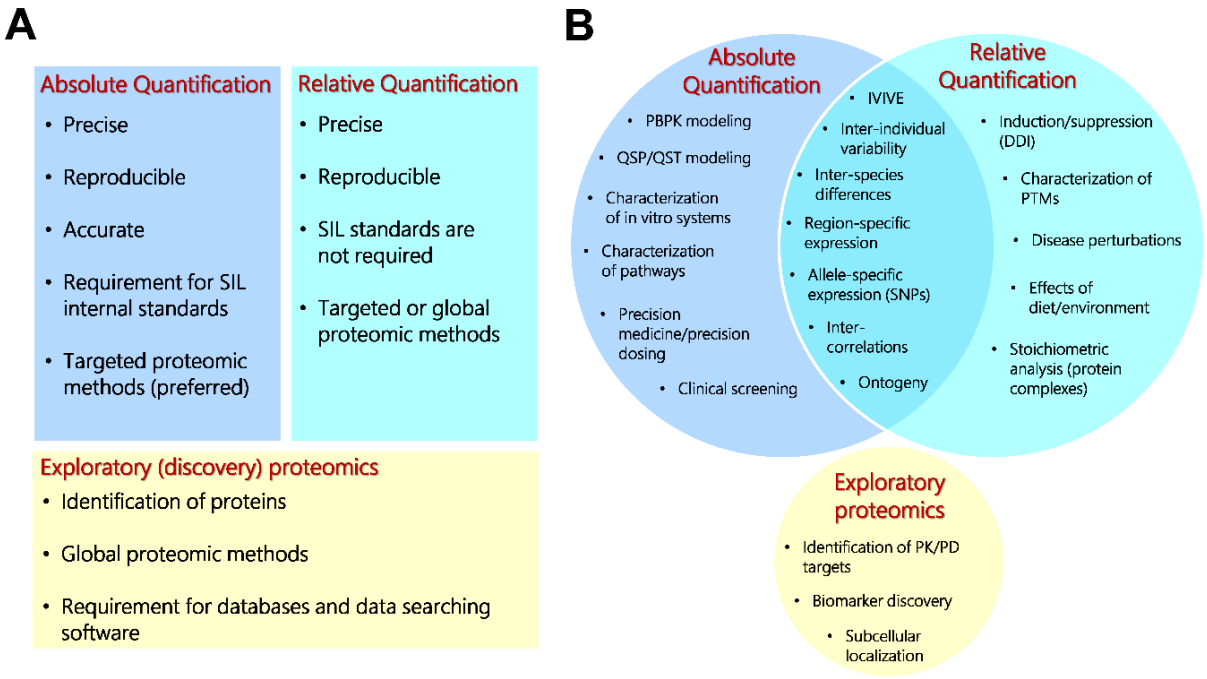

Figure 2-3 The characteristics and applications of absolute quantification, relative quantification and discovery proteomic approaches. **A.** The requirements and characteristics of different levels of quantitative proteomic analysis. Absolute quantification requires assays that are accurate and precise; relative quantification requires reproducibility. **B.** Applications of data generated using absolute quantification, relative quantification and exploratory proteomics in translational PK and PD research. Several applications overlap between absolute and relative quantification. Abbreviations: DDI, drug-drug interaction; PBPK, physiology-based pharmacokinetics; PD, pharmacodynamics; PK, pharmacokinetics; PTM, post-translational modification; QSP, quantitative systems pharmacology; QST, quantitative systems toxicology; SIL, stable isotope label; SNP, single nucleotide polymorphism.

2.7.1 Physiology-based pharmacokinetic (PBPK) modeling and IVIVE

The use of PBPK models has now become firmly embedded in practices within the pharmaceutical industry and evidence from these models is used in different phases of drug

development (Huang et al., 2013; Jamei, 2016). PBPK modeling has gained wide acceptance with regulatory agencies (Rowland et al., 2015), with PBPK data being used in the labels of 21% of new drug applications approved by US Food and Drug Administration (FDA) in 2015 (Marsousi et al., 2017). Modeling is commonly used for prediction of human pharmacokinetic parameters and evaluation of the effects of factors affecting a patient population, such as genetics and lifestyle (Heikkinen et al., 2015; Prasad et al., 2017). PBPK models are built by integrating drug profiles with physiological data, including blood flow, organ size, protein binding, and abundances of enzymes and transporters (Figure 2-2) (Jones and Rowland-Yeo, 2013). Various commercial and non-commercial platforms, e.g. Simcyp, GastroPlus, and PK-Sim, have facilitated the use of PBPK modeling (Kuepfer et al., 2016), but all require data describing protein abundance and population variability, and such data are still in short supply (Heikkinen et al., 2015). Key areas where PBPK models suffer from limited data include non-CYP and non-UGT metabolic pathways, extra-hepatic drug-metabolism and disposition, effects of differences in special populations (e.g. hepatically/renally-impaired, pediatric and geriatric patients) and inter-species variability. These limitations have started to be addressed in recent years mainly because of increased availability of (biopsy and surgical) tissue samples, advances in sample preparation methods and increased application of LC-MS proteomic techniques.

The use of IVIVE has extended the utility of PBPK modeling and made biosimulation more widely usable by linking modeling to in vitro studies using animal and human systems (Sager et al., 2015). The application of IVIVE-PBPK requires integration of absolute abundance data in tissue relative to the in vitro system and system-specific scaling factors (e.g. microsomal protein content or hepatocellularity) with various patient-derived physiological parameters (Barter et al., 2007) to predict pharmacokinetic profiles and account for metabolic differences among specific populations (Rostami-Hodjegan, 2012). A recent systematic survey of the literature showed that the majority of PBPK models are used for the assessment of clinical pharmacokinetics and DDIs (Sager et al., 2015). Recently reported PBPK models that used proteomic data were developed for an array of applications, such as the prediction of variability in clearance (Matthew D Harwood, Achour, et al., 2016; Kumar et al., 2018; Vildhede et al., 2018), variability in DDIs (Doki et al., 2018), impact of formulation (Johnson et al., 2014), effects of liver disease (Wang et al., 2016; Prasad et al., 2018) and kidney impairment (Zhao et al., 2012) on drug pharmacokinetics, and predicting drug kinetics in pediatrics (Jiang et al., 2013; Johnson et al., 2014; Ladumor et al., 2019), older patients (Polasek et al., 2013) and

during pregnancy (Gaohua et al., 2012; Ke et al., 2013, 2014). In addition to these applications, PBPK models represent a valuable tool for learning and internal decision making in the pharmaceutical industry as well as storing and integrating compound-specific information throughout drug discovery and development.

2.7.2 Quantitative systems pharmacology (QSP) models

Models with broader pharmacological applications include QSP models which represent new tools for drug development (Danhof, 2016), with several applications, including prediction of the effects of therapeutic agents, mechanisms of interaction between therapeutic targets and elucidating the biological processes underlying disease and resistance to drugs (Kirouac et al., 2015; Dimitrova et al., 2017; Kirouac, 2018). The US FDA has recently adopted the use of these models and the first case was the assessment of a novel parathyroid hormone replacement biologic (Peterson and Riggs, 2015). The use of QSP models for supporting new drug submissions is therefore expected to increase (Niu et al., 2019). In particular, a promising application of QSP models is the assessment of phamcodynamic DDI potential by probing the mechanisms of interaction of a drug combination in the system and exploring the outcomes of target perturbations, as reported recently for the interaction between glibenclamide and the glucose-insulin-glucagon system in Type 2 diabetes (Choy et al., 2013). The requirement for multi-omic data is emphasized for building pharmacology and toxicology models with the essential role of pharmaco- and toxico-proteomics in identifying and quantifying critical proteins in pathways affected by drug, chemical and environmental exposure (Wetmore and Merrick, 2004). This normally follows a strategy consisting of a discovery method followed by robust targeted quantification (Gillet et al., 2016). Proteomic data were previously used as the basis for developing QSP models to predict the effects of drugs, such as gemcitabine and birinapant in pancreatic cancer (Zhu et al., 2018) and 5-flurouracil in colorectal cancer (Hector et al., 2012).

2.7.3 Disease perturbation

Disease perturbation models are QSP models that aim to simulate disease progression and assess the effects of different drug regimens on a diseased population. Modeling disease perturbations requires relative abundance data for the diseased tissue compared with a healthy set of samples used as control. Disease-scale models have been applied to several disease states, including cirrhosis and different types of cancer. Cirrhosis is a disease of the liver that

significantly affects drug metabolism and disposition and hence disease modeling can help with tailoring dosage regimens that are both safe and efficacious. Liver fibrosis generally leads to a reduction in expression of phase I and phase II enzymes (including CYPs, UGTs and sulfotransferases), and consequently, progressive decline in their abundance and activity is observed as the disease advances (Fisher et al., 2009; Hardwick et al., 2013). Proteomic evidence of changes in the abundance of CYPs, UGTs and other hepatic enzymes was reported in cirrhotic livers and was shown to be dependent on the cause of cirrhosis (Prasad et al., 2018). Phase I metabolizing enzymes are reported to be more influenced by disease progression than phase II pathways which can be attributed to shortage in blood supply reaching the scarred tissue (Yang et al., 2003). Incorporating proteomic data into disease-scale PBPK models has led to improved model performance in cirrhosis as reported for zidovudine, morphine (Prasad et al., 2018), repaglinide, bosentan, telmisartan, valsartan and olmesartan (Li et al., 2015; Wang et al., 2016).

Applications of disease models have also been highlighted for different malignancies, including breast cancer (Hodgkinson et al., 2012) and colon cancer (Hector et al., 2012). These models were mainly used to predict the prognosis in certain populations and assess the effect of anti-cancer regimens at different stages of the disease. Because of the difficulty in recruiting cancer patient populations in clinical studies and the ethical issues related to the exposure of healthy subjects to toxic anti-cancer drugs, PBPK models are better accepted in oncology drug development compared with other disease states (Yoshida et al., 2017). There is currently a lack of abundance data in cancer, and LC-MS proteomics is set to address this gap by providing quantitative measurements of enzymes and transporters from biopsies and archived surgical samples (Prasad et al., 2017).

2.7.4 Protein inter-correlations

Inter-individual variation in drug PK and PD can largely be predicted by integration of known sources of variability, including demographic factors (e.g. age and ethnicity) and physiological parameters (e.g. blood flow, levels of enzymes and transporters) (Jamei et al., 2009). In silico approaches, such as PBPK models, can simulate the interaction between different covariates, such as changes in enzyme/transporter abundance, and predict their effects on clearance and DDIs (Doki et al., 2018; Melillo et al., 2019). Considering the inter-correlation between the expression levels of pharmacologically active proteins, and indeed between other physiological parameters (e.g. liver size and blood flow), can lead to more plausible parameter combinations

when sampling from a population distribution (Tsamandouras et al., 2015). Multiplexed quantitative proteomics can measure multiple enzymes and transporters in individual biological samples simultaneously, allowing robust assessment of inter-correlations between these proteins (Achour, Barber, et al., 2014; Prasad et al., 2019). Due to the nature of correlation analysis, technical bias can in some cases lead to apparent relationships in protein expression and therefore caution should be exercised in order to use only verified biological inter-correlations in modeling applications (Heikkinen et al., 2015).

While various inter-correlations between drug-metabolizing enzymes and transporters have been confirmed both at the RNA (Wortham et al., 2007; Izukawa et al., 2009; Zhang et al., 2016) and protein levels (Achour, Russell, et al., 2014; Mooij et al., 2016; Cheung et al., 2019; Couto et al., 2019), the quantitative impact of such relationships on pharmacokinetic outcomes has only recently started to be explored, with models incorporating inter-correlations outperforming those that do not (Barter et al., 2010; Doki et al., 2018). It is expected that the use of more realistic combinations of physiological parameters will be widely practiced in PK and PD modeling and simulation (Melillo et al., 2019).

2.7.5 Precision dosing

Model-informed precision dosing (MIPD) aims to predict the right dose of a drug for a specific patient based on individual characteristics. This is expected to lead to improved efficacy and reduced toxicity and pave the way to individualized therapy (Darwich et al., 2017). This approach is most applicable to drugs with a narrow therapeutic index and for special populations, such as pediatrics, geriatrics and patients with hepatic and renal impairment (Polasek et al., 2018). Multi-omic approaches and recent developments in 'liquid biopsy' assays (Rowland et al., 2019) are expected to facilitate the construction of 'virtual twins' as a useful strategy to enable precision dosing. A 'virtual twin' is an *in silico* model that represents an individual patient, created by integrating system parameters (i.e. demographic, clinical and enzyme/transporter abundance data) from the patient in order to simulate individualized drug response (Patel et al., 2018). This requires collection of absolute and relative expression data (Polasek et al., 2018) measured in individual patients using innovative sampling techniques, such as the use of biofluids (Boukouris and Mathivanan, 2015).

2.7.6 Ontogeny

The process of growth and maturation is thought to be the main contributor to observed differences in drug PK profiles across the pediatric population age range and when compared with adult populations (Fernandez et al., 2011). For example, physiological changes, such as gastric pH and emptying and intestinal motility that occur from birth to adulthood affect the rate of drug absorption. This is particularly evident in neonates in which absorption is generally delayed (Lu and Rosenbaum, 2014; Batchelor and Marriott, 2015). In addition, the ontogeny of drug-metabolizing enzymes, such as CYPs and UGTs, and transporter proteins within the liver and other organs contributes to variable rates of drug metabolism and excretion (Bhatt et al., 2017, 2019; Boberg et al., 2017; van Groen et al., 2018; Badée et al., 2019), with consequences for toxicity and efficacy profiles (Batchelor and Marriott, 2015; Elmorsi et al., 2016).

Current drug dosing regimens for pediatrics are based on allometric scaling from adult populations or reliant on local guidance and clinician experience because of lack of data from clinical trials (Calvier et al., 2017). Regulators are increasingly supportive of mechanistic PBPK models to inform drug labels in lieu of clinical trials in pediatric applications (Jones et al., 2015; Miller et al., 2019). There is still, however, a paucity of data to feed these paediatric models, in large part because pediatric samples are obtained opportunistically (Howard et al., 2018; Templeton et al., 2018).

Despite the difficulties of sample collection, there is consensus that the abundance and function of the majority of enzyme and transporter proteins are comparatively low in fetal and neonatal samples, increasing at varying rates as a function of age toward adult equivalent levels (Chen et al., 2016; Upreti and Wahlstrom, 2016; Badée et al., 2019; Cheung et al., 2019). For example, CYP3A4, UGT2B7 and P-gp are present in small amounts in neonatal samples, increasing toward or surpassing adult equivalent levels by 1-3 years of age (Mehrotra et al., 2015; van Groen et al., 2018; Bhatt et al., 2019). Conversely, CYP3A7 abundance is relatively high in fetal and neonatal samples, decreasing rapidly toward adult equivalent levels within 1 year (Mehrotra et al., 2015; Leeder and Meibohm, 2016). Incorporation of ontogeny profiles with in silico models led to useful pharmacokinetic predictions for several drugs, such as theophylline (Ginsberg et al., 2004), propofol (Michelet et al., 2018), tramadol (T'jollyn et al., 2015) and valproic acid (Ogungbenro and Aarons, 2014), in children.

2.7.7 Characterization of polymorphisms

Most drug-metabolizing enzymes, particularly CYPs, and transporters, such as organic anion transporting polypeptides, are polymorphic with a range of clinical consequences (Zhou et al., 2017; Oswald, 2018). Various genetic polymorphisms are non-synonymous and can be characterized at the protein level, while polymorphisms occurring in the regulatory region of a gene can affect gene expression and mRNA stability in a particular tissue but do not result in modifications to the protein sequence. The effect of polymorphism becomes significant when it causes variability to an extent that necessitates a change in the administered dose of a specific drug (Gentry et al., 2002); a case in point is CYP2C9 polymorphism and its effects on the required dose of the anti-coagulant warfarin. Our group has previously developed an allele-specific proteomic workflow that can distinguish different polymorphic variants of CYP2B6 (Russell et al., 2013; Achour, Russell, et al., 2014). Shi et al. (2018) showed applicability of this approach to UGT2B15 with the aim of elucidating the regulatory mechanisms of UGT expression. Although relative quantification is as applicable to studying polymorphisms as absolute quantification, this application requires accurate and reproducible assessment of the stoichiometry of target enzymes (or transporters), and therefore targeted proteomic methods that employ a QconCAT standard are especially suitable (Achour et al., 2019).

2.7.8 Disease biomarker discovery

Identification of biomarkers assists in understanding the pathophysiology of a disease and its progression, as well as monitoring patient response during therapy (O'Dwyer et al., 2011; Hector et al., 2012). This is applicable not only to traditional drugs but also to testing the efficacy of new candidates and comparing them to already available therapeutic agents. Often more than one biomarker is necessary to characterize a disease state, where the synergy between several targets in the same (or related) disease pathway makes a composite test more effective than monitoring a single biomarker of disease (Russell et al., 2017). A rigorous discovery proteomics workflow should consist of a preliminary discovery phase using global proteomics, such as shotgun DDA or SWATH profiling, followed by verification or validation of target proteins using more quantitative targeted techniques, such as MRM or PRM. The settings of the targeted experiment will depend on information collected in the discovery phase (Prasad et al., 2019).

The initial step can be performed on a small set of well-characterized samples from patients with the relevant disease state relative to control with the aim of identifying differentially

expressed proteins (O'Dwyer et al., 2011; Gillet et al., 2016). Global proteomics has led to the discovery of various diagnostic biomarkers, such as proteins related to resistance to cancer chemotherapy, and biomarkers for monitoring treatment (Russell et al., 2016; Srivastava and Creek, 2018). These biomarkers are normally associated with critical cell function pathways, such as survival, proliferation (Shruthi et al., 2016), apoptosis (Hector et al., 2012) and post-translational modification of proteins (Held et al., 2010). After conclusive identification of a set of biomarkers, targets are quantified in samples from different populations, such as patients at different stages of the disease, and a healthy cohort (Elschenbroich et al., 2011; Sjöström et al., 2015).

A promising application of global proteomics showed differences in expression profiles between Crohn's disease and ulcerative colitis, which are symptomatically very similar but require entirely different treatment regimens (Starr et al., 2017). In cancer, a wide range of signalling pathways can be perturbed, including the function of protein kinases and phosphatases, which can be monitored as disease biomarkers and targeted by novel drug therapies (Bollu et al., 2017; Bhullar et al., 2018). Recently characterized cancer biomarkers for the assessment of prognosis and therapy-related considerations include HER2 for decision-making in cancer treatment (Kirouac et al., 2015), cAMP-CREB1 axis as a key mechanism associated with resistance to platinum-based therapy (Dimitrova et al., 2017), caspase networks associated with prognosis of colorectal cancer (Hector et al., 2012), Stathmin-1 in relation to cell migration in colon cancer metastasis (Tan et al., 2012), and protein Z as an early biomarker for the detection of ovarian cancer (Russell et al., 2016).

2.8. Recommendations for best practice in applying proteomic techniques

With the recent expansion in the use of proteomic techniques in clinical and pharmacology research, robust guidelines have become crucially required for choosing the most appropriate method for a specific application. The decision-making process tends to be complex and will depend on multiple factors including the biological question, the type of sample, the number of samples, the number of targets, and the available budget. Figure 2-4 shows a simplified decision tree intended to guide the choice of proteomic methods used for pharmacology applications. In the same line, a workshop was recently held by the International Society for the Study of Xenobiotics (ISSX), with the aim of reaching a consensus on the use of proteomics in translational pharmacology research. Various recommendations for the choice and

application of different techniques were proposed but a general consensus was not achieved (Prasad et al., 2019).

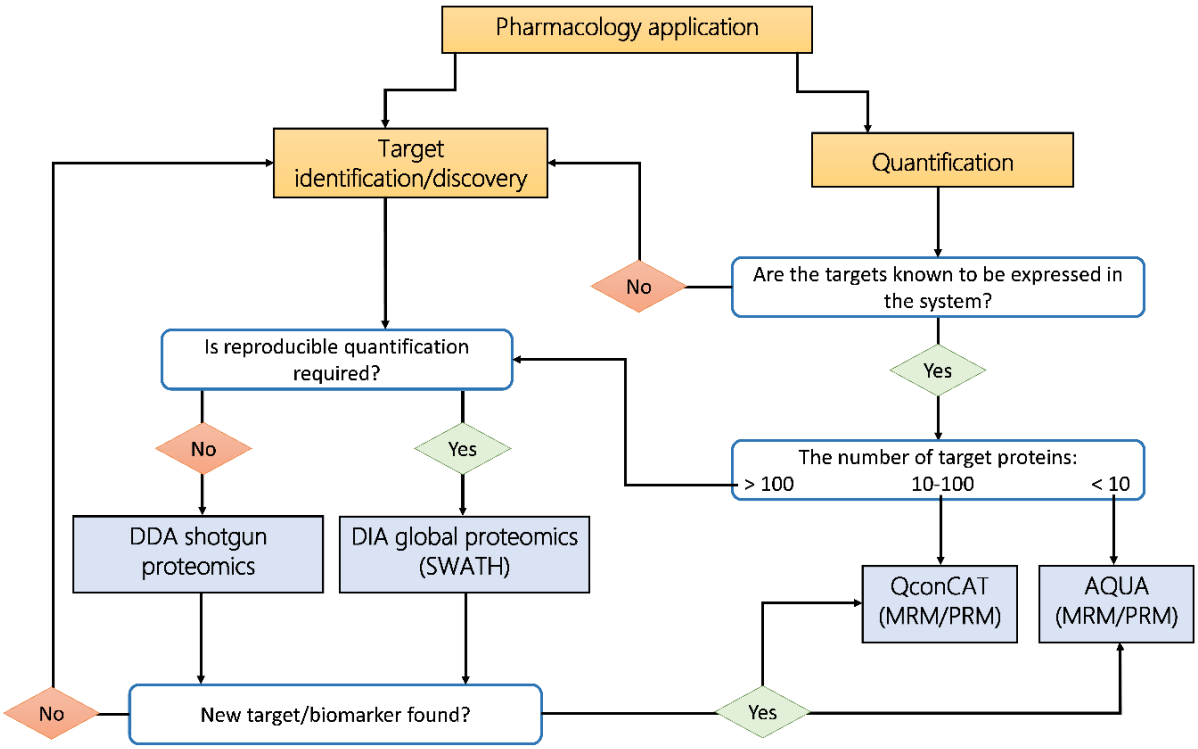

Figure 2-4 Decision tree for choosing suitable proteomic techniques intended for pharmacology applications. A typical number of samples (~30) is used as input for the decision tree. The application can be hypothesis-driven and focused on quantification or hypothesis-generating and intended for discovery. If the application is focused on discovery, global proteomics are most suitable, with preference for data-independent acquisition when reproducible quantification of differential expression is required. When a target or a biomarker is discovered, more accurate quantification is achieved with targeted proteomics. If the target proteins are known to be expressed in the system and are well-defined, targeted proteomics are preferred. If the number of targets is small (< 10), AQUA-based methods (in conjunction with MRM or PRM techniques) are cost-effective. When the number of targets is higher (10-100), QconCAT methodology is preferred. Quantification of larger numbers of targets (> 100) and characterization of proteomes is better achieved using global proteomics. Orange boxes denote applications and blue boxes represent proteomic methods.

Considerations for choosing a technique will generally differ for targeted and global proteomic methods. In targeted analysis, isotopically labeled standards are used to improve precision and accuracy of measurements and reduce bias caused by variations in sample preparation and matrix effects (Bhatt and Prasad, 2018). This is desirable when accurate quantification of inter-individual variability is required for QSP models and MIPD. Techniques recommended for these applications include MRM applied on triple quadrupole instruments and PRM conducted

on higher resolution platforms, such as Orbitraps and Q-TOF instruments. Both methods can be used for multiplexed quantification and they offer a wide dynamic range, typically two orders of magnitude, and therefore spiking of standards should be guided by the range of targeted proteins. One of the main advantages of targeted analysis is possibly its unparalleled sensitivity achieved even in the presence of a complex biological matrix (Holman *et al.*, 2012). Therefore, recommended practice is to quantify protein expressed at very low abundance in a targeted manner. MRM is currently the 'gold standard' in clinical and pharmacological research (Carr et al., 2014), and recent guidelines by the Clinical Proteomic Tumor Analysis Consortium (CPTAC) provides recommendations and standard operating procedures (SOPs) for the development, application and reporting of MRM assays (Whiteaker et al., 2014; Abbatiello et al., 2017). Large-scale cross-laboratory assessment of plasma proteins showed improved quantification when harmonized SOPs are followed (Abbatiello et al., 2015). Triple quadrupole instruments used for MRM are less expensive than higher resolution mass spectrometers and the use of scheduled MRM improves the reproducibility of the data and increases the number of peptides that can be analyzed in one experiment (Oswald et al., 2013), thus reducing the cost and time of analysis. PRM methodology offers advantages in selectivity, resolution and sensitivity while requiring a lower level of method development compared with MRM (Peterson et al., 2012). Orbitrap and Q-TOF instruments tend to be expensive but they represent versatile platforms capable of targeted (PRM) and global analyses (Peterson et al., 2012; Schilling et al., 2015).

Targeted techniques rely on the use of labeled standards and the choice of suitable standards depends on the type of experiment and available budget and expertise. Isotope-labeled internal standards tends to be expensive, but they provide better quality quantification (higher precision and accuracy) than label-free methods. AQUA peptides are ideal for screening applications where a small number of proteins (< 10) are monitored in a large number of samples. QconCATs are more applicable when higher numbers of proteins are targeted and for applications that require strict stoichiometry, such as allele-specific proteomics (Shi et al., 2018; Achour et al., 2019). QconCAT standards have the advantage of sustainability and transferability across laboratories (Russell et al., 2013); a plasmid can be shared by different groups with access to protein expression facilities. We have previously developed a cost-benefit framework to assess the use of quantitative proteomic methods based on cost and application (Al Feteisi, Achour, Barber, et al., 2015). This assessment showed that the high

cost of PSAQ standards hinders their application when a considerable set of proteins are targeted.

For applications that aim to identify novel proteins or quantify a large number of targets (> 100 proteins), the method of choice is global proteomics. Shotgun global proteomics, in conjunction with the TPA approach, can be cheaper than targeted methods because they do not require the use of labeled standards. This method is applied with Q-TOF and Orbitrap instruments and has a wide range of hypothesis-generating applications, including proteome-wide analysis, assessment of disease perturbations and biomarker discovery. Data-independent methods, such as SWATH, offer increased depth of analysis and quantitative reproducibility (Gillet et al., 2012), making them very suitable for generating protein network data for systems pharmacology applications. Their use is however still restricted to core facilities, and sophisticated bioinformatics tools are required for data analysis and interpretation (Distler et al., 2014; Röst et al., 2014). A combined discovery-quantification strategy is recommended when characterizing a novel target or disease pathway (Gillet et al., 2016). This requires using global analysis (e.g. SWATH) on well-defined (disease and control) samples followed by targeted (MRM or PRM) quantification.

The concept of a 'proteomic map of disease' has recently been proposed (Guo et al., 2015; Xu et al., 2019), supported by highly reproducible sample preparation and global proteomic workflows. We recommend that major academic centres should conduct harmonized efforts to generate and share similar proteomic maps in health and disease for available biopsy and surgical samples from different tissues, as demonstrated recently (Uhlen et al., 2015). This will likely require the use of highly reproducible methods capable of wide proteome coverage, such as SWATH-MS (Gillet et al., 2012), and these digital maps can be interrogated retrospectively by various groups for future applications.

2.9. Conclusion

Quantitative proteomic measurements can make a significant contribution to the advance of quantitative systems pharmacology and can be relatively quickly translated into the clinic, where they directly benefit patients. These measurements are powerful, providing selectivity and sensitivity unparalleled by other protein-level techniques. The disadvantage of the unparalleled sensitivity is that independent orthogonal verification of a measurement is often challenging. Further, the cost of these experiments and small sample sizes preclude extensive sample sharing and cross-laboratory analyses. Prasad et al. (2019) have highlighted the

difficulty in obtaining consensus as to appropriate protocols for different measurements, especially as the most thorough approaches are beyond the budgets of many laboratories.

We can however make a number of broad observations. Firstly, targeted methods are preferred where a specific, poorly expressed set of proteins is to be quantified, whereas global methods are better adapted to gaining a general picture of the functional proteome in a cell. Secondly, while there is merit in terms of accuracy in analyzing unfractionated samples, the loss of precision and sensitivity compared with the use of fractions is often critical. Thirdly, neither QconCAT proteins nor AQUA peptides are ideal as standards for targeted proteomics; QconCATs are favorable where large numbers of similar samples are to be analyzed for several proteins, whereas AQUA peptides are effective for small numbers of target proteins. When a decision is made, the minimal requirement is that the use of a particular quantitative proteomic technique should be 'fit for purpose'. Ultimately, the selected method and the level of proteomic quantification will have a substantial impact on the quality and validity of model-informed predictions.

2.10 References

Abbatiello SE, Ackermann BL, Borchers C, Bradshaw RA, Carr SA, Chalkley R, Choi M, Deutsch E, Domon B, Hoofnagle AN, Keshishian H, Kuhn E, Liebler DC, MacCoss M, MacLean B, Mani D, Neubert H, Smith D, Vitek O, and Zimmerman L (2017) New Guidelines for Publication of Manuscripts Describing Development and Application of Targeted Mass Spectrometry Measurements of Peptides and Proteins. *Mol Cell Proteomics* **16**:327–328.

Abbatiello SE, Schilling B, Mani DR, Zimmerman LJ, Hall SC, MacLean B, Albertolle M, Allen S, Burgess M, Cusack MP, Gosh M, Hedrick V, Held JM, Inerowicz HD, Jackson A, Keshishian H, Kinsinger CR, Lyssand J, Makowski L, Mesri M, Rodriguez H, Rudnick P, Sadowski P, Sedransk N, Shaddox K, Skates SJ, Kuhn E, Smith D, Whiteaker JR, Whitwell C, Zhang S, Borchers CH, Fisher SJ, Gibson BW, Liebler DC, MacCoss MJ, Neubert TA, Paulovich AG, Regnier FE, Tempst P, and Carr SA (2015) Large-Scale Interlaboratory Study to Develop, Analytically Validate and Apply Highly Multiplexed, Quantitative Peptide Assays to Measure Cancer-Relevant Proteins in Plasma. *Mol Cell Proteomics* **14**:2357–2374.

Achour B, Al-Majdoub ZM, Al Feteisi H, Elmorsi Y, Rostami-Hodjegan A, and Barber J (2015) Ten years of QconCATs: Application of multiplexed quantification to small medically relevant proteomes. *Int J Mass Spectrom* **391**:93–104.

Achour B, Al Feteisi H, Lanucara F, Rostami-Hodjegan A, and Barber J (2017) Global proteomic analysis of human liver microsomes: Rapid characterization and quantification of hepatic drug-metabolizing enzymes. *Drug Metab Dispos*, **45**:666–675.

Achour B, and Barber J (2013) The activities of Achromobacter lysyl endopeptidase and Lysobacter lysyl endoproteinase as digestive enzymes for quantitative proteomics. *Rapid Commun Mass Spectrom* **27**:1669–1672.

Achour B, Barber J, and Rostami-Hodjegan A (2014) Expression of hepatic drug-metabolizing cytochrome P450 enzymes and their intercorrelations: A meta-analysis. *Drug Metab Dispos* **42**:1349–1356.

Achour B, Dantonio A, Niosi M, Novak JJ, Fallon JK, Barber J, Smith PC, Rostami-Hodjegan A, and Goosen TC (2017) Quantitative Characterization of Major Hepatic UDP-Glucuronosyltransferase Enzymes in Human Liver Microsomes: Comparison of Two Proteomic Methods and Correlation with Catalytic Activity. *Drug Metab Dispos* **45**:1102–1112.

Achour B, Rostami-Hodjegan A, and Barber J (2019) Response to "Determining Allele-

Specific Protein Expression (ASPE) Using a Novel Quantitative Concatamer Based Proteomics Method". *J Proteome Res* **18**:574–574.

Achour B, Russell MR, Barber J, and Rostami-Hodjegan A (2014) Simultaneous quantification of the abundance of several cytochrome P450 and uridine 5′-diphospho-glucuronosyltransferase enzymes in human liver microsomes using multiplexed targeted proteomics. *Drug Metab Dispos*, **42**:500–510.

Adrait A, Lebert D, Trauchessec M, Dupuis A, Louwagie M, Masselon C, Jaquinod M, Chevalier B, Vandenesch F, Garin J, Bruley C, and Brun V (2012) Development of a Protein Standard Absolute Quantification (PSAQ^{TM}) assay for the quantification of Staphylococcus aureus enterotoxin A in serum. *J Proteomics* **75**:3041–3049.

Aebersold R, Burlingame AL, and Bradshaw RA (2013) Western blots versus selected reaction monitoring assays: time to turn the tables? *Mol Cell proteomics* **12**:2381–2.

Al-Majdoub ZM, Al Feteisi H, Achour B, Warwood S, Neuhoff S, Rostami-Hodjegan A, and Barber J (2019) Proteomic quantification of human blood–brain barrier SLC and ABC transporters in healthy individuals and dementia patients. *Mol Pharm* **16**:1220–1233.

Al-Majdoub ZM, Carroll KM, Gaskell SJ, and Barber J (2014) Quantification of the proteins of the bacterial ribosome using QconCAT technology. *J Proteome Res* **13**:1211–1222.

Al Feteisi H, Achour B, Barber J, and Rostami-Hodjegan A (2015) Choice of LC-MS Methods for the Absolute Quantification of Drug-Metabolizing Enzymes and Transporters in Human Tissue: a Comparative Cost Analysis. *AAPS J* **17**:438–446.

Al Feteisi H, Achour B, Rostami-hodjegan A, and Barber J (2015) Translational value of liquid chromatography coupled with tandem mass spectrometry-based quantitative proteomics for in vitro -- in vivo extrapolation of drug metabolism and transport and considerations in selecting appropriate techniques. *Expert Opin Drug Metab Toxicol* **11**:1357–1369.

Al Feteisi H, Al-Majdoub ZM, Achour B, Couto N, Rostami-Hodjegan A, and Barber J (2018) Identification and quantification of blood–brain barrier transporters in isolated rat brain microvessels. *J Neurochem* **146**:670-685.

Badée J, Fowler S, de Wildt SN, Collier AC, Schmidt S, and Parrott N (2019) The Ontogeny of UDP-glucuronosyltransferase Enzymes, Recommendations for Future Profiling Studies and Application Through Physiologically Based Pharmacokinetic Modelling. *Clin Pharmacokinet* **58**:189–211.

Barter Z, Bayliss M, Beaune P, Boobis A, Carlile D, Edwards R, Brian Houston J, Lake B, Lipscomb J, Pelkonen O, Tucke G, and Rostami-Hodjegan A (2007) Scaling Factors for the Extrapolation of In Vivo Metabolic Drug Clearance From In Vitro Data: Reaching a

Consensus on Values of Human Micro-somal Protein and Hepatocellularity Per Gram of Liver. *Curr Drug Metab* **8**:33–45.

Barter ZE, Perrett HF, Yeo KR, Allorge D, Lennard MS, and Rostami-Hodjegan A (2010) Determination of a quantitative relationship between hepatic CYP3A5*1/*3 and CYP3A4 expression for use in the prediction of metabolic clearance in virtual populations. *Biopharm Drug Dispos* **31**:516–532.

Batchelor HK, and Marriott JF (2015) Paediatric pharmacokinetics: Key considerations. *Br J Clin Pharmacol* **79**:395–404.

Batth TS, Papetti M, Pfeiffer A, Tollenaere MAX, Francavilla C, and Olsen J V. (2018) Large-Scale Phosphoproteomics Reveals Shp-2 Phosphatase-Dependent Regulators of Pdgf Receptor Signaling. *Cell Rep* **22**:2784–2796.

Bhatt DK, Gaedigk A, Pearce RE, Leeder JS, and Prasad B (2017) Age-dependent Protein Abundance of Cytosolic Alcohol and Aldehyde Dehydrogenases in Human Liver. *Drug Metab Dispos* **45**:1044–1048.

Bhatt DK, Mehrotra A, Gaedigk A, Chapa R, Basit A, Zhang H, Choudhari P, Boberg M, Pearce RE, Gaedigk R, Broeckel U, Leeder JS, and Prasad B (2019) Age- and Genotype-Dependent Variability in the Protein Abundance and Activity of Six Major Uridine Diphosphate-Glucuronosyltransferases in Human Liver. *Clin Pharmacol Ther* **105**:131–141.

Bhatt DK, and Prasad B (2018) Critical Issues and Optimized Practices in Quantification of Protein Abundance Level to Determine Interindividual Variability in DMET Proteins by LC-MS/MS Proteomics. *Clin Pharmacol Ther* **103**:619–630.

Bhullar KS, Lagarón NO, McGowan EM, Parmar I, Jha A, Hubbard BP, and Rupasinghe HPV (2018) Kinase-targeted cancer therapies: progress, challenges and future directions. *Mol Cancer* **17**:48.

Bi Y, Qiu X, Rotter CJ, Kimoto E, Piotrowski M, Varma M V, Ei-Kattan AF, and Lai Y (2013) Quantitative assessment of the contribution of sodium-dependent taurocholate co-transporting polypeptide (NTCP) to the hepatic uptake of rosuvastatin, pitavastatin and fluvastatin. *Biopharm Drug Dispos* **34**:452–61.

Bilbao A, Varesio E, Luban J, Strambio-De-Castillia C, Hopfgartner G, Müller M, and Lisacek F (2015) Processing strategies and software solutions for data-independent acquisition in mass spectrometry. *Proteomics* **15**:964–980.

Billington S, Ray AS, Salphati L, Xiao G, Chu X, Humphreys WG, Liao M, Lee CA, Mathias A, Hop CECA, Rowbottom C, Evers R, Lai Y, Kelly EJ, Prasad B, and Unadkat JD (2018)

Transporter Expression in Noncancerous and Cancerous Liver Tissue from Donors with Hepatocellular Carcinoma and Chronic Hepatitis C Infection Quantified by LC-MS/MS Proteomics. *Drug Metab Dispos* **46**:189–196.

Billington S, Salphati L, Hop CECA, Chu X, Evers R, Burdette D, Rowbottom C, Lai Y, Xiao G, Humphreys WG, Nguyen TB, Prasad B, and Unadkat JD (2019) Interindividual and Regional Variability in Drug Transporter Abundance at the Human Blood–Brain Barrier Measured by Quantitative Targeted Proteomics. *Clin Pharmacol Ther* cpt.1373.

Boberg M, Vrana M, Mehrotra A, Pearce RE, Gaedigk A, Bhatt DK, Leeder JS, and Prasad B (2017) Age-Dependent Absolute Abundance of Hepatic Carboxylesterases (CES1 and CES2) by LC-MS/MS Proteomics: Application to PBPK Modeling of Oseltamivir In Vivo Pharmacokinetics in Infants. *Drug Metab Dispos* **45**:216–223.

Bollu LR, Mazumdar A, Savage MI, and Brown PH (2017) Molecular pathways: Targeting protein tyrosine phosphatases in cancer. *Clin Cancer Res* **23**:2136–2142.

Boukouris S, and Mathivanan S (2015) Exosomes in bodily fluids are a highly stable resource of disease biomarkers. *Proteomics - Clin Appl* **9**:358–367.

Brownridge P, Holman SW, Gaskell SJ, Grant CM, Harman VM, Hubbard SJ, Lanthaler K, Lawless C, O'Cualain R, Sims P, Watkins R, and Beynon RJ (2011) Global absolute quantification of a proteome: Challenges in the deployment of a QconCAT strategy. *Proteomics* **11**:2957–70.

Calderón-Celis F, Encinar JR, and Sanz-Medel A (2018) Standardization approaches in absolute quantitative proteomics with mass spectrometry. *Mass Spectrom Rev* **37**:715–737.

Calvier EAM, Krekels EHJ, Välitalo PAJ, Rostami-Hodjegan A, Tibboel D, Danhof M, and Knibbe CAJ (2017) Allometric Scaling of Clearance in Paediatric Patients: When Does the Magic of 0.75 Fade? *Clin Pharmacokinet* **56**:273–285.

Carr SA, Abbatiello SE, Ackermann BL, Borchers C, Domon B, Deutsch EW, Grant RP, Hoofnagle AN, Huttenhain R, Koomen JM, Liebler DC, Liu T, MacLean B, Mani D, Mansfield E, Neubert H, Paulovich AG, Reiter L, Vitek O, Aebersold R, Anderson L, Bethem R, Blonder J, Boja E, Botelho J, Boyne M, Bradshaw RA, Burlingame AL, Chan D, Keshishian H, Kuhn E, Kinsinger C, Lee JSH, Lee S-W, Moritz R, Oses-Prieto J, Rifai N, Ritchie J, Rodriguez H, Srinivas PR, Townsend RR, Van Eyk J, Whiteley G, Wiita A, and Weintraub S (2014) Targeted Peptide Measurements in Biology and Medicine: Best Practices for Mass Spectrometry-based Assay Development Using a Fit-for-Purpose Approach. *Mol Cell Proteomics* **13**:907–917.

Chen B, Liu L, Ho H, Chen Y, Yang Z, Liang X, Payandeh J, Dean B, Hop CECA, and Deng Y (2017) Strategies of Drug Transporter Quantitation by LC-MS: Importance of Peptide Selection and Digestion Efficiency. *AAPS J* **19**:1469–1478.

Chen Y, Zane NR, Thakker DR, and Wang MZ (2016) Quantification of Flavin-containing Monooxygenases 1, 3, and 5 in Human Liver Microsomes by UPLC-MRM-Based Targeted Quantitative Proteomics and Its Application to the Study of Ontogeny. *Drug Metab Dispos* **44**:975–983.

Cheung CSF, Anderson KW, Wang M, and Turko I V. (2015) Natural Flanking Sequences for Peptides Included in a Quantification Concatamer Internal Standard. *Anal Chem* **87**:1097–1102.

Cheung KWK, van Groen BD, Spaans E, van Borselen MD, C.J.M. de Bruijn A, Simons-Oosterhuis Y, Tibboel D, Samsom JN, Verdijk RM, Smeets B, Zhang L, Huang S, Giacomini KM, and de Wildt SN (2019) A comprehensive analysis of ontogeny of renal drug transporters: mRNA analyses, quantitative proteomics and localization. *Clin Pharmacol Ther* **106**:1083-1092.

Choksawangkarn W, Edwards N, Wang Y, Gutierrez P, and Fenselau C (2012) Comparative study of workflows optimized for In-gel, In-solution, and on-filter proteolysis in the analysis of plasma membrane proteins. *J Proteome Res* **11**:3030–3034.

Choy S, Hénin E, van der Walt J-S, Kjellsson MC, and Karlsson MO (2013) Identification of the primary mechanism of action of an insulin secretagogue from meal test data in healthy volunteers based on an integrated glucose-insulin model. *J Pharmacokinet Pharmacodyn* **40**:1–10.

Cieślak A, Kelly I, Trottier J, Verreault M, Wunsch E, Milkiewicz P, Poirier G, Droit A, and Barbier O (2016) Selective and sensitive quantification of the cytochrome P450 3A4 protein in human liver homogenates through multiple reaction monitoring mass spectrometry. *Proteomics* **16**:2827–2837.

Couto N, Al-Majdoub ZM, Achour B, Wright PC, Rostami-Hodjegan A, and Barber J (2019) Quantification of Proteins Involved in Drug Metabolism and Disposition in the Human Liver Using Label-Free Global Proteomics. *Mol Pharm* **16**:632–647.

Cox J, and Mann M (2008) MaxQuant enables high peptide identification rates, individualized p.p.b.-range mass accuracies and proteome-wide protein quantification. *Nat Biotechnol* **26**:1367–1372.

Danhof M (2016) Systems pharmacology -- Towards the modeling of network interactions. *Eur J Pharm Sci* **94**:4–14.

Darwich AS, Ogungbenro K, Vinks AA, Powell JR, Reny JL, Marsousi N, Daali Y, Fairman D, Cook J, Lesko LJ, McCune JS, Knibbe CAJ, de Wildt SN, Leeder JS, Neely M, Zuppa AF, Vicini P, Aarons L, Johnson TN, Boiani J, and Rostami-Hodjegan A (2017) Why has model-informed precision dosing not yet become common clinical reality? lessons from the past and a roadmap for the future. *Clin Pharmacol Ther* **101**:646–656.

den Braver-Sewradj SP, den Braver MW, Baze A, Decorde J, Fonsi M, Bachellier P, Vermeulen NPE, Commandeur JNM, Richert L, and Vos JC (2017) Direct comparison of UDP-glucuronosyltransferase and cytochrome P450 activities in human liver microsomes, plated and suspended primary human hepatocytes from five liver donors. *Eur J Pharm Sci* **109**:96–110.

Dimitrova N, Nagaraj AB, Razi A, Singh S, Kamalakaran S, Banerjee N, Joseph P, Mankovich A, Mittal P, Difeo A, and Varadan V (2017) InFlo: A novel systems biology framework identifies cAMP-CREB1 axis as a key modulator of platinum resistance in ovarian cancer. *Oncogene* **36**:2472–2482.

Distler U, Kuharev J, Navarro P, Levin Y, Schild H, and Tenzer S (2014) Drift time-specific collision energies enable deep-coverage data-independent acquisition proteomics. *Nat Methods* **11**:167–70.

Doki K, Darwich AS, Achour B, Tornio A, Backman JT, and Rostami-Hodjegan A (2018) Implications of intercorrelation between hepatic CYP3A4-CYP2C8 enzymes for the evaluation of drug-drug interactions: a case study with repaglinide. *Br J Clin Pharmacol* **84**:972–986.

Drozdzik M, Busch D, Lapczuk J, Müller J, Ostrowski M, Kurzawski M, and Oswald S (2018) Protein Abundance of Clinically Relevant Drug-Metabolizing Enzymes in the Human Liver and Intestine: A Comparative Analysis in Paired Tissue Specimens. *Clin Pharmacol Ther* **104**:515–524.

Drozdzik M, Gröer C, Penski J, Lapczuk J, Ostrowski M, Lai Y, Prasad B, Unadkat JD, Siegmund W, and Oswald S (2014) Protein Abundance of Clinically Relevant Multidrug Transporters along the Entire Length of the Human Intestine. *Mol Pharm* **11**:3547–3555.

Dupuis A, Hennekinne J-A, Garin J, and Brun V (2008) Protein Standard Absolute Quantification (PSAQ) for improved investigation of staphylococcal food poisoning outbreaks. *Proteomics* **8**:4633–4636.

Elmorsi Y, Barber J, and Rostami-Hodjegan A (2016) Ontogeny of Hepatic Drug Transporters and Relevance to Drugs Used in Pediatrics. *Drug Metab Dispos* **44**:992–998.

Elschenbroich S, Ignatchenko V, Clarke B, Kalloger SE, Boutros PC, Gramolini AO, Shaw P,

Jurisica I, and Kislinger T (2011) In-Depth Proteomics of Ovarian Cancer Ascites: Combining Shotgun Proteomics and Selected Reaction Monitoring Mass Spectrometry. *J Proteome Res* **10**:2286–2299.

Fallon JK, Harbourt DE, Maleki SH, Kessler FK, Ritter JK, and Smith PC (2008) Absolute quantification of human uridine-diphosphate glucuronosyl transferase (UGT) enzyme isoforms 1A1 and 1A6 by tandem LC-MS. *Drug Metab Lett* **2**:210–22.

Fallon JK, Houvig N, Booth-Genthe CL, and Smith PC (2018) Quantification of membrane transporter proteins in human lung and immortalized cell lines using targeted quantitative proteomic analysis by isotope dilution nanoLC-MS/MS. *J Pharm Biomed Anal* **154**:150–157.

Fallon JK, Neubert H, Hyland R, Goosen TC, and Smith PC (2013) Targeted quantitative proteomics for the analysis of 14 UGT1As and -2Bs in human liver using NanoUPLC-MS/MS with selected reaction monitoring. *J Proteome Res* **12**:4402-4413.

Fernandez E, Perez R, Hernandez A, Tejada P, Arteta M, and Ramos JT (2011) Factors and mechanisms for pharmacokinetic differences between pediatric population and adults. *Pharmaceutics* **3**:53–72, Multidisciplinary Digital Publishing Institute (MDPI).

Fisher CD, Lickteig AJ, Augustine LM, Ranger-Moore J, Jackson JP, Ferguson SS, and Cherrington NJ (2009) Hepatic Cytochrome P450 Enzyme Alterations in Humans with Progressive Stages of Nonalcoholic Fatty Liver Disease. *Drug Metab Dispos* **37**:2087–2094.

Freue GVC, Sasaki M, Meredith A, Günther OP, Bergman A, Takhar M, Mui A, Balshaw RF, Ng RT, Opushneva N, Hollander Z, Li G, Borchers CH, Wilson-McManus J, McManus BM, Keown PA, and McMaster WR (2010) Proteomic Signatures in Plasma during Early Acute Renal Allograft Rejection. *Mol Cell Proteomics* **9**:1954–1967.

Fu C, Di L, Han X, Soderstrom C, Snyder M, Troutman MD, Obach RS, and Zhang H (2013) Aldehyde Oxidase 1 (AOX1) in Human Liver Cytosols: Quantitative Characterization of AOX1 Expression Level and Activity Relationship. *Drug Metab Dispos* **41**:1797–1804.

Gallien S, Bourmaud A, Kim SY, and Domon B (2014) Technical considerations for large-scale parallel reaction monitoring analysis. *J Proteomics* **100**:147–159.

Gallien S, Duriez E, Crone C, Kellmann M, Moehring T, and Domon B (2012) Targeted Proteomic Quantification on Quadrupole-Orbitrap Mass Spectrometer. *Mol Cell Proteomics* **11**:1709–1723.

Gallien S, Duriez E, Demeure K, and Domon B (2013) Selectivity of LC-MS/MS analysis: Implication for proteomics experiments. *J Proteomics* **81**:148–158.

Gaohua L, Abduljalil K, Jamei M, Johnson TN, and Rostami-Hodjegan A (2012) A pregnancy physiologically based pharmacokinetic (p-PBPK) model for disposition of drugs metabolized by CYP1A2, CYP2D6 and CYP3A4. *Br J Clin Pharmacol* **74**:873–885.

Geiger T, Cox J, Ostasiewicz P, Wisniewski JR, and Mann M (2010) Super-SILAC mix for quantitative proteomics of human tumor tissue. *Nat Methods* **7**:383–5.

Gentry PR, Hack CE, Haber L, Maier A, and Clewell HJ (2002) An approach for the quantitative consideration of genetic polymorphism data in chemical risk assessment: Examples with warfarin and parathion. *Toxicol Sci* **70**:120–139.

Geromanos SJ, Vissers JPC, Silva JC, Dorschel CA, Li GZ, Gorenstein M V., Bateman RH, and Langridge JI (2009) The detection, correlation, and comparison of peptide precursor and product ions from data independent LC-MS with data dependant LC-MS/MS. *Proteomics* **9**:1683–1695.

Gillet LC, Leitner A, and Aebersold R (2016) Mass Spectrometry Applied to Bottom-Up Proteomics: Entering the High-Throughput Era for Hypothesis Testing. *Annu Rev Anal Chem* **9**:449–72.

Gillet LC, Navarro P, Tate S, Röst H, Selevsek N, Reiter L, Bonner R, and Aebersold R (2012) Targeted Data Extraction of the MS/MS Spectra Generated by Data-independent Acquisition: A New Concept for Consistent and Accurate Proteome Analysis. *Mol Cell Proteomics* **11**:O111.016717.

Gillette MA, and Carr SA (2013) Quantitative analysis of peptides and proteins in biomedicine by targeted mass spectrometry. *Nat Methods* **10**:28–34.

Gilquin B, Louwagie M, Jaquinod M, Cez A, Picard G, El Kholy L, Surin B, Garin J, Ferro M, Kofman T, Barau C, Plaisier E, Ronco P, and Brun V (2017) Multiplex and accurate quantification of acute kidney injury biomarker candidates in urine using Protein Standard Absolute Quantification (PSAQ) and targeted proteomics. *Talanta* **164**:77–84.

Ginsberg G, Hattis D, Russ A, and Sonawane B (2004) Physiologically based pharmacokinetic (PBPK) modeling of caffeine and theophylline in neonates and adults: implications for assessing children's risks from environmental agents. *J Toxicol Environ Heal Part A* **67**:297–329.

Gröer C, Brück S, Lai Y, Paulick A, Busemann A, Heidecke CD, Siegmund W, and Oswald S (2013) LC-MS/MS-based quantification of clinically relevant intestinal uptake and efflux transporter proteins. *J Pharm Biomed Anal* **85**:253–261.

Gröer C, Busch D, Patrzyk M, Beyer K, Busemann A, Heidecke CD, Drozdzik M, Siegmund W, and Oswald S (2014) Absolute protein quantification of clinically relevant cytochrome

P450 enzymes and UDP-glucuronosyltransferases by mass spectrometry-based targeted proteomics. *J Pharm Biomed Anal* **100**.

Guo T, Kouvonen P, Koh CC, Gillet LC, Wolski WE, Röst HL, Rosenberger G, Collins BC, Blum LC, Gillessen S, Joerger M, Jochum W, and Aebersold R (2015) Rapid mass spectrometric conversion of tissue biopsy samples into permanent quantitative digital proteome maps. *Nat Med* **21**:407–413.

Hansen J, Palmfeldt J, Pedersen KW, Funder AD, Frost L, Hasselstrøm JB, and Jornil JR (2019) Postmortem protein stability investigations of the human hepatic drug-metabolizing cytochrome P450 enzymes CYP1A2 and CYP3A4 using mass spectrometry. *J Proteomics* **194**:125-131.

Harbourt DE, Fallon JK, Ito S, Baba T, Ritter JK, Glish GL, and Smith PC (2012) Quantification of human uridine-diphosphate glucuronosyl transferase 1A isoforms in liver, intestine, and kidney using nanobore liquid chromatography-tandem mass spectrometry. *Anal Chem* **84**:98-105.

Hardwick RN, Ferreira DW, More VR, Lake AD, Lu Z, Manautou JE, Slitt AL, and Cherrington NJ (2013) Altered UDP-Glucuronosyltransferase and Sulfotransferase Expression and Function during Progressive Stages of Human Nonalcoholic Fatty Liver Disease. *Drug Metab Dispos* **41**:554–561.

Harwood MD, Achour B, Neuhoff S, Russell MR, Carlson G, Warhurst G, and Rostami-Hodjegan A (2016) In Vitro-In Vivo Extrapolation Scaling Factors for Intestinal P-Glycoprotein and Breast Cancer Resistance Protein: Part I: A Cross-Laboratory Comparison of Transporter-Protein Abundances and Relative Expression Factors in Human Intestine and Caco-2 Cells. *Drug Metab Dispos* **44**:297–307.

Harwood MD, Achour B, Neuhoff S, Russell MR, Carlson G, Warhurst G, and Rostami-Hodjegan A (2016) In Vitro–In Vivo Extrapolation Scaling Factors for Intestinal P-glycoprotein and Breast Cancer Resistance Protein: Part II. The Impact of Cross-Laboratory Variations of Intestinal Transporter Relative Expression Factors on Predicted Drug Disposition. *Drug Metab Dispos* **44**:476 LP-480.

Harwood MD, Achour B, Russell MR, Carlson GL, Warhurst G, and Rostami-Hodjegan A (2015) Application of an LC–MS/MS method for the simultaneous quantification of human intestinal transporter proteins absolute abundance using a QconCAT technique. *J Pharm Biomed Anal* **110**:27–33.

Harwood MD, Neuhoff S, Rostami-Hodjegan A, and Warhurst G (2016) Breast Cancer Resistance Protein Abundance, but Not mRNA Expression, Correlates with Estrone-3-

Sulfate Transport in Caco-2. *J Pharm Sci* **105**:1370–1375.

Harwood MD, Russell MR, Neuhoff S, Warhurst G, and Rostami-Hodjegan A (2014) Lost in centrifugation: Accounting for transporter protein losses in quantitative targeted absolute proteomics. *Drug Metab Dispos* **42**:1766–1772.

Havliš J, and Shevchenko A (2004) Absolute quantification of proteins in solutions and in polyacrylamide gels by mass spectrometry. *Anal Chem* **76**:3029–3036.

Hector S, Rehm M, Schmid J, Kehoe J, McCawley N, Dicker P, Murray F, McNamara D, Kay EW, Concannon CG, Huber HJ, and Prehn JHM (2012) Clinical application of a systems model of apoptosis execution for the prediction of colorectal cancer therapy responses and personalisation of therapy. *Gut* **61**:725–733.

Heikkinen AT, Lignet F, Cutler P, and Parrott N (2015) The role of quantitative ADME proteomics to support construction of physiologically based pharmacokinetic models for use in small molecule drug development. *PROTEOMICS - Clin Appl* **9**:732–744.

Held JM, Danielson SR, Behring JB, Atsriku C, Britton DJ, Puckett RL, Schilling B, Campisi J, Benz CC, and Gibson BW (2010) Targeted quantitation of site-specific cysteine oxidation in endogenous proteins using a differential alkylation and multiple reaction monitoring mass spectrometry approach. *Mol Cell Proteomics* **9**:1400–10.

Hodgkinson VC, Agarwal V, ELFadl D, Fox JN, McManus PL, Mahapatra TK, Kneeshaw PJ, Drew PJ, Lind MJ, and Cawkwell L (2012) Pilot and feasibility study: comparative proteomic analysis by 2-DE MALDI TOF/TOF MS reveals 14-3-3 proteins as putative biomarkers of response to neoadjuvant chemotherapy in ER-positive breast cancer. *J Proteomics* **75**:2745–2752.

Holman SW, Sims PFG, and Eyers CE (2012) The use of selected reaction monitoring in quantitative proteomics. *Bioanalysis* **4**:1763–1786.

Hoshi Y, Uchida Y, Tachikawa M, Inoue T, Ohtsuki S, and Terasaki T (2013) Quantitative Atlas of blood-brain barrier transporters, receptors, and tight junction proteins in rats and common marmoset. *J Pharm Sci* **102**:3343–55.

Howard M, Barber J, Alizai N, and Rostami-Hodjegan A (2018) Dose adjustment in orphan disease populations: the quest to fulfill the requirements of physiologically based pharmacokinetics. *Expert Opin Drug Metab Toxicol* **14**:1315–1330.

Hu A, Noble WS, and Wolf-Yadlin A (2016) Technical advances in proteomics: new developments in data-independent acquisition. *F1000Research* **5**:419.

Huang S-M, Abernethy DR, Wang Y, Zhao P, and Zineh I (2013) The utility of modeling and simulation in drug development and regulatory review. *J Pharm Sci* **102**:2912–23.

Huillet C, Adrait A, Lebert D, Picard G, Trauchessec M, Louwagie M, Dupuis A, Hittinger L, Ghaleh B, Le Corvoisier P, Jaquinod M, Garin J, Bruley C, and Brun V (2012) Accurate Quantification of Cardiovascular Biomarkers in Serum Using Protein Standard Absolute Quantification (PSAQ^{TM}) and Selected Reaction Monitoring. *Mol Cell Proteomics* **11**:M111.008235.

Ibarrola N, Kalume DE, Gronborg M, Iwahori A, and Pandey A (2003) A Proteomic Approach for Quantitation of Phosphorylation Using Stable Isotope Labeling in Cell Culture. *Anal Chem* **75**:6043–6049.

Ishida K, Ullah M, Tóth B, Juhasz V, and Unadkat JD (2018) Successful Prediction of In Vivo Hepatobiliary Clearances and Hepatic Concentrations of Rosuvastatin Using Sandwich-Cultured Rat Hepatocytes, Transporter-Expressing Cell Lines, and Quantitative Proteomics. *Drug Metab Dispos* **46**:66–74.

Ishihama Y, Oda Y, Tabata T, Sato T, Nagasu T, Rappsilber J, and Mann M (2005) Exponentially Modified Protein Abundance Index (emPAI) for Estimation of Absolute Protein Amount in Proteomics by the Number of Sequenced Peptides per Protein. *Mol Cell Proteomics* **4**:1265–1272.

Izukawa T, Nakajima M, Fujiwara R, Yamanaka H, Fukami T, Takamiya M, Aoki Y, Ikushiro SS -i., Sakaki T, and Yokoi T (2009) Quantitative analysis of UGT1A and UGT2B expression levels in human livers. *Drug Metab Dispos* **37**:1759–1768.

Jamei M (2016) Recent Advances in Development and Application of Physiologically-Based Pharmacokinetic (PBPK) Models: a Transition from Academic Curiosity to Regulatory Acceptance. *Curr Pharmacol Reports* **2**:161–169.

Jamei M, Dickinson GL, and Rostami-Hodjegan A (2009) A framework for assessing inter-individual variability in pharmacokinetics using virtual human populations and integrating general knowledge of physical chemistry, biology, anatomy, physiology and genetics: A tale of "bottom-up" vs "top-down" recognition . *Drug Metab Pharmacokinet* **24**:53–75.

Jamwal R, Barlock BJ, Adusumalli S, Ogasawara K, Simons BL, and Akhlaghi F (2017) Multiplex and Label-Free Relative Quantification Approach for Studying Protein Abundance of Drug Metabolizing Enzymes in Human Liver Microsomes Using SWATH-MS. *J Proteome Res* **16**:4134–4143.

Jiang X-L, Zhao P, Barrett JS, Lesko LJ, and Schmidt S (2013) Application of Physiologically Based Pharmacokinetic Modeling to Predict Acetaminophen Metabolism and Pharmacokinetics in Children. *CPT Pharmacometrics Syst Pharmacol* **2**:e80.

Johnson TN, Zhou D, and Bui KH (2014) Development of physiologically based pharmacokinetic model to evaluate the relative systemic exposure to quetiapine after administration of IR and XR formulations to adults, children and adolescents. *Biopharm Drug Dispos* **35**:341–352.

Jones HM, Chen Y, Gibson C, Heimbach T, Parrott N, Peters SA, Snoeys J, Upreti V V., Zheng M, and Hall SD (2015) Physiologically based pharmacokinetic modeling in drug discovery and development: a pharmaceutical industry perspective. *Clin Pharmacol Ther* **97**:247–262.

Jones HM, and Rowland-Yeo K (2013) Basic Concepts in Physiologically Based Pharmacokinetic Modeling in Drug Discovery and Development. *CPT Pharmacometrics Syst Pharmacol* **2**:e63.

Kamiie J, Ohtsuki S, Iwase R, Ohmine K, Katsukura Y, Yanai K, Sekine Y, Uchida Y, Ito S, and Terasaki T (2008) Quantitative Atlas of membrane transporter proteins: Development and application of a highly sensitive simultaneous LC/MS/MS method combined with novel in-silico peptide selection criteria. *Pharm Res* **25**:1469–1483.

Kawakami H, Ohtsuki S, Kamiie J, Suzuki T, Abe T, and Terasaki T (2011) Simultaneous absolute quantification of 11 cytochrome P450 isoforms in human liver microsomes by liquid chromatography tandem mass spectrometry with In silico target peptide selection. *J Pharm Sci* **100**:341-352.

Ke AB, Nallani SC, Zhao P, Rostami-Hodjegan A, Isoherranen N, and Unadkat JD (2013) A Physiologically Based Pharmacokinetic Model to Predict Disposition of CYP2D6 and CYP1A2 Metabolized Drugs in Pregnant Women. *Drug Metab Dispos* **41**:801–813.

Ke AB, Nallani SC, Zhao P, Rostami-Hodjegan A, and Unadkat JD (2014) Expansion of a PBPK model to predict disposition in pregnant women of drugs cleared via multiple CYP enzymes, including CYP2B6, CYP2C9 and CYP2C19. *Br J Clin Pharmacol* **77**:554–570.

Keller A, Bader SL, Kusebauch U, Shteynberg D, Hood L, and Moritz RL (2016) Opening a SWATH Window on Posttranslational Modifications: Automated Pursuit of Modified Peptides. *Mol Cell Proteomics* **15**:1151–1163.

Kettenbach AN, Rush J, and Gerber SA (2011) Absolute quantification of protein and post-translational modification abundance with stable isotope–labeled synthetic peptides. *Nat Protoc* **6**:175–186.

Kim YJ, Gallien S, El-Khoury V, Goswami P, Sertamo K, Schlesser M, Berchem G, and Domon B (2015) Quantification of SAA1 and SAA2 in lung cancer plasma using the isotype-specific PRM assays. *Proteomics* **15**:3116–3125.

Kirkpatrick DS, Gerber SA, and Gygi SP (2005) The absolute quantification strategy: a general procedure for the quantification of proteins and post-translational modifications. *Methods* **35**:265–273.

Kirouac DC (2018) How Do We "Validate" a QSP Model? *CPT Pharmacometrics Syst Pharmacol* **7**:547–548.

Kirouac DC, Lahdenranta J, Du J, Yarar D, Onsum MD, Nielsen UB, and McDonagh CF (2015) Model-Based Design of a Decision Tree for Treating HER2+ Cancers Based on Genetic and Protein Biomarkers. *CPT pharmacometrics Syst Pharmacol* **4**:e00019.

Kito K, Ota K, Fujita T, and Ito T (2007) A synthetic protein approach toward accurate mass spectrometric quantification of component stoichiometry of multiprotein complexes. *J Proteome Res* **6**:792–800.

Kitteringham NR, Jenkins RE, Lane CS, Elliott VL, and Park BK (2009) Multiple reaction monitoring for quantitative biomarker analysis in proteomics and metabolomics. *J Chromatogr B* **877**:1229–1239.

Knights KM, Spencer SM, Fallon JK, Chau N, Smith PC, and Miners JO (2016) Scaling factors for the in vitro - in vivo extrapolation (IV-IVE) of renal drug and xenobiotic glucuronidation clearance. *Br J Clin Pharmacol* **81**:1153–1164.

Kumar V, Prasad B, Patilea G, Gupta A, Salphati L, Evers R, Hop CECA, and Unadkat JD (2015) Quantitative transporter proteomics by liquid chromatography with tandem mass spectrometry: Addressing methodologic issues of plasma membrane isolation and expression-activity relationship. *Drug Metab Dispos* **43**:284–288.

Kumar V, Salphati L, Hop CECA, Xiao G, Lai Y, Mathias A, Chu X, Humphreys WG, Liao M, Heyward S, and Unadkat JD (2019) A Comparison of Total and Plasma Membrane Abundance of Transporters in Suspended, Plated, Sandwich-Cultured Human Hepatocytes Versus Human Liver Tissue Using Quantitative Targeted Proteomics and Cell Surface Biotinylation. *Drug Metab Dispos* **47**:350–357.

Kumar V, Yin J, Billington S, Prasad B, Brown CDA, Wang J, and Unadkat JD (2018) The Importance of Incorporating OCT2 Plasma Membrane Expression and Membrane Potential in IVIVE of Metformin Renal Secretory Clearance. *Drug Metab Dispos* **46**:1441–1445.

Kurokawa N, Kishimoto T, Tanaka K, Kondo J, Takahashi N, and Miura Y (2019) New approach to evaluating the effects of a drug on protein complexes with quantitative proteomics, using the SILAC method and bioinformatic approach. *Biosci Biotechnol Biochem* **83**:2034-2048.

Ladumor MK, Bhatt DK, Gaedigk A, Sharma S, Thakur A, Pearce RE, Leeder JS, Bolger MB, Singh S, and Prasad B (2019) Ontogeny of Hepatic Sulfotransferases (SULTs) and Prediction of Age-Dependent Fractional Contribution of Sulfation in Acetaminophen Metabolism. *Drug Metab Dispos* **47**:818-831.

Langenfeld E, Zanger UM, Jung K, Meyer HE, and Marcus K (2009) Mass spectrometry-based absolute quantification of microsomal cytochrome P450 2D6 in human liver. *Proteomics* **9**:2313–23.

Leeder JS, and Meibohm B (2016) Challenges and opportunities for increasing the knowledge base related to drug biotransformation and pharmacokinetics during growth and development. *Drug Metab Dispos* **44**:916–923.

Li R, Barton H, and Maurer T (2015) A Mechanistic Pharmacokinetic Model for Liver Transporter Substrates Under Liver Cirrhosis Conditions. *CPT Pharmacometrics Syst Pharmacol* **4**:338–349.

Linghu D, Guo L, Zhao Y, Liu Z, Zhao M, Huang L, and Li X (2017) iTRAQ-based quantitative proteomic analysis and bioinformatics study of proteins in pterygia. *Proteomics – Clin Appl* **11**:1600094.

Lu H, and Rosenbaum S (2014) Developmental pharmacokinetics in pediatric populations. *J Pediatr Pharmacol Ther* **19**:262–76.

Ludwig C, Gillet L, Rosenberger G, Amon S, Collins BC, and Aebersold R (2018) Data-independent acquisition-based SWATH-MS for quantitative proteomics: a tutorial. *Mol Syst Biol* **14**:e8126.

MacLeod AK, Fallon PG, Sharp S, Henderson CJ, Wolf CR, and Huang JT-J (2015) An enhanced in vivo stable isotope labeling by amino acids in cell culture (SILAC) model for quantification of drug metabolism enzymes. *Mol Cell Proteomics* **14**:750–60.

Margaillan G, Rouleau M, Fallon JK, Caron P, Villeneuve L, Turcotte V, Smith PC, Joy MS, and Guillemette C (2015) Quantitative profiling of human renal UDP-glucuronosyltransferases and glucuronidation activity: a comparison of normal and tumoral kidney tissues. *Drug Metab Dispos* **43**:611–9.

Marsousi N, Desmeules JA, Rudaz S, and Daali Y (2017) Usefulness of PBPK Modeling in Incorporation of Clinical Conditions in Personalized Medicine. *J Pharm Sci* **106**:2380–2391.

Mehrotra A, Boberg M, Vrana M, Gaedigk A, Pearce RE, Leeder S, and Prasad B (2015) Age-dependent Expression Analysis of Major Drug Metabolizing Enzymes in Human Liver. *FASEB J* **30**:713.11.

Meiqun C, Zifan G, Kehuan S, and Zhengzhi W (2011) Application of iTRAQ quantitative proteomics in identification of serum biomarkers in breast cancer, in *2011 4th International Conference on Biomedical Engineering and Informatics (BMEI)* pp 1658–1663, IEEE.

Melillo N, Darwich AS, Magni P, and Rostami-Hodjegan A (2019) Accounting for inter-correlation between enzyme abundance: a simulation study to assess implications on global sensitivity analysis within physiologically-based pharmacokinetics. *J Pharmacokinet Pharmacodyn* **46**:137–154.

Merrill AE, Hebert AS, MacGilvray ME, Rose CM, Bailey DJ, Bradley JC, Wood WW, El Masri M, Westphall MS, Gasch AP, and Coon JJ (2014) NeuCode labels for relative protein quantification. *Mol Cell Proteomics* **13**:2503–12.

Michalski A, Cox J, and Mann M (2011) More than 100,000 detectable peptide species elute in single shotgun proteomics runs but the majority is inaccessible to data-dependent LC-MS/MS. *J Proteome Res* **10**:1785–93.

Michelet R, Van Bocxlaer J, Allegaert K, and Vermeulen A (2018) The use of PBPK modeling across the pediatric age range using propofol as a case. *J Pharmacokinet Pharmacodyn* **45**:765–785.

Miller NA, Reddy MB, Heikkinen AT, Lukacova V, and Parrott N (2019) Physiologically Based Pharmacokinetic Modelling for First-In-Human Predictions: An Updated Model Building Strategy Illustrated with Challenging Industry Case Studies. *Clin Pharmacokinet* **58**:727–746.

Mirzaei H, McBee JK, Watts J, and Aebersold R (2008) Comparative evaluation of current peptide production platforms used in absolute quantification in proteomics. *Mol Cell Proteomics* **7**:813–23.

Mooij MG, van de Steeg E, van Rosmalen J, Windster JD, de Koning BAE, Vaes WHJ, van Groen BD, Tibboel D, Wortelboer HM, and de Wildt SN (2016) Proteomic Analysis of the Developmental Trajectory of Human Hepatic Membrane Transporter Proteins in the First Three Months of Life. *Drug Metab Dispos* **44**:1005–13.

Morales AG, Lachén-Montes M, Ibáñez-Vea M, Santamaría E, and Fernández-Irigoyen J (2017) Application of Isobaric Tags for Relative and Absolute Quantitation (iTRAQ) to Monitor Olfactory Proteomes During Alzheimer's Disease Progression. In *Current Proteomic Approaches Applied to Brain Function*, in pp 29-42.

Nakamura K, Hirayama-Kurogi M, Ito S, Kuno T, Yoneyama T, Obuchi W, Terasaki T, and Ohtsuki S (2016) Large-scale multiplex absolute protein quantification of drug-

metabolizing enzymes and transporters in human intestine, liver, and kidney microsomes by SWATH-MS: Comparison with MRM/SRM and HR-MRM/PRM. *Proteomics* **16**:2106–17.

Niu J, Straubinger RM, and Mager DE (2019) Pharmacodynamic Drug–Drug Interactions. *Clin Pharmacol Ther* **105**:1395–1406.

O'Dwyer D, Ralton LD, O'Shea A, and Murray GI (2011) The proteomics of colorectal cancer: identification of a protein signature associated with prognosis. *PLoS One* **6**:e27718.

Ogungbenro K, and Aarons L (2014) A physiologically based pharmacokinetic model for Valproic acid in adults and children. *Eur J Pharm Sci* **63**:45–52.

Ohtsuki S, Schaefer O, Kawakami H, Inoue T, Liehner S, Saito A, Ishiguro N, Kishimoto W, Ludwig-Schwellinger E, Ebner T, and Terasaki T (2012) Simultaneous Absolute Protein Quantification of Transporters, Cytochromes P450, and UDP-Glucuronosyltransferases as a Novel Approach for the Characterization of Individual Human Liver: Comparison with mRNA Levels and Activities. *Drug Metab Dispos* **40**:83–92.

Ong S-E, Blagoev B, Kratchmarova I, Kristensen DB, Steen H, Pandey A, and Mann M (2002) Stable isotope labeling by amino acids in cell culture, SILAC, as a simple and accurate approach to expression proteomics. *Mol Cell Proteomics* **1**:376–86.

Ong S-E, and Mann M (2005) Mass spectrometry-based proteomics turns quantitative. *Nat Chem Biol* **1**:252–262.

Oswald S (2018) Organic Anion Transporting Polypeptide (OATP) transporter expression, localization and function in the human intestine. *Pharmacol Ther* **195**:39-53.

Oswald S, Gröer C, Drozdzik M, and Siegmund W (2013) Mass spectrometry-based targeted proteomics as a tool to elucidate the expression and function of intestinal drug transporters. *AAPS J* **15**:1128–40.

Patel N, Wiśniowska B, Jamei M, and Polak S (2018) Real Patient and its Virtual Twin: Application of Quantitative Systems Toxicology Modelling in the Cardiac Safety Assessment of Citalopram. *AAPS J* **20**:6.

Peng K, Bacon J, Zheng M, Guo Y, and Wang MZ (2015) Ethnic variability in the expression of hepatic drug transporters: absolute quantification by an optimized targeted quantitative proteomic approach. *Drug Metab Dispos* **43**:1045–55.

Peterson AC, Russell JD, Bailey DJ, Westphall MS, and Coon JJ (2012) Parallel Reaction Monitoring for High Resolution and High Mass Accuracy Quantitative, Targeted Proteomics. *Mol Cell Proteomics* **11**:1475–1488.

Peterson MC, and Riggs MM (2015) FDA advisory meeting clinical pharmacology review

utilizes a quantitative systems pharmacology (QSP) model: A watershed moment? *CPT Pharmacometrics Syst Pharmacol* **4**:189–192.

Polasek TM, Patel F, Jensen BP, Sorich MJ, Wiese MD, and Doogue MP (2013) Predicted metabolic drug clearance with increasing adult age. *Br J Clin Pharmacol* **75**:1019–1028.

Polasek TM, Shakib S, and Rostami-Hodjegan A (2018) Precision dosing in clinical medicine: present and future. *Expert Rev Clin Pharmacol* **11**:743-746.

Prasad B, Achour B, Artursson P, Hop CECA, Lai Y, Smith PC, Barber J, Wisniewski JR, Spellman D, Uchida Y, Zientek MA, Unadkat JD, and Rostami-Hodjegan A (2019) Toward a Consensus on Applying Quantitative Liquid Chromatography-Tandem Mass Spectrometry Proteomics in Translational Pharmacology Research: A White Paper. *Clin Pharmacol Ther* **106**:525–543.

Prasad B, Bhatt DK, Johnson K, Chapa R, Chu X, Salphati L, Xiao G, Lee C, Hop CECA, Mathias A, Lai Y, Liao M, Humphreys WG, Kumer SC, and Unadkat JD (2018) Abundance of Phase 1 and 2 Drug-Metabolizing Enzymes in Alcoholic and Hepatitis C Cirrhotic Livers: A Quantitative Targeted Proteomics Study. *Drug Metab Dispos* **46**:943–952.

Prasad B, Evers R, Gupta A, Hop CECA, Salphati L, Shukla S, Ambudkar S V., and Unadkat JD (2013) Interindividual variability in hepatic organic anion-transporting polypeptides and P-glycoprotein (ABCB1) protein expression: quantification by liquid chromatography tandem mass spectroscopy and influence of genotype, age, and sex. *Drug Metab Dispos* **42**:78–88.

Prasad B, Gaedigk A, Vrana M, Gaedigk R, Leeder J, Salphati L, Chu X, Xiao G, Hop C, Evers R, Gan L, and Unadkat J (2016) Ontogeny of Hepatic Drug Transporters as Quantified by LC-MS/MS Proteomics. *Clin Pharmacol Ther* **100**:362–370.

Prasad B, Johnson K, Billington S, Lee C, Chung GW, Brown CDA, Kelly EJ, Himmelfarb J, and Unadkat JD (2016) Abundance of Drug Transporters in the Human Kidney Cortex as Quantified by Quantitative Targeted Proteomics. *Drug Metab Dispos* **44**:1920–1924.

Prasad B, and Unadkat JD (2014) Comparison of Heavy Labeled (SIL) Peptide versus SILAC Protein Internal Standards for LC-MS/MS Quantification of Hepatic Drug Transporters. *Int J Proteomics* **2014**:451510, Hindawi Publishing Corporation.

Prasad B, Vrana M, Mehrotra A, Johnson K, and Bhatt DK (2017) The Promises of Quantitative Proteomics in Precision Medicine.

Ronsein GE, Pamir N, von Haller PD, Kim DS, Oda MN, Jarvik GP, Vaisar T, and Heinecke JW (2015) Parallel reaction monitoring (PRM) and selected reaction monitoring (SRM)

exhibit comparable linearity, dynamic range and precision for targeted quantitative HDL proteomics. *J Proteomics* **113**:388–399.

Ross PL, Huang YN, Marchese JN, Williamson B, Parker K, Hattan S, Khainovski N, Pillai S, Dey S, Daniels S, Purkayastha S, Juhasz P, Martin S, Bartlet-Jones M, He F, Jacobson A, and Pappin DJ (2004) Multiplexed Protein Quantitation in *Saccharomyces cerevisiae* Using Amine-reactive Isobaric Tagging Reagents. *Mol Cell Proteomics* **3**:1154–1169.

Röst HL, Rosenberger G, Navarro P, Gillet L, Miladinoviä SM, Schubert OT, Wolski W, Collins BC, Malmström J, Malmström L, and Aebersold R (2014) OpenSWATH enables automated, targeted analysis of data-independent acquisition MS data. *Nat Biotechnol* **32**:219–223.

Rostami-Hodjegan A (2012) Physiologically based pharmacokinetics joined with in vitro-in vivo extrapolation of ADME: A marriage under the arch of systems pharmacology. *Clin Pharmacol Ther* **92**:50–61.

Rowland A, Ruanglertboon W, van Dyk M, Wijayakumara D, Wood LS, Meech R, Mackenzie PI, Rodrigues AD, Marshall J-C, and Sorich MJ (2019) Plasma extracellular nanovesicle (exosome)-derived biomarkers for drug metabolism pathways: a novel approach to characterize variability in drug exposure. *Br J Clin Pharmacol* **85**:216–226.

Rowland M, Lesko LJ, and Rostami-Hodjegan A (2015) Physiologically based pharmacokinetics is impacting drug development and regulatory decision making. *CPT Pharmacometrics Syst Pharmacol* **4**:313–315.

Russell MR, Achour B, McKenzie EA, Lopez R, Harwood MD, Rostami-Hodjegan A, and Barber J (2013) Alternative fusion protein strategies to express recalcitrant QconCAT proteins for quantitative proteomics of human drug metabolizing enzymes and transporters. *J Proteome Res* **12**:5934–5942.

Russell MR, Graham C, D'Amato A, Gentry-Maharaj A, Ryan A, Kalsi JK, Ainley C, Whetton AD, Menon U, Jacobs I, and Graham RLJ (2017) A combined biomarker panel shows improved sensitivity for the early detection of ovarian cancer allowing the identification of the most aggressive type II tumours. *Br J Cancer* **117**:666–674.

Russell MR, Walker MJ, Williamson AJK, Gentry-Maharaj A, Ryan A, Kalsi J, Skates S, D'Amato A, Dive C, Pernemalm M, Humphryes PC, Fourkala E-O, Whetton AD, Menon U, Jacobs I, and Graham RLJ (2016) Protein Z: A putative novel biomarker for early detection of ovarian cancer. *Int J Cancer* **138**:2984–2992.

Sager JE, Yu J, Ragueneau-Majlessi I, and Isoherranen N (2015) Physiologically Based Pharmacokinetic (PBPK) Modeling and Simulation Approaches: A Systematic Review of

Published Models, Applications, and Model Verification. *Drug Metab Dispos* **43**:1823–1837.

Sato Y, Nagata M, Kawamura A, Miyashita A, and Usui T (2012) Protein quantification of UDP-glucuronosyltransferases 1A1 and 2B7 in human liver microsomes by LC-MS/MS and correlation with glucuronidation activities. *Xenobiotica* **42**:823–829.

Sato Y, Nagata M, Tetsuka K, Tamura K, Miyashita A, Kawamura A, and Usui T (2014) Optimized methods for targeted peptide-based quantification of human uridine 59-diphosphate-glucuronosyltransferases in biological specimens using liquid chromatography-tandem mass spectrometry. *Drug Metab Dispos* **42**:885–889.

Schaefer O, Ohtsuki S, Kawakami H, Inoue T, Liehner S, Saito A, Sakamoto A, Ishiguro N, Matsumaru T, Terasaki T, and Ebner T (2012) Absolute quantification and differential expression of drug transporters, cytochrome P450 enzymes, and UDP-glucuronosyltransferases in cultured primary human hepatocytes. *Drug Metab Dispos* **40**:93–103.

Schiffmann C, Hansen R, Baumann S, Kublik A, Nielsen PH, Adrian L, von Bergen M, Jehmlich N, and Seifert J (2014) Comparison of targeted peptide quantification assays for reductive dehalogenases by selective reaction monitoring (SRM) and precursor reaction monitoring (PRM). *Anal Bioanal Chem* **406**:283–291.

Schilling B, MacLean B, Held JM, Sahu AK, Rardin MJ, Sorensen DJ, Peters T, Wolfe AJ, Hunter CL, MacCoss MJ, and Gibson BW (2015) Multiplexed, Scheduled, High-Resolution Parallel Reaction Monitoring on a Full Scan QqTOF Instrument with Integrated Data-Dependent and Targeted Mass Spectrometric Workflows. *Anal Chem* **87**:10222–10229.

Shawahna R, Uchida Y, Declèves X, Ohtsuki S, Yousif S, Dauchy S, Jacob A, Chassoux F, Daumas-Duport C, Couraud P-O, Terasaki T, and Scherrmann J-M (2011) Transcriptomic and Quantitative Proteomic Analysis of Transporters and Drug Metabolizing Enzymes in Freshly Isolated Human Brain Microvessels. *Mol Pharm* **8**:1332–1341.

Shi J, Wang X, Zhu H, Jiang H, Wang D, Nesvizhskii A, and Zhu H-J (2018) Determining Allele-Specific Protein Expression (ASPE) Using a Novel Quantitative Concatamer Based Proteomics Method. *J Proteome Res* **17**:3606–3612.

Shruthi B, Vinodhkumar P, and Selvamani M (2016) Proteomics: A new perspective for cancer. *Adv Biomed Res* **5**:67.

Silva JC, Denny R, Dorschel CA, Gorenstein M, Kass IJ, Li GZ, McKenna T, Nold MJ, Richardson K, Young P, and Geromanos S (2005) Quantitative proteomic analysis by

accurate mass retention time pairs. *Anal Chem* **77**:2187–2200.

Silva JC, Gorenstein M V., Li G-Z, Vissers JPC, and Geromanos SJ (2006) Absolute Quantification of Proteins by LCMSE: a virtue of parallel MS acquisition. *Mol Cell Proteomics* **5**:144–156.

Sjöström M, Ossola R, Breslin T, Rinner O, Malmström L, Schmidt A, Aebersold R, Malmström J, and Niméus E (2015) A Combined Shotgun and Targeted Mass Spectrometry Strategy for Breast Cancer Biomarker Discovery. *J Proteome Res* **14**:2807–2818.

Smith BJ, Martins-de-Souza D, and Fioramonte M (2019) A Guide to Mass Spectrometry-Based Quantitative Proteomics. *Methods in Molecular Biology* **1916**:3–39.

Srivastava A, and Creek DJ (2018) Discovery and Validation of Clinical Biomarkers of Cancer: a Review Combining Metabolomics and Proteomics. *Proteomics* **19**:1700448.

Starr AE, Deeke SA, Ning Z, Chiang CK, Zhang X, Mottawea W, Singleton R, Benchimol EI, Wen M, Mack DR, Stintzi A, and Figeys D (2017) Proteomic analysis of ascending colon biopsies from a paediatric inflammatory bowel disease inception cohort identifies protein biomarkers that differentiate Crohn's disease from UC. *Gut* **66**:1573–1583.

T'jollyn H, Snoeys J, Vermeulen A, Michelet R, Cuyckens F, Mannens G, Van Peer A, Annaert P, Allegaert K, Van Bocxlaer J, and Boussery K (2015) Physiologically Based Pharmacokinetic Predictions of Tramadol Exposure Throughout Pediatric Life: an Analysis of the Different Clearance Contributors with Emphasis on CYP2D6 Maturation. *AAPS J* **17**:1376–87.

Takemori N, Beynon RJ, Endo Y, Hurst JL, Tanaka Y, Gómez-Baena G, Harman VM, and Takemori A (2017) MEERCAT: Multiplexed Efficient Cell Free Expression of Recombinant QconCATs For Large Scale Absolute Proteome Quantification. *Mol Cell Proteomics* **16**:2169–2183.

Tan HT, Wu W, Ng YZ, Zhang X, Yan B, Ong CW, Tan S, Salto-Tellez M, Hooi SC, and Chung MCM (2012) Proteomic analysis of colorectal cancer metastasis: Stathmin-1 revealed as a player in cancer cell migration and prognostic marker. *J Proteome Res* **11**:1433–1445.

Templeton IE, Jones NS, and Musib L (2018) Pediatric Dose Selection and Utility of PBPK in Determining Dose. *AAPS J* **20**:31.

Tsamandouras N, Wendling T, Rostami-Hodjegan A, Galetin A, and Aarons L (2015) Incorporation of stochastic variability in mechanistic population pharmacokinetic models: handling the physiological constraints using normal transformations. *J Pharmacokinet*

Pharmacodyn **42**:349–73.

Tsuchida S, Satoh M, Kawashima Y, Sogawa K, Kado S, Sawai S, Nishimura M, Ogita M, Takeuchi Y, Kobyashi H, Aoki A, Kodera Y, Matsushita K, Izumi Y, and Nomura F (2013) Application of quantitative proteomic analysis using tandem mass tags for discovery and identification of novel biomarkers in periodontal disease. *Proteomics* **13**:2339–2350.

Uchida Y, Ohtsuki S, Katsukura Y, Ikeda C, Suzuki T, Kamiie J, and Terasaki T (2011) Quantitative targeted absolute proteomics of human blood-brain barrier transporters and receptors. *J Neurochem* **117**:333–45.

Uhlen M, Fagerberg L, Hallstrom BM, Lindskog C, Oksvold P, Mardinoglu A, Sivertsson A, Kampf C, Sjostedt E, Asplund A, Olsson I, Edlund K, Lundberg E, Navani S, Szigyarto CA-K, Odeberg J, Djureinovic D, Takanen JO, Hober S, Alm T, Edqvist P-H, Berling H, Tegel H, Mulder J, Rockberg J, Nilsson P, Schwenk JM, Hamsten M, von Feilitzen K, Forsberg M, Persson L, Johansson F, Zwahlen M, von Heijne G, Nielsen J, and Ponten F (2015) Tissue-based map of the human proteome. *Science (80-)* **347**:1260419–1260419.

Upreti V V, and Wahlstrom JL (2016) Meta-analysis of hepatic cytochrome P450 ontogeny to underwrite the prediction of pediatric pharmacokinetics using physiologically based pharmacokinetic modeling. *J Clin Pharmacol* **56**:266–83.

Välikangas T, Suomi T, and Elo LL (2017) A comprehensive evaluation of popular proteomics software workflows for label-free proteome quantification and imputation. *Brief Bioinform* **19**:1344–1355.

van Groen BD, van de Steeg E, Mooij MG, van Lipzig MMH, de Koning BAE, Verdijk RM, Wortelboer HM, Gaedigk R, Bi C, Leeder JS, van Schaik RHN, van Rosmalen J, Tibboel D, Vaes WH, and de Wildt SN (2018) Proteomics of human liver membrane transporters: A focus on fetuses and newborn infants. *Eur J Pharm Sci* **124**:217–227.

Venkatakrishnan K, von Moltke LL, Court MH, Harmatz JS, Crespi CL, and Greenblatt DJ (2000) Comparison between cytochrome P450 (CYP) content and relative activity approaches to scaling from cDNA-expressed CYPs to human liver microsomes: ratios of accessory proteins as sources of discrepancies between the approaches. *Drug Metab Dispos* **28**:1493–504.

Vildhede A, Karlgren M, Svedberg EK, Wisniewski JR, Lai Y, Norén A, and Artursson P (2014) Hepatic uptake of atorvastatin: influence of variability in transporter expression on uptake clearance and drug-drug interactions. *Drug Metab Dispos* **42**:1210–8.

Vildhede A, Mateus A, Khan EK, Lai Y, Karlgren M, Artursson P, and Kjellsson MC (2016)

Mechanistic Modeling of Pitavastatin Disposition in Sandwich-Cultured Human Hepatocytes: A Proteomics-Informed Bottom-Up Approach. *Drug Metab Dispos* **44**:505–516.

Vildhede A, Nguyen C, Erickson B, Kunz R, Jones R, Kimoto E, Bourbonais F, Rodrigues D, and Manthena V (2018) Comparison of proteomic quantification approaches for hepatic drug transporters: Multiplexed global quantitation correlates with targeted proteomic quantitation. *Drug Metab Dispos* **46**:692-696.

Vildhede A, Wiśniewski JR, Norén A, Karlgren M, and Artursson P (2015) Comparative Proteomic Analysis of Human Liver Tissue and Isolated Hepatocytes with a Focus on Proteins Determining Drug Exposure. *J Proteome Res* **14**:3305–3314.

Vrana M, Whittington D, Nautiyal V, and Prasad B (2017) Database of Optimized Proteomic Quantitative Methods for Human Drug Disposition-Related Proteins for Applications in Physiologically Based Pharmacokinetic Modeling. *CPT Pharmacometrics Syst Pharmacol* **6**:267–276.

Walsky RL, Bauman JN, Bourcier K, Giddens G, Lapham K, Negahban A, Ryder TF, Obach RS, Hyland R, and Goosen TC (2012) Optimized assays for human UDP-glucuronosyltransferase (UGT) activities: Altered alamethicin concentration and utility to screen for UGT inhibitors. *Drug Metab Dispos* **40**:1051–1065.

Walsky RL, and Obach RS (2004) Validated assays for human cytochrome P450 activities. *Drug Metab Dispos* **32**:647–660.

Wang H, Zhang H, Li J, Wei J, Zhai R, Peng B, Qiao H, Zhang Y, and Qian X (2015) A new calibration curve calculation method for absolute quantification of drug metabolizing enzymes in human liver microsomes by stable isotope dilution mass spectrometry. *Anal Methods* **7**:5934–5941.

Wang L, Collins C, Kelly EJ, Chu X, Ray AS, Salphati L, Xiao G, Lee C, Lai Y, Liao M, Mathias A, Evers R, Humphreys W, Hop CECACA, Kumer SC, and Unadkat JD (2016) Transporter expression in liver tissue from subjects with alcoholic or hepatitis C cirrhosis quantified by targeted quantitative proteomics. *Drug Metab Dispos* **44**:1752–1758.

Wang X, Shi J, and Zhu H-J (2019) Functional Study of Carboxylesterase 1 Protein Isoforms. *Proteomics* **19**:1800288.

Wegler C, Gaugaz FZ, Andersson TB, Wiśniewski JR, Busch D, Gröer C, Oswald S, Norén A, Weiss F, Hammer HS, Joos TO, Poetz O, Achour B, Rostami-Hodjegan A, Van De Steeg E, Wortelboer HM, and Artursson P (2017) Variability in Mass Spectrometry-based Quantification of Clinically Relevant Drug Transporters and Drug Metabolizing

Enzymes. *Mol Pharm* **14**:3142–3151.

Weiß F, Hammer HS, Klein K, Planatscher H, Zanger UM, Norén A, Wegler C, Artursson P, Joos TO, and Poetz O (2018) Direct Quantification of Cytochromes P450 and Drug Transporters—A Rapid, Targeted Mass Spectrometry-Based Immunoassay Panel for Tissues and Cell Culture Lysates. *Drug Metab Dispos* **46**:387–396.

Wetmore BA, and Merrick BA (2004) Invited Review: Toxicoproteomics: Proteomics Applied to Toxicology and Pathology. *Toxicol Pathol* **32**:619–642.

Whiteaker JR, Halusa GN, Hoofnagle AN, Sharma V, MacLean B, Yan P, Wrobel JA, Kennedy J, Mani DR, Zimmerman LJ, Meyer MR, Mesri M, Rodriguez H, Abbatiello SE, Boja E, Carr SA, Chan DW, Chen X, Chen J, Davies SR, Ellis MJC, Fenyö D, Hiltke T, Ketchum KA, Kinsinger C, Kuhn E, Liebler DC, Lin D, Liu T, Loss M, MacCoss MJ, Qian W-J, Rivers R, Rodland KD, Ruggles K V, Scott MG, Smith RD, Thomas S, Townsend RR, Whiteley G, Wu C, Zhang H, Zhang Z, and Paulovich AG (2014) CPTAC Assay Portal: a repository of targeted proteomic assays. *Nat Methods* **11**:703–704.

Wiese S, Reidegeld KA, Meyer HE, and Warscheid B (2007) Protein labeling by iTRAQ: a new tool for quantitative mass spectrometry in proteome research. *Proteomics* **7**:340–50.

Wiśniewski JR, and Mann M (2012) Consecutive Proteolytic Digestion in an Enzyme Reactor Increases Depth of Proteomic and Phosphoproteomic Analysis. *Anal Chem* **84**:2631–2637.

Wiśniewski JR, Ostasiewicz P, Duś K, Zielińska DF, Gnad F, and Mann M (2012) Extensive quantitative remodeling of the proteome between normal colon tissue and adenocarcinoma. *Mol Syst Biol* **8**.

Wiśniewski JR, Vildhede A, Norén A, and Artursson P (2016) In-depth quantitative analysis and comparison of the human hepatocyte and hepatoma cell line HepG2 proteomes. *J Proteomics* **136**:234–247.

Wiśniewski JR, Wegler C, and Artursson P (2019) Multiple-Enzyme-Digestion Strategy Improves Accuracy and Sensitivity of Label- and Standard-Free Absolute Quantification to a Level That Is Achievable by Analysis with Stable Isotope-Labeled Standard Spiking. *J Proteome Res* **18**:217–224.

Wiśniewski JR, Wegler C, and Artursson P (2016) Subcellular fractionation of human liver reveals limits in global proteomic quantification from isolated fractions. *Anal Biochem* **509**:82–88.

Wiśniewski JR, Zougman A, Nagaraj N, and Mann M (2009) Universal sample preparation method for proteome analysis. *Nat Methods* **6**:359–362.

Wortham M, Czerwinski M, He L, Parkinson A, and Wan YJY (2007) Expression of constitutive androstane receptor, hepatic nuclear factor 4α, and P450 oxidoreductase genes determines interindividual variability in basal expression and activity of a broad scope of xenobiotic metabolism genes in the human liver. *Drug Metab Dispos* **35**:1700–1710.

Xie C, Yan T, Chen J, Li X, Zou J, Zhu L, Lu L, Wang Y, Zhou F, Liu Z, and Hu M (2017) LC-MS/MS quantification of sulfotransferases is better than conventional immunogenic methods in determining human liver SULT activities: implication in precision medicine. *Sci Rep* **7**:3858.

Xu J, Patassini S, Rustogi N, Riba-Garcia I, Hale BD, Phillips AM, Waldvogel H, Haines R, Bradbury P, Stevens A, Faull RLM, Dowsey AW, Cooper GJS, and Unwin RD (2019) Regional protein expression in human Alzheimer's brain correlates with disease severity. *Commun Biol* **2**:43.

Yang LQ, Li SJ, Cao YF, Man XB, Yu WF, Wang HY, and Wu MC (2003) Different alterations of cytochrome P450 3A4 isoform and its gene expression in livers of patients with chronic liver diseases. *World J Gastroenterol* **9**:359–363.

Yoshida K, Budha N, and Jin JY (2017) Impact of physiologically based pharmacokinetic models on regulatory reviews and product labels: Frequent utilization in the field of oncology. *Clin Pharmacol Ther* **101**:597–602.

Yoshitake S, McKay-Daily M, Tanaka M, and Huang Z (2017) Quantification of Sulfotransferases 1A1 and 1A3/4 in Tissue Fractions and Cell Lines by Multiple Reaction Monitoring Mass Spectrometry. *Drug Metab Lett* **11**:35–47.

Zhang F, Xiao Y, and Wang Y (2017) SILAC-Based Quantitative Proteomic Analysis Unveils Arsenite-Induced Perturbation of Multiple Pathways in Human Skin Fibroblast Cells. *Chem Res Toxicol* **30**:1006–1014.

Zhang H-F, Wang H-H, Gao N, Wei J-Y, Tian X, Zhao Y, Fang Y, Zhou J, Wen Q, Gao J, Zhang Y-J, Qian X-H, and Qiao H-L (2016) Physiological Content and Intrinsic Activities of 10 Cytochrome P450 Isoforms in Human Normal Liver Microsomes. *J Pharmacol Exp Ther* **358**:83-93.

Zhao P, Vieira M de LT, Grillo JA, Song P, Wu T-C, Zheng JH, Arya V, Berglund EG, Atkinson AJ, Sugiyama Y, Pang KS, Reynolds KS, Abernethy DR, Zhang L, Lesko LJ, and Huang S-M (2012) Evaluation of Exposure Change of Nonrenally Eliminated Drugs in Patients With Chronic Kidney Disease Using Physiologically Based Pharmacokinetic Modeling and Simulation. *J Clin Pharmacol* **52**:91S–108S.

Zhou Y, Ingelman-Sundberg M, and Lauschke VM (2017) Worldwide Distribution of Cytochrome P450 Alleles: A Meta-analysis of Population-scale Sequencing Projects. *Clin Pharmacol Ther* **102**:688–700.

Zhu X, Shen X, Qu J, Straubinger RM, and Jusko WJ (2018) Multi-Scale Network Model Supported by Proteomics for Analysis of Combined Gemcitabine and Birinapant Effects in Pancreatic Cancer Cells. *CPT pharmacometrics Syst Pharmacol* **7**:549–561.

Chapter Three: Complementarity of MaxQuant and Progenesis in Identification of Drug-Metabolising Enzymes and Transporters in Human Liver

Declaration

Areti-Maria Vasilogianni, Eman El-Khateeb, Sarah Alrubia, Zubida M. Al-Majdoub, Narciso Couto, Brahim Achour, Amin Rostami-Hodjegan, and Jill Barber

The literature search, data analysis and writing of the manuscript were equally divided among the first three authors who share the first-authorship. The sample analysis was performed by Zubida M. Al-Majdoub and Narciso Couto. I also contributed to the study design, data interpretation and manuscript revision, along with all co-authors. I retained editorial control.

3.1 Abstract

Several software packages are available for the analysis of proteomic LC-MS/MS data, including commercial (e.g. Mascot/Progenesis LC-MS) and open access software (e.g. MaxQuant). In this study, Progenesis and MaxQuant were used to analyse the same data set from human liver microsomes (n = 23). Comparison focussed on the total number of peptides and proteins identified by the two packages. For the peptides exclusively identified by each software, distribution of peptide length, hydrophobicity, molecular weight, isoelectric point and score was compared. At the protein level, we focussed on drug-metabolising enzymes and transporters, by comparing the number of unique peptides detected by the two packages. On average, there was a 65% overlap in detected peptides, with surprisingly little consistency in the characteristics of peptides exclusively detected by each software. Generally, MaxQuant detected more peptides than Progenesis, and the additional peptides were short and had relatively poor scores. Progenesis-specific peptides tended to be more hydrophilic and basic relative to peptides detected only by MaxQuant. In conclusion, in order to maximise the use of MS datasets, we recommend processing with more than one software package. Together, Progenesis and MaxQuant provided excellent coverage, with a core of common peptides identified in a very robust way.

3.2 Introduction

Recent years have witnessed increased use of mass spectrometry-based proteomics for the identification and quantification of pharmacologically relevant proteins in different populations (Yan, Gao, et al., 2015; Yan, Lu, et al., 2015; Wegler et al., 2017; Billington et al., 2018; Prasad et al., 2018; Al-Majdoub et al., 2019). This powerful analytical technique allows characterisation of complex biological matrices (such as enriched fractions, cell culture lysates, tissue extracts, and biopsies) as well as quantification of specific proteins of special interest (Al Feteisi et al., 2015; Välikangas et al., 2017). A wide variety of mass spectrometry-based strategies are available, taking advantage of the technique's selectivity, sensitivity and ability to detect many proteins simultaneously (Pan et al., 2009; Aebersold and Mann, 2016).

Drug metabolising enzymes (DMEs), such as cytochrome P450 (CYP450) (Kawakami et al., 2011; Ohtsuki et al., 2012; Achour et al., 2014; Li et al., 2015; Vildhede et al., 2015; Wang et al., 2015; Zhang et al., 2016; Achour, Dantonio, et al., 2017; Couto et al., 2020) and uridine 5'-diphospho-glucuronosyltransferase (UGT) enzymes, have received significant attention in recent years owing to their role in determining the kinetics of the majority of drugs on the market (Wienkers and Heath, 2005). However, even with recent advances in technology, measuring UGT enzymes remains challenging because of their membrane topology and high sequence homology (Harwood et al., 2016). Similarly, transporters are difficult to quantify because of low abundance and membrane localization, and therefore their characterization requires enrichment of plasma membrane fractions and the use of highly sensitive instrumentation (Achour, Al-Majdoub, et al., 2020).

The increased availability of data, however, has highlighted inter-laboratory and inter-methodological variation in quantification (Wegler et al., 2017). There is no simple relationship between the size of a mass spectrometry signal and the concentration of analyte. Worse, the LC-MS/MS workflow does not normally sample every available peptide but selects the most intense signals at any time point. Quantification of DMEs and transporters is important – it provides numbers used in silico to represent patients in virtual clinical trials (Rostami-Hodjegan, 2012; Jamei, 2016; Sharma et al., 2020). The community therefore assembled in September 2018 to address best practice in proteomic analysis and quantification methods, resulting in a white paper (Prasad et al., 2019).

Differences in quantification can arise from differences in sample preparation (Bhatt and Prasad, 2018; Howard et al., 2018), quantification methodology (Gillet et al., 2016; Bhatt and Prasad, 2018), including whether measurement is targeted or untargeted (Prasad et al., 2013;

Wegler et al., 2017; Couto et al., 2019), LC-MS/MS parameters and instrumentation, even when the sample is the same. In practice, we are not especially interested in measuring the same sample because biological differences between samples are the main subject of our investigations. Multivariate statistical techniques, such as principal components analysis (PCA), have been used to discern biological and technical variation within groups of samples (Jehmlich et al., 2013; Howard et al., 2018; Leoni et al., 2019) but are of limited utility in assessing cross-laboratory measurements.

At this stage, strategies for overcoming these differences would inevitably involve many replicate analyses, which are at best costly, and often impossible where samples are small and of human origin. There is, however, less excuse for differences in quantification resulting from data analysis. The commonly used data analysis tools, required to convert RAW data files into quantification of proteins, have different algorithms that can generate variable results, and one useful idea is to assess their complementarity. Comparative reports for different data analysis tools have been generated (Table 3-1) with varied conclusions. A single 2012 study sought to compare data processing using complex samples from animal retinas, concluding that the total number of proteins identified by MaxQuant and Progenesis is highly comparable (74% overlap) (Merl et al., 2012). Another study using five different data analysis tools to identify potato and human synthetic peptides concluded that MaxQuant achieved the highest peptide coverage based on charge-state merging, while Progenesis was the best based on the obtained original data, as a result of all alignment feature and normalization before LC-MS/MS (Chawade et al., 2015). Comparison of different tools using a plant-derived standard proteins mix demonstrated high variability in protein abundance measured by the different tools, suggesting caution should be applied with discovery proteomics data (Al Shweiki et al., 2017). Finally, a study using Universal Proteomics Standard Set and yeast concluded that Progenesis performed consistently well in differential expression analysis and produced few missing intensity values, whereas data filtering or imputation methods improved the performance of MaxQuant, Proteios, PEAKS, and OpenMS (Välikangas et al., 2017).

In the present work, we analysed a dataset obtained by analysing 23 human liver membrane samples using two widely used software packages, MaxQuant and Progenesis, commonly used for peptide/protein identification and quantification. MaxQuant (Cox and Mann, 2008; Cox et al., 2014) uses its own search engine, Andromeda, for identification, which relies on a probability calculation for scoring a peptide-spectrum match (Neuhauser et al., 2011). Quantification of proteins is based on maximum peptide ratio information from extracted peptide ion signal intensities. These are normalised to minimise the overall fold change of all

peptides across all fractions (Al Shweiki et al., 2017). Progenesis uses Mascot for identification (Perkins et al., 1999) and quantifies proteins based on peptide ion peak intensity while allowing full operator control (Al Shweiki et al., 2017).

Table 3-1 A summary of previous investigations that compared data analysis software and the outcomes compared.

Study	Sample	Compared software	Analysis technique (instrument)	Outcomes compared
Merl et al. 2012	Retinal cells (healthy animals)	Progenesis MaxQuant	Label free versus SILAC (Orbitrap)	Quantification accuracy Dynamic range Sensitivity
Chawade et al. 2015	Synthetic peptides (potato and human)	Progenesis MaxQuant Proteios Skyline Anubis	DDA and SRM (Orbitrap XL ETD)	Peptide coverage F1-Score (harmonic mean of precision and sensitivity) Mean accuracy (proportion of true positive and negative identifications) Number of unique peptides
Välikangas et al. 2017	Universal Proteomics Standard Set and yeast *Saccharomyces cerevisiae*	Progenesis MaxQuant Proteios PEAKS OpenMS	DDA (Orbitrab Velos)	The number of proteins quantified The extent of missing data
Al Shweiki et al. 2017	Standard Proteins mix (plant)	Proteome Discoverer Scaffold MaxQuant Progenesis	DDA (Orbitrap Velos)	Biological variability Protein abundance estimates Protein fold change

DDA, Data dependent acquisition; SRM, Selected reaction monitoring; SILAC, Stable isotope labelling by amino acids in cell culture.

3.3 Materials and methods

3.3.1 Dataset

The dataset analysed in this study was previously generated by Couto et al. (Couto et al., 2019) using 23 human liver microsomes (HLM) samples provided by Pfizer (Groton, CT, USA). Suppliers of these samples were Vitron (Tucson, AZ, USA) and BD Gentest (San Jose, CA, USA). Demographic details, sample preparation, LC-MS/MS analysis workflow and data analysis were reported previously (Couto et al., 2019). The primary goal for which these data were generated is to evaluate the expression of proteins responsible for the metabolism and transport of drugs and xenobiotic in human liver (Couto et al., 2019).

3.3.2 Database Fasta file

UniProtKB human proteome fasta file containing 71599 entries (May 2017) was used for analysis by both Progenesis and MaxQuant (Bateman et al., 2017).

3.3.3 Data processing

Data analysis was performed using MaxQuant 1.6.1.0 (Max Planck Institute of Biochemistry, Munich, Germany) and Progenesis QI 4.0 (Nonlinear Dynamics, Newcastle-upon-Tyne, UK). Replicates (two of each sample) were analysed in the same batch. Progenesis LC-MS takes raw data of the MS/MS scans and transforms them to peak lists. One sample was selected as a reference after checking the two-dimensional mapping (m/z versus retention time), and the retention times of the other samples within the batch were aligned. The 2D map uses as visual quality control and highlights any problems in a sample run. Default peak-picking settings were used and the resulting aggregate spectra were filtered to include + 2, and + 3 charge states only. These aligned spectra contain all peak information, allowing the detection of all ions. An .mgf file representing the aggregate spectra was exported and searched for peptide identification using in-house Mascot server (Matrix Science, London, UK) using human SwissProt and Tremble databases containing 75,004 protein sequences. Search parameters used were: 5 ppm precursor mass tolerance, 0.5 Da fragment mass tolerance, cysteine carbamidomethylation was set as fixed modification, M oxidation, NQ deamidation, label 13C(6) (K), label 13C(6) were used as variable modifications. Trypsin/P was set as the proteolytic enzyme, and one missed

cleavage was allowed (for more details on Progenesis and Mascot processing see (Couto et al., 2019)). The resulting .xml file was re-imported to assign peptides to features using the following thresholds: Mascot determined peptides with ion scores of 15 and above and only proteins with at least one unique peptide ranked as top candidate were considered and re-imported into Progenesis. Maximum number of hits was set to "AUTO" to ensure only statistically significant and high-quality identification is applied. Mascot scores corresponding to a false discovery rate (FDR) of <0.01 was set as a threshold for peptide identification. FDR of <0.01 was also used for protein-level identification. Quantitative analysis was carried out using the "Hi3" intensity-based method on Progenesis as previously described (Al-Majdoub et al., 2019). The reference protein, in this case bovine serum albumin (BSA), was assigned at a known amount. Knowing the spiked amount of BSA and the accession number, abundance of all proteins in the sample was quantified from Progenesis output.

The parameters applied in MaxQuant were changed from default to match their counterparts in Progenesis and Mascot as presented in Table 3-2. Full details of all the parameter settings used for MaxQuant are listed in Supplementary Table 3-1. No filters were applied for the scores in data processing and cut-off scores were applied manually after exporting the data.

Table 3-2 Processing parameters applied in MaxQuant and Progenesis.

Parameter description	Parameter setting
Label free quantification	Yes
Multiplicity	1
Digestion Enzyme	Trypsin/P
Variable Modifications	Oxidation (M) & Deamidation (NQ)
Fixed modifications	Carbamidomethyl (C)
Max number of modifications per peptide	11
Max charge	7
Main search peptide tolerance	5 ppm
Min pep length	7
Min pep length for unspecific	70
Max peptide mass [Da]	6000 Da
Peptides for quantification	Unique + razor
MS/MS match tolerance	0.5 Da
False discovery rate (FDR)	1%

3.3.4 Comparison of peptides identified by MaxQuant and Progenesis

The comparison aimed to identify the differences between performance of the two software tools in terms of the number, nature and identity of identified peptides.

3.3.4.1 Peptide score correlation between software tools

Using Smallvoice v1.0, an in-house tool for sorting assessment data (Ellis and Barber, 2016), peptides detected by the two software tools were combined in one sheet with their corresponding scores (MaxQuant score, Progenesis score, or both in cases of overlap). Linear regression analysis (using Excel 2016) was applied to correlate MaxQuant and Progenesis peptide scores for each sample independently, yielding an equation in the form y = m x, where y represents the Progenesis score and x represents the MaxQuant score. All peptides with MaxQuant scores below 40 were disregarded, as were the equivalent Progenesis peptides.

3.3.4.2 Numbers and sequences of peptides

Sequences of peptides above the threshold scores were collated for each software, and from these data, the total number of peptides identified by either MaxQuant, Progenesis or both were calculated.

3.3.4.3 Correlation of peptide signal intensities between software tools

The signal intensities generated by the two tools were correlated in the same way as the scores, yielding for each sample regression equations in the form y = m x. This was used to assess reproducibility of quantification across software.

3.3.4.4 Characteristics of identified software-specific peptides

Software-specific peptides (i.e. peptides only detected by a single package) were characterised to identify the effect of algorithm differences on preferentially identified peptides. Lengths, scores and number of modifications were calculated in Excel. Hydrophobicity/hydrophilicity of each peptide was calculated using GRAVY score calculator (http://www.gravy-calculator.de/index.php) and isoelectric points were estimated using http://isoelectric.org/index.html. Unpaired student's *t*-test was used to determine differences between means of the estimated characteristics of the peptides.

3.3.4.5 Calculation of percentage identical peptides

As an indicator of reproducibility, the quality control parameter 'percentage identical peptides' (PIP) was calculated (Al Feteisi et al., 2018) both between samples for the two processing packages. Of particular interest were PIP values for the same samples processed by MaxQuant and Progenesis. Principal components analysis (PCA) was performed on R 3.5.1 using PIP values to assess proteome-wide similarity data across the 23 samples.

3.3.5 Comparison at the protein level

All peptide sequences were matched against UniProt human proteome database, and accordingly each peptide was assigned to a certain human protein. The numbers of samples, in which a specific protein (CYP, UGT, or transporter) was identified based on unique peptides by each software, were counted and compared. In order to assign the detected peptides to appropriate human proteins, the following approach was applied:

- All peptides were matched against the UniProt human proteome fasta file (May 2017) (The UniProt Consortium, 2019). Proteins were prioritised according to the following criteria: (a) full length proteins were preferred over cDNA; (b) characterised sequences were prioritised over uncharacterised ones; and (c) longer sequences of the same proteins were preferred over shorter ones. The final order was arranged alphabetically.
- The remaining peptides that did not match any protein were deleted. Single peptides that appeared in two or fewer samples and did not appear in the UniProt fasta file were also deleted.
- A best-fit analysis was then run to minimise the number of accession codes that account for all the peptides.

For each sample, the number of proteins identified with at least one unique or razor peptide by each software package was determined. The number of CYP450s, UGTs, ABC and SLC transporters were calculated separately. Percentage identical proteins (PIPr) was calculated for all pairs of results, both inter- and intra-sample.

3.3.6 Software availability and processing time

MaxQuant is as an open access cross-platform software available online from https://www.maxquant.org/, while Progenesis is a commercial software package provided by Waters Corporation (NYSE: WAT) and it requires a licence. The average time taken to process a sample was determined for both tools in hours and compared. MaxQuant processing time

includes only one step from the raw data to the processed Excel sheets, while Progenesis requires an additional step to generate and export the mgf file, which represents the post-alignment aggregate spectrum, then this file is searched using Mascot.

The raw files were processed by MaxQuant on personal computers that have the following specifications: Processor Intel® Core™ i7-6600U CPU @ 2.6 GHz; RAM 20 GB; 64-bit operating system; Windows 10. The computer used for Progenesis processing has the following specifications: Dell Precision T7600 Tower workstation; Processor 2x Intel Xeon-E5-2643 CPU @ 3.30 GHz; RAM 128 GB; 64-bit operating system; Windows 7.

3.4 Results

3.4.1 Comparison of peptide scores between Progenesis and MaxQuant

The scores of peptides identified by the two software packages were plotted against one another, as shown in Figure 3-1A for sample HLM76. Linear regression gave rise to a best fit equation in the form y = m x, with R^2 values (typically around 0.23 – 0.43) reflecting considerable scatter; peptide scores were far from consistent between the two software packages. Equations linking scores for all samples are shown in Supplementary Table 3-2. Peptides with scores below 40 in MaxQuant were disregarded and the corresponding cut-off scores in Progenesis were calculated according to these equations. For sample HLM76, the Progenesis cut-off score was 13.4. The average for all samples was 14.03, so a cut-off score of 14 for Progenesis could be used as an *ad hoc* equivalent to MaxQuant 40. Figure 3-1B depicts all the trend lines for all the samples. The red line represents the trend line for collated data from all samples. Equation 3-1 represents the fit of data from all of the samples, allowing a slope of 0.35 to be used in the general case.

$$Progenesis\ score = 0.3508 \times MaxQuant\ score \quad \text{(Equation 3-1)}$$

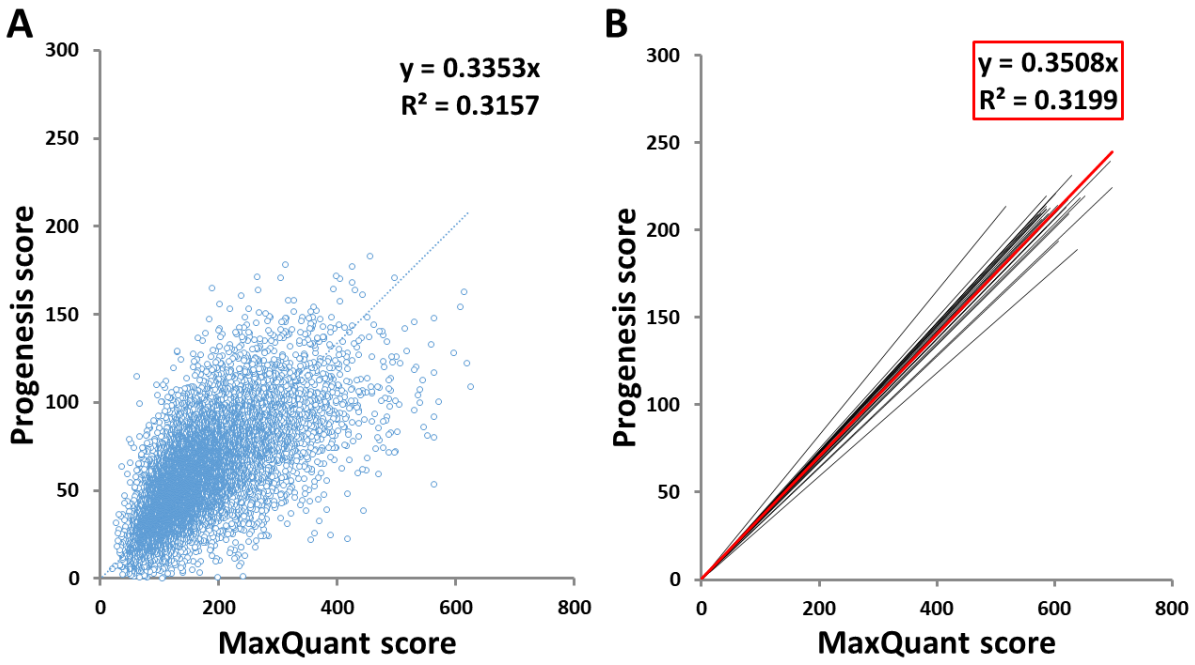

Figure 3-1 Linear regression of MaxQuant and Progenesis peptide scores. A representative linear regression analysis for one sample, HLM76, is shown (**A**), with the trend lines for the linear regression equations for each sample shown in black and for the collated data from all samples shown in red (**B**).

3.4.2 Total number of peptides and modified peptides

Prior to filtering, the total number of peptides identified by the two packages averaged 20736 for Progenesis and 17963 for MaxQuant (Supplementary Table 3-4). Filtering the data led to identification of 14870 (range 11490-16126) by Progenesis, compared with 17534 (range 15991-20129) by MaxQuant. The default parameters in MaxQuant have a cut-off for modified peptides of 40, and these are generally the peptides with the lowest scores. Modified peptides in this study represent peptides with asparagine/glutamine deamidation and/or methionine oxidation. Table 3-3 summarises the numbers of peptides detected by the two software packages after data filtering. There was from 52–72% overlap (65% on average) between the peptides detected by the two packages; 10% of the peptides identified by Progenesis were modified but only 6% of those identified by MaxQuant.

Sample HLM73 (and to a lesser extent HLM41) is an interesting case, with much higher levels of modification than the norm, identified by both software packages. It is not clear whether the high level of modification is the result of technical differences in handling the samples, or biological differences (for example in response to ageing).

Table 3-3 Comparison of the total number of peptides, peptides specific for each software and modified peptides as identified by MaxQuant and Progenesis. This comparison was done after removing the peptides with low scores.

Sample	MaxQuant *total peptides*	Progenesis *total peptides*	MaxQuant only *peptides*		Progenesis only *peptides*		Overlap		MaxQuant *modified*		Progenesis *modified*	
			Number	Percent	Number	Percent	Number	Percent	Number	Percent	Number	Percent
HLM01	15991	11490	3280	18%	2193	12%	12711	70%	673	4%	1337	9%
HLM02	20129	14838	7313	33%	2022	9%	12816	58%	1182	6%	1397	9%
HLM06	18343	14437	6092	30%	2186	11%	12251	60%	892	5%	1405	10%
HLM08	17563	15876	3906	20%	2219	11%	13657	69%	789	4%	1267	8%
HLM11	17509	15947	3931	20%	2369	12%	135784	68%	833	5%	1507	9%
HLM25	18421	15483	5407	26%	2469	12%	13014	62%	961	5%	1553	10%
HLM38	17480	16126	3735	19%	2381	12%	13745	69%	861	5%	1461	9%
HLM41	17335	14589	5076	26%	2330	12%	12259	62%	1338	8%	1828	13%
HLM48	17270	15113	4265	22%	2108	11%	13005	67%	910	5%	1343	9%
HLM71	16012	15644	2746	15%	2378	13%	13266	72%	786	5%	1522	10%
HLM72	16883	15406	3637	19%	2160	11%	13246	70%	829	5%	1425	9%
HLM73	16727	15225	3707	20%	2205	12%	13020	69%	2921	17%	3137	21%
HLM74	17828	14352	5691	28%	2215	11%	12137	61%	827	5%	1391	10%

HLM75	16447	15058	3537	19%	2148	12%	12910	69%	752	5%	1388	9%
HLM76	18744	14454	6447	31%	2157	10%	12297	59%	1006	5%	1431	10%
HLM77	16802	14847	3872	21%	1917	10%	12930	69%	907	5%	1285	9%
HLM78	18361	14256	6294	31%	2189	11%	12067	59%	987	5%	1457	10%
HLM80	16918	15075	4037	21%	2194	12%	12881	67%	758	4%	1365	9%
HLM89	17379	15941	3827	19%	2389	12%	13552	69%	1492	9%	2004	13%
HLM90	17071	12205	4009	20%	2731	14%	13062	66%	931	5%	1140	9%
HLM91	16812	15111	4045	21%	2344	12%	12767	67%	790	5%	1399	9%
HLM100	17722	15666	4334	22%	2278	11%	13388	67%	854	5%	1388	9%
HLM117	19535	14884	6998	32%	2347	11%	12537	57%	921	5%	1517	10%
Mean	**17534**	**14870**	**4617**	**23%**	**2258**	**11%**	**18231**	**65%**	**1009**	**6%**	**1519**	**10%**
SD	1027	1102	1273	5%	165	1%	25630	5%	458	3%	394	3%
CV	6%	7%	28%	23%	7%	8%	141%	7%	45%	47%	26%	26%

3.4.3 Correlation between intensities in MaxQuant and Progenesis

Good correlations were observed between intensities of peptide signals reported by MaxQuant and Progenesis, with each sample giving a relationship in the form y = m x, with average R^2 of 0.75 (Figure 3-2B). Although each sample had an independent linear regression equation (Figure 3-2A), intensities reported by MaxQuant were always higher than corresponding intensities reported by Progenesis. Individual regression equations for intensities for each individual sample are shown in Supplementary Table 3-3. The average trend line for all data was described by the equation below:

$$Progenesis\ intensity = 0.0149 \times MaxQuant\ intensity \quad \text{(Equation 3-2)}$$

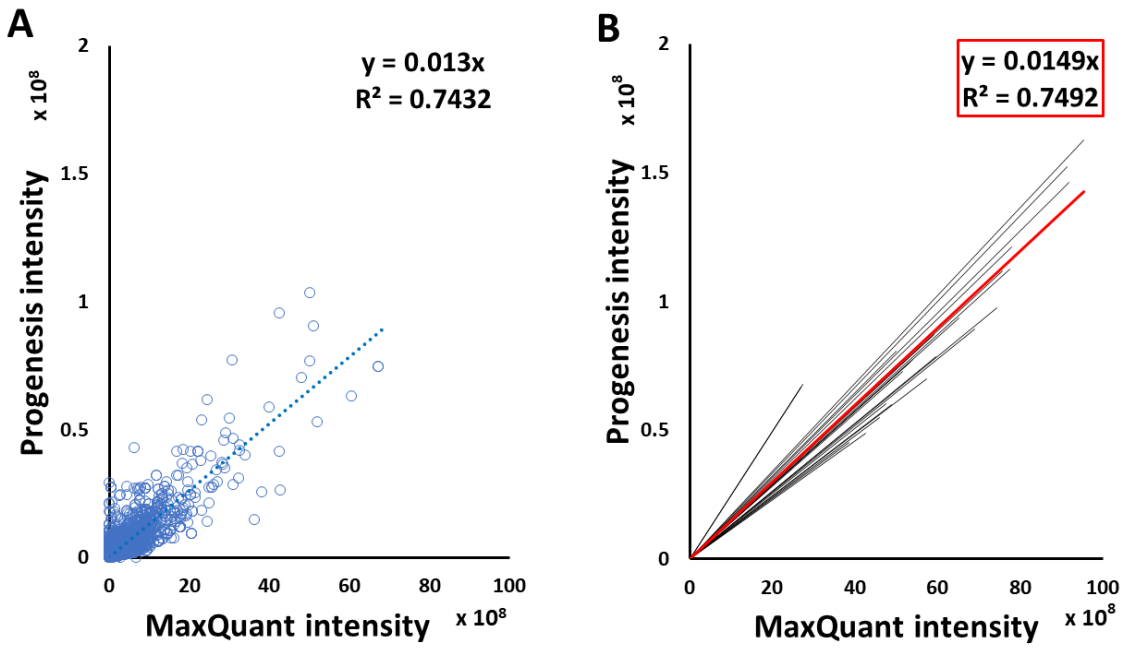

Figure 3-2 Linear regression of MaxQuant and Progenesis peptide signal intensities. A representative linear regression analysis for one sample, HLM76, is shown (**A**). The trend lines for the linear regression equations for each sample are shown in black and for the collated data from all samples shown in red (**B**).

3.4.5 Peptide characteristics

Several characteristics of the peptides detected by a single tool were now investigated, as these were thought to be indicative of any possible bias by the software algorithm. These are illustrated in Figure 3-3, using sample HLM76 as an example. Firstly, any bias towards long or short peptides was probed. The median and mode lengths of MaxQuant specific peptides (n=6447, non-Gaussian distribution) were 13 and 11, whereas median and mode lengths of Progenesis-specific peptides (n=2157, non-Gaussian distribution) were 13 and 7, showing that Progenesis favoured relatively shorter peptides. The scores of software-specific peptides were treated similarly. The ranges of median and mode scores of the MaxQuant specific peptides for all the samples were 74.6 to 199.7 and 46.5 to 367.2, whereas ranges of median and mode scores of the Progenesis-specific peptides were 23.9 to 53.1 and 13.6 to 88.6, which, when adjusted to be equivalent to the MaxQuant values (using equations in Supplementary Table 3-2) were 57.9 to 164.7 and 40.4 to 257.2 (Supplementary Table 3-7). Thus, MaxQuant detects a higher number of software-specific peptides with relatively greater confidence than Progenesis. The same trends were observed across all samples.

Figure 3-3C shows GRAVY scores for MaxQuant-specific and Progenesis-specific peptides; the more negative the value, the more hydrophilic the peptide. Each peptide is represented by a line starting from 0 on the y axis and ending either in the positive or the negative side of the y axis, depending on the actual value of hydrophobicity (GRAVY score). The median and mode GRAVY scores of the MaxQuant specific peptides in all samples ranged from –0.35 to 0.09 and from –0.7 to 0.4, respectively, whereas median and mode GRAVY scores of the Progenesis-specific peptides were ranging from –0.53 to –0.43 and from –0.9 to 0.1 (Supplementary Table 3-8). Therefore, the peptides identified by Progenesis (Figure 3-3C) had more negative GRAVY scores, indicating higher hydrophilicity than those identified solely by MaxQuant (Figure 3-3C).

Supplementary Table 3-5 provides an example of statistical analysis in relation to the peptide length, GRAVY score (hydrophobicity), isoelectric point (PI), and molecular weight of peptides from sample HLM76. Comparison of these characteristics showed that Progenesis-specific peptides were generally shorter, more hydrophilic, and more basic, with lower mass.

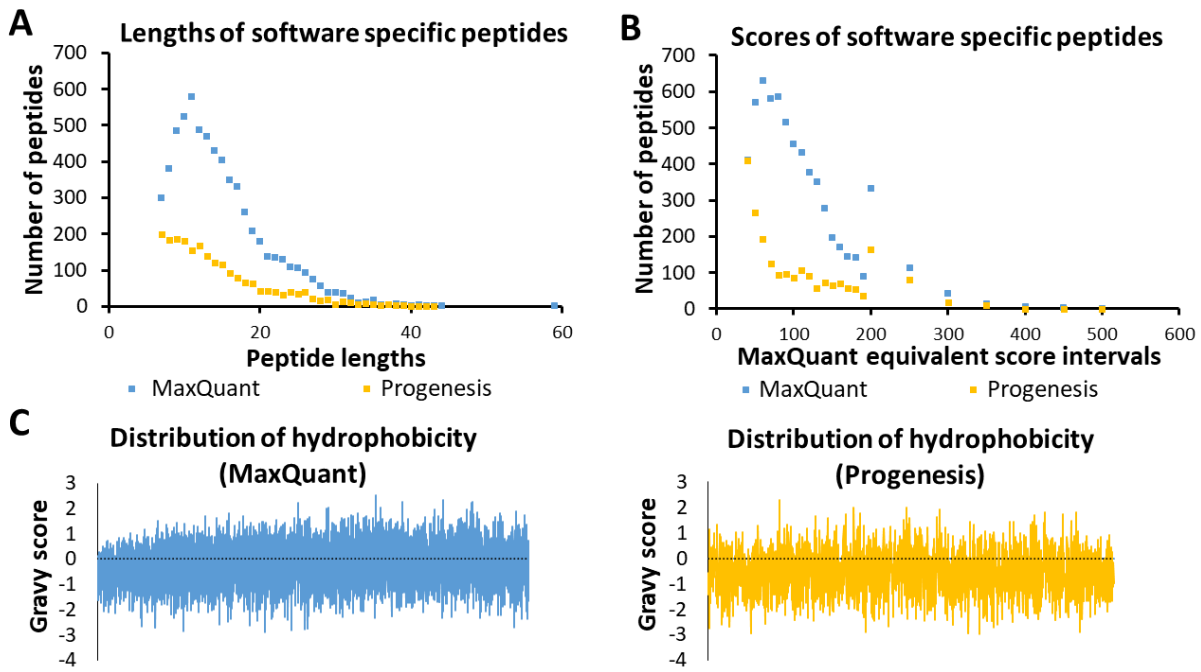

Figure 3-3 Characteristics of sample HLM76 peptides identified by the two software packages in terms of length (**A**), score (**B**) and hydrophobicity (**C**).

3.4.6 Multivariate analysis of peptide and protein data

PIP (percentage identical peptides) and PIPr (percentage identical proteins) were calculated between samples for each software package as previously described (Al Feteisi et al., 2018), and the results were analysed by principal components analysis (PCA). PCA results are presented in Figure 3-4. PCA on PIP and PIPr values returned two distinct clusters for each package. Clustering of PIP and PIPr data generated with Progenesis and MaxQuant were quite similar and the % variance explained by each dimension were almost identical. The clusters contained the same patient samples and the difference between PIP and PIPr (regardless of the software) was the outlier with PIP (sample HLM73) and PIPr (sample HLM2). Sample HLM73 is different at the peptide level possibly due to extensive modification as shown in Table 3-3. Importantly, PCA provides more information in relation to explained variance when technical and biological factors are tractable.

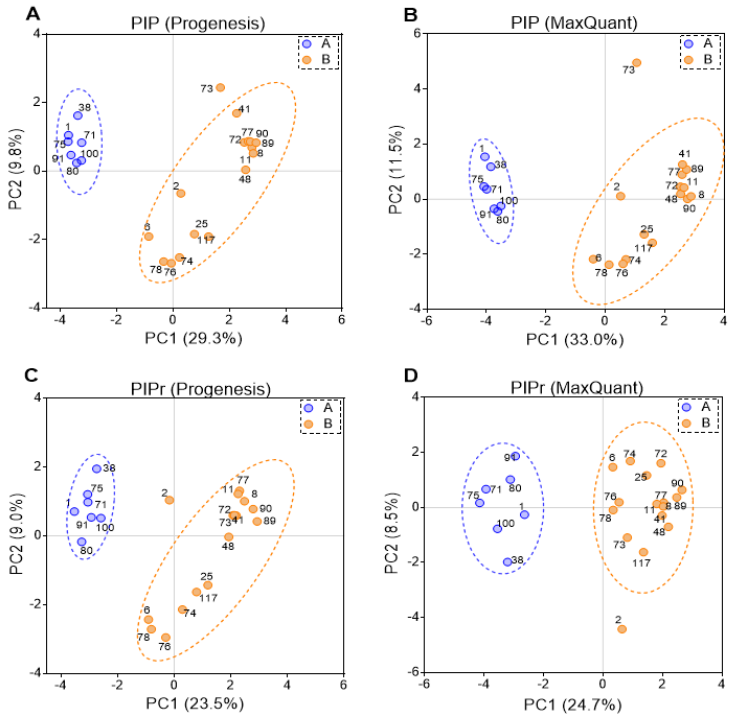

Figure 3-4 Principal components analysis (PCA) for 23 human liver samples based on percentage identical peptides (PIP) identified by Progenesis (**A**) and MaxQuant (**B**), and percentage identical proteins (PIPr) identified by Progenesis (**C**) and MaxQuant (**D**).

3.4.7 Drug-metabolising enzymes and transporters

We now focused on membrane proteins of particular interest in drug metabolism and disposition: CYPs, UGTs, ABC and SLC transporters. For each of these proteins, the number of samples in which the protein could be detected (with unique peptides) by each software package is shown in Supplementary Table 3-6. Figure 3-5, 3-6 and 3-7 shown the results for (CYP and UGT) enzymes, ABC transporters and SLCs, respectively. The more abundant proteins (for example, CYP3A4, UGT1A1, ABCD3, SLC3A1) were found in all 23 samples, regardless of the software. More interesting in the context of this paper are examples such as CYP1A1, CYP2F1, UGT1A7, ABCA2, and many SLC transporters which, in many samples, achieve a positive identification using one software package only (Figure 3-5, 3-6, 3-7). In these cases, the use of two software packages permits additional identification and higher coverage of important proteins relative to the use of a single package. However, these uniquely identified proteins require additional rigour to establish confidence in their identification. The most important cases are summarised in Table 3-4.

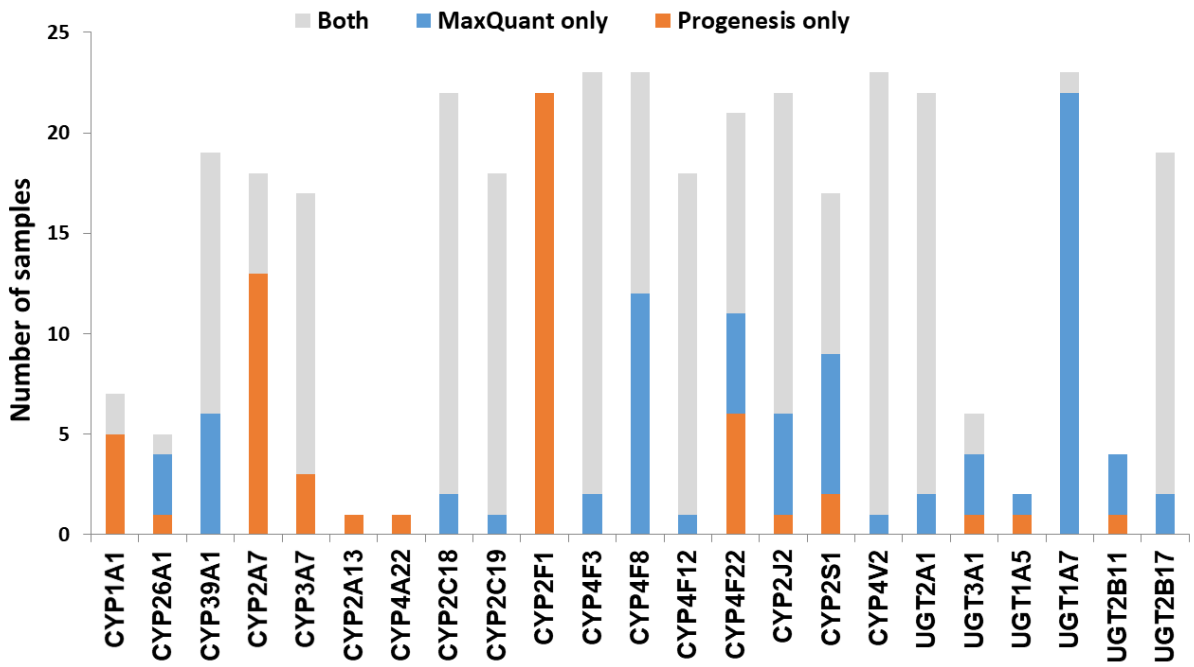

Figure 3-5 The number of samples in which CYPs and UGTs identified by each software tool. Other CYPs and UGTs that have been identified by both software (overlap) in all samples are not included.

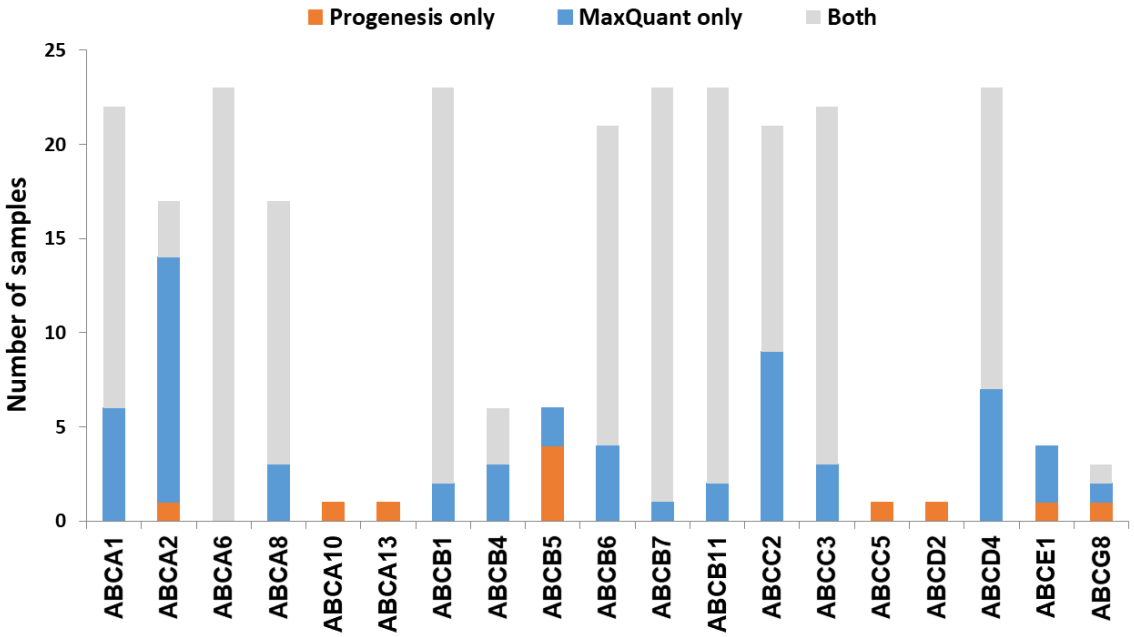

Figure 3-6 The number of samples in which ABC transporters were identified by each software tool. Other ABC transporters that have been identified by both software (overlap) in all samples are not included.

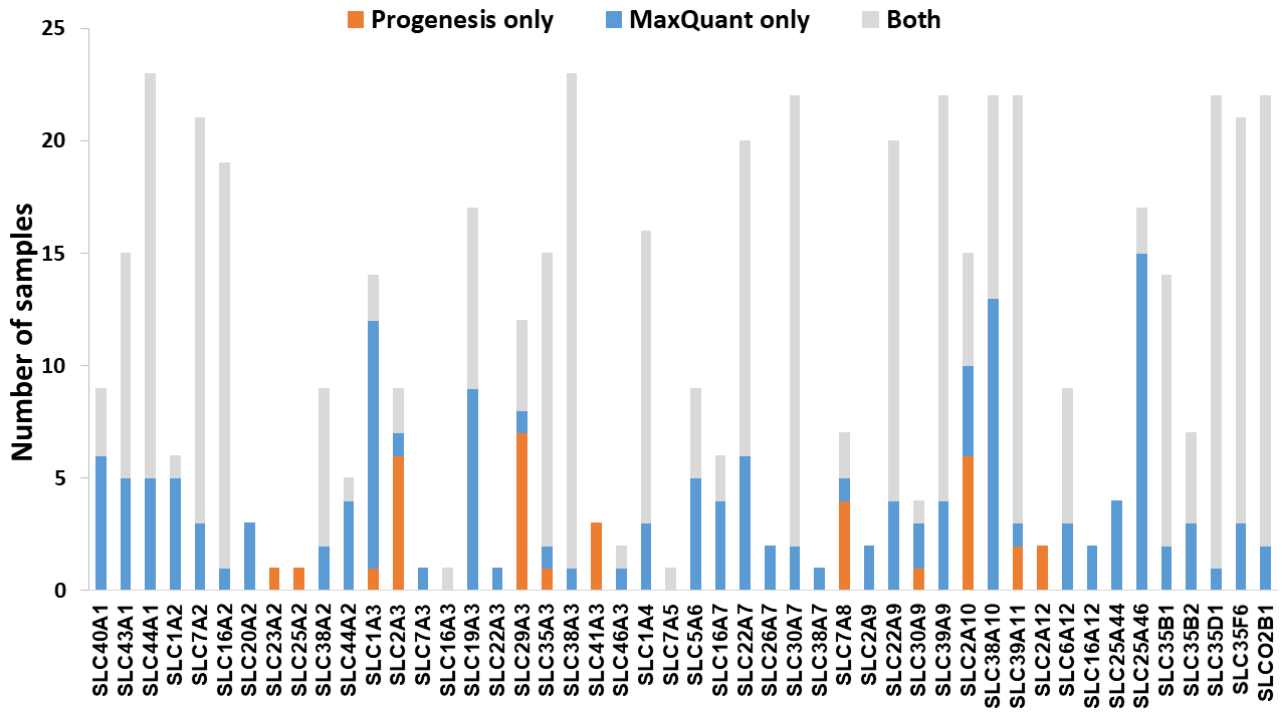

Figure 3-7 The number of samples in which solute carriers (SLCs) were identified by each software tool. Other SLC transporters that have been identified by both software (overlap) in all samples are not included.

Table 3-4 Drug-metabolising enzymes and transporters identified by the two software packages.

Protein	Number of samples with reliable detection by Progenesis	Number of samples with reliable detection by MaxQuant	Comments
CYP1A1	7	2	Involved in steroid hormone biosynthesis (Schwarz et al., 2004), fatty acid (Schwarz et al., 2004), and retinol metabolism (Chen et al., 2000).
CYP39A1	13	19	Involved in cholesterol degradation and bile acid biosynthesis (Stiles et al., 2014).
CYP2A7	18	5	
CYP2F1	22	0	Possibly involved in the metabolism of naphthalene (Li et al., 2017).
CYP4F8	11	23	Involved in fatty acid metabolism (Bylund et al., 2000).
CYP4F22	16	15	Autosomal recessive loss of function mutations associated with congenital

			ichthyosiform erythroderma (Sugiura et al., 2013; Sugiura and Akiyama, 2015).
CYP2J2	17	21	Involved in arachidonate metabolism (Lucas et al., 2010).
CYP2S1	10	15	Involved in fatty acid metabolism (Bui et al., 2011).
ABCA1 (ABC1)	16	22	Involved in the transport of cholesterol and high density lipoproteins (Quazi and Molday, 2013). Mutations lead to Tangier disease (Rust et al., 1999).
ABCA2 (ABC2)	4	16	Associated with drug resistance in cancer cells, and one SNP of ABCA2 is linked to early onset of Alzheimer's disease (Mack et al., 2008).
ABCB5 (ABCB5 P-gp)	4	2	Associated with drug resistance in colorectal cancer and melanoma (Wilson et al., 2011, 2014).
ABCC2 (MRP2)	12	22	Mutations are associated with Dubin-Johnson syndrome(Schuetz et al., 2014).
ABCD4 (PMP70)	16	23	Involved in vitamin B12 transport (Deme et al., 2014).
SLC2A1 (GLUT-1)	10	5	Involved in glucose transport and when mutated, associated with GLUT1 deficiency syndrome (Lee et al., 2015).
SLC29A1 (ENT1)	12	17	Mutations are associated with inherited H syndrome, pigmented hypertrichosis with insulin-dependent diabetes, and Faisalabad histiocytosis (Bolze et al., 2012).
SLC29A3 (ENT3)	11	5	Mutations associated with disorders, such as H syndrome, pigmented hypertrichotic dermatosis with insulin-dependent diabetes syndrome, and histiocytosis with massive lymphadenopathy (Kang et al., 2010).
SLC22A7 (OAT2)	14	20	Acts as sodium–independent organic anion/dimethyldicarboxylate exchanger (Kobayashi et al., 2005).

3.4.8 Processing time

Although computer specifications were superior with Progenesis, it took approximately 3 hours to process 2 raw files (2 replicates of the same sample with average size 1.5 GB) with Progenesis and 2-4 hours by MaxQuant. Notably, Progenesis requires an additional step to run a search on Mascot in order to generate the final output for identification and quantification of the protein targets, which might take 1 extra hour. Both software processing procedures are time consuming but being an open access tool, MaxQuant can be used on personal computers while commercially available tools (e.g. Progenesis) are expensive and are normally operated on dedicated PCs.

3.5 Discussion

Mass spectrometry-based global proteomics is a powerful tool, allowing thousands of proteins to be identified and quantified simultaneously, with very high sensitivity and selectivity. Many commentators have noted, however, that such sensitivity and selectivity come at a price – the lack of independent verification. Perhaps the most oft-quoted summary is that of Professor Ian Wilson of Imperial College, London "Nuclear magnetic resonance (NMR) is like a mother that is reliable and doesn't lie to you but is often insensitive. LC-MS is like a lover that lies to you." (https://factor.niehs.nih.gov/2013/9/science-metabolomics/index.htm). Sample preparation and sampling by the mass spectrometer can lead to reasonably well-understood differences between the results reported by different laboratories, even when many replicates are run and/or many fractionation steps performed. It remains, however, somewhat disturbing that different processing software, even when (as here) well-respected packages are used, can yield different results using the same input.

There have been a relatively small number of studies devoted to understanding the role of the processing package in interpreting global proteomic data and many of these focus on quite simple model systems, such as yeast and plants (Nesvizhskii, 2010; Tsai et al., 2012). The real importance of differences in processing will only be apparent when different packages are used to process clinical samples, especially precious human samples where sample availability is limited and where the proteins under study are of low abundance, membrane bound, or show high homology and therefore yield few unique peptides.

Duplicate MS output files, generated from duplicate tryptic digests of 23 human liver samples were processed by two different software packages, Progenesis and MaxQuant. Peptide score

correlation obtained for each sample by the two software tools was performed and an average trend line was created to establish a score cut-off equivalent to a MaxQuant score of 40. A comparison between the remaining sets of peptides was performed. The overlap between the peptides detected by the two packages ranged from 52–72% (mean 65%) with the total number of peptides identified by MaxQuant typically 18% higher. Progenesis, on average detected more modified peptides (10% compared to 6% for MaxQuant). A comparison of the characteristics of the software-specific peptides showed that, in general, Progenesis identified shorter peptides than MaxQuant, and they tended to be more basic and more hydrophilic.

We used consistent parameters for both software tools (mass tolerance, enzyme specificity, missed cleavages and modifications) and both search engines use a peptide score to match the experimental MS/MS data with a theoretical spectrum. The scoring of the peptide-spectrum match (PSM) by both tools is based on a probability calculation. The more recently developed Andromeda (MaxQuant) tool bases the scores on a binomial distribution probability, taking into account peptide fragments, neutral losses (water, ammonia) and diagnostic peaks (Neuhauser et al., 2011; Tyanova et al., 2016). Mascot (Progenesis) scoring uses peptide fragments for spectral correlation with a probabilistic modelling approach and applies an ion score cut-off to filter the PSMs (Tu et al., 2016). Although the scoring systems seem very similar, the processes necessary for assigning a PSM can yield different outcomes because the algorithms used for peak picking and subsequent peptide sequencing differ between search engines (Paulo, 2013). False positive PSMs present a challenge, as the false peptide/protein identification interferes with the interpretation of the data. Therefore, ways to measure and control the number of false identifications are required. These measures discriminate correct PSMs from false identifications and ultimately allow controlling the false discovery rate (FDR) (Nesvizhskii, 2010).

The scoring algorithms aim to describe the match quality, for instance, the number of shared fragment ions between a spectrum and a candidate peptide sequence (Perkins et al., 1999) or similarity in general. In the case of Mascot/Andromeda the number of shared fragment ions is converted into a probabilistic match score using the negative logarithm of the determined probability that the computed PSM is an incorrect assignment (Neuhauser et al., 2011). This generates a measure of match quality with high scores representing more likely hits and a high proportion of matching fragment ions. An expectation value is calculated for all sequence candidates based on the score distribution. Low quality peaks can either be used for scoring or filtered out by the search engine, leading to differences in the quality of the PSMs. Matches of

medium to high quality spectra tend to be scored robustly by the two software, leading to the observed significant overlap.

For the purpose of comparison in this study, the score cut-off values were normalized based on a predefined cut-off score of 40 for MaxQuant. An equivalent value was determined for Mascot (ranging from 11.9 to 16.5). This finding is in agreement with the literature, which reported that MaxQuant score is about three times Mascot score (Neuhauser et al., 2011). The cut-off values of ≥ 40 for MaxQuant and ≥ 20 for Mascot were reported to offer a high identification probability in proteomics (Tsai et al., 2012; Dudekula and Le, 2016). Higher score was associated with unmodified peptides, with a clear indication of higher confidence in unmodified peptide identification across the 23 analysed samples; the average proportion of unmodified peptides associated with scores ≥ 40 for MaxQuant and Mascot was 94% and 90%, respectively. This is in line with a previous assessment reporting 89.1% unmodified peptides (in mouse dendritic cells) (Neuhauser et al., 2011).

At the protein level, our comparison focused on hepatic drug-metabolising enzymes and transporters involved in drug metabolism and disposition. There is considerable inter-individual variability in the expression of these proteins, and this results in different efficacy and toxicity of drugs among different patients (Turner et al., 2015). The distribution and abundances of these proteins can be used for the prediction of the pharmacokinetics of drugs in pharmacologically based pharmacokinetics models. More specifically, they can be used as scaling factors for the in vitro to in vivo extrapolation of drug clearance (Rostami-Hodjegan, 2012).

In most of the samples, unique peptides corresponding to CYP and UGT proteins were detected by both software tools; in general, Progenesis and MaxQuant identified similar numbers of CYP and UGT peptides (Chi-squared test, $p>0.05$). There were some discrepancies, however, with the most interesting cases being CYP1A1, 2A7, 2F1, 4F8 and UGT1A7 (Table 3-4 and Figure 3-5). These are important for the metabolism of steroids, pneumotoxicants, naphthalene, fatty acids, and many other endogenous and xenobiotic substances (Table 3-4) (Tournel et al., 2007).

The present study uses label-free proteomics and one of its objectives is to compare the peptides unique for MaxQuant and those unique for Progenesis. The peptides are assigned to proteins by Uniprot and are unique for the protein group. The expression of UGT1A5 and UGT1A7 in human livers has not been reported. The peptides used for the identification of UGT1A5 and

UGT1A7 are unique for the group UGT1A, but not for UGT1A5 and UGT1A7. For the purpose of this study, this shouldn't be considered as a limitation as the main aim is the comparison between the two software tools. However, further investigation of this observation is required using targeted proteomics, in order to confirm the presence or absence of these UGTs in human liver samples.

Transporters are generally expressed at very low levels and in the plasma membrane, rather than endoplasmic reticulum, so they are not well enriched in microsomal preparations. We have previously demonstrated that microsomes are a crude membrane fraction that comprises membranes from various intracellular compartments as well as the plasma membrane (Achour, Al Feteisi, et al., 2017; Couto et al., 2019). Endoplasmic reticulum is highly enriched in microsomes while plasma membrane tends to be less enriched; enrichment factors are normally less than 2 fold for plasma membrane, whereas reticular proteins have higher enrichment (>5 fold) (Weiß et al., 2018) This is mainly because of different levels of loss of membrane protein; in-house data showed 50-80% recovery of reticular protein compared to 30-60% recovery of cell membrane protein (Achour, Al-Majdoub, et al., 2020). Microsomal crude membrane extracts are not perfect but they are the best available enriched membrane preparation. Extracting purer fractions such as plasma membrane fractions is fraught with unmitigated levels of protein loss. Like UGTs, transporters are membrane embedded, and, like UGTs, they tended to be more readily detected by MaxQuant. However, count differences (Chi-squared statistics) showed non-significant differences. Table 3-4 and Figure 3-5, 3-6 and 3-7 show that in some cases, MaxQuant identifies more unique peptides for CYPs, UGTs and transporters, whereas in other cases the opposite trend is observed. Table 3-4 also illustrates how the peptides detected only by Progenesis (for example, GNGIAFSSGDRWK and KSPAFMPFSAGR from CYP2F1) tend to be hydrophilic and basic whereas those detected only in MaxQuant (for example, TLDFIDVLLLSEDKNGK and SVINTSDAITDK from CYP4F8) tend to be slightly longer, less hydrophilic and weak acids, in line with the characteristics preferred by MaxQuant compared to Progenesis. The ABC transporters' dataset illustrates that any search conditions will inevitably lead to some loss of genuine peptides together with the noise. When this dataset was subjected to MaxQuant processing with deamidation not permitted, most of the peptides detected here only with Progenesis appeared.

The PCA analysis of the data shown in Figure 3-4 is gratifying. The two software packages are in broad agreement, especially with respect to inter-individual variability. For example, both packages agree that sample 75 is similar to 71, and 77 is similar to 89. Where they disagree,

we have developed some understanding of the reasons. It is therefore possible carefully to augment the data obtained using a Progenesis single package (Couto et al., 2019) with the additional data obtained here using MaxQuant. A representative sample of the peptides unique to MaxQuant was checked manually. Supplementary Table 3-9 shows quantification of transporters, which was only achieved with the contribution of the second software package.

To conclude, when two software packages (in this case MaxQuant and Progenesis) are used to analyse the same proteomic LC-MS/MS dataset, different results are obtained with on average 65% identical peptides. MaxQuant favours short, hydrophobic, more acidic peptides while Progenesis favours shorter, hydrophilic, basic peptides, including those with post-translational modification. The overlap gives a set of very robust identifications, and these are sufficient for many purposes where abundant proteins from reproducible samples are being detected. The present samples, however, are precious, from human donors and the proteins under study are of low abundance. In this case, the additional effort of extracting information readily verifiable with only one of the software packages is worthwhile.

3.6 References

Achour B, Al-Majdoub ZM, Rostami-Hodjegan A, and Barber J (2020) Mass Spectrometry of Human Transporters. *Annu Rev Anal Chem* **13**:223–247.

Achour B, Al-Majdoub ZM, Grybos-Gajniak A, Lea K, Kilford P, Zhang M, Knight D, Barber J, Schageman J, and Rostami-Hodjegan A (2020) Liquid Biopsy Enables Quantification of the Abundance and Interindividual Variability of Hepatic Enzymes and Transporters. *Clin Pharmacol Ther* **109**:222-232.

Achour B, Al Feteisi H, Lanucara F, Rostami-Hodjegan A, and Barber J (2017) Global proteomic analysis of human liver microsomes: Rapid characterization and quantification of hepatic drug-metabolizing enzymes. *Drug Metab Dispos* **45**:666-675.

Achour B, Dantonio A, Niosi M, Novak JJ, Fallon JK, Barber J, Smith PC, Rostami-Hodjegan A, and Goosen TC (2017) Quantitative Characterization of Major Hepatic UDP-Glucuronosyltransferase Enzymes in Human Liver Microsomes: Comparison of Two Proteomic Methods and Correlation with Catalytic Activity. *Drug Metab Dispos* **45**:1102–1112.

Achour B, Russell MR, Barber J, and Rostami-Hodjegan A (2014) Simultaneous quantification of the abundance of several cytochrome P450 and uridine 5′-diphospho-glucuronosyltransferase enzymes in human liver microsomes using multiplexed targeted proteomics. *Drug Metab Dispos*, **42**:500–510.

Aebersold R, and Mann M (2016) Mass-spectrometric exploration of proteome structure and function. *Nature* **537**:347–355.

Al-Majdoub ZM, Al Feteisi H, Achour B, Warwood S, Neuhoff S, Rostami-Hodjegan A, and Barber J (2019) Proteomic quantification of human blood–brain barrier SLC and ABC transporters in healthy individuals and dementia patients. *Mol Pharm* **16**:1220–1233.

Al Feteisi H, Achour B, Rostami-hodjegan A, and Barber J (2015) Translational value of liquid chromatography coupled with tandem mass spectrometry-based quantitative proteomics for in vitro -- in vivo extrapolation of drug metabolism and transport and considerations in selecting appropriate techniques. *Expert Opin Drug Metab Toxicol* **11**:1357–1369.

Al Feteisi H, Al-Majdoub ZM, Achour B, Couto N, Rostami-Hodjegan A, and Barber J (2018) Identification and quantification of blood–brain barrier transporters in isolated rat brain

microvessels. *J Neurochem* **146**:670-685.

Al Shweiki MR, Mönchgesang S, Majovsky P, Thieme D, Trutschel D, and Hoehenwarter W (2017) Assessment of Label-Free Quantification in Discovery Proteomics and Impact of Technological Factors and Natural Variability of Protein Abundance. *J Proteome Res* **16**:1410–1424.

Bateman A, Martin MJ, O'Donovan C, Magrane M, Alpi E, Antunes R, Bely B, Bingley M, Bonilla C, Britto R, Bursteinas B, Bye-AJee H, Cowley A, Da Silva A, De Giorgi M, Dogan T, Fazzini F, Castro LG, Figueira L, Garmiri P, Georghiou G, Gonzalez D, Hatton-Ellis E, Li W, Liu W, Lopez R, Luo J, Lussi Y, MacDougall A, Nightingale A, Palka B, Pichler K, Poggioli D, Pundir S, Pureza L, Qi G, Rosanoff S, Saidi R, Sawford T, Shypitsyna A, Speretta E, Turner E, Tyagi N, Volynkin V, Wardell T, Warner K, Watkins X, Zaru R, Zellner H, Xenarios I, Bougueleret L, Bridge A, Poux S, Redaschi N, Aimo L, ArgoudPuy G, Auchincloss A, Axelsen K, Bansal P, Baratin D, Blatter MC, Boeckmann B, Bolleman J, Boutet E, Breuza L, Casal-Casas C, De Castro E, Coudert E, Cuche B, Doche M, Dornevil D, Duvaud S, Estreicher A, Famiglietti L, Feuermann M, Gasteiger E, Gehant S, Gerritsen V, Gos A, Gruaz-Gumowski N, Hinz U, Hulo C, Jungo F, Keller G, Lara V, Lemercier P, Lieberherr D, Lombardot T, Martin X, Masson P, Morgat A, Neto T, Nouspikel N, Paesano S, Pedruzzi I, Pilbout S, Pozzato M, Pruess M, et al. (2017) UniProt: the universal protein knowledgebase. *Nucleic Acids Res* **45**:D158–D169.

Bhatt DK, and Prasad B (2018) Critical Issues and Optimized Practices in Quantification of Protein Abundance Level to Determine Interindividual Variability in DMET Proteins by LC-MS/MS Proteomics. *Clin Pharmacol Ther* **103**:619–630.

Billington S, Ray AS, Salphati L, Xiao G, Chu X, Humphreys WG, Liao M, Lee CA, Mathias A, Hop CECA, Rowbottom C, Evers R, Lai Y, Kelly EJ, Prasad B, and Unadkat JD (2018) Transporter Expression in Noncancerous and Cancerous Liver Tissue from Donors with Hepatocellular Carcinoma and Chronic Hepatitis C Infection Quantified by LC-MS/MS Proteomics. *Drug Metab Dispos* **46**:189–196.

Bolze A, Abhyankar A, Grant A V., Patel B, Yadav R, Byun M, Caillez D, Emile J-F, Pastor-Anglada M, Abel L, Puel A, Govindarajan R, de Pontual L, and Casanova J-L (2012) A Mild Form of SLC29A3 Disorder: A Frameshift Deletion Leads to the Paradoxical Translation of an Otherwise Noncoding mRNA Splice Variant. *PLoS One* **7**:e29708.

Bui P, Imaizumi S, Beedanagari SR, Reddy ST, and Hankinson O (2011) Human CYP2S1 Metabolizes Cyclooxygenase- and Lipoxygenase-Derived Eicosanoids. *Drug Metab Dispos* **39**:180–190.

Bylund J, Hidestrand M, Ingelman-Sundberg M, and Oliw EH (2000) Identification of CYP4F8 in Human Seminal Vesicles as a Prominent 19-Hydroxylase of Prostaglandin Endoperoxides. *J Biol Chem* **275**:21844–21849.

Chawade A, Sandin M, Teleman J, Malmström J, and Levander F (2015) Data processing has major impact on the outcome of quantitative label-free LC-MS analysis. *J Proteome Res* **14**:676–687.

Chen H, Howald WN, and Juchau MR (2000) Biosynthesis of all-trans-retinoic acid from all-trans-retinol: catalysis of all-trans-retinol oxidation by human P-450 cytochromes. *Drug Metab Dispos* **28**:315–22.

Couto N, Al-Majdoub ZM, Achour B, Wright PC, Rostami-Hodjegan A, and Barber J (2019) Quantification of Proteins Involved in Drug Metabolism and Disposition in the Human Liver Using Label-Free Global Proteomics. *Mol Pharm* **16**:632–647.

Couto N, Al-Majdoub ZM, Gibson S, Davies PJ, Achour B, Harwood MD, Carlson G, Barber J, Rostami-Hodjegan A, and Warhurst G (2020) Quantitative Proteomics of Clinically Relevant Drug-Metabolizing Enzymes and Drug Transporters and Their Intercorrelations in the Human Small Intestine. *Drug Metab Dispos* **48**:245–254.

Cox J, Hein MY, Luber CA, Paron I, Nagaraj N, and Mann M (2014) Accurate Proteome-wide Label-free Quantification by Delayed Normalization and Maximal Peptide Ratio Extraction, Termed MaxLFQ. *Mol Cell Proteomics* **13**:2513–2526.

Cox J, and Mann M (2008) MaxQuant enables high peptide identification rates, individualized p.p.b.-range mass accuracies and proteome-wide protein quantification. *Nat Biotechnol* **26**:1367–1372.

Deme JC, Hancock MA, Xia X, Shintre CA, Plesa M, Kim JC, Carpenter EP, Rosenblatt DS, and Coulton JW (2014) Purification and interaction analyses of two human lysosomal vitamin B 12 transporters: LMBD1 and ABCD4. *Mol Membr Biol* **31**:250–261.

Dudekula K, and Le T (2016) Data in Brief Data from quantitative label free proteomics analysis of rat spleen. *Data Br* **8**:494–500.

Ellis S, and Barber J (2016) Expanding and personalising feedback in online assessment: A case study in a school of pharmacy. *Pract Res High Educ* **10**:121–129.

Gillet LC, Leitner A, and Aebersold R (2016) Mass Spectrometry Applied to Bottom-Up Proteomics: Entering the High-Throughput Era for Hypothesis Testing. *Annu Rev Anal Chem* **9**:449–72.

Harwood MD, Achour B, Neuhoff S, Russell MR, Carlson G, and Warhurst G (2016) In Vitro-In Vivo Extrapolation Scaling Factors for Intestinal P-Glycoprotein and Breast Cancer Resistance Protein: Part I: A Cross-Laboratory Comparison of Transporter-Protein Abundances and Relative Expression Factors in Human Intestine and Caco-2 Cells. *Drug Metab Dispos* **44**:297–307.

Howard M, Achour B, Al-Majdoub Z, Rostami-Hodjegan A, and Barber J (2018) GASP and FASP are complementary for LC-MS/MS proteomic analysis of drug-metabolising enzymes and transporters in pig liver. *Proteomics* **18**:1800200.

Jamei M (2016) Recent Advances in Development and Application of Physiologically-Based Pharmacokinetic (PBPK) Models: a Transition from Academic Curiosity to Regulatory Acceptance. *Curr Pharmacol Reports* **2**:161–169.

Jehmlich N, Dinh KHD, Gesell-Salazar M, Hammer E, Steil L, Dhople VM, Schurmann C, Holtfreter B, Kocher T, and Völker U (2013) Quantitative analysis of the intra- and inter-subject variability of the whole salivary proteome. *J Periodontal Res* **48**:392–403.

Kang N, Jun AH, Bhutia YD, Kannan N, Unadkat JD, and Govindarajan R (2010) Human Equilibrative Nucleoside Transporter-3 (hENT3) Spectrum Disorder Mutations Impair Nucleoside Transport, Protein Localization, and Stability. *J Biol Chem* **285**:28343–28352.

Kawakami H, Ohtsuki S, Kamiie J, Suzuki T, Abe T, and Terasaki T (2011) Simultaneous absolute quantification of 11 cytochrome P450 isoforms in human liver microsomes by liquid chromatography tandem mass spectrometry with In silico target peptide selection. *J Pharm Sci* **100**:341-352.

Kobayashi Y, Ohshiro N, Sakai R, Ohbayashi M, Kohyama N, and Yamamoto T (2005) Transport mechanism and substrate specificity of human organic anion transporter 2 (hOat2 [SLC22A7]). *J Pharm Pharmacol* **57**:573–578.

Lee EE, Ma J, Sacharidou A, Mi W, Salato VK, Nguyen N, Jiang Y, Pascual JM, North PE,

Shaul PW, Mettlen M, and Wang RC (2015) A Protein Kinase C Phosphorylation Motif in GLUT1 Affects Glucose Transport and is Mutated in GLUT1 Deficiency Syndrome. *Mol Cell* **58**:845–853.

Leoni E, Bremang M, Mitra V, Zubiri I, Jung S, Lu C-H, Adiutori R, Lombardi V, Russell C, Koncarevic S, Ward M, Pike I, and Malaspina A (2019) Combined Tissue-Fluid Proteomics to Unravel Phenotypic Variability in Amyotrophic Lateral Sclerosis. *Sci Rep* **9**:4478.

Li J, Zhou L, Wang H, Yan H, Li N, Zhai R, Jiao F, Hao F, Jin Z, Tian F, Peng B, Zhang Y, and Qian X (2015) A new sample preparation method for the absolute quantitation of a target proteome using ^{18} O labeling combined with multiple reaction monitoring mass spectrometry. *Analyst*, **140**:1281-1290.

Li L, Carratt S, Hartog M, Kovalchuk N, Jia K, Wang Y, Zhang Q-Y, Edwards P, Van Winkle L, and Ding X (2017) Human CYP2A13 and CYP2F1 Mediate Naphthalene Toxicity in the Lung and Nasal Mucosa of CYP2A13/2F1-Humanized Mice. *Environ Health Perspect* **125**:067004.

Lucas D, Goulitquer S, Marienhagen J, Fer M, Dreano Y, Schwaneberg U, Amet Y, and Corcos L (2010) Stereoselective epoxidation of the last double bond of polyunsaturated fatty acids by human cytochromes P450. *J Lipid Res* **51**:1125–1133.

Mack JT, Brown CB, and Tew KD (2008) ABCA2 as a therapeutic target in cancer and nervous system disorders. *Expert Opin Ther Targets* **12**:491–504.

Merl J, Ueffing M, Hauck SM, and von Toerne C (2012) Direct comparison of MS-based label-free and SILAC quantitative proteome profiling strategies in primary retinal Müller cells. *Proteomics* **12**:1902-1911.

Nesvizhskii AI (2010) A survey of computational methods and error rate estimation procedures for peptide and protein identification in shotgun proteomics. *J Proteomics* **73**:2092–2123.

Neuhauser N, Michalski A, Scheltema RA, Olsen J V, and Mann M (2011) Andromeda : A Peptide Search Engine Integrated into the MaxQuant Environment. *J Proteome Res* **10**:1794-1805.

Ohtsuki S, Schaefer O, Kawakami H, Inoue T, Liehner S, Saito A, Ishiguro N, Kishimoto W, Ludwig-Schwellinger E, Ebner T, and Terasaki T (2012) Simultaneous absolute protein

quantification of transporters, cytochromes P450, and UDP-glucuronosyltransferases as a novel approach for the characterization of individual human liver: Comparison with mRNA levels and activities. *Drug Metab Dispos* **40**:83–92.

Pan S, Aebersold R, Chen R, Rush J, Goodlett DR, McIntosh MW, Zhang J, and Brentnall TA (2009) Mass Spectrometry Based Targeted Protein Quantification: Methods and Applications. *J Proteome Res* **8**:787–797.

Paulo JA (2013) Practical and Efficient Searching in Proteomics: A Cross Engine Comparison. *Webmedcentral* **4**.

Perkins DN, Pappin DJC, Creasy DM, and Cottrell JS (1999) Probability-based protein identification by searching sequence databases using mass spectrometry data. *Electrophoresis* **20**:3551–3567.

Prasad B, Achour B, Artursson P, Hop CECA, Lai Y, Smith PC, Barber J, Wisniewski JR, Spellman D, Uchida Y, Zientek MA, Unadkat JD, and Rostami-Hodjegan A (2019) Toward a Consensus on Applying Quantitative Liquid Chromatography-Tandem Mass Spectrometry Proteomics in Translational Pharmacology Research: A White Paper. *Clin Pharmacol Ther* **106**:525–543.

Prasad B, Bhatt DK, Johnson K, Chapa R, Chu X, Salphati L, Xiao G, Lee C, Hop CECA, Mathias A, Lai Y, Liao M, Humphreys WG, Kumer SC, and Unadkat JD (2018) Abundance of Phase 1 and 2 Drug-Metabolizing Enzymes in Alcoholic and Hepatitis C Cirrhotic Livers: A Quantitative Targeted Proteomics Study. *Drug Metab Dispos* **46**:943–952.

Prasad B, Evers R, Gupta A, Hop CECA, Salphati L, Shukla S, Ambudkar S V., and Unadkat JD (2013) Interindividual variability in hepatic organic anion-transporting polypeptides and P-glycoprotein (ABCB1) protein expression: quantification by liquid chromatography tandem mass spectroscopy and influence of genotype, age, and sex. *Drug Metab Dispos* **42**:78–88.

Quazi F, and Molday RS (2013) Differential Phospholipid Substrates and Directional Transport by ATP-binding Cassette Proteins ABCA1, ABCA7, and ABCA4 and Disease-causing Mutants. *J Biol Chem* **288**:34414–34426.

Rostami-Hodjegan A (2012) Physiologically based pharmacokinetics joined with in vitro-in vivo extrapolation of ADME: A marriage under the arch of systems pharmacology. *Clin*

Pharmacol Ther **92**:50–61.

Rust S, Rosier M, Funke H, Real J, Amoura Z, Piette J-C, Deleuze J-F, Brewer HB, Duverger N, Denèfle P, and Assmann G (1999) Tangier disease is caused by mutations in the gene encoding ATP-binding cassette transporter 1. *Nat Genet* **22**:352–355.

Schuetz JD, Swaan PW, and Tweedie DJ (2014) The Role of Transporters in Toxicity and Disease. *Drug Metab Dispos* **42**:541–545.

Schwarz D, Kisselev P, Ericksen SS, Szklarz GD, Chernogolov A, Honeck H, Schunck W-H, and Roots I (2004) Arachidonic and eicosapentaenoic acid metabolism by human CYP1A1: highly stereoselective formation of 17(R),18(S)-epoxyeicosatetraenoic acid. *Biochem Pharmacol* **67**:1445–1457.

Sharma S, Suresh Ahire D, and Prasad B (2020) Utility of Quantitative Proteomics for Enhancing the Predictive Ability of Physiologically Based Pharmacokinetic Models Across Disease States. *J Clin Pharmacol* **60**:S17–S35.

Stiles AR, Kozlitina J, Thompson BM, McDonald JG, King KS, and Russell DW (2014) Genetic, anatomic, and clinical determinants of human serum sterol and vitamin D levels. *Proc Natl Acad Sci* **111**:E4006–E4014.

Sugiura K, and Akiyama M (2015) Update on autosomal recessive congenital ichthyosis: mRNA analysis using hair samples is a powerful tool for genetic diagnosis. *J Dermatol Sci* **79**:4–9.

Sugiura K, Takeichi T, Tanahashi K, Ito Y, Kosho T, Saida K, Uhara H, Okuyama R, and Akiyama M (2013) Lamellar ichthyosis in a collodion baby caused by CYP4F22 mutations in a non-consanguineous family outside the Mediterranean. *J Dermatol Sci* **72**:193–195.

The UniProt Consortium (2019) UniProt: a worldwide hub of protein knowledge. *Nucleic Acids Res* **47**:D506–D515.

Tournel G, Cauffiez C, Billaut-Laden I, Allorge D, Chevalier D, Bonnifet F, Mensier E, Lafitte J-J, Lhermitte M, Broly F, and Lo-Guidice J-M (2007) Molecular analysis of the CYP2F1 gene: Identification of a frequent non-functional allelic variant. *Mutat Res Mol Mech Mutagen* **617**:79–89.

Tsai S, Tsou C, Mao W, Chang W, Han H, and Hsu W (2012) Label-free quantitative

proteomics of CD133-positive liver cancer stem cells. *Proteome Sci* **10**: 1-14

Tu C, Li J, Shen S, Sheng Q, Shyr Y, and Qu J (2016) Performance Investigation of Proteomic Identification by HCD/CID Fragmentations in Combination with High/Low-Resolution Detectors on a Tribrid, High-Field Orbitrap Instrument. *PLoS One* **11**:e0160160.

Turner RM, Park BK, and Pirmohamed M (2015) Parsing interindividual drug variability: an emerging role for systems pharmacology. *Wiley Interdiscip Rev Syst Biol Med* **7**:221–241.

Tyanova S, Temu T, and Cox J (2016) The MaxQuant computational platform for mass spectrometry-based shotgun proteomics. *Nat Protoc* **11**:2301–2319.

Välikangas T, Suomi T, and Elo LL (2017) A comprehensive evaluation of popular proteomics software workflows for label-free proteome quantification and imputation. *Brief Bioinform* **19**:1344–1355.

Vildhede A, Wiśniewski JR, Norén A, Karlgren M, and Artursson P (2015) Comparative Proteomic Analysis of Human Liver Tissue and Isolated Hepatocytes with a Focus on Proteins Determining Drug Exposure. *J Proteome Res* **14**:3305–3314.

Wang H, Zhang H, Li J, Wei J, Zhai R, Peng B, Qiao H, Zhang Y, and Qian X (2015) A new calibration curve calculation method for absolute quantification of drug metabolizing enzymes in human liver microsomes by stable isotope dilution mass spectrometry. *Anal Methods* **7**:5934–5941.

Wegler C, Gaugaz FZ, Andersson TB, Wiśniewski JR, Busch D, Gröer C, Oswald S, Norén A, Weiss F, Hammer HS, Joos TO, Poetz O, Achour B, Rostami-Hodjegan A, van de Steeg E, Wortelboer HM, and Artursson P (2017) Variability in Mass Spectrometry-based Quantification of Clinically Relevant Drug Transporters and Drug Metabolizing Enzymes. *Mol Pharm* **14**:3142–3151.

Weiß F, Hammer HS, Klein K, Planatscher H, Zanger UM, Norén A, Wegler C, Artursson P, Joos TO, and Poetz O (2018) Direct Quantification of Cytochromes P450 and Drug Transporters—A Rapid, Targeted Mass Spectrometry-Based Immunoassay Panel for Tissues and Cell Culture Lysates. *Drug Metab Dispos* **46**:387–396.

Wienkers LC, and Heath TG (2005) Predicting in vivo drug interactions from in vitro drug discovery data. *Nat Rev Drug Discov* **4**:825–833.

Wilson BJ, Saab KR, Ma J, Schatton T, Putz P, Zhan Q, Murphy GF, Gasser M, Waaga-Gasser

AM, Frank NY, and Frank MH (2014) ABCB5 Maintains Melanoma-Initiating Cells through a Proinflammatory Cytokine Signaling Circuit. *Cancer Res* **74**:4196–4207.

Wilson BJ, Schatton T, Zhan Q, Gasser M, Ma J, Saab KR, Schanche R, Waaga-Gasser A-M, Gold JS, Huang Q, Murphy GF, Frank MH, and Frank NY (2011) ABCB5 Identifies a Therapy-Refractory Tumor Cell Population in Colorectal Cancer Patients. *Cancer Res* **71**:5307–5316.

Yan T, Gao S, Peng X, Shi J, Xie C, Li Q, Lu L, Wang Y, Zhou F, Liu Z, and Hu M (2015) Significantly decreased and more variable expression of major CYPs and UGTs in liver microsomes prepared from HBV-positive human hepatocellular carcinoma and matched pericarcinomatous tissues determined using an isotope label-free UPLC-MS/MS method. *Pharm Res* **32**:1141–1157.

Yan T, Lu L, Xie C, Chen J, Peng X, Zhu L, Wang Y, Li Q, Shi J, Zhou F, Hu M, and Liu Z (2015) Severely Impaired and Dysregulated Cytochrome P450 Expression and Activities in Hepatocellular Carcinoma: Implications for Personalized Treatment in Patients. *Mol Cancer Ther* **14**:2874–2886.

Zhang H-F, Wang H-H, Gao N, Wei J-Y, Tian X, Zhao Y, Fang Y, Zhou J, Wen Q, Gao J, Zhang Y-J, Qian X-H, and Qiao H-L (2016) Physiological Content and Intrinsic Activities of 10 Cytochrome P450 Isoforms in Human Normal Liver Microsomes. *J Pharmacol Exp Ther* **358**:83-93.

3.7 Supplementary Information

Supplementary Table 3-1 Detailed parameters applied with MaxQuant.

Group specific Parameters	
1- Type Standard: none	Multiplicity: 1
2- Digestion mode: Specific	Enzyme: Trypsin/P
	Max. missed: 1
3- Modifications	Variable modifications: Oxidation (M) & Deamidation (NQ)
	Max number of modifications per peptide: 11
4- Instrument	Orbitrap
First search peptide tolerance 20	Main search peptide tolerance 5
Peptide tolerance unit ppm	Individual peptide mass tolerance (Checked)
Isotop match tolerance **2**	Isotop match tolerance unit ppm
Centroid match tolerance 8	Centroid match tolerance unit ppm
Centroid half width 35	Centroid half width unit ppm
Time Valley Factor 1.4	Isotop Valley factor 1.2
Isotop time correlation 0.6	Theoretical isotope correlation 0.6
Recalibration unit ppm	Min Peak length 2
Max charge **7**	Min score for recalibration 70
Cut peaks (checked)	Gap scans 1
Intensity threshold 0	Intensity determination Value at Maximum
5- Label free quantification: yes	
Global parameters	
1- **Sequence**	include contaminants (checked)
Fixed modifications Carbamidomethyl (C)	Min pep length 7
Max peptide mass [Da] 4500	Min peptide length for unspecific search 8
Max. peptide length for unspecific search 25	
2- **Identification**	PSM FDR 0.01
XPSM FDR 0.01	Protein FDR 0.01
Site decoy fraction 0.01	Min. peptides 1
Min.razor + unique peptides 1	Min. unique peptides 0

Min. score for unmodified peptides 0	Min. score for modified peptides 0
Min. delta score for unmodified peptides 0	Min. delta score for modified peptides 6
Main search max. combinations 200	Base FDR calculations on delta score (unchecked)
Razor protein FDR checked	
3- **Protein Quantification**	Label min. ratio count 2
Peptides for quantification Unique + razor	Use only unmodified peptides
Modifications used in protein quantification	Oxidation (M) & Deamidation (NQ)
Discard unmodified counterpart peptides (checked)	Advanced ratio estimation (checked)
4- Advanced	Calculate peak properties (unchecked)
Decoy mode Revert	Use for occupancies Normalized ratios
5- Label free quantification	Separate LFQ in parameter groups unchecked
Stabilize large LFQ ratios (checked)	Require MS/MS for LFQ comparisons (checked)
¡BAQ (unchecked)	Advanced site intensities (checked)
LFQ norm for sites and peptides (unchecked)	6- **MS/MS FTMS**
FTMS MS/MS match tolerance 20	FTMS MS/MS match tolerance unit ppm
FTMS MS/MS de novo tolerance 10	FTMS MS/MS de novo tolerance unit ppm
FTMS MS/MS deisotoping tolerance 7	FTMS MS/MS deisotoping tolerance unit ppm
FTMS top peaks per Da interval 12	FTMS top x mass window [Da] 100
FTMS de isotoping (checked)	FTMS higher charges (checked)
FTMS water loss (checked)	FTMS ammonia loss (checked)
FTMS dependent losses (checked)	FTMS recalibration (unchecked)
7- MS/MS ITMS	ITMS MS/MS match tolerance 0.5
ITMS MS/MS match tolerance unit Da	ITMS MS/MS de novo tolerance 0.25
ITMS MS/MS de novo tolerance unit Da	ITMS MS/MS deisotoping tolerance 0.15
ITMS MS/MS deisotoping tolerance unit Da	ITMS top peaks per Da interval 8
ITMStop x mass window [Da] 100	ITMS de-isotoping (unchecked)
ITMS higher charges (checked)	ITMS water loss (checked)
ITMS ammonia loss (checked)	ITMS dependent losses checked
ITMS recalibration (unchecked)	**8- MS/MS- TOF**
TOF MS/MS match tolerance 40	TOF MS/MS match tolerance unit ppm
TOF MS/MS de novo tolerance 0.02	TOF MS/MS de novo tolerance unit Da
TOF MS/MS deisotoping tolerance 0.01	TOF MS/MS deisotoping tolerance unit Da
TOF top peaks per Da interval 10	TOF top x mass window [Da] 100

TOF de isotoping (checked)	TOF higher charges (checked)
TOF water loss (checked)	TOF ammonia loss (checked)
TOF dependent losses (checked)	TOF recalibration (unchecked)
9- MS/MS unknown	Unknown MS/MS match tolerance 0.5
Unknown MS/MS match tolerance unit Da	Unknown MS/MS de novo tolerance 0.25
Unknown MS/MS de novo tolerance unit Da	Unknown MS/MS deisotoping tolerance 0.15
Unknown MS/MS deisotoping tolerance unit Da	Unknown top peaks per Da interval 8
Unknown top x mass window [Da] 100	Unknown de isotoping (unchecked)
Unknown higher charges (checked)	Unknown water loss (checked)
Unknown ammonia loss (checked)	Unknown dependent losses checked
Unknown recalibration (unchecked)	**10- tables**
Write msScans table (checked)	Write msms Scans table (checked)
Write ms3Scans table (checked)	Write all Peptides table (checked)
Write mzRange table (checked)	Write pasefMsms Scans table (checked)
Write accumulatedPasef Msms Scans table (checked)	

Supplementary Table 3-2 Range of cut-off scores in Progenesis. The cut-off scores for Progenesis are equivalent to a cut-off score of 40 in MaxQuant. The equation represents a mathematical relationship that allows conversion of cut-off scores from one software to the other. Progenesis score is represented by y and MaxQuant score by x.

Sample	Equation to convert cut-off scores	R^2	Cut-off score for Progenesis
HLM76	y=0.3353x	0.32	13.4
HLM02	y=0.3445x	0.34	13.8
HLM25	y=0.3386x	0.35	13.5
HLM48	y=0.359x	0.41	14.4
HLM73	y=0.374x	0.43	15.0
HLM80	y=0.3539x	0.34	14.2
HLM91	y=0.3617x	0.35	14.5
HLM06	y=0.3439x	0.32	13.8
HLM11	y=0.3552x	0.41	14.2
HLM38	y=0.3673x	0.40	14.7
HLM41	y=0.3187x	0.25	12.8
HLM72	y=0.3489x	0.41	14
HLM75	y=0.3675x	0.37	14.7
HLM90	y=0.2964x	0.30	11.9
HLM117	y=0.3215x	0.28	12.9
HLM08	y = 0.4129x	0.23	16.5
HLM71	y = 0.3682x	0.32	14.7
HLM77	y = 0.3651x	0.40	14.6
HLM78	y = 0.3371x	0.31	13.5
HLM74	y = 0.3446x	0.33	13.8
HLM100	y = 0.3561x	0.36	14.2
HLM89	y = 0.3643x	0.43	14.6
HLM01	y = 0.363x	0.35	14.5

Supplementary Table 3-3 Regression equation for the relationship between Progenesis intensities (y) and MaxQuant intensities (x) and the coefficient of determination for each individual human liver microsome (HLM) sample.

Sample	Regression equation to convert intensities	R^2
HLM01	y=0.0248x	0.68
HLM02	y=0.012x	0.62
HLM06	y=0.0123x	0.59
HLM08	y=0.0145x	0.62
HLM11	y=0.0162x	0.50
HLM25	y=0.0146x	0.60
HLM38	y=0.0118x	0.66
HLM41	y=0.01242x	0.59
HLM48	y=0.0144x	0.59
HLM71	y=0.0132x	0.65
HLM72	y=0.0171x	0.57
HLM73	y=0.0151x	0.59
HLM74	y=0.0123x	0.61
HLM75	y=0.0115x	0.65
HLM76	y=0.013x	0.74
HLM77	y=0.0147x	0.67
HLM78	y=0.0131x	0.56
HLM80	y=0.0144x	0.67
HLM89	y=0.0156x	0.57
HLM90	y=0.016x	0.57
HLM91	y=0.025x	0.63
HLM100	y=0.0127x	0.53
HLM117	y=0.0149x	0.49

Supplementary Table 3-4 Comparison of the total number of peptides, peptides specific for a software and modified peptides identified by MaxQuant and Progenesis. This comparison was done before removing peptides with scores lower than 40 in MaxQuant or equivalent for Progenesis.

Sample	MaxQuant total peptides	Progenesis total peptides	MaxQuant only peptides		Progenesis only peptides		Overlap		MaxQuant modified		Progenesis modified	
			Number	Percent	Number	Percent	Number	Percent	Number	Percent	Number	Percent
HLM01	16366	20284	3280	14%	7198	31%	13086	56%	714	4%	5053	25%
HLM02	20584	19950	7485	27%	6851	25%	13099	48%	1259	6%	4919	24%
HLM06	18725	19236	6531	25%	7042	27%	12194	47%	937	5%	4784	25%
HLM08	18169	22645	3934	15%	8410	32%	14235	54%	872	5%	5801	26%
HLM11	17912	21733	4351	17%	8172	31%	13561	52%	946	5%	5534	26%
HLM25	18773	20558	5475	21%	7260	28%	13298	51%	1037	6%	5130	25%
HLM38	17909	22449	4212	16%	8752	33%	13697	51%	929	5%	5841	26%
HLM41	17789	21019	4580	18%	7810	31%	13209	52%	1470	8%	5656	27%
HLM48	17743	20701	4388	17%	7346	29%	13355	53%	917	6%	5258	25%
HLM71	16413	21986	2772	11%	8345	34%	13641	55%	847	5%	5990	27%
HLM72	17269	21027	4028	16%	7786	31%	13241	53%	936	5%	5305	25%
HLM73	17393	20847	3946	16%	7400	30%	13447	54%	3236	19%	7199	35%
HLM74	18170	19150	5741	23%	6721	27%	12429	50%	879	5%	4728	25%
HLM75	16809	20901	3957	16%	8049	32%	12852	52%	842	5%	5487	26%
HLM76	19091	19107	6554	26%	6570	26%	12537	49%	1103	6%	4673	24%
HLM77	17348	20466	3916	16%	7034	29%	13432	55%	1014	6%	5115	25%
HLM78	18794	18989	6467	25%	6662	26%	12327	48%	1113	6%	4790	25%
HLM80	17326	20734	4113	17%	7521	30%	13213	53%	839	5%	5366	26%
HLM89	17801	22059	3853	15%	8111	31%	13948	54%	1603	9%	6258	28%
HLM90	17497	21586	4142	16%	8231	32%	13355	52%	1030	6%	5693	26%
HLM91	17149	20650	4061	16%	7562	31%	13088	53%	836	5%	5224	25%
HLM100	18207	21220	4477	17%	7490	29%	13730	53%	988	5%	5242	25%
HLM117	19923	19628	7491	28%	7196	27%	12432	46%	1031	5%	4886	25%
Mean	**17963**	**20736**	**4772**	**19%**	**7544**	**30%**	**13192**	**52%**	**1103**	**6%**	**5388**	**26%**
SD	1021	1059	1311	5%	611	2%	531	3%	508	3%	581	2%
CV	6%	5%	27%	25%	8%	8%	4%	5%	46%	47%	11%	8%

Supplementary Table 3-5 Statistical comparison between peptide characteristics for sample HLM76 in relation to peptide length, GRAVY score (hydrophobicity), isoelectric point (PI), and molecular weight of peptides detected by only one software tool MaxQuant (*Max.*) and Progenesis (*Pro.*).

	Length		**GRAVY score**		**PI**		**Molecular weight**	
	Max.	***Pro.***	***Max.***	***Pro.***	***Max.***	***Pro.***	***Max.***	***Pro.***
Median	13	13	-0.1667	-0.4692	5.848	6.613	1530.69	1450.72
Mode	11	7	-0.1	-0.3	9.831	9.831	1264.4	785.939
n	6447	2157	6447	2157	6447	2157	6447	2157
Mann-Whitney test P value	<0.0001		<0.001		<0.001		<0.001	

Supplementary Table 3-6 Enzyme and transporter proteins detected in 23 human liver samples by the two software tools.

Gene name	Number of samples where unique/distinct peptides are identified			
	Progenesis only	**MaxQuant only**	**Both**	**Neither**
CYPs				
CYP1A1	5	0	2	16
CYP1A2	0	0	23	0
CYP17A1	0	0	1	22
CYP20A1	0	0	0	23
CYP26A1	1	3	1	18
CYP27A1	0	0	23	0
CYP39A1	0	6	13	4
CYP51A1	0	0	23	0
CYP3A4	0	0	23	0
CYP3A5	0	0	23	0
CYP2A6	0	0	23	0
CYP2A7	13	0	5	5
CYP3A7	3	0	14	6
CYP4A11	0	0	23	0
CYP2A13	1	0	0	22
CYP4A22	1	0	0	22
CYP1B1	0	0	2	21
CYP7B1	0	0	23	0
CYP8B1	0	0	23	0
CYP2B6	0	0	23	0
CYP2C8	0	0	23	0
CYP2C9	0	0	23	0
CYP2C18	0	2	20	1
CYP2C19	0	1	17	5
CYP2D6	0	0	23	0
CYP2E1	0	0	23	0
CYP2F1	22	0	0	1
CYP4F2	0	0	23	0

CYP4F3	0	2	21	0
CYP4F8	0	12	11	0
CYP4F11	0	0	23	0
CYP4F12	0	1	17	5
CYP4F22	6	5	10	2
CYP2J2	1	5	16	1
CYP2S1	2	7	8	6
CYP4V2	0	1	22	0
UGTs				
UGT1A1	0	0	23	0
UGT2A1	0	2	20	1
UGT3A1	1	3	2	17
UGT1A3	0	0	23	0
UGT2A3	0	0	23	0
UGT1A4	0	0	23	0
UGT1A5	1	1	0	21
UGT1A6	0	0	23	0
UGT1A9	0	0	23	0
UGT2B4	0	0	23	0
UGT2B7	0	0	23	0
UGT2B10	0	0	23	0
UGT2B11	1	3	0	19
UGT2B15	0	0	23	0
UGT2B17	0	2	17	4
SLC transporters				
SLC1A1	1	11	7	4
SLC2A1	6	1	4	12
SLC16A1	0	0	23	0
SLC22A1	0	1	22	0
SLC23A1	0	3	0	20
SLC26A1	0	6	7	10
SLC27A1	2	3	16	2
SLC28A1	0	1	0	22

SLC29A1	0	5	12	6
SLC30A1	0	8	9	6
SLC33A1	0	0	23	0
SLC40A1	0	6	3	14
SLC43A1	0	5	10	8
SLC44A1	0	5	18	0
SLC48A1	0	1	0	22
SLC1A2	0	5	1	17
SLC2A2	0	0	23	0
SLC7A2	0	3	18	2
SLC16A2	0	1	18	4
SLC20A2	0	3	0	20
SLC23A2	1	0	0	22
SLC25A2	1	0	0	22
SLC38A2	0	2	7	14
SLC43A2	5	0	0	18
SLC44A2	0	4	1	18
SLC1A3	1	11	2	9
SLC2A3	6	1	2	14
SLC7A3	0	1	0	22
SLC16A3	0	0	1	22
SLC19A3	0	9	8	6
SLC22A3	0	1	0	22
SLC29A3	7	1	4	11
SLC35A3	1	1	13	8
SLC38A3	0	1	22	0
SLC41A3	3	0	0	20
SLC43A3	0	0	23	0
SLC46A3	0	1	1	21
SLC1A4	0	3	13	7
SLC38A4	0	0	23	0
SLC7A5	0	0	1	22
SLC5A6	0	5	4	14

SLC16A7	0	4	2	17
SLC22A7	0	6	14	3
SLC26A7	0	2	0	21
SLC30A7	0	2	20	0
SLC38A7	0	1	0	22
SLC39A7	0	0	23	0
SLC7A8	4	1	2	16
SLC2A9	0	2	0	21
SLC22A9	0	4	16	3
SLC30A9	1	2	1	19
SLC39A9	0	4	18	1
SLC2A10	6	4	5	8
SLC38A10	0	13	9	1
SLC39A11	2	1	19	1
SLC2A12	2	0	0	21
SLC6A12	0	3	6	14
SLC16A12	0	2	0	21
SLC2A13	0	0	1	22
SLC39A14	0	0	23	0
SLC25A15	0	0	23	0
SLC22A18	0	0	23	0
SLC25A40	1	4	0	18
SLC25A42	0	0	23	0
SLC25A44	0	4	0	19
SLC25A46	0	15	2	6
SLC35B1	0	2	12	9
SLC35B2	0	3	4	16
SLC35C1	0	0	4	19
SLC35C2	0	1	0	22
SLC35D1	0	1	21	1
SLC35F6	0	3	18	2
SLCO1B1	0	0	23	0
SLCO1B3	0	0	23	0

SLCO2B1	0	2	20	1
ABC transporters				
ABCA1	0	6	16	1
ABCA2	1	13	3	6
ABCA6	0	0	23	0
ABCA8	0	3	14	6
ABCA10	1	0	0	22
ABCA13	1	0	0	22
ABCB1 (MDR1)	0	2	21	0
ABCB4 (MDR3)	0	3	3	17
ABCB5	4	2	0	17
ABCB6	0	4	17	2
ABCB7	0	1	22	0
ABCB8	0	0	23	0
ABCB10	0	0	23	0
ABCB11	0	2	21	0
ABCC1 (MRP1)	0	2	0	21
ABCC2 (MRP2)	0	9	12	2
ABCC3 (MRP3)	0	3	19	1
ABCC5 (MRP5)	1	0	0	22
ABCC6 (MRP6)	0	0	23	0
ABCD1	0	0	23	0
ABCD2	1	0	0	22
ABCD3	0	0	23	0
ABCD4	0	7	16	0
ABCE1	1	3	0	19
ABCG8	1	1	1	20

Supplementary Table 3-7 Median and mode scores for software-specific peptides in each sample.

	MaxQuant		Progenesis	
Sample	**Median score**	**Mode score**	**Median score (MaxQuant Equivalent)**	**Mode score (MaxQuant Equivalent)**
HLM01	78.2	64.3	32.4 (89.3)	15.5 (42.6)
HLM02	123	114.9	51.4 (149)	88.6 (257.2)
HLM06	126.9	94.7	53.1 (154.2)	56.3 (163.7)
HLM08	74.6	60.5	23.9 (57.9)	17.7 (42.9)
HLM11	124.7	114.5	51.9 (146.1)	30.5 (85.9)
HLM25	92.8	91.6	30.6 (90.5)	17.5 (51.7)
HLM38	122.8	108.9	51.9 (141.4)	58.5 (159.2)
HLM41	123.7	101.6	49.8 (156.1)	61.9 (197.2)
HLM48	199.7	252.4	29.8 (83.1)	17.5 (48.7)
HLM71	79.6	58.4	31.7 (86.2)	14.9 (40.4)
HLM72	128.4	114.5	52.9 (151.6)	37.3 (106.9)
HLM73	77.7	50	32.3 (86.3)	18.6 (49.8)
HLM74	96.1	58.9	29.6 (85.9)	14.4 (41.8)
HLM75	122.6	122.1	52.5 (142.9)	35.3 (96.1)
HLM76	98.7	367.2	29.5 (87.9)	13.6 (40.4)
HLM77	79.2	46.5	34.5 (86.3)	16.2 (40.6)
HLM78	97.3	125.9	29.5 (87.5)	13.6 (40.5)
HLM80	87.4	47.6	29.8 (84.2)	15.3 (43.2)
HLM89	77.6	47.2	30.4 (83.5)	15.7 (42.9)
HLM90	123.1	108.9	45.5 (153.4)	23.2 (78.3)
HLM91	86.8	110.4	32.4 (89.6)	20.1 (55.5)
HLM100	86.1	62.5	32.2 (90.4)	14.9 (41.7)
HLM117	133.1	114.9	52.9 (164.7)	31.5 (98.1)

Supplementary Table 3-8 Median and mode Gravy scores for software-specific peptides in each sample.

	MaxQuant		Progenesis	
Sample	**Median Gravy score**	**Mode Gravy score**	**Median Gravy score**	**Mode Gravy score**
HLM01	-0.20	-0.30	-0.49	-0.50
HLM02	-0.13	0.30	-0.52	-0.70
HLM06	-0.16	-0.30	-0.48	0.10
HLM08	-0.12	0.30	-0.49	-0.40
HLM11	0.09	0.20	-0.51	-0.70
HLM25	-0.14	-0.10	-0.51	-0.50
HLM38	-0.17	-0.40	-0.48	-0.52
HLM41	-0.35	-0.30	-0.50	-0.50
HLM48	-0.13	0.30	-0.52	-0.70
HLM71	-0.28	-0.70	-0.47	-0.50
HLM72	-0.14	-0.60	-0.48	-0.90
HLM73	-0.09	0.40	-0.47	-0.70
HLM74	-0.19	-0.20	-0.51	-0.50
HLM75	-0.21	-0.20	-0.43	-0.70
HLM76	-0.17	-0.10	-0.47	-0.30
HLM77	-0.14	0.10	-0.44	0.10
HLM78	-0.20	-0.20	-0.46	-0.30
HLM80	-0.20	-0.10	-0.50	-0.70
HLM89	-0.14	0.30	-0.47	-0.70
HLM90	-0.09	-0.1	-0.53	-0.50
HLM91	-0.20	-0.20	-0.43	-0.70
HLM100	-0.17	-0.10	-0.50	-0.70
HLM117	-0.16	-0.30	-0.47	-0.20

Supplementary Table 3-9 Quantification of transporters only achieved with MaxQuant.

Transporter	Sample	Abundance (pmol/mg)
SLC2A9	HLM41	0.37
	HLM89	0.41
SLC7A3	HLM75	0.003
SLC16A12	HLM11	1.75
	HLM48	3.36
SLC20A2	HLM76	0.16
	HLM100	2.87
	HLM117	0.49
SLC22A3	HLM06	8.25
SLC25A44	HLM02	0.16
	HLM06	1.27
	HLM77	0.19
	HLM117	0.31
SLC26A7	HLM25	0.46
	HLM77	0.18
SLC38A7	HLM02	0.75

Chapter Four: Hepatic Scaling Factors for In Vitro-In Vivo Extrapolation (IVIVE) of Metabolic Drug Clearance in Patients with Colorectal Cancer with Liver Metastasis

Declaration

This chapter constitutes a manuscript accepted for publication in the journal Drug Metabolism and Disposition, and it is in press.

Vasilogianni A. M., Achour B., Scotcher D., Peters S.A., Al-Majdoub Z.M., Barber J., and Rostami-Hodjegan A. (**2021**). Hepatic Scaling Factors for In Vitro-In Vivo Extrapolation (IVIVE) of Metabolic Drug Clearance in Patients with Colorectal Cancer with Liver Metastasis. *Drug Metab Dispos* (in press).

I carried out the literature search, generation and analysis of data, contributed to the study design and wrote the manuscript. Dr Brahim Achour was consulted on experimental methodology and statistical analysis and edited the manuscript. Dr Daniel Scotcher was consulted on PBPK modelling and edited the manuscript. Dr Sheila Annie Peters, Dr Zubida M. Al-Majdoub, Dr Jill Barber and Prof. Amin Rostami-Hodjegan edited the manuscript. I retained editorial control. Dr Brahim Achour, Dr Sheila Annie Peters, Dr Jill Barber and Prof. Amin Rostami-Hodjegan contributed to the study design.

4.1 Abstract

In vitro-in vivo extrapolation (IVIVE) linked with physiologically based pharmacokinetic (PBPK) modelling is used to predict the fates of drugs in patients. Ideally, the IVIVE-PBPK models should incorporate "systems" information accounting for characteristics of the specific target population. There is a paucity of such scaling factors in cancer, particularly microsomal protein per gram of liver (MPPGL) and cytosolic protein per gram of liver (CPPGL). In this study, cancerous and histologically normal liver tissue from 16 patients with colorectal liver metastasis (CRLM) were fractionated to microsomes and cytosol. Protein content was measured in homogenates, microsomes and cytosol. The loss of microsomal protein during fractionation was accounted for using corrections based on NADPH cytochrome P450 reductase activity in different matrices. MPPGL was significantly lower in cancerous tissue (24.8 ± 9.8 mg/g) than histologically normal tissue (39.0 ± 13.8 mg/g). CPPGL in cancerous tissue was 42.1 ± 12.9 mg/g compared with 56.2 ± 16.9 mg/g in normal tissue. No correlations between demographics (sex, age and BMI) and MPPGL or CPPGL were apparent in the data. The generated scaling factors together with assumptions regarding the relative volumes of cancerous versus non-cancerous tissue were used to simulate plasma exposure of drugs with different extraction ratios. The PBPK simulations revealed a substantial difference in drug exposure (AUC), up to 3.3-fold, when using typical scaling factors (healthy population) instead of disease-related parameters in cancer population. These indicate the importance of using population-specific scalars in IVIVE-PBPK for different disease states.

4.2 Introduction

Cancer is a multifaceted disease characterized by deregulated cell growth with the potential to invade tissues and form metastases. Colorectal cancer is the third most common type of cancer and is associated with the second highest number of deaths caused by cancer (Bray et al., 2018). Metastasis to the liver constitutes one of the main causes of mortality in patients with colorectal cancer (Siegel et al., 2018) as it accounts for 70% of metastases from colorectal cancer, followed by metastasis to the lungs, distant lymph nodes, and peritoneum (Holch et al., 2017). Metastasis to the liver can affect hepatic function as the resultant lesions occupy space in liver tissue leading to abnormal liver function tests (Jiang et al., 2018). Inflammation is a condition that may also affect the hepatic function, as inflammatory markers have been shown to be associated positively with the size of metastases (Wong et al., 2007).

Challenges in the development of new drugs in the area of oncology include the difficulty of recruiting from the appropriate patient population and safety issues when testing anti-cancer drugs of high toxicity in healthy volunteers (Gutierrez et al., 2009; Bates et al., 2015). Given these challenges, and the high medical need, model-informed precision dosing (MIDD) and, in particularly, physiologically based pharmacokinetics (PBPK) are widely employed (Darwich et al., 2017). PBPK modelling has generally higher regulatory acceptance in the development of anti-cancer drugs than other disease areas (Yoshida et al., 2017), and models are used to inform dosing of cancer patients.

In vitro-in vivo extrapolation (IVIVE) employs models that incorporate “systems” information and in vitro drug data to predict plasma and tissue concentration-time profiles, which are critical components of bottom-up PBPK models (Rostami-Hodjegan, 2012). Data obtained using population-specific in vitro systems taking into account potential differences in functional activity need to be scaled to in vivo outcomes. For IVIVE of hepatic drug clearance, different in vitro systems can be used, including recombinantly expressed enzymes, hepatocytes, liver microsomes and cytosol. The scalars related to liver microsomes and cytosol are microsomal protein per gram of liver (MPPGL) and cytosolic protein per gram of liver (CPPGL), respectively (Barter et al., 2007).

To obtain microsomal and cytosolic fractions required for in vitro data, it is necessary to homogenize liver tissue and fractionate the homogenate using differential centrifugation. During tissue fractionation, membrane protein is subject to significant losses (Wilson et al., 2003). Accounting for protein losses is necessary for obtaining correct MPPGL values and

thus, more accurate clearance predictions. For the correction of microsomal protein loss, different microsomal markers can be used, such as NADPH cytochrome P450 reductase or total P450 content measured in the homogenate and microsomal fractions (Barter et al., 2008). Cytosolic markers for the correction of cytosolic protein loss include alcohol dehydrogenase and glutathione-S-transferase (Cubitt et al., 2011); however, loss of cytosolic protein is expected to be negligible (soluble fraction). MPPGL and CPPGL values have been reported in healthy human liver with mean values of 32 mg/g liver and 80.7 mg/g liver, respectively (Barter et al., 2007; Cubitt et al., 2011).

Although scalars have been reported for healthy liver, such data are scarce in disease populations, such as cancer. Available scalar data in liver cancer suggest that MPPGL is different in livers with hepatocellular carcinoma relative to normal liver tissue (Zhang et al., 2015; Gao et al., 2016). To our knowledge, there are no reports of scalars or IVIVE-PBPK models for colorectal liver metastasis (CRLM) for the prediction of in vivo hepatic drug clearance. The aim of this study was to generate MPPGL and CPPGL scaling factors in cancerous liver tissue from CRLM patients and compare the values with scalars from matched histologically normal tissue. The scalars were applied in PBPK simulations to predict in vivo hepatic clearance. This study highlights the importance of applying appropriate population-specific scalars for IVIVE of metabolic drug clearance in CRLM patients.

4.3 Materials and Methods

4.3.1 Materials and chemicals

All chemicals were purchased from Sigma-Aldrich (Poole, Dorset, UK) unless otherwise stated. EDTA-free protease inhibitor cocktail was obtained from Roche Applied Sciences (Mannheim, Germany).

4.3.2 Liver samples

Matched cancerous and histologically normal liver tissue specimens from 16 adult CRLM patients were obtained opportunistically following hepatectomy from the Manchester University NHS Foundation Trust (MFT) Biobank, Manchester, UK. The study was covered under the MFT Biobank generic ethics approval (NRES 14/NW/1260 and 19/NW/0644). Among the 16 donors, 7 were female and 9 were male, and their ages ranged from 34 to 85

years. The body mass index (BMI) of the patients ranged from 21.6 to 36.3 kg/m^2. Supplementary Table 4-1 presents demographic and clinical details of the donors.

4.3.3 Preparation of human liver microsomal and cytosolic fractions

Microsomal and cytosolic fractions were generated from liver tissue using differential centrifugation as previously described (Achour et al., 2017). Liver tissue was homogenized by a mechanical homogenizer (Thermo Fisher Scientific, UK) in homogenization buffer (150 mM KCl, 2 mM EDTA, 50 mM Tris, 1 mM dithiothreitol, and EDTA-free protease inhibitor cocktail, pH 7.4) at 10 ml for each gram of liver tissue. The homogenate was centrifuged at 10,000 *g* for 20 min at 4°C using an Optima^{TM} L-100 ultracentrifuge (Beckman Coulter, Fullerton, CA). The first pellet (cell debris) was stored at -80°C and then the supernatant was further centrifuged at 100,000 *g* for 75 min at 4 °C. The cytosol (the supernatant) was stored at -80°C and the pellet (microsomes) was re-suspended in 1 ml of storage buffer (0.25 M potassium phosphate, pH 7.25) per gram of liver tissue and stored at -80°C.

4.3.4 Measurement of total protein content in homogenates and fractions

The protein content of liver homogenates, microsomes and cytosolic samples was measured using bicinchoninic acid (BCA) protein assay (Pierce® Microplate BCA Protein Assay Kit – Reducing Agent Compatible) in triplicate. Absorbance was measured at 562 nm using a SpectraMax 190 platereader (Molecular Devices, Sunnyvale, CA) with bovine serum albumin used as calibration standard. For the homogenates and the cytosolic samples that contained dithiothreitol, a compatibility reagent solution was used. The cytosolic protein per gram of liver (CPPGL), and the homogenate protein per gram of liver (HomPPGL) were calculated based on the total protein content, and no further correction for loss was required.

4.3.5 Measurement of NADPH cytochrome P450 reductase activity

In the current study, NADPH P450 reductase activity was used to account for microsomal membrane loss during fractionation. The activity of NADPH P450 reductase was measured in homogenates and microsomes from the same liver samples in order to estimate loss of microsomal protein during fractionation. The protocol was adapted from methods by Guengerich et al. (2009) and Achour et al. (2011). In a 1 ml cuvette, oxidised equine cytochrome c (0.5 mM, 80 µL) was mixed with potassium phosphate buffer (0.25 M, 980 µl, pH 7.25), KCN (1 mM, 10 µl) and homogenates (10 µl, equivalent to 1 mg of tissue) or 1:10

diluted microsomes (10 µl, equivalent to 1 mg of tissue). The absorbance of the mixtures was measured using a Jenway 7315 UV-Visible spectrophotometer (Thermo Fisher Scientific) at 550 nm in kinetic mode. The absorbance was monitored for 2 min to establish the baseline, followed by addition of reduced NADPH solution (10 mM, 10 µl) to start the reaction of cytochrome c reduction, which was monitored for 5 min.

The slope of the initial linear phase of the reaction is directly proportional to the amount of cytochrome P450 reductase in the sample. The enzyme activity (units/mg liver tissue) was calculated using Equation 4-1 and fractional loss of microsomal protein was estimated based on the ratio of activity in microsomes relative to the homogenate from the same liver sample (Equation 4-2), using the ratio of the slope from the microsomal fraction (1 mg of tissue) to the slope from the homogenate (1 mg of total protein) for each individual. The ratios also allowed calculation of microsomal membrane enrichment. MPPGL for each sample was corrected using the recovery factors according to Equation 4-3 (Barter et al., 2008). Recovery factor is equal to 1-fractional loss of microsomal protein.

$$Enzyme\ activity = \frac{\Delta A_{550}/min \times dil \times total\ volume}{21.1 \times V}$$ (Equation 4-1)

ΔA550/min: rate of change in the absorbance at 550 nm

dil: dilution factor of the original enzyme sample

Total volume: volume of the reaction mixture (ml)

21.1 is the extinction coefficient for reduced cytochrome c ($mM^{-1}\ cm^{-1}$)

V: volume of the enzyme sample (ml), corresponding to 1 mg of liver tissue

$$Microsomal\ loss = 1 - \frac{activity\ in\ microsomes}{activity\ in\ homogenate}$$ (Equation 4-2)

$$MPPGL\ (mg\ g^{-1}) = \frac{Yield\ of\ microsomal\ protein\ (mg\ g^{-1})}{1 - Fraction\ loss\ of\ microsomal\ protein}$$ (Equation 4-3)

4.3.6 Statistical data analysis

Statistical data analysis was performed and graphs were generated using GraphPad Prism 8.1.2 (La Jolla, California USA). The data is presented as mean ± standard deviation (SD). Coefficient of variation (CV) was used to describe variability in datasets and the Kolmogorov-Smirnov test was used to assess the normality of distribution of the datasets. Several datasets did not follow normal distribution, and therefore non-parametric statistical tests for differences

were used. Differences in HomPPGL, uncorrected MPPGL and CPPGL values between histologically normal and matched cancerous tissues were assessed using Wilcoxon test. Differences in MPPGL values between histologically normal and matched cancerous tissues were assessed using Mann-Whitney test. This test was also used for the assessment of the effect of hepatic lobe of origin and sex of donors on MPPGL and CPPGL in normal and cancerous tissues. For the assessment of the effect of BMI and age on MPPGL and CPPGL, Spearman correlation and linear regression analysis were used. In each of the above cases, the probability cut-off value for statistical significance was set at 0.05.

4.3.7 Physiologically based pharmacokinetic (PBPK) simulations

The effect of using the generated scaling factors in a cancer population was assessed using PBPK modelling on Simcyp V18 Release 1 (Certara, Sheffield, UK) in healthy and cancer populations. For the assessment of effects of MPPGL changes on simulated plasma drug exposure, four cytochrome P450 substrates with different hepatic extraction ratios (see Table 4-1) were used: alfentanil (predominantly metabolized by CYP3A4), alprazolam (predominantly metabolized by CYP3A4 and CYP3A5), midazolam (predominantly metabolized by CYP3A4 and CYP3A5), and desipramine (predominantly metabolized by CYP2D6). CYP isoforms are responsible for the metabolism of the majority of clinically used drugs in all fields of treatment (anti-cancer and non-anti-cancer drugs), with CYP3A4/5 being the most prevalent, followed by CYP2D6. For this reason, we used CYP3A4, CYP3A5 and CYP2D6 enzymes for our simulations. The compound files were not changed from those provided within the Simcyp simulator. PBPK simulations were performed using system parameters already available on the simulator for healthy ("Sim-Healthy Volunteers") and cancer ("Sim-Cancer") virtual populations, without or with inclusion of MPPGL data measured in current study. The effects of MPPGL changes in cancer on drug exposure following oral administration were assessed using four different MPPGL models:

MPPGL model 1 (Healthy; Healthy population): the default MPPGL in Simcyp was used for the healthy population; mean MPPGL was 39.8 mg/g tissue (defined by the Simcyp model), (Equation 4-4, Barter et al., 2008).

$$Mean\ MPPGL\ \left(\frac{mg}{g}\right) = 10\text{^}(1.407\ +\ 0.0158 * \text{Age}\ -\ 0.00038 * \text{Age\^2}\ +\ 0.000024 * \text{Age\^3})$$

(Equation 4-4), coefficient of variabilities (CV)% is 26.9

MPPGL model 2 (Cancer-D; Cancer-Default population): the default MPPGL in Simcyp was used for the cancer population; mean MPPGL was 39.8 mg/g tissue (defined by the Simcyp model), (Equation 4-4, Barter et al., 2008).

These two models were used to assess any effects on drug exposure between healthy and cancer populations without changing MPPGL values. The key differences in the systems parameters between Healthy and Cancer-D involve age distribution, haematocrit, Alpha-1-acid glycoprotein (AAG) and albumin levels.

MPPGL model 3 (New Cancer-ALN; New Cancer population-assuming liver is obtained from cancer patients but entire liver tissue is histologically normal, ALN = All Liver Normal): experimentally-derived MPPGL in histologically normal tissue was used for the cancer population; mean MPPGL was 39 mg/g tissue, (Equation 4-5, adapted from Barter et al., 2008 with revised baseline).

$Mean\ MPPGL\ \left(\frac{mg}{g}\right) = 10\text{^}(1.59106462)$ (Equation 4-5), CV% is 35.36

Model 3 assumes that the whole liver remains histologically normal, and this implies the maximum metabolic capacity of microsomal enzymes. CV% used for this model is experimentally-derived based on MPPGL in histologically normal tissue.

MPPGL model 4 (New Cancer-ALC; New Cancer population-assuming liver is obtained from cancer patients and entire liver tissue is histologically cancerous, ALC = All Liver Cancerous): experimentally-derived MPPGL in cancerous tissue was used for the cancer population; mean MPPGL was 24.8 mg/g tissue, (Equation 4-6, adapted from Barter et al., 2008 with revised baseline).

$Mean\ MPPGL\ \left(\frac{mg}{g}\right) = 10\text{^}(1.3944516)$ (Equation 4-6), CV% is 39.7

Model 4 assumes that the whole liver is cancerous and this implies the minimum metabolic capacity of microsomal enzymes. It also assumes that the liver mass does not change and that each pmol of enzyme has the same activity, irrespective of disease state. CV% used for this model is experimentally-derived based on MPPGL in cancerous tissue.

The size of the liver being normal is important, as this will define how much of the liver will be fully functional. If a proportion of liver is not normal, this may lead to decreased scaled intrinsic clearance, with effect on clearance being compound dependent. In cases of a surgical

resection, clearance should be calculated based on healthy MPPGL and remnant liver size. Although surgical resection is the ideal solution for CRLM patients, this is not feasible for many patients that have to live with a liver with histologically normal and cancerous parts, with unchangeable liver size. Therefore, metabolic capacities of enzymes come from 2 different sources: histologically normal and cancerous liver (relative contributions of normal and cancerous parts are unknown in the current study). In this case, it is more appropriate to use MPPGL for histologically normal tissue with the weight of the liver being histologically normal and MPPGL for cancerous tissue with the weight of the liver being cancerous.

For Equation 4-4, the age was plotted against MPPGL values for Healthy population; for both observed and predicted (Barter et al., 2008) values (Supplementary Figure 4-1). For each model and for each drug, a generic trial design was used, with the following characteristics. The age range of the cancerous donors is 34-85 and the age range in the virtual population is 20 - 50 years old, which consists a limitation of our study. However, this limitation wouldn't have any effect on the final observations, as the age range is kept consistent in all the models, and additionally, age-dependent MPPGL in cancer samples was not apparent (Figure 4-4D). The mean (for all 100 virtual subjects) systemic concentration (C_{sys})-time profiles were plotted and the area under the curve from time 0 to infinity ($AUC_{0\text{-}inf}$) and maximum plasma concentration (C_{max}) values were compared across the four MPPGL methods/ models (Table 4-1). Parameters used for PBPK simulations are listed in Supplementary Table 4-2. Oral doses for alfentanil, alprazolam, midazolam and desipramine are 0.043 mg/kg, 0.5 mg, 5 mg, and 50 mg respectively.

Lack of differences in CPPGL between normal and cancerous tissue (see Results) meant that significant effects on the clearance and systemic concentrations of drugs metabolized by cytosolic enzymes were not expected. Therefore, no PBPK simulations were performed to assess possible effects on pharmacokinetics of drugs metabolized by cytosolic enzymes.

4.4 Results

4.4.1 Protein content of liver homogenates and fractions

Total protein content was measured in homogenates, microsomes, and cytosols from histologically normal and matched cancerous (n = 16) liver samples (Figure 4-1; Supplementary Table 4-3). The mean HomPPGL was 126.1 ± 46.7 mg/g in histologically normal samples and 86.9 ± 50.2 mg/g in matched cancer samples (range: 75.1-266.7 and 37.1-204.8 mg/g, respectively). The mean CPPGL was 56.2 ± 16.9 mg/g in histologically normal samples and 42.1 ± 12.9 mg/g in cancer samples (range: 32.3-80.7 and 24.8-67.2 mg/g, respectively). There was no statistically significant difference in HomPPGL (Wilcoxon test, $p = 0.0654$) and CPPGL between histologically normal and cancerous samples (Wilcoxon test, $p = 0.0654$). The mean microsomal protein isolated from liver, before correction for membrane loss was 15.8 ± 3.9 mg/g in histologically normal samples and 6.5 ± 3.3 mg/g in matched cancer samples (8.8-22.8 and 2.6-15.2 mg/g, respectively), and a 2.4-fold statistically significant difference (Wilcoxon test, $p < 0.0001$).

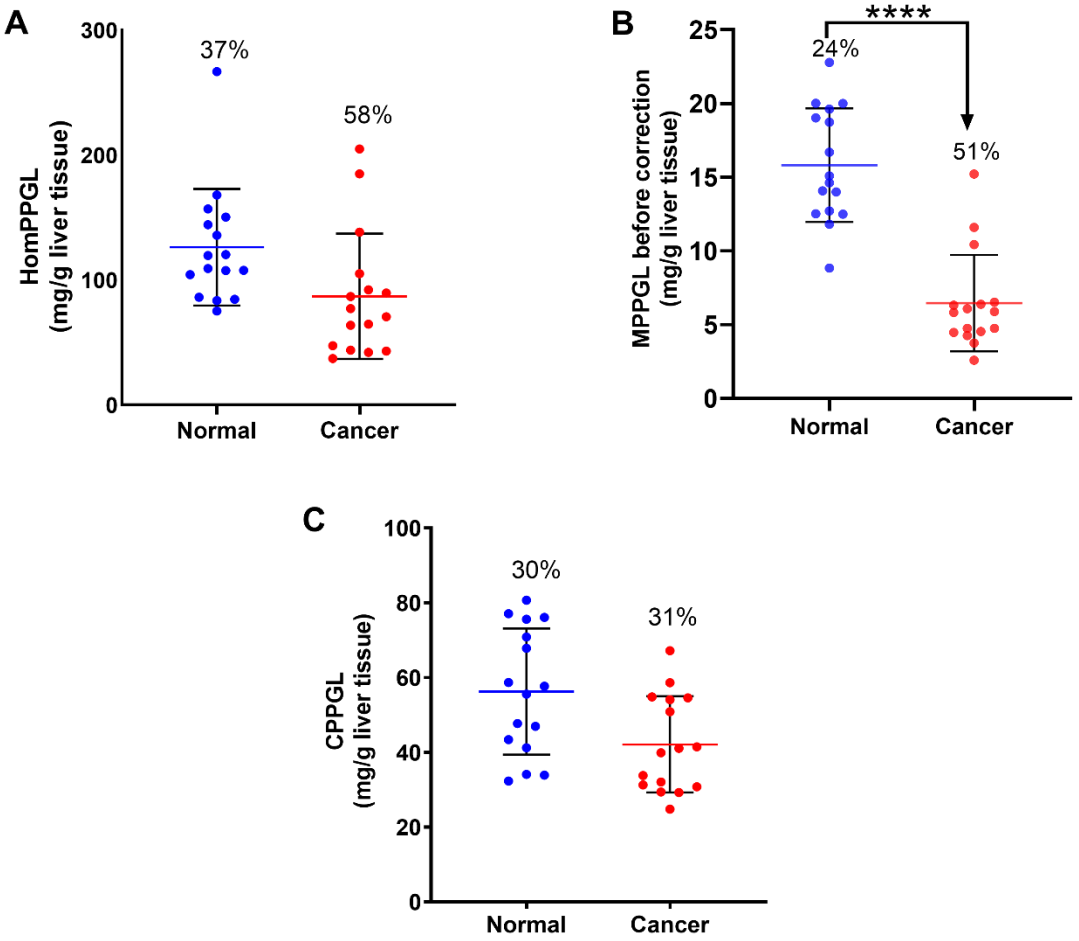

Figure 4-1 Total protein content (mg per gram of liver) in homogenates (HomPPGL, **A**), microsomal fractions (MPPGL before correction for losses, **B**) and cytosolic fractions (CPPGL, **C**) from histologically normal and matched tumor samples (n=16). The MPPGL values in panel **B** are not corrected for loss of membrane protein. Blue and red symbols represent normal and cancer samples. The lines represent means, error bars represent standard deviations, and percentages represent CVs. The asterisks (****) represent statistical differences with $p < 0.0001$ between histologically normal and cancerous tissues. Wilcoxon test was used for comparison of HomPPGL, uncorrected MPPGL, and CPPGL between matched cancerous and histologically normal samples.

4.4.2 NADPH cytochrome P450 reductase activity in homogenates and microsomes

Activity of NADPH cytochrome P450 reductase was used to assess recovery and enrichment of microsomal membrane. Activity measurements were made in homogenates and microsomal fractions of histologically normal (n = 16) and matched cancer samples (n = 11) (Figure 4-2A and Supplementary Table 4-4). Activity measurements in 5 tumorous samples were below the limit of quantitation and thus, only data for 11 tumorous samples are presented. The mean enzymatic activity in homogenates was 2.36 ± 0.73 units/mg in histologically normal tissues, and 0.58 ± 0.37 units/mg of tissue in cancer samples (range: 0.8-3.58 and 0.14-1.42 units/mg, respectively). In microsomal fractions, activity was 1.03 ± 0.44 units/mg of tissue in histologically normal tissues and 0.18 ± 0.19 units/mg of tissue in cancer samples (range: 0.34-1.72 and 0.03-0.71 units/mg of tissue, respectively).

Enrichment and recovery of microsomal proteins relative to homogenates were calculated for histologically normal (n = 16) and matched cancerous samples (n = 11), as shown in Figure 4-2B and C, respectively. Mean enrichment was 3.5 ± 1.5 fold (range: 1.5-7.3) for histologically normal and 3.3 ± 1.4 (range: 1.4-5.7 fold) for cancerous samples. Microsomal protein recovery was 0.4 ± 0.2 (range: 0.2-0.8) for histologically normal and 0.3 ± 0.1 (range: 0.1-0.5), with minimal difference in mean recovery for the normal (0.4) and cancerous samples (0.3).

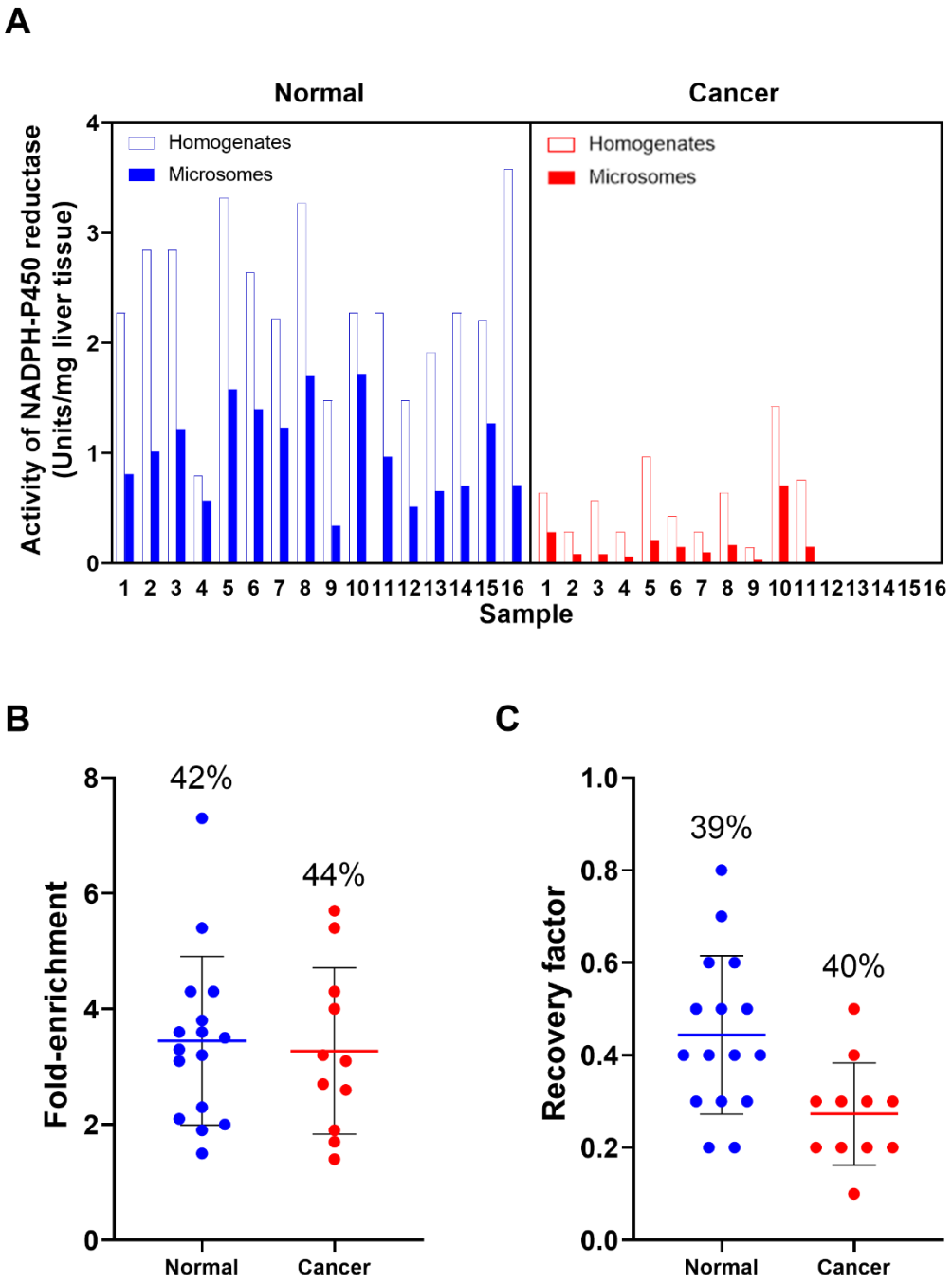

Figure 4-2 Activity of NADPH cytochrome P450 reductase in homogenates and microsomes from histologically normal (n = 16) and tumor samples (n = 11) from CRLM patients (**A**). Each bar represent the mean value of triplicate measurements of each individual sample. Blue open and solid bars correspond to normal homogenates and microsomes, respectively. Red open and solid bars correspond to cancer homogenates and microsomes, respectively. Fold-enrichment (**B**) and recovery (**C**) of microsomal proteins from histologically normal (n = 16) and tumor (n = 13) samples from CRLM patients. Lines represent means, error bars represent standard deviations, and percentages represent CVs. Blue and red symbols represent histologically normal and tumor samples, respectively.

4.4.3 Corrected microsomal protein per gram of liver (MPPGL)

The MPPGL values were corrected using the recovery factors for histologically normal (n = 16) and cancer tissues (n = 11) (Figure 4-3). The mean corrected MPPGL was 39 ± 13.8 mg/g histologically normal tissue and 24.8 ± 9.8 mg/g cancerous tissue (range: 16.5-63.1 mg/g and 8.7-43.9 mg/g, respectively). MPPGL values were significantly lower in tumorous samples compared with histologically normal samples (Mann-Whitney test, $p = 0.0109$).

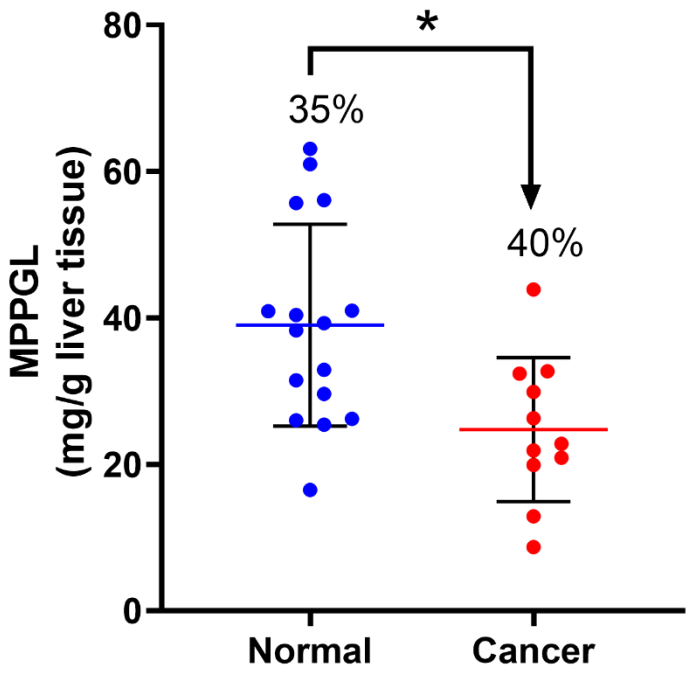

Figure 4-3 Corrected microsomal protein content (mg) per gram tissue (MPPGL) from histologically normal (n = 16) and tumor samples (n = 11). Lines represent means, error bars represent standard deviations, and percentages represent CVs. The asterisk (*) represent statistical difference (Mann-Whitney test, $p < 0.05$).

4.4.4 Effect of demographics on MPPGL values

The effects of anatomical origin of liver tissue (left or right liver lobe), sex, BMI and age on MPPGL values were tested for histologically normal and cancerous tissues (Figure 4-4). Some demographics information are not available for each sample. For example, the liver lobe (right or left) from which the sample has been taken is not available for 3 of the patients. Similarly, BMI is not available for 3 of the patients. Therefore, only 13 samples are used for the correlation of liber lobe or BMI with MPPGL. The mean MPPGL was 38.7 ± 13.1 mg/g in histologically normal tissue from the left liver lobe (n = 4; 25.4-56.1 mg/g) and 37.0 ± 14.4 mg/g in histologically normal tissue from the right liver lobe (n = 9; 16.5-61.0 mg/g). By contrast, MPPGL was 29.4 ± 4.3 mg/g in cancerous tissue from the left liver lobe (n = 2; 26.3-32.4) and 22.4 ± 7.7 mg/g in cancerous tissue from the right liver lobe (n = 7; 8.7-32.7 mg/g). The difference in MPPGL from different lobes for histologically normal was not statistically significant (Mann-Whitney test, $p = 0.9399$). The statistical test was not applied to data from tumorous samples due to the low sample size from the left liver lobe (n = 2) (Figure 4-4A). The MPPGL was 38.3 ± 14.3 mg/g and 39.5 ± 14.3 mg/g for female (n = 7; 6.5-56.1 mg/g) and male (n = 9; 25.4-63.1 mg/g) donors of histologically normal tissue, respectively. MPPGL was 23.3 ± 7.2 mg/g and 26.0 ± 12.2 mg/g for female (n = 5; 12.9-32.7 mg/g) and male (n = 6; 8.7-43.9 mg/g) donors of cancerous tissues, respectively. No significant differences in MPPGL between male and female donors of histologically normal (Mann-Whitney test, $p = 0.8371$) and tumorous tissues were observed (Mann-Whitney test, $p > 0.9999$) (Figure 4-4B). There was no trend in MPPGL values with BMI (Spearman test, $p = 0.6338$) or age (Spearman test, $p = 0.8711$) (Figure 4-4C and D, respectively).

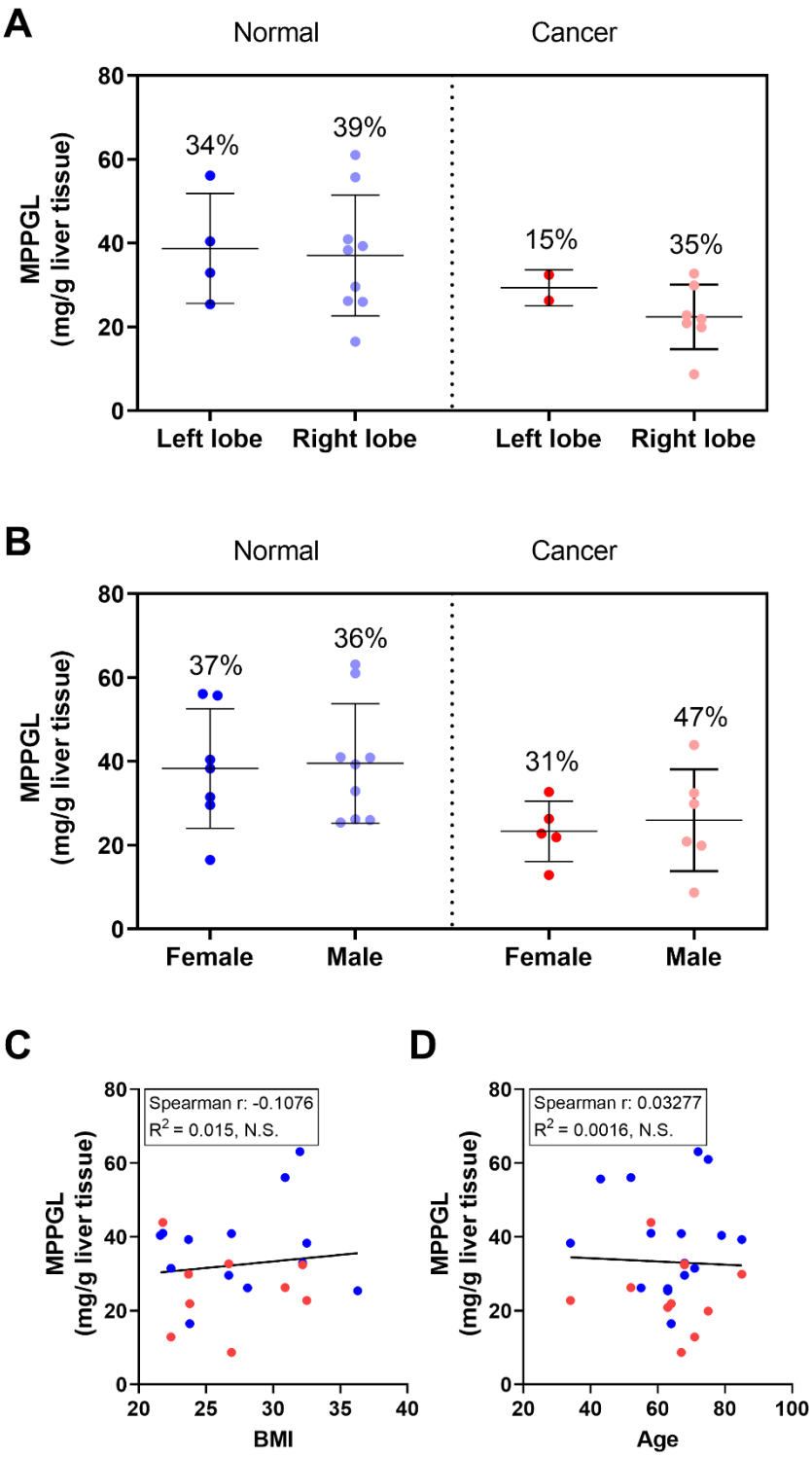

Figure 4-4 Effects of liver lobe (**A**), sex (**B**), BMI (**C**) and age (**D**) on MPPGL values for histologically normal and cancer samples. In panels A and B, lines represent means, error bars represent standard deviation values and percentages represent CVs. Mann-Whitney test was used to assess the effect of hepatic lobes and sex. Spearman correlation and linear regression were used to assess the effect of BMI and age. Blue symbols represent histologically normal samples and red symbols represent cancer samples. N.S. means no significant relation ($p > 0.05$).

4.4.5 Effect of demographics on CPPGL values

The effects of anatomical origin of tissue (left or right liver lobe), sex, BMI and age on CPPGL values were tested for histologically normal and cancerous tissues (Figure 4-5). Some demographics information are not available for each sample. For example, the liver lobe (right or left) from which the sample has been taken is not available for 3 of the patients. Similarly, BMI is not available for 3 of the patients. Therefore, only 13 samples are used for the correlation of liber lobe or BMI with CPPGL. The mean CPPGL was 47.7 ± 11.1 mg/g in histologically normal tissue from the left liver lobe (n = 4; 33.9-57.7 mg/g) and 58.3 ± 18.8 mg/g in histologically normal tissue from the right lobe (n = 9; 32.3-80.7 mg/g). CPPGL was 45.2 ± 11.4 mg/g in cancerous tissue from the left liver lobe (n = 4; 30.8-54.6 mg/g) and 38.5 ± 11.5 mg/g in cancerous tissue from the right liver lobe (n = 9; 24.8-58.6 mg/g). There was no statistically significant difference in CPPGL from different lobes for histologically normal (Mann-Whitney test, p = 0.3301) or tumorous samples (Mann-Whitney test, p = 0.6042) (Figure 4-5A). The CPPGL was 61.4 ± 14.9 mg/g and 52.2 ± 18 mg/g for female (n = 7; 34.1-77.1 mg/g) and male (n = 9; 32.3-80.7 mg/g) donors of histologically normal tissue, respectively. CPPGL was 37.8 ± 12.4 mg/g and 45.5 ± 12.9 mg/g for female (n = 7; 24.8-54.8 mg/g) and male (n = 9; 30.8-67.2 mg/g) donors of cancerous tissues. There was no statistically significant difference in CPPGL between male and female donors of histologically normal (Mann-Whitney test, p = 0.2991) or tumorous tissues (Mann-Whitney test, p = 0.1738) (Figure 4-5B). There was no specific correlation between CPPGL values and BMI (Spearman test, p = 0.2191) or age (Spearman test, p = 0.27415) (Figure 4-5C and D, respectively).

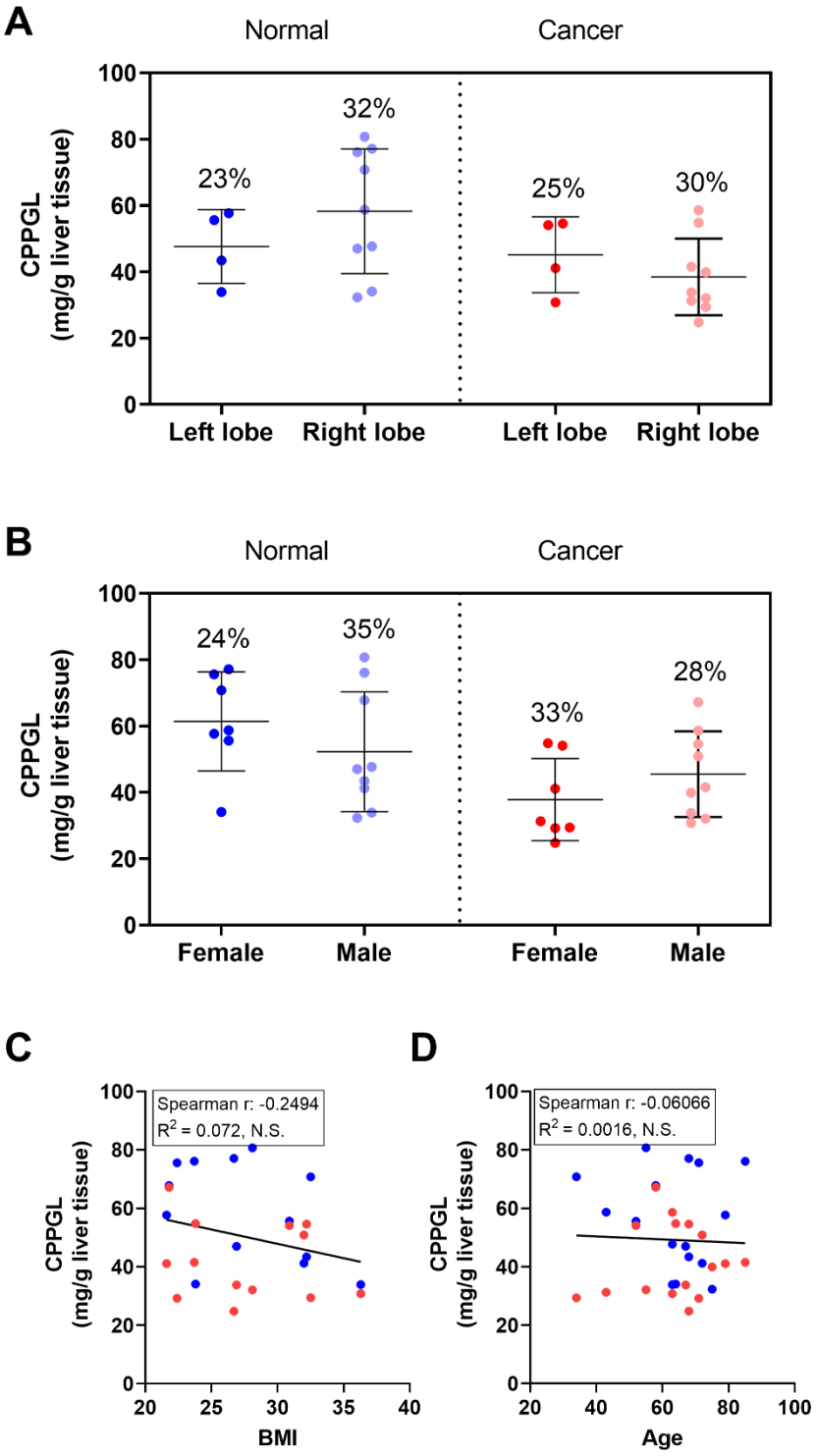

Figure 4-5 Effects of liver lobe (**A**), sex (**B**), BMI (**C**) and age (D) on CPPGL values for histologically normal and cancer samples. In panels A and B, lines represent means, error bars represent standard deviation values and percentages represent CVs. Mann-Whitney test was used to assess the effect of hepatic lobes and sex. Spearman correlation and linear regression were used to assess the effect of BMI and age. Blue symbols represent histologically normal samples and red symbols represent cancer samples. N.S. means no significant relation ($p > 0.05$).

4.4.6 Physiologically based pharmacokinetic (PBPK) simulations

Simulations for four different drugs (alfentanil, alprazolam, midazolam, desipramine) were performed using four different methods (Figure 4-6); Model 1 (Healthy) used default MPPGL (Simcyp) with a healthy population, Model 2 (Cancer-D) used default MPPGL with a cancer population, Model 3 (New Cancer-ALN) used MPPGL measured in this study in histologically normal tissue with a cancer population, and Model 4 (New Cancer-ALC) used MPPGL measured in this study in cancer tissue with a cancer population. Table 4-1 lists pharmacokinetic parameter values (T_{max}, C_{max}, and $AUC_{0\text{-}inf}$) for all simulations. Cmax is the maximum drug concentration observed in plasma, and Tmax is the time at which the highest drug concentration occurs after drug administration. AUC0-inf is the area under the plasma drug concentration-time curve from time 0 to infinity. New Cancer-ALN assumes that the whole liver is histologically normal, whereas New Cancer-ALC assumes that the whole liver is cancerous. For alfentanil, $AUC_{0\text{-}inf}$ predicted using MPPGL of cancerous tissue (New Cancer-ALC) was approximately 3.3 fold higher of that obtained using default MPPGL (Simcyp) with a healthy population (Healthy), whereas for midazolam, alprazolam and desipramine, this value was approximately 1.4 fold higher.

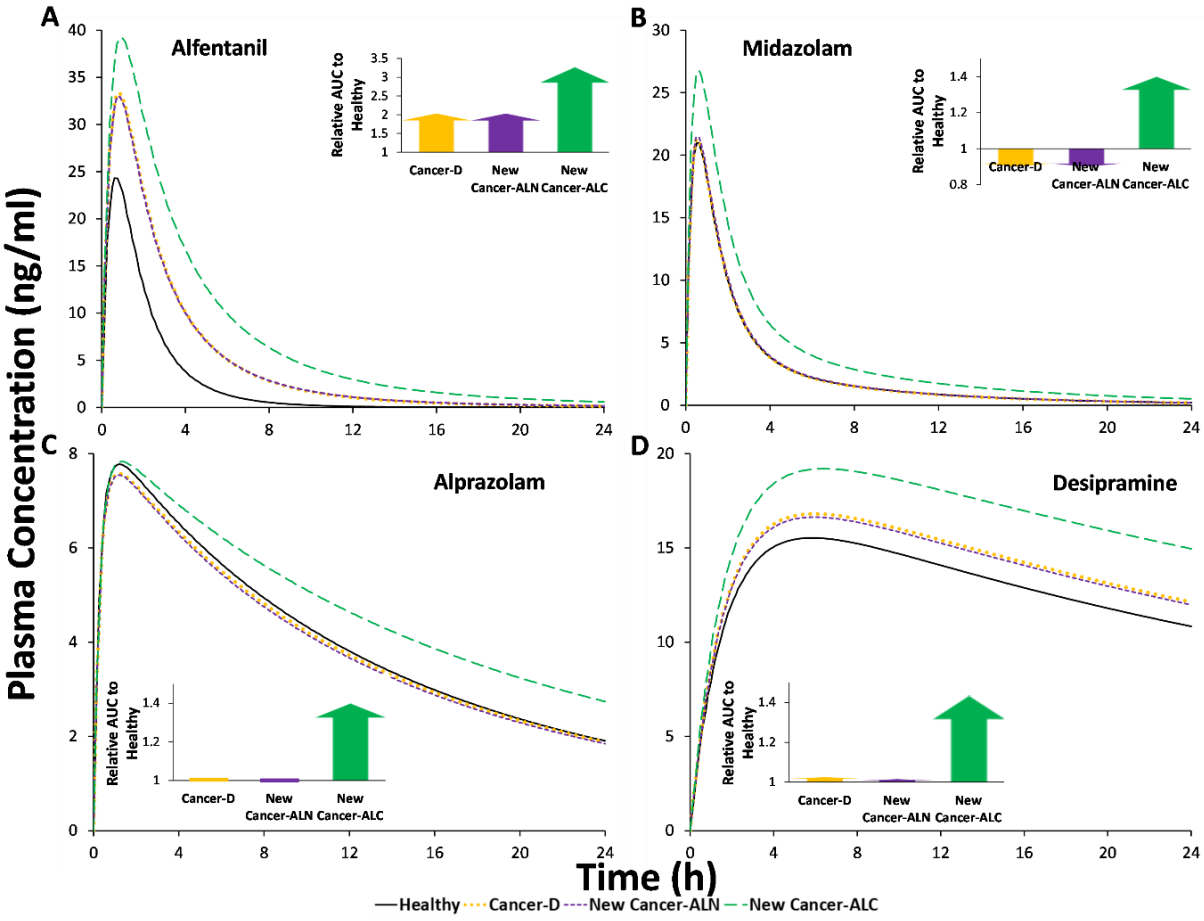

Figure 4-6 Mean predicted systemic concentration over time (24 hours) after oral administration of alfentanil (**A**), midazolam (**B**), alprazolam (**C**), and desipramine (**D**) For each drug, four different methods of scaling were used. Healthy: default MPPGL (Simcyp) with a healthy population. Cancer-D: default MPPGL with a cancer population. New Cancer-ALN: MPPGL measured in this study for histologically normal tissue with a cancer population. New Cancer-ALC: MPPGL measured in this study for cancer tissue with a cancer population. Inset graphs show the Relative $AUC_{0\text{-}inf}$ (0 to infinity) ratios of Cancer-D, New Cancer-ALN, and New Cancer-ALC to Healthy.

Table 4-1 Mean predicted E_H, Tmax, Cmax, and $AUC_{0\text{-}inf}$ for oral alfentanil, alprazolam, midazolam, and desipramine using four different scaling methods within PBPK model. $AUC_{0\text{-}inf}$ ratios using different methods are also provided.

Drug	Model	E_H	Cmax (ng/ml)	$AUC_{0\text{-}inf}$ (ng/ml.h)	Tmax (h)	Relative $AUC_{0\text{-}inf}$ ratios to Healthy
Alfentanil	Healthy	0.36	24	59	0.6	
	Cancer-D	0.24	33	120	0.9	2
	New Cancer-ALN	0.25	33	120	0.9	2
	New Cancer-ALC	0.17	39	193	0.9	3.3
Alprazolam	Healthy	0.04	8	144	1.2	
	Cancer-D	0.04	8	142	1.2	1
	New Cancer-ALN	0.04	8	140	1.2	1
	New Cancer-ALC	0.03	8	199	1.3	1.4
Midazolam	Healthy	0.43	24	76	0.6	
	Cancer-D	0.48	21	65	0.6	0.9
	New Cancer-ALN	0.48	21	65	0.5	0.9
	New Cancer-ALC	0.38	27	104	0.6	1.4
Desipramine	Healthy	0.42	16	1385	5.9	
	Cancer-D	0.34	17	1421	5.9	1
	New Cancer-ALN	0.35	17	1406	5.9	1
	New Cancer-ALC	0.27	19	1989	6.4	1.4

Hepatic extraction ratio = E_H, Cmax = maximum plasma concentration, $AUC_{0\text{-}inf}$ = Area under the curve from time 0 to infinity, T_{max} = time at which C_{max} is observed. For each simulation, ten trials and ten subjects per trial were included.

Healthy: default MPPGL (Simcyp) with a healthy population. Cancer-D: default MPPGL with a cancer population. New Cancer-ALN: MPPGL measured in this study for histologically normal tissue with a cancer population. New Cancer-ALC: MPPGL measured in this study for cancer tissue with a cancer population.

4.5 Discussion

Scaling factors, including MPPGL and CPPGL, are used for IVIVE of data generated in in vitro systems to predict metabolic clearance of drugs (Wilson et al., 2003; Barter et al., 2007; Cubitt et al., 2011). Inter-individual variability of MPPGL has been reported previously (Wilson et al., 2003; Barter et al., 2008) and may explain part of the variation in metabolic clearance in the absence of genetic differences in the abundance and activity of enzymes in individuals. The data describing scalars in special populations and in disease states, such as cancer, are scarce. In addition, the effects of changes in these scalars (MPPGL, CPPGL) in cancer patients on metabolic clearance have not been investigated. As cancer is not a uniform disease (for example, drug metabolizing enzymes and transporters may vary in different cancer types), the effects in each cancer type should be addressed independently. Changes in MPPGL for primary hepatocellular carcinoma compared with histologically normal tissue have been reported (Zhang et al., 2015; Gao et al., 2016), but corresponding data for metastatic liver cancer are currently lacking. To our knowledge, our study is the first to describe scaling factors for CRLM.

In this study, CPPGL and HomPPGL values were measured as the total protein content of each fraction, while MPPGL was calculated by correcting for protein loss during fractionation using cytochrome P450 reductase activity, a microsomal membrane marker. MPPGL values for histologically normal tissues (39.0 ± 13.8 mg/g of tissue) were consistent with the literature (Pelkonen et al., 1973; Wilson et al., 2003; Barter et al., 2007; Zhang et al., 2015), while values in cancerous tissues were significantly lower (24.8 ± 12.9 mg/g of tissue). A difference in the CV% was also observed between the histologically normal (CV% = 35) and the cancer tissues (CV% = 40). Higher CV% in cancer tissues may reflect the heterogeneity of cancer tissues or the different number of samples (smaller in cancer) that could increase the variability in cancer. The global reduction in microsomal protein content suggests that the abundance (pmol/g liver) of microsomal proteins, such as cytochrome P450 enzymes, in liver tissue may decrease in CRLM. Reported data on cytochrome P450 are limited to qualitative evidence that identify specific enzymes in histologically normal and tumorous tissues from CRLM patients (Lane et al., 2004) and therefore, future proteomics studies involving quantification of such enzymes would be valuable. Functional activity studies with probe substrates would also be useful but require larger samples than are available to us currently. CPPGL and HomPPGL values showed little difference between cancerous and histologically normal tissues, and CPPGL in

histologically normal tissue (56.2 ± 16.9 mg/g of tissue) was consistent with the literature (45-134 mg/g) (Boogaard et al., 1996; Renwick et al., 2002; Mutch et al., 2007).

The potential effects of donor demographics (such as age, sex, BMI) and sampled liver lobe on MPPGL and CPPGL values were evaluated. Statistical analysis showed no relationship between the examined variables and changes in MPPGL and CPPGL values. Barter et al. (2007) performed a meta-analysis of literature data from 114 individuals and reported a relationship between age and MPPGL; values decreased with increasing age (40 mg/g liver for a 30 years old individual and 31 mg/g liver for a 60 years old individual). This effect of age on MPPGL had not been discernible in the component individual studies (Pelkonen et al., 1974; Lipscomb et al., 1998, 2003; Wilson et al., 2003; Hakooz et al., 2006). A more recent study by Barter et al. (2008) showed that MPPGL values increased from childhood until the age of 28 years, then decreased thereafter. The small sample size and large underlying variability in the data of the present study meant that any correlation of MPPGL with age could not be delineated. Likewise, BMI did not affect MPPGL and CPPGL in either normal or cancerous tissues based on data from this study. There is no published literature on correlation between BMI and MPPGL or CPPGL in cancer. The sex of donors had no discernible effect on MPPGL or CPPGL in normal or cancerous tissues, consistent with earlier studies (Wilson et al., 2003; Schmucker et al., 1990). In addition, the liver lobe from which the tissues were samples did not have an effect on MPPGL or CPPGL values from either normal or cancerous tissues. There are no reported data in the literature about regional differences in human liver, but studies in mice showed that microsomal P450 activity is variable in different lobes (Rudeck et al., 2018). Additionally, there was an effort to correlate the MPPGL values to the disease severity. No trend was observed, although the way that the samples were categorized according to the disease severity was not completely quantitative. This is a result of the small number of samples, and the lack of the information about the disease severity for all the patients.

The impact of applying different MPPGL values as scalars was studied using PBPK simulations on different drugs (alfentanil, alprazolam, midazolam, desipramine) metabolized by CYP enzymes with different extraction ratios. Generally, PK profiles of drugs are expected to differ in cancer populations compared with profiles in healthy subjects. In many cases, clearance of anti-cancer drugs decreases in cancer patients compared with healthy individuals (Piotrovsky et al., 1998; Houk et al., 2009; Hudachek et al., 2010) for various reasons, including co-morbidities, such as hepatic and renal impairment in cancer patients (Suri et al., 2015). Another possible reason may be changes in MPPGL or CPPGL and differences in the

expression of enzymes and transporters (Gao et al., 2016; Billington et al., 2018). Our data showed little difference in CPPGL between normal and cancerous tissues, but significantly lower MPPGL in cancer samples. Therefore, only the effect of MPPGL on drug pharmacokinetics was assessed in the simulations. MPPGL was used in other studies for scaling in hepatocellular carcinoma and glioblastoma (Gao et al., 2016; Li et al., 2017), and the present study is the first to assess the effect of changes in MPPGL in CRLM. The results for all the drugs showed that the MPPGL value affected drug exposure, suggesting that the proportion of the liver affected by cancer affects drug levels reaching the systemic circulation. More specifically, when the whole liver was assumed to be tumorous, higher systemic concentration was predicted compared with a histologically normal liver. Our simulations show that using appropriate MPPGL values for a certain population is important for the prediction of drug exposure; however, the applied MPPGL value should be accompanied by the percentage of cancerous liver in each patient. Although the percentage of cancerous liver is not known for the present study, it is common practice for major hepatectomy to resect up to 70% of the total liver for a sufficient liver function, including histologically normal and cancerous tissue (Hemming et al., 2003; Jiang et al, 2018). As a result, there may be a significant contribution of the tumour to the overall liver activity in CRLM patients. If we know the proportion of normal to cancerous tissue for an individual, then such data can be incorporated into the PBPK model. Otherwise, sensitivity and uncertainty analysis should be performed between two extreme cases (100% normal vs 100% cancerous) to establish worst-case scenario. It is important to clarify that the predicted PK profiles are not compared with clinical data, which are not available for CRLM patients. Therefore, our simulations are not indicative of which method is correct with observations, but they point out the assumption that MPPGL affect the PK in cancer patients. Further work is needed to verify this updated PBPK cancer population model against clinical data. PK may also depend on cancer stage, starting with a small amount of liver being affected (New Cancer-ALN) resulting in a high amount of liver being cancerous (New Cancer-ALC). In this study, we assumed that the abundance of CYPs in CRLM was the same as for the generic healthy and cancer population in Simcyp. Although there are no published data on the abundance in CRLM, potential differences in the abundance of CYPs may have additive effects on the PK (Vasilogianni et al., in preparation).

In summary, this study assessed, for the first time, scaling factors specific for CRLM patients and showed significantly lower MPPGL in cancerous tissue compared with histologically normal tissue from CRLM patients. HomPPGL and CPPGL did not differ significantly between

cancerous and histologically normal samples. Donor demographics (age, sex, BMI) and the anatomical origin of samples (liver lobe) had no effect on MPPGL and CPPGL values. PBPK simulations on drugs with different extraction ratios metabolized by CYPs revealed substantial difference in drug exposure, up to 3.3-fold, when comparing default scaling factors to population-specific scalars. It is therefore recommended that appropriate population-specific MPPGL values, accounting for percentage of liver/tumorous liver tissue, should be considered for prediction of drug exposure in cancer patients. Future studies should quantify enzyme abundance differences to improve understanding of metabolic drug clearance in cancer.

4.6 References

Achour B, Al Feteisi H, Lanucara F, Rostami-Hodjegan A, and Barber J (2017) Global proteomic analysis of human liver microsomes: Rapid characterization and quantification of hepatic drug-metabolizing enzymes. *Drug Metab Dispos* **45**:666-675.

Achour B, Barber J, and Rostami-Hodjegan A (2011) Cytochrome P450 Pig Liver Pie: Determination of Individual Cytochrome P450 Isoform Contents in Microsomes from Two Pig Livers Using Liquid Chromatography in Conjunction with Mass Spectrometry. *Drug Metab Dispos* **39**:2130–2134.

Barter ZE, Bayliss M, Beaune P, Boobis A, Carlile D, Edwards R, Houston BJ, Lake B, Lipscomb J, and Pelkonen O, et al. (2007) Scaling Factors for the Extrapolation of In Vivo Metabolic Drug Clearance From In Vitro Data: Reaching a Consensus on Values of Human Micro-somal Protein and Hepatocellularity Per Gram of Liver. *Curr Drug Metab* **8**:33–45.

Barter ZE, Chowdry JE, Harlow JR, Snawder JE, Lipscomb JC, and Rostami-Hodjegan A (2008) Covariation of human microsomal protein per gram of liver with age: Absence of influence of operator and sample storage may justify interlaboratory data pooling. *Drug Metab Dispos* **36**:2405–2409.

Bates SE, Berry DA, Balasubramaniam S, Bailey S, LoRusso PM, and Rubin EH (2015) Advancing Clinical Trials to Streamline Drug Development. *Clin Cancer Res* **21**:4527–4535.

Billington S, Ray AS, Salphati L, Xiao G, Chu X, Humphreys WG, Liao M, Lee CA, Mathias A, and Hop C, et al. (2018) Transporter expression in non-cancerous and cancerous liver tissue from subjects with hepatocellular carcinoma and chronic hepatitis C infection quantified by LC-MS/MS proteomics. *Drug Metab Dispos* **46**:189-96.

Boogaard PJ, Sumner SC-J, and Bond JA (1996) Glutathione Conjugation of 1,2:3,4-Diepoxybutane in Human Liver and Rat and Mouse Liver and Lungin Vitro. *Toxicol Appl Pharmacol* **136**:307–316.

Bray F, Ferlay J, Soerjomataram I, Siegel RL, Torre LA, and Jemal A (2018) Global cancer statistics 2018: GLOBOCAN estimates of incidence and mortality worldwide for 36 cancers in 185 countries. *CA Cancer J Clin* **68**:394–424.

Cubitt HE, Houston JB, and Galetin A (2011) Prediction of Human Drug Clearance by Multiple Metabolic Pathways: Integration of Hepatic and Intestinal Microsomal and Cytosolic Data. *Drug Metab Dispos* **39**:864–873.

Darwich AS, Ogungbenro K, Hatley OJ, and Rostami-Hodjegan A (2017) Role of pharmacokinetic modeling and simulation in precision dosing of anticancer drugs. *Transl Cancer Res* **6**:1512–1529.

Gao J, Zhou J, He XP, Zhang YF, Gao N, Tian X, Fang Y, Wen Q, Jia LJ, and Jin H, et al. (2016) Changes in cytochrome P450s-mediated drug clearance in patients with hepatocellular carcinoma in vitro and in vivo: A bottom-up approach. *Oncotarget* **7**:28612–28623.

Guengerich FP, Martin M V, Sohl CD, and Cheng Q (2009) Measurement of cytochrome P450 and NADPH–cytochrome P450 reductase. *Nat Protoc* **4**:1245–1251.

Gutierrez ME, Kummar S, and Giaccone G (2009) Next generation oncology drug development: opportunities and challenges. *Nat Rev Clin Oncol* **6**:259–265.

Hakooz N, Ito K, Rawden H, Gill H, Lemmers L, Boobis AR, Edwards RJ, Carlile DJ, Lake BG, and Houston JB (2006) Determination of a Human Hepatic Microsomal Scaling Factor for Predicting in Vivo Drug Clearance. *Pharm Res* **23**:533–539.

Hemming AW, Reed AI, Howard RJ, Fujita S, Hochwald SN, Caridi JG, Hawkins IF, and Vauthey JN (2003) Preoperative portal vein embolization for extended hepatectomy. *Ann Surg* **237**:686–693.

Holch JW, Demmer M, Lamersdorf C, Michl M, Schulz C, von Einem JC, Modest DP, and Heinemann V (2017) Pattern and Dynamics of Distant Metastases in Metastatic Colorectal Cancer. *Visc Med* **33**:70–75.

Houk BE, Bello CL, Kang D, and Amantea M (2009) A population pharmacokinetic meta-analysis of sunitinib malate (SU11248) and its primary metabolite (SU12662) in healthy volunteers and oncology patients. *Clin Cancer Res* **15**:2497–2506.

Hudachek SF, Eckhardt SG, Hicks B, and Gustafson DL (2010) Population pharmacokinetic model of PI88, a heparanase inhibitor. *Cancer Chemoth Pharmacol* **65**:743-753.

Jiang Z, Li C, Zhao Z, Liu Z, Guan X, Yang M, Li X, Yuan D, Qiu S, and Wang X (2018) Abnormal Liver Function Induced by Space-Occupying Lesions Is Associated with

Unfavorable Oncologic Outcome in Patients with Colorectal Cancer Liver Metastases. *Biomed Res Int* **2018**:1–7.

Lane CS, Nisar S, Griffiths WJ, Fuller BJ, Davidson BR, Hewes J, Welham KJ, and Patterson LH (2004) Identification of cytochrome P450 enzymes in human colorectal metastases and the surrounding liver: A proteomic approach. *Eur J Cancer* **40**:2127–2134.

Li J, Wu J, Bao X, Honea N, Xie Y, Kim S, Sparreboom A, and Sanai N (2017) Quantitative and mechanistic understanding of AZD1775 penetration across human blood-brain barrier in glioblastoma patients using an IVIVE-PBPK modeling approach. *Clin Cancer Res* **23**:7454–7466.

Lipscomb JC, Fisher JW, Confer PD, and Byczkowski JZ (1998) In Vitro t oin Vivo Extrapolation for Trichloroethylene Metabolism in Humans. *Toxicol Appl Pharmacol* **152**:376–387.

Lipscomb JC, Teuschler LK, Swartout JC, Striley CAF, and Snawder JE (2003) Variance of Microsomal Protein and Cytochrome P450 2E1 and 3A Forms in Adult Human Liver. *Toxicol Mech Methods* **13**:45–51.

Mutch E, Nave R, McCracken N, Zech K, and Williams FM (2007) The role of esterases in the metabolism of ciclesonide to desisobutyryl-ciclesonide in human tissue. *Biochem Pharmacol* **73**:1657–1664.

Pelkonen O, Kaltiala EH, Larmi TKI, and Kärki NT (1973) Comparison of activities of drug-metabolizing enzymes in human fetal and adult livers. *Clin Pharmacol Ther* **14**:840–846.

Pelkonen O, Kaltiala EH, Larmi TKI, and Kärki NT (1974) Cytochrome P-450-linked monooxygenase system and drug-induced spectral interactions in human liver microsomes. *Chem Biol Interact* **9**:205–216.

Piotrovsky VK, Huang ML, Van Peer A, and Langenaecken C (1998) Effects of demographic variables on vorozole pharmacokinetics in healthy volunteers and in breast cancer patients. *Cancer Chemother Pharmacol* **42**:221–228.

Renwick AB, Ball SE, Tredger JM, Price RJ, Walters DG, Kao J, Scatina JA, and Lake BG (2002) Inhibition of zaleplon metabolism by cimetidine in the human liver: in vitro studies with subcellular fractions and precision-cut liver slices. *Xenobiotica* **32**:849–862.

Rostami-Hodjegan A (2012) Physiologically based pharmacokinetics joined with in vitro-in

vivo extrapolation of ADME: A marriage under the arch of systems pharmacology. *Clin Pharmacol Ther* **92**:50–61.

Rudeck J, Bert B, Marx-Stoelting P, Schönfelder G, and Vogl S (2018) Liver lobe and strain differences in the activity of murine cytochrome P450 enzymes. *Toxicology* **404**–**405**:76–85.

Schmucker DL, Woodhouse KW, Wang RK, Wynne H, James OF, McManus M, and Kremers P (1990) Effects of age and gender on in vitro properties of human liver microsomal monooxygenases. *Clin Pharmacol Ther* **48**:365–374.

Siegel RL, Miller KD, and Jemal A (2018) Cancer statistics, 2018. *CA Cancer J Clin* **68**:7–30.

Suri A, Chapel S, Lu C, and Venkatakrishnan K (2015) Physiologically based and population PK modeling in optimizing drug development: A predict-learn-confirm analysis. *Clin Pharmacol Ther* **98**:336–344.

Wilson ZE, Rostami-Hodjegan A, Burn JL, Tooley A, Boyle J, Ellis SW, and Tucker GT (2003) Inter-individual variability in levels of human microsomal protein and hepatocellularity per gram of liver. *Br J Clin Pharmacol* **56**:433–440.

Wong VKH, Malik HZ, Hamady ZZR, Al-Mukhtar A, Gomez D, Prasad KR, Toogood GJ, and Lodge JPA (2007) C-reactive protein as a predictor of prognosis following curative resection for colorectal liver metastases. *Br J Cancer* **96**:222–225.

Yoshida K, Budha N, and Jin JY (2017) Impact of physiologically based pharmacokinetic models on regulatory reviews and product labels: Frequent utilization in the field of oncology. *Clin Pharmacol Ther* **101**:597–602.

Zhang H, Gao N, Tian X, Liu T, Fang Y, Zhou J, Wen Q, Xu B, Qi B, and Gao J, et al. (2015) Content and activity of human liver microsomal protein and prediction of individual hepatic clearance in vivo. *Sci Rep* **5**:17671.

4.7 Supplementary Information

Supplementary Table 4-1 Demographic and clinical details of CRLM patients.

Sample ID	Age at surgery (years)	Race	Sex	Body mass index, BMI (kg/m^2)	Smoking/ Alcohol use	Liver lobe	Diagnosis	Medical history	Treatment
389	52	Caucasian	Female	30.86	No/ Occasionally	Left	Metastatic moderately well differentiated adenocarcinoma	Deep vein thrombosis, asthma, duodenal ulcer, thyroid problem, liver lesions	Fragmin, levothyroxine, betamethasone, ventolin, ferrous fumarate
590	72	Caucasian	Male	32	Pipe/ 22 units per week	-	Metastatic moderate to Well differentiated adenocarcinoma (dirty necrosis)	Asthma, polypectomy, tonsillectomy, Hemicolectomy Dukes B	Salbutamol, tiotropium, lansaprozole, nasonex
633	67	Caucasian	Male	26.85	Ex-stopped/ -	Right	Metastatic adenocarcinoma & fatty liver disease	Peripheral neuropathy secondary to oxaliplatin, type 2 diabetes, hypercholesterolemia, valvular heart disease, prostate cancer with bone metastasis, colonic	Metformin, zoladex, oxaplatin and 5FU, irinotecan and 5FU with cetuximab

								cancer T3N0, colorectal liver metastasis	
674	68	Caucasian	Female	26.67	No/ -	Right	Metastatic moderately differentiated adenocarcinoma	Rectosigmoid cancer 10/10 Dukes B	-
734	64	Caucasian	Female	23.84	No/ Occasionally	Right	Moderately to focally poorly differentiated metastatic adenocarcinoma	Primary colorectal	Dalteparin, short course of radiotherapy, adjuvant OXmdG and 5FU
746	85	Caucasian	Male	23.67	Ex (40 years)/ Moderately	Right	Metastatic papillary carcinoma	Laparoscopic R hemicolectomy T2M0, Squamous cell carcinoma (scalp), hypothyroidism, hypertension, Chronic obstructive pulmonary disease	Irbesartan, levothyroxine, bisoprolol, aspirin, omeprazole, budesamide, formoterol
794	71	Caucasian	Female	22.41	No/ No	-	Metastatic adenocarcinoma with extensive intra-acinar necrosis	R hemicolectomy, pT3N2, high blood pressure, depression	Tomudex chemotherapy
818	58	Caucasian	Male	21.78	Ex (25 years)/ 18 units per week	-	Moderately differentiated metastatic adenocarcinoma	Sigmoid adenocarcinoma pT3pN2	Loperamide, carboplatin/5FU and modified de Gramont and radiotherapy

1492	34	-	Female	32.53	Ex-stopped/ Approximately 20 units per week	Right	Metastatic moderate and poorly differentiated adenocarcinoma	Bowel resection, pilonodal abcess x2, grometts (as a child), tonsillectomy (as a child), egg collection, occasional palpitations, asthma (as a child), reflux, joint problems in knees, treated for Irritable bowel syndrome	Omeprazole, amitryptyline, microgynon, glucosamine sulphate, ibuprofen, peppermint oil
1493	75	-	Male	-	No/ No	Right	Metastatic moderately differentiated adenocarcinoma	Sigmoid tumour, sleep apnoea, asthma	Cod liver oil, salbutamol inhaler, seretide inhaler, movicol
1498	63	Caucasian	Male	-	No/ Rarely	Right	Metastatic adenocarcinoma	Previous gout, anaemia, cataract operation	Doxycycline regime completed, Nil regular
1795	63		Male	36.32	Ex - stopped (previously 30cpd)/ Approximately 75 units per week	Left	Metastatic well differentiated adenocarcinoma	Adenocarcinoma, hypertension, intermittent claudication of left leg	Omeprazole, irbesartan, simvastatin, clopidogrel
1957	68	-	Male	32.16	No/ -	Left	Metastatic moderately differentiated adenocarcinoma	Primary rectal cancer, pneumonia post-operative, liver	Nil regular

								cancer, late lung metastasis	
2036	43	-	Female	-	-/ -	Right	Metastatic moderate to poorly differentiated adenocarcinoma	Primary colorectal	Omeprazole, paracetamol
2058	79	Caucasian	Female	21.6	-/ -	Left	Metastatic adenocarcinoma	Below the knee amputation, primary colorectal, lung metastasis	Lansoprazole, ferrous sulphate, alendronic acid, paracetamol, codeine phosphate, senna, natecal D3
2095	55	Caucasian	Male	28.1	-/ -	Right	Metastatic moderately differentiated adenocarcinoma	Primary colorectal	Nil regular

Supplementary Table 4-2 Input parameters for PBPK modelling using Simcyp v18 R1 for alfentanil (predominantly metabolized by CYP3A4), alprazolam (predominantly metabolized by CYP3A4 and CYP3A5), desipramine (predominantly metabolized by CYP2D6), and midazolam (predominantly metabolized by CYP3A4 and CYP3A5).

Input Parameters				
Compound Name	**SV-Alfentanil**	**SV-Alprazolam**	**SV-Desipramine**	**Sim-Midazolam**
Mol Weight (g/mol)	416.520	308.800	266.400	325.800
log P	2.160	2.120	4.570	3.530
Compound Type	Monoprotic Base	Monoprotic Base	Monoprotic Base	Monoprotic Base
pKa 1	6.500	2.400	10.260	6.000
pKa 2	n/a	n/a	n/a	n/a
B/P	0.630	0.825	1.160	0.603
Haematocrit	45.000	45.000	45.000	45.000
fu	0.104	0.290	0.240	0.032
GI Absorption Model	1st order	1st order	1st order	1st order
GI Permeability Assay	n/a	n/a	Entered	n/a
GI Peff,man	Regional	Regional	Regional	Regional
Distribution Model	Minimal PBPK Model	Minimal PBPK Model	Minimal PBPK Model	Minimal PBPK Model
Vss (L/kg)	0.370	0.760	20.800	0.880
Prediction Method	Entered	Entered	Entered	Entered
Clearance Type	Enzyme Kinetics	Enzyme Kinetics	Enzyme Kinetics	Enzyme Kinetics
Trial Design				
Population Name	Sim-Healthy Volunteers/Cancer	Sim-Healthy Volunteers/Cancer	Sim-Healthy Volunteers/Cancer	Sim-Healthy Volunteers/Cancer
Use Pop Representative	No	No	No	No
Population Size	100.000	100.000	100.000	100.000
Number of Trials	10.000	10.000	10.000	10.000
No. of Subjects per Trial	10.000	10.000	10.000	10.000
Start Day/Time	Day 1, 09:00	Day 1, 09:00	Day 1, 09:00	Day 1, 09:00
End Day/Time	Day 2, 09:00	Day 2, 09:00	Day 2, 09:00	Day 2, 09:00
Study Duration (h)	24.000	24.000	24.000	24.000
Sampling Time	Pre-defined Uniform	Pre-defined Uniform	Pre-defined Uniform	Pre-defined Uniform
Sampling Site Selection	Off	Off	Off	Off
Prandial State	Fasted	Fasted	Fasted	Fasted
Route	Oral	Oral	Oral	Oral
Dose Units	Dose (mg/kg)	Dose (mg)	Dose (mg)	Dose (mg)
Dose	0.043	0.500	50.000	5.000
Start Day/Time	Day 1, 09:00	Day 1, 09:00	Day 1, 09:00	Day 1, 09:00
Dosing Regimen	Single Dose	Single Dose	Single Dose	Single Dose

Supplementary Table 4-3 Protein content (mg/g liver tissue) in homogenates, microsomes, and cytosols from histologically normal and cancerous tissues of CRLM patients.

	HomPPGL (mg/g liver tissue)																		
sample	**1957**	**818**	**1493**	**1498**	**389**	**734**	**746**	**1492**	**794**	**674**	**590**	**633**	**1795**	**2095**	**2058**	**2036**	**mean**	**SD**	**cv**
normal	119.5	150.2	167.9	144.1	83.4	266.7	107.4	156.7	75.1	107.6	109.1	135.7	120.2	104.2	84.4	86.0	126.1	46.7	0.37
tumor	138.2	89.5	92.0	104.9	184.9	37.1	64.6	70.4	86.6	204.8	77.0	63.7	42.0	43.0	47.3	43.7	86.9	50.2	0.58
	Uncorrected MPPGL (mg/g liver tissue)																		
sample	**1957**	**818**	**1493**	**1498**	**389**	**734**	**746**	**1492**	**794**	**674**	**590**	**633**	**1795**	**2095**	**2058**	**2036**	**mean**	**SD**	**cv**
normal	14.0	22.8	14.1	19.6	20.0	11.8	18.7	20.0	16.7	12.7	12.5	14.6	8.8	15.1	12.5	19.0	15.8	3.9	0.24
tumor	6.4	15.2	4.3	10.4	11.6	4.7	6.5	5.9	4.5	4.8	6.3	2.6	3.7	6.1	5.8	4.5	6.5	3.3	0.51
	CPPGL (mg/g liver tissue)																		
sample	**1957**	**818**	**1493**	**1498**	**389**	**734**	**746**	**1492**	**794**	**674**	**590**	**633**	**1795**	**2095**	**2058**	**2036**	**mean**	**SD**	**cv**
normal	43.4	67.8	32.3	47.7	55.6	34.1	76.1	70.8	75.6	77.1	41.2	47.0	33.9	80.7	57.7	58.7	56.2	16.9	0.30
tumor	54.6	67.2	39.9	58.6	54.1	54.8	41.5	29.4	29.2	24.8	50.9	33.8	30.8	32.1	41.1	31.3	42.1	12.9	0.31

Supplementary Table 4-4 NADPH cytochrome 450 reductase activities (units/mg tissue) in homogenates and microsomes from histologically normal and tumor tissues of CRLM patients.

	NADPH CYP450 reductase activity in homogenates (unit/mg)	NADPH CYP450 reductase activity in microsomes (unit/mg)	NADPH CYP450 reductase activity in homogenates (unit/mg)	NADPH CYP450 reductase activity in microsomes (unit/mg)
Sample ID	**Normal**		**Tumor**	
389	2.275	0.811	0.640	0.282
633	2.844	1.015	0.284	0.085
674	2.844	1.219	0.569	0.083
734	0.796	0.570	0.284	0.062
746	3.318	1.580	0.967	0.211
794	2.640	1.398	0.427	0.148
818	2.218	1.232	0.284	0.099
1492	3.270	1.708	0.640	0.165
1493	1.479	0.341	0.142	0.030
1498	2.275	1.719	1.422	0.708
1957	2.275	0.968	0.758	0.150
1795	1.479	0.513	-	-
2036	1.919	0.656	-	-
2058	2.275	0.704	-	-
2095	2.204	1.270	-	-
590	3.583	0.711	-	-
Mean	2.356	1.026	0.583	0.184
SD	0.73	0.44	0.37	0.19

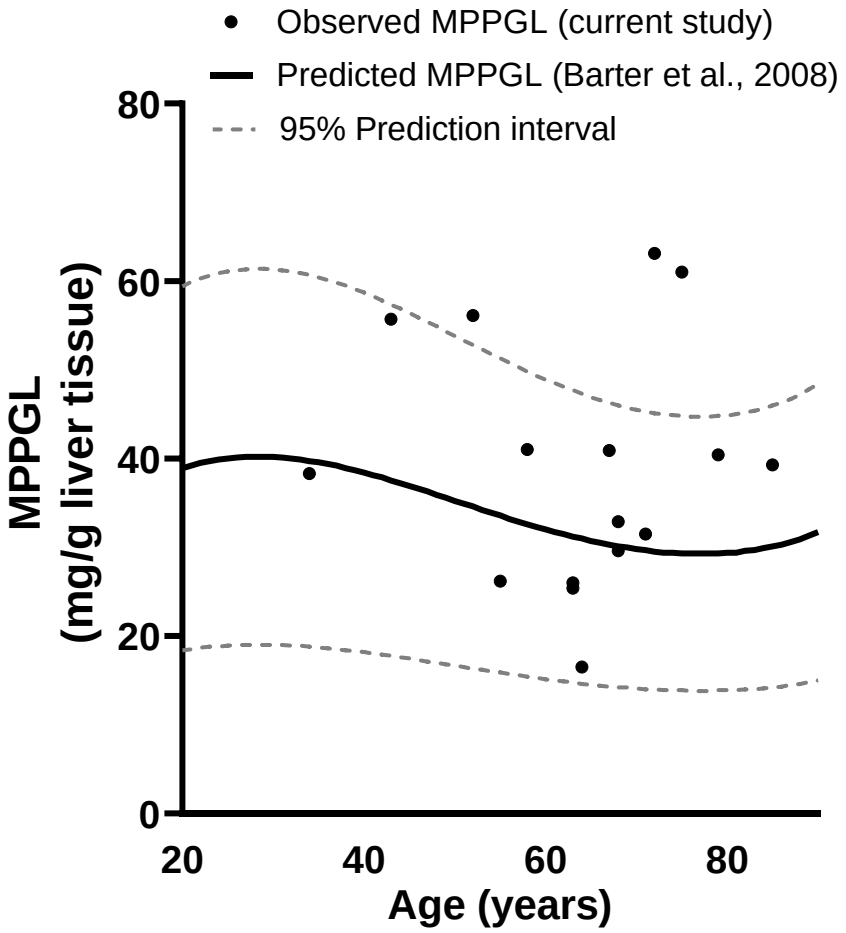

Supplementary Figure 4-1 Relationship between observed (current study) and predicted MPPGL values and age (Barter et al., 2008), with 95% confidence intervals for the predicted values for Model 1. The observed MPPGL values correspond to the histologically normal samples.

Chapter Five: Changes in Abundance of Proteins Involved in Drug Pharmacokinetics and Pharmacodynamics in Colorectal Cancer Liver Metastasis Relative to Healthy Liver

Declaration

Areti-Maria Vasilogianni, Zubida M. Al-Majdoub, Brahim Achour, Sheila Annie Peters, Amin Rostami-Hodjegan, and Jill Barber

I carried out the literature search, generation and analysis of data, contributed to the study design and wrote the manuscript. Dr Zubida M. Al-Majdoub and Dr Brahim Achour were consulted on experimental methodology and analysis of data, and suggested edits to the manuscript. Dr Sheila Annie Peters, Dr Jill Barber and Prof. Amin Rostami-Hodjegan contributed to the study design and provided guidance. I retained editorial control.

5.1 Abstract

This study aims to quantify drug-metabolising enzymes (DMEs), transporters, receptor tyrosine kinases (RTKs) and protein markers (involved in pathways affected in cancer) in pooled healthy, histologically normal, and matched cancerous liver microsomes from colorectal cancer liver metastasis (CRLM) patients. Microsomal fractionation was performed and pooled microsomes were prepared. Global and accurate mass and retention time (AMRT) LC-MS proteomics were used to quantify proteins. A QconCAT ('KinCAT') for the quantification of RTKs was designed and applied for the first time. Physiologically-based pharmacokinetic (PBPK) simulations were performed to assess the contribution of altered abundance of CYPs to changes in pharmacokinetics (PK). Most CYPs and UGTs were downregulated in histologically normal relative to healthy samples, and were further reduced in cancer samples (up to 54-fold). The transporters, MRP2/3, OAT2/7 and OATP2B1/1B3/1B1 were downregulated in CRLM. Application of CYP abundance data in PBPK models for CYP-substrates (alfentanil, midazolam, and nebivolol) indicated substantially higher (up to 13-fold) drug exposure in cancer compared with healthy populations. Liver function markers were downregulated, while inflammation proteins were upregulated (by up to 76-fold) in cancer samples. Various pharmacodynamics (PD) markers (e.g. RTKs) were altered in CRLM. Using global proteomics, we examined proteins in pathways relevant to cancer (such as metastasis and desmoplasia), including caveolins and collagen chains, and confirmed general over-expression of such pathways. This study highlights impaired drug metabolism, perturbed drug transport and altered abundance of cancer markers in CRLM, demonstrating the importance of population-specific abundance data in PBPK models for cancer.

5.2 Introduction

Colorectal cancer (CRC) is the third most common type of cancer worldwide (Bray et al., 2018), with half of patients having liver metastasis (Maher et al., 2017). Surgical resection is the ideal intervention for colorectal cancer liver metastasis (CRLM), but this is not always possible and other adjuvant therapies (e.g. chemotherapy) are available (Mitchell et al., 2019). Because liver metastasis is common, pharmacokinetics (PK) of many drugs differ in CRC patients due to perturbed system parameters (Cheeti et al., 2013; Yan, Gao, et al., 2015; Shinko et al., 2017; Billington et al., 2018; Vasilogianni et al., 2021). Pharmacodynamics (PD) is also expected to change due to altered expression of drug targets during cancer progression (Adeyinka et al., 2002), which has been reported across different cancer types (Koivunen et al., 2006).

To translate the effects of changes in expression under disease conditions to in vivo outcomes, proteomics data are used within the framework of *in vitro-in vivo* extrapolation (IVIVE) linked to physiologically-based pharmacokinetic/pharmacodynamic (PBPK/PD) modelling (Rostami-Hodjegan, 2012; Prasad et al., 2017). However, protein abundance data are limited in cancer populations. The limited qualitative data available on CRLM on the expression of drug-metabolising enzymes (DMEs) (Lane et al., 2004) suggest that cancer may alter drug metabolism. Quantitative transporter data in CRLM are limited to mRNA measurements (Wlcek et al., 2011) or comparison of expression in livers from healthy donors with that in histologically normal livers from CRLM patients (Kurzawski et al., 2019). Expression of pharmacodynamic targets including receptors is also affected by cancer. Of particular interest are receptor tyrosine kinases (RTKs), which regulate cellular processes and many anti-cancer drugs, such as regorafenib, inhibit them, thus improving survival of CRLM patients (Lee and Oh, 2016; García-Aranda and Redondo, 2019). RTK mRNA and protein expression data have been measured in cell lines (Kao et al., 2003; Kim et al., 2016; Potratz et al., 2016) but human studies are only limited to immunohistochemistry (Saito et al., 2004; Ljuslinder et al., 2009; Steller et al., 2013; Yao et al., 2013).

This study, therefore, aimed to apply global and QconCAT-based proteomics to quantify PK and PD proteins in pooled liver samples from healthy (healthy donors), histologically normal (peri-carcinomatous) and matched cancerous liver tissue from CRLM patients. The target proteins are involved in drug metabolism, transport and pathways affected in cancer. Notably, we designed, for the first time, a QconCAT standard ('KinCAT') for absolute quantification of RTKs. We additionally assessed the contribution of altered abundance of CYPs using PBPK

models. The generated abundance data will fill key gaps in current knowledge about human enzymes, transporters and PD targets in CRLM.

5.3 Materials and Methods

5.3.1 Liver samples and donor characteristics

Matched cancerous and histologically normal liver tissues from adult CRLM patients were supplied by the Manchester University NHS Foundation Trust (MFT) Biobank, Manchester, UK, following hepatectomy. Ethics were covered under the MFT Biobank generic ethical approval (NRES 14/NW/1260 and 19/NW/0644). Healthy human liver microsomal samples (tumour-free) from healthy subjects were provided by Pfizer (Groton, CT, USA), and prepared previously by Vitron (Tucson, AZ, USA) and BD Gentest (San Jose, CA, USA). Supplementary Tables 5-1 and 5-2 present demographic and clinical information about the donors of CRLM and healthy samples.

5.3.2 QconCATs standards

MetCAT and TransCAT standards have been used in this study, as described previously (Russell et al., 2013; Harwood et al., 2015). A modified version of the TransCAT was used (Supplementary Information). The "KinCAT" is a novel QconCAT for the quantification of human RTKs. It consists of concatenated tryptic peptides representative of the following proteins: macrophage colony-stimulating factor 1 receptor (CSF1R), epidermal growth factor receptor (EGFR), ephrin type-A receptor 2 (EPH2A), erythroblastic oncogene B2 (ERBB2), fibroblast growth factor receptors (FGFR1/2/3), FMS-like tyrosine kinase (FLT3), insulin-like growth factor 1 receptor (IGF1R), insulin receptor (INSR), mast/stem cell growth factor receptor (KIT), hepatocyte growth factor receptor (MET), neurotrophic tyrosine kinase receptor type 2 (NTRK2), platelet-derived growth factor receptors (PGFRA/B), proto-oncogene tyrosine-protein kinase receptor (RET), angiopoietin-1 receptor (TIE2), tyrosine-protein kinase receptor UFO (AXL), vascular endothelial growth factor receptors (VGFR1/2/3). These proteins were selected for their crucial role in cancer biology and treatment. Details are provided in Supplementary Information and Figure 5-1.

5.3.3 Sample preparation for proteomics

Liver tissue samples were fractionated to microsomes (Vasilogianni et al., 2021), as described in Supplementary Methods. Pooled samples were made up by combining equal volumes of individual microsomes from either 15 healthy samples (HP), 16 histologically normal samples (NP) from CRLM patients or 16 matched cancerous liver samples (TP) from the same CRLM patients. Each pooled sample (70 µg) was spiked with known amounts (Supplementary Methods) of each isotopically-labelled QconCAT, and prepared using filter-aided sample preparation (FASP) (Al-Majdoub et al., 2019; Couto et al., 2019, 2020). Samples were denaturated (sodium dexoycholate, 10% w/v final concentration), reduced (dithiothreitol, 0.1 M final concentration), alkylated (iodoacetamide, 100 µl of 50 mM), and digested (2 doses of LysC 2% w/w, 30°C, 4 h, and trypsin 4% w/w, 37°C, 16 h) (Al-Majdoub et al., 2014). Unlabelled peptide standards, GVNDNEEGFFSAR, VGFLPDGVIK and SEGVNDNEEGFFSAR, were added to quantify the QconCATs (MetCAT, TransCAT and KinCAT, respectively). Samples were lyophilized by vacuum centrifugation after sample preparation and stored at -20°C until mass spectrometric analysis. Additional details are provided in Supplementary Methods.

5.3.4 Liquid chromatography and tandem mass spectrometry (LC-MS/MS)

Dried samples were re-suspended in loading buffer and loaded onto an UltiMate® 3000 Rapid Separation LC system (RSLC, Dionex Corporation, Sunnyvale, CA) coupled to a Q Exactive HF Hybrid Quadrupole-Orbitrap mass spectrometer (Thermo Fisher Scientific, Waltham, MA). Details are provided in Supplementary Methods.

5.3.5 Analysis and annotation of proteomic data

Proteomic data were processed using MaxQuant 1.6.7.0 (Max Planck Institute, Martinsried, Germany), and searched against a customized database, comprising human UniprotKB database (74,788 sequences) and QconCAT sequences. For targeted accurate mass and retention time (AMRT) analysis, light-to-heavy intensity ratios were used with QconCAT concentrations to calculate protein amounts based on accurate mass and retention time for each peptide (Al-Majdoub et al., 2019; Al-Majdoub, Couto, et al., 2020). Peptides selected for quantification of CYPs/UGTs, transporters and RTKs are presented in Supplementary Tables 5-6, 5-7 and 5-8, respectively. For global analysis, data were processed using the total protein

approach (TPA) based on the ratio of individual protein to total proteome MS signal intensity (Al-Majdoub, Achour, et al., 2020).

5.3.6 Physiologically-based pharmacokinetic (PBPK) simulations

The effect of abundance of CYPs on simulated plasma drug exposure was assessed using PBPK modelling on Simcyp V20 Release 1 (Certara, Sheffield, UK) on CYP-substrates with different hepatic extraction ratios (E_H): alfentanil (CYP3A4 substrate, E_H=0.36 in healthy), midazolam (CYP3A4 and CYP3A5 substrate, E_H=0.44), and nebivolol (CYP3A4 and CYP2D6 substrate, E_H=0.74). The compound files were available in Simcyp library, and PBPK simulations used system parameters available on the simulator for healthy and cancer populations. The effects of abundance changes (based on TPA) in CRLM were assessed using previously described models (Vasilogianni et al., 2021):

Model 1 (Healthy): default MPPGL and abundance levels for the healthy population (Simcyp).

Model 2 (Cancer-D): default MPPGL and abundance for the cancer population (Simcyp).

MPPGL model 3 (New Cancer-ALN): MPPGL of histologically normal tissue (Vasilogianni et al., 2021) and abundances of CYPs in histologically normal relative to healthy tissue were used for the cancer population, assuming the whole liver is histologically normal (maximum metabolic capacity).

MPPGL model 4 (New Cancer-ALC): MPPGL of cancerous tissue (Vasilogianni et al., 2021) and abundance of CYPs in tumor relative to healthy tissue were used for the cancer population, assuming the whole liver is cancerous (minimum metabolic capacity) and liver mass is unchangeable.

The mean systemic concentration (C_{sys})-time profiles were plotted, and the area under the curve (AUC) and clearance (dose/AUC) were compared. Supplementary Table 5-5 summarises the parameters used in PBPK simulations.

5.3.7 Data analysis

Ratios were calculated for abundances in histologically normal and tumor samples relative to healthy control samples. Expression levels with ratios within 2-fold (0.5-2.0) were considered

similar. Graphs were generated using GraphPad Prism 8.1.2 (GraphPad Software, La Jolla, California USA).

5.4 Results

5.4.1 Novel QconCAT (KinCAT) for the quantification of kinases

Kinases regulate cellular processes and are involved in the development and progression of cancer. Protein expression levels of kinases have not been quantified in human tissue. We have therefore designed, for the first time, a QconCAT (KinCAT) to quantify RTKs (Figure 5-1A and C). KinCAT migrated on SDS-PAGE (molecular mass 82 kDa), including N-terminal core ribosomal protein to improve expression of the KinCAT (Al-Majdoub et al., 2014) with a histidine tag for purification, demonstrating that the intact QconCAT was expressed (Figure 5-1B) and confirmed by Mascot sequence coverage (88%) (Figure 5-1D). The ^{13}C-labelling efficiency was >97% (Figure 5-1E). The LC-MS traces of the digested KinCAT peptides are shown in Figure 5-1A, using Skyline (version 19.01.193) (www.sciex.com/products/software/skyline-software). More details about the KinCAT are provided in the Supplementary Table 5-4.

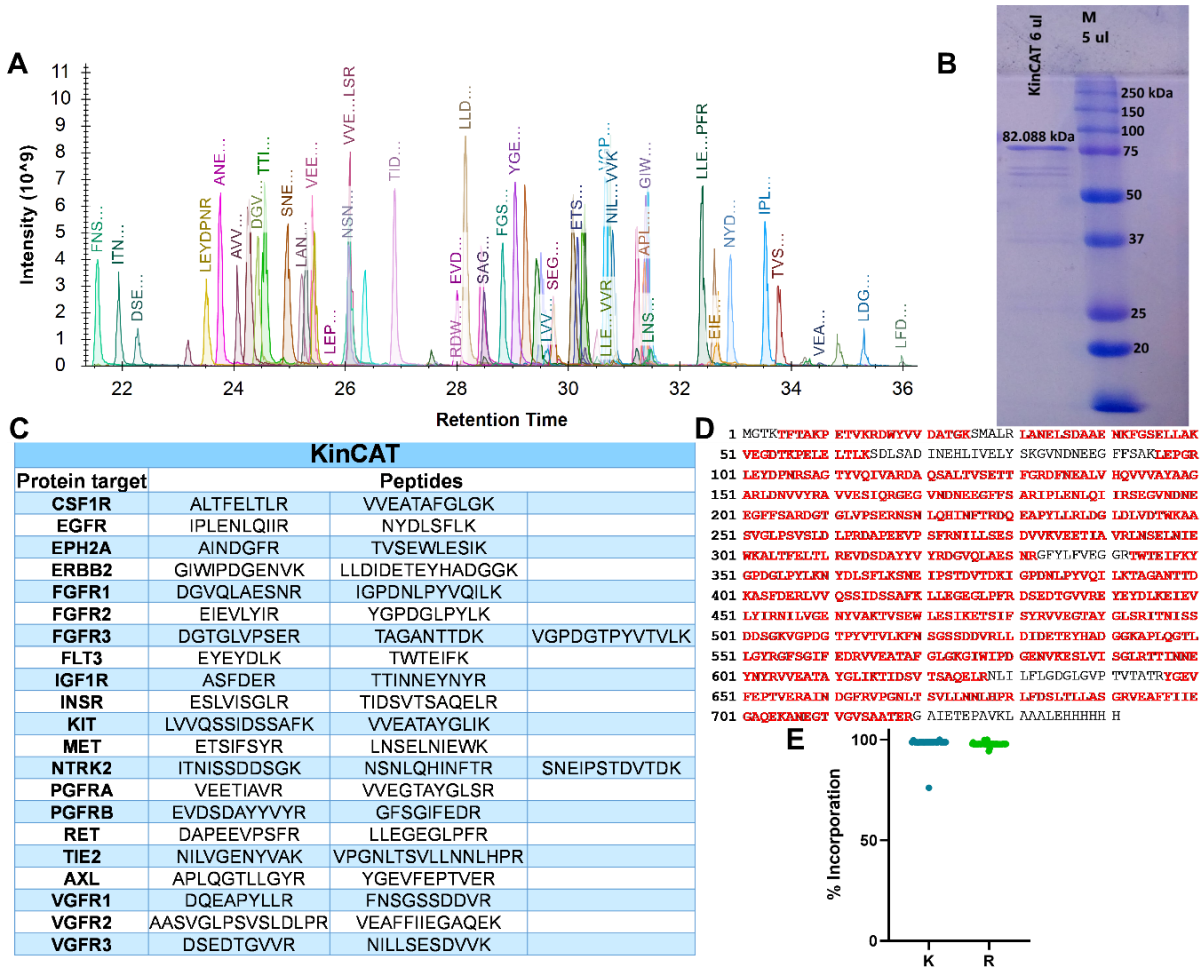

Figure 5-1 Design and characterization of the KinCAT. LC-MS traces of peptides included in the KinCAT sequence (**A**). SDS-PAGE gel showing the expression and purity of KinCAT; M = molecular weight marker (**B**). Sequences of KinCAT peptides and the RTK proteins they represent (**C**). Sequence coverage of the KinCAT protein, showing complete expression (**D**). Incorporation efficiency of $^{13}C_6$-lysines (K) and arginines (R) in the KinCAT peptides (**E**).

5.4.2 Abundance of CYPs and UGTs in healthy, histologically normal, and cancerous liver

5.4.2.1 Absolute abundance of CYP and UGT enzymes

The effect of cancer on the expression of DMEs was evaluated by comparing the expression in 1 pooled healthy (HP), 1 pooled histologically normal (NP) and 1 pooled tumorous sample (TP) from CRLM patients using AMRT. With the exception of CYP2J2, protein expression of CYPs (Figure 5-2A) and UGTs (Figure 5-2D) in HP is similar to that in NP. Abundance of CYPs and UGTs in HP ranged from 0.16 to 90.2 and 7.7 to 60.7 pmol/mg microsomal protein,

respectively. Interestingly, enzyme expression was significantly decreased for all CYPs and UGTs in TP (Figure 5-2A and D). The most abundant CYP in HP was CYP3A4 (90.2 pmol/mg microsomal protein), followed by 2E1 and 2C9 (79.4 and 76.1 pmol/mg microsomal protein, respectively). CYP2C9 was the most abundant (17.4 pmol/mg microsomal protein) in TP, followed by 2E1, and 3A4 (9.5 and 9 pmol/mg, respectively). The most abundant UGT was UGT2B7 (60.7, 80.9, and 9.1 pmol/mg microsomal protein in HP, NP, and TP, respectively). CYP2D6 and UGT1A3 were not detected in HP, whereas, CYP3A5 was not detected in NP and TP.

5.4.2.2 Replicate of measurement of CYPs and UGTs

To confirm the quantification of CYPs and UGTs, we measured replicate samples (HP, NP and TP) and assessed the results from the two studies against one another (Supplementary Table 5-9), which were consistent.

5.4.2.3 Abundance distribution of CYPs and UGTs in HP and TP

The pie charts in Figure 5-2 represent the abundance distribution (based on targeted analysis) of CYPs (Figure 5-2B and C) and UGTs (Figure 5-2E and F) in HP and TP. The overall distribution patterns of the enzymes had similarities between the two groups, with some differences, particularly for the abundance of CYP3A4 (28%), which was the highest in HP, whereas CYP2C9 (30%) was the most abundant in TP.

5.4.2.4 Fold change in the expression of CYPs and UGTs in TP and NP relative to HP

Fold change in expression of CYPs and UGTs in TP and NP relative to HP was assessed using TPA. In Figure 5-2G and 2H, the abundance of enzymes in NP and TP is expressed as relative ratios to levels in HP. Most of the CYPs in NP were within 2-fold of levels in HP, except CYP3A4 and CYP3A5 (3-fold lower), and CYP2J2 (5-fold lower in NP). Similar trends were observed for UGTs, most of which were downregulated by more than 2-fold (up to 7-fold for UGT1A1) in NP. CYPs were further downregulated in TP (up to 54-fold). Notably, CYP3A4 and CYP3A5 were 11 and 10-fold lower in TP, respectively. Similarly, UGT expression levels were decreased further in TP (up to 26-fold).

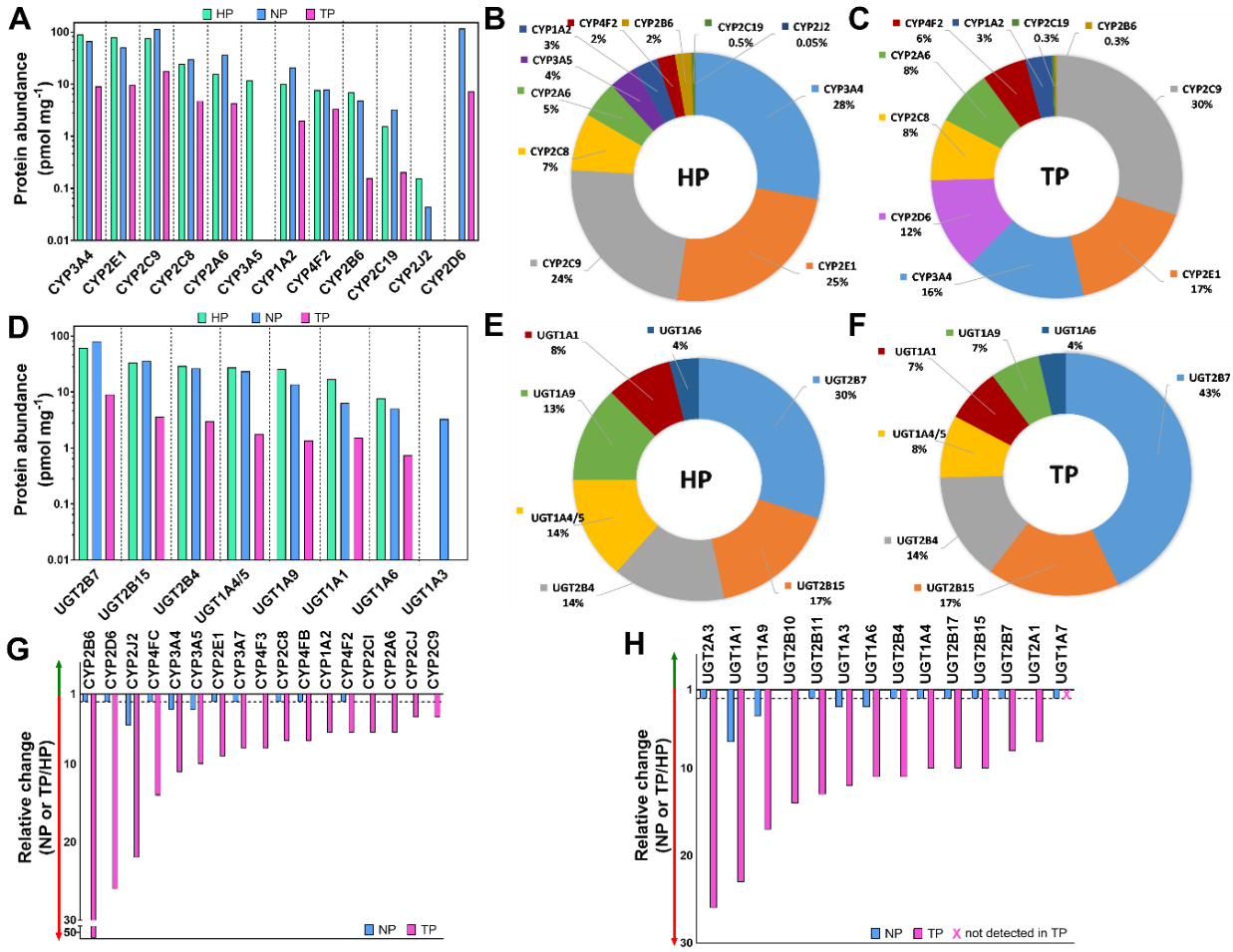

Figure 5-2 Protein expression of cytochrome P450 enzymes (CYPs) and UDP-glucuronosyltransferases (UGTs) in healthy (HP), histologically normal (NP) and tumorous (TP) pooled HLM samples. Absolute abundance of CYPs (**A**) and UGTs (**D**) is expressed in pmol per mg of microsomal protein. Pie charts represent the distribution of CYPs (**B**, **C**), and UGTs (**E**, **F**) in HP and TP, respectively, based on their absolute abundance. The relative changes in expression of CYPs (**G**) and UGTs (**H**) in NP and TP compared with HP. The green and red arrows indicate increased and decreased expression relative to HP, respectively. The dotted line represents 2-fold change.

5.4.3 Abundance of transporters in healthy, histologically normal and cancerous liver

Protein expression of ABC and SLC transporters, plasma membrane protein (ATP1A1) and cadherin-like transporter (CDH17) was measured using AMRT targeted method (Figure 5-3A and B). With the exception of P-gp (0.71 and 0.46 pmol/mg protein in TP and HP), ABC transporters were either not detected (BCRP, MRP6 and BSEP) or, in the case of MDR3, MRP2 and MRP3, lower in cancer (0.14, 0.18 and 0.47 pmol/mg protein, respectively) compared with HP (0.52, 0.85, 0.70 pmol/mg protein, respectively) (Figure 5-3A). ATP1A1 was moderately abundant in healthy liver, as indicated previously (Couto *et al.*, 2019), and its abundance was higher in cancer (16.3 pmol/mg in TP and 7.3 pmol/mg in HP). CDH17 was only quantifiable in NP and TP. Expression of SLCs was perturbed in cancer, with lower abundance of OAT7, OAT2B1, OATP1B3, OATP1B1 and OAT2 in TP (0.25, 0.69, 0.36, 0.54, and 0.16 pmol/mg, respectively) compared with HP (3.3, 2.4, 2.4, 2.0, and 1.5 pmol/mg, respectively).

5.4.3.1 Fold changes in the expression of transporters

TPA revealed relative changes in the abundance of ABC (Figure 5-3C) and SLC (Figure 5-3D) transporters in NP and TP compared with HP. Only MRP2 and MRP3 were lower in NP by more than 2-fold. In TP, we observed reduced expression of MRP2 and MRP3, and an increase in MRP4, P-gp and MDR3, relative to HP. BCRP was similar in TP and HP. Most SLCs, with exception of OATP1A2, were lower by more than 2-fold in NP. Up to 51-fold reduction in expression was observed in SLC transporters in TP. The magnitude of change in abundance followed the rank order: OAT7>OATP1B3>OAT2 >OCT3>OATP1B1>OATP2B1>MOT1 (Figure 5-3D).

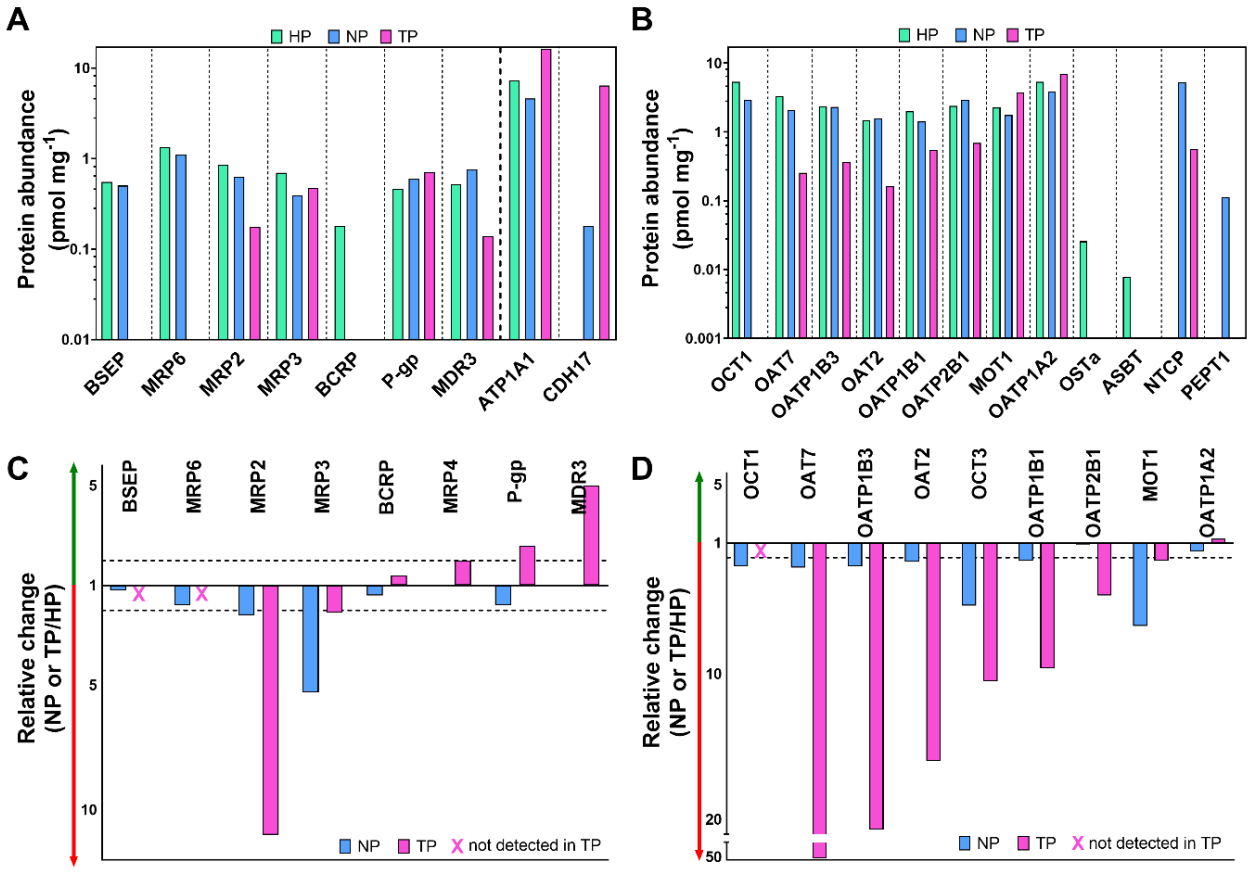

Figure 5-3 Abundance of transporters in healthy (HP), histologically normal (NP) and tumorous (TP) pooled HLM samples. Absolute abundance of ABC transporters, plasma membrane marker (ATP1A1) and one adhesion protein (CDH17) (**A**) and solute carriers (SLCs) (**B**), expressed in pmol of protein per mg of total protein. Relative change in expression of ABC (**C**) and SLC (**D**) transporters in NP and TP, compared with HP. The green and red arrows indicate increased and decreased expression relative to HP, respectively. The dotted line represents 2-fold change.

5.4.4 Differential protein abundance of non-CYP non-UGT and anti-oxidant enzymes

We also assessed the relative change in abundance of non-CYP non-UGT DMEs and anti-oxidant enzymes using the TPA (Figure 5-4A, B and C), in NP and TP compared with HP. Among non-CYP non-UGT enzymes (Figure 5-4A), FMO4, ALDH2, SULT1A2, SULT1B1, ADH4, ADH6, ADH1B and AOXA were more abundant in NP compared with HP, whereas CES3, POR, MGST2 and MGST3 were less abundant (>2-fold change). The suppressive effect of cancer on expression was observed with CES1/2, FMO3/5, MGST1/2/3, POR, MGST1/2/3, ALDH1A/1G, ADH6, ADHX, EPHX1, and SULT2A1, with up to 7.3-fold lower levels (Figure 5-4A and B).

Anti-oxidant enzymes (Figure 5-4C) protect cells from oxidative stress, which may lead to carcinogenesis. Heme-oxygenase 1 and 2 (heme degradation) (HMOX1 and HMOX2) were expressed at lower levels in NP compared with HP (69.7 and 4.1-fold). HMOX1 was not detected in TP. Peroxiredoxins (involved in detoxification of peroxides), PRDX4 and PRDX5, and HMOX2 were downregulated (up to 4.1-fold), while catalase, CAT (neutralises hydrogen peroxide), and PRDX2 were expressed at higher levels in NP. PRDX4, PRDX6, HMOX2, superoxide dismutase (dismutation of superoxide) SOD1, and CAT were downregulated, while PRDX5 and PRDX2 were up to 12.3-fold higher in TP.

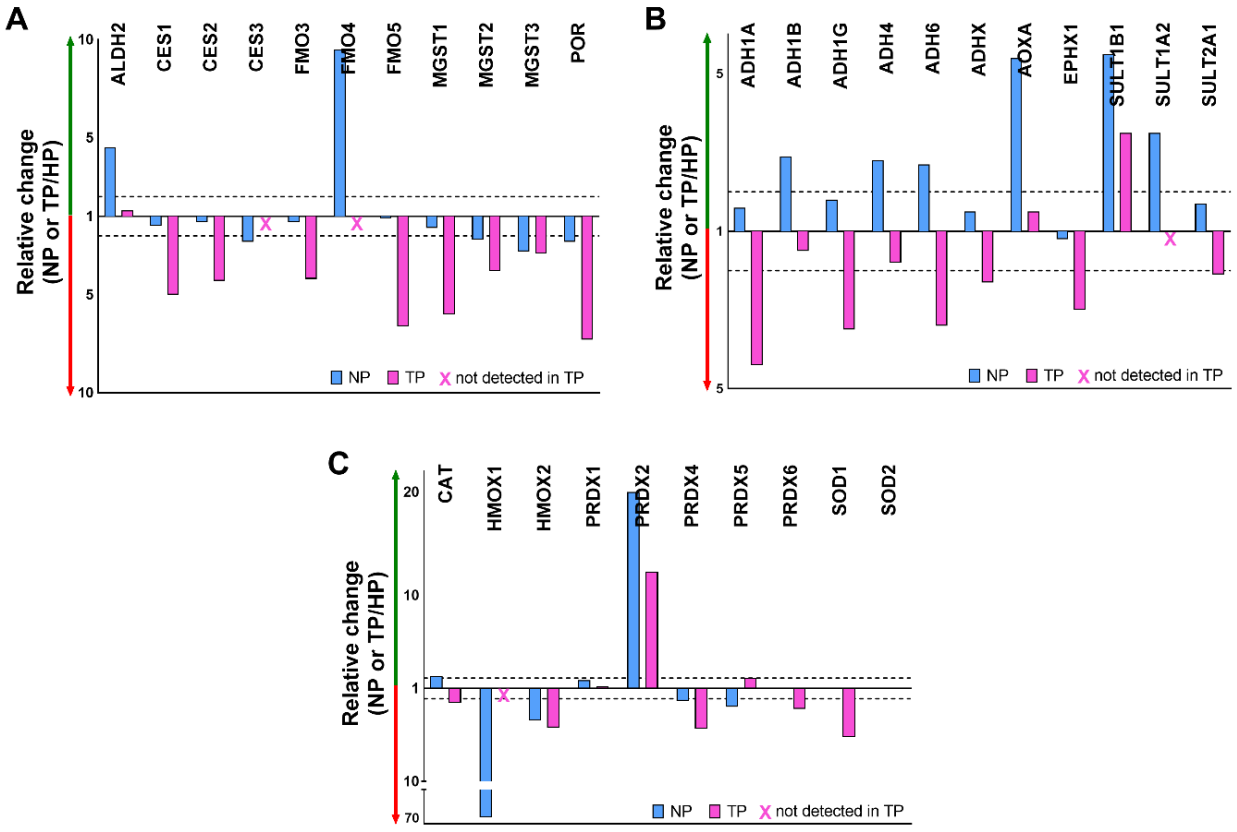

Figure 5-4 Relative abundance of non-CYP non-UGT enzymes (**A**, **B**), and anti-oxidant enzymes (**C**) measured in healthy (HP), histologically normal (NP) and tumorous (TP) pooled HLM samples. The green and red arrows indicate higher or lower expression relative to HP, respectively. The dotted line is set to 2-fold change. (**A**) ALDH, aldehyde dehydrogenase; CES, carboxylesterase; FMO, flavin-containing monooxygenase; MGST, microsomal glutathione S-transferase; POR, NADPH-cytochrome P450 reductase. (**B**) ADH, alcohol dehydrogenase; AOX, aldehyde oxidase; EPHX, epoxide hydrolase; SULT, sulfotransferase. (**C**) CAT, catalase; HMOX, heme-oxygenase; PRDX, peroxiredoxin; SOD, Superoxide dismutase.

5.4.5 Assessment of changes in expression of kinases in NP and TP compared with HP

5.4.5.1 Expression levels of RTKs

To assess the expression of RTKs, AMRT targeted analysis using KinCAT was carried out in HP, NP and TP liver samples (Figure 5-5A). Expression of VGFR1, TIE2, FGFR3, ERBB2 and IGF1R was higher in NP relative to HP, whereas AXL and VGFR3 were less abundant in NP, and RET was exclusively expressed in NP (at 0.04 pmol/mg protein). Compared with HP, expression levels of INSR, EGFR, AXL were lower, and those of NTRK2, ERBB2, IGF1R were higher in TP. KIT was only expressed in NP and TP. FGFR1 (0.01 pmol/mg), VGFR2 (0.02 pmol/mg), FGFR2 (0.04 pmol/mg), and PGFRB (3.8 pmol/mg) were exclusively expressed in TP.

5.4.5.2 Non-RTKs exclusively expressed in TP

Additional kinases expressed in the pooled cancer sample were assessed using global proteomics and quantified by the TPA. Figure 5-5B shows kinases involved in various biological pathways that were exclusively expressed in TP, including creatine kinases (KCR), mitogen-activated protein kinase (MK), STRAP, PAK1 and GAK.

5.4.5.3 Fold change in expression of RTKs between HP to NP and TP

Fold changes in the abundance of RTKs were assessed by the TPA (Figure 5-5C). The abundance of VGFR3/1, FGFR2, INSR and NTRK2 was lower (>2-fold) in NP compared with HP, whereas KIT and VGFR2 were higher (>2-fold). In TP, we observed decreased expression of TIE2, EGFR, FGFR2, and INSR and increased abundance of KIT, VGFR2 and EPHA2 compared with HP.

5.4.5.4 RTK-related pathways affected in cancer

Figure 5-5D describes the role of RTKs (tumor cell survival/proliferation, angiogenesis, differentiation/apoptosis, and extracellular matrix formation/metastasis) and biological pathways affected by RTKs with altered expression. Compared with HP, our data show an increase in expression of phosphatidylinositol 3-kinase (PI3K) and serine/threonine-protein kinase mTOR (tumor cell survival). Ras-related protein R-Ras, serine/threonine-protein kinase Raf, and extracellular signal-regulated kinases ERK were upregulated (tumor cell

proliferation). Additionally, proto-oncogene tyrosine-protein kinase SRC and Ras-related C3 botulinum toxin substrate 1 (RAC1) (Metastasis) were higher in TP compared with HP.

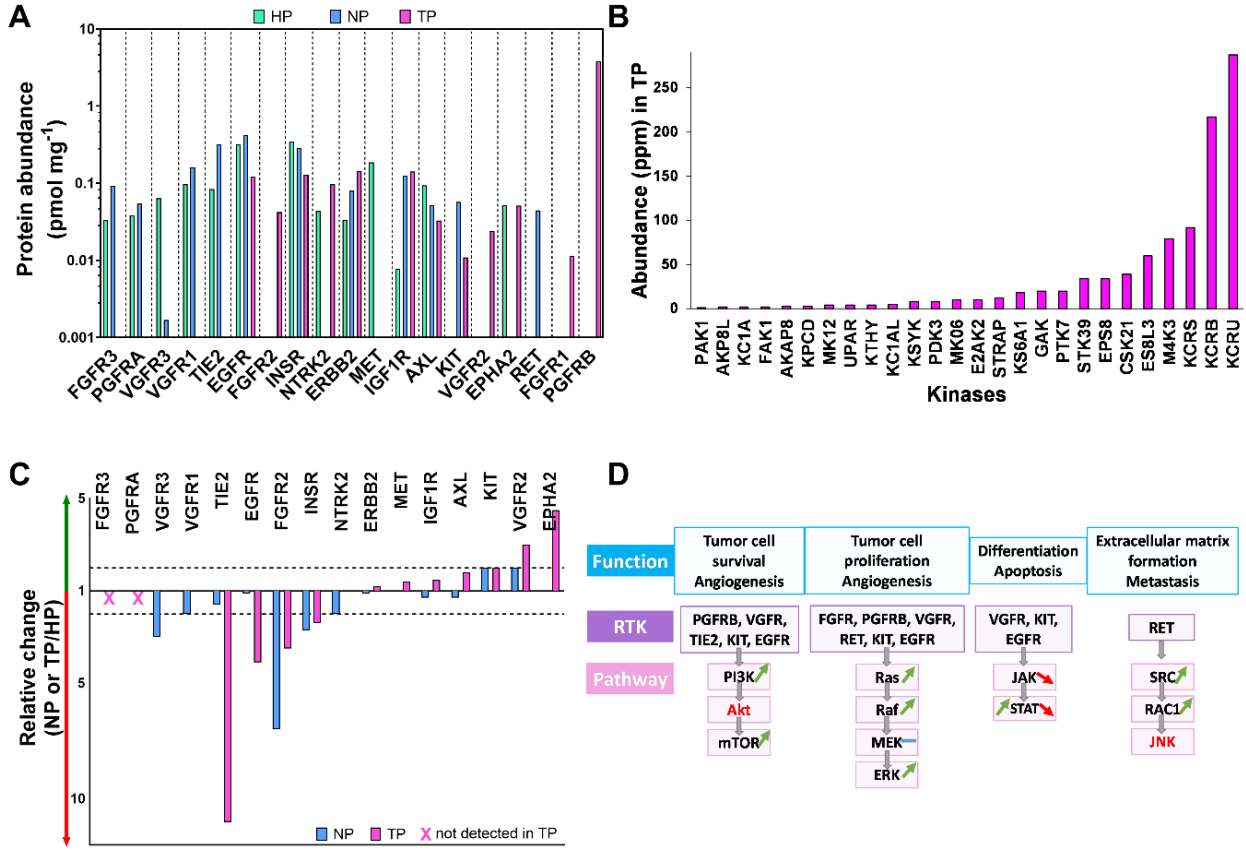

Figure 5-5 Abundance of kinases in healthy (HP), histologically normal (NP) and tumorous (TP) pooled HLM. (**A**) Absolute abundance of receptor tyrosine kinases (RTKs), expressed in pmol of protein per mg of liver microsomal protein using KinCAT as standard. (**B**) Relative abundance of kinases (not RTKs) exclusively identified in TP, expressed as ppm (parts per million) using the total protein approach (TPA). (**C**) Relative change of RTKs in NP and TP compared with HP. When a bar is not present, this means that there was no change in NP or TP compared with HP. The crosses indicate the absence of a protein from a sample. The green and red arrows indicate increased and decreased expression relative to HP, respectively. The dotted line is set to 2-fold change. (**D**) Functions of RTKs (targeted by anti-cancer tyrosine kinase inhibitors, TKIs) and biological pathways that are affected by the altered abundances of RTKs. Green and red arrows show increased and decreased abundance of proteins in TP, respectively. The blue line represents exclusive expression (low) in HP, and red font means the target was not detected in any of the samples.

5.4.6 Abundance of markers of liver function, inflammation, desmoplasia and metastasis

By applying the TPA, we assessed fold changes in the abundance of various markers of liver function and cancer in NP and TP relative to HP.

5.4.6.1 Liver function

Figure 5-6A shows 3.5-fold higher expression of liver function marker, alanine aminotransferase (ALT1), and 4-fold reduction in that of alkaline phosphatase (ALP), in NP compared with HP. However, liver function markers, ALT1, ALP, and aspartate aminotransferase (AST), were downregulated in TP by 7.6, 2.3, and 1.8-fold, respectively, suggesting impaired liver function in CRLM.

5.4.6.2 Inflammation

Expression of inflammatory markers (Figure 5-6B) showed variable trends. Abundance of cytochrome c oxidase (COX1), interferon-induced transmembrane protein 3 (IFM3), catenin beta-1 (CTNNB1) was lower in NP compared with HP (up to 6.3-fold), while that of interleukin enhancer-binding factor (ILF2) was significantly higher (32-fold). COX1 was downregulated and ILF2 was significantly upregulated (76-fold) in TP. ILF3 and macrophage migration inhibitory factor (MIF) were not expressed in HP, but had higher levels in TP compared with NP. Arachidonate 5-lipoxygenase (LOX5) and nuclear factor NF-kappa-B (NFKB1) were exclusively expressed in TP.

5.4.6.3 Desmoplasia

We also measured desmoplasia markers (Figure 5-6C) involved in the growth of fibrous tissue. Consistent with fibrotic appearance of the tumorous samples observed during tissue fractionation, we found exclusive expression of GPX3, GPX8, tenascin (TENA) in TP. Additionally, glutathione peroxidase (GPX4), and caveolins (CAV) 1 and 2 were expressed at higher levels (>2-fold) in TP compared with HP.

5.4.6.4 Metastasis markers

Expression of metastasis markers was perturbed in CRLM. Collagen chains (Figure 5-6D), COIA1 and COEA1 were upregulated (165-fold) in NP, and almost all collagen chains were significantly higher (up to 1065-fold) or exclusively expressed (COCA1, COC4A1) in TP compared with HP. Cathepsins (Figure 5-6E) were generally unchanged across all samples, with only CATG being significantly higher (9.9-fold) in TP relative to HP. Other metastasis markers (Figure 5-6F), such as cystatin-N (CYTN), matrix metalloproteinase 12 (MM12), desmocollin 2 (DSC2) and metalloproteinase inhibitor (TIMP3), were exclusively expressed in TP. Expression of MM8 and MM9 was (up to 3.7-fold) lower in TP compared with HP.

Integrin alpha-M (ITAM), vimentin (VIME), clusterin (CLUS), syntenin-1 (SDCB1) and TIMP1 were upregulated in TP (up to 38-fold).

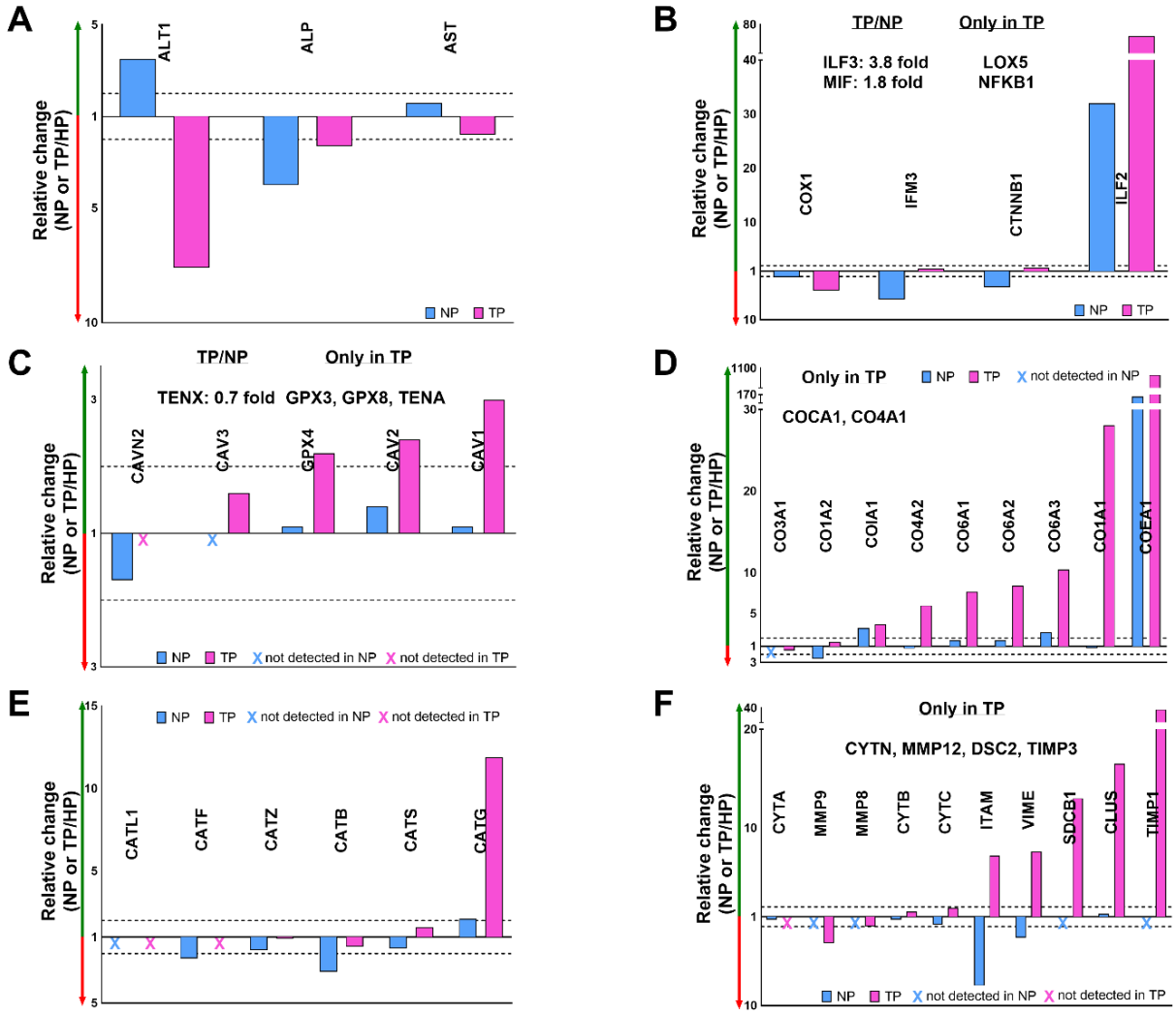

Figure 5-6 Relative change of markers of liver function (**A**), inflammation (**B**), desmoplasia (**C**), collagen chains (metastasis markers) (**D**), cathepsins (metastasis markers) (**E**), and other metastasis markers (**F**) in NP and TP compared with HP. HP is set to 1 and NP and TP are expressed as relative changes to HP. When a bar is not present, this means that there was no change of expression in NP or TP relative to HP. The crosses indicate absence of a protein from a sample. The green and red arrows indicate increased and decreased expression relative to HP, respectively. The dotted line is set to 2-fold change.

5.4.7 Physiologically-based pharmacokinetic (PBPK) simulations

Simulations for CYP-substrates (alfentanil, midazolam, nebivolol) were performed (Figure 5-7) using either default healthy population in Simcyp (Healthy), default cancer population in Simcyp (Cancer-D), or experimentally-derived data (New Cancer-ALN, New Cancer-ALC).

AUC predicted using New Cancer-ALC was 13, 6, 4-fold higher than that obtained using the Healthy model for alfentanil, midazolam and nebivolol, respectively. Similarly, when using New Cancer-ALC, the clearance (dose/AUC) of alfentanil, midazolam, and nebivolol was 14, 8 and 4-fold lower than in the Healthy scenario.

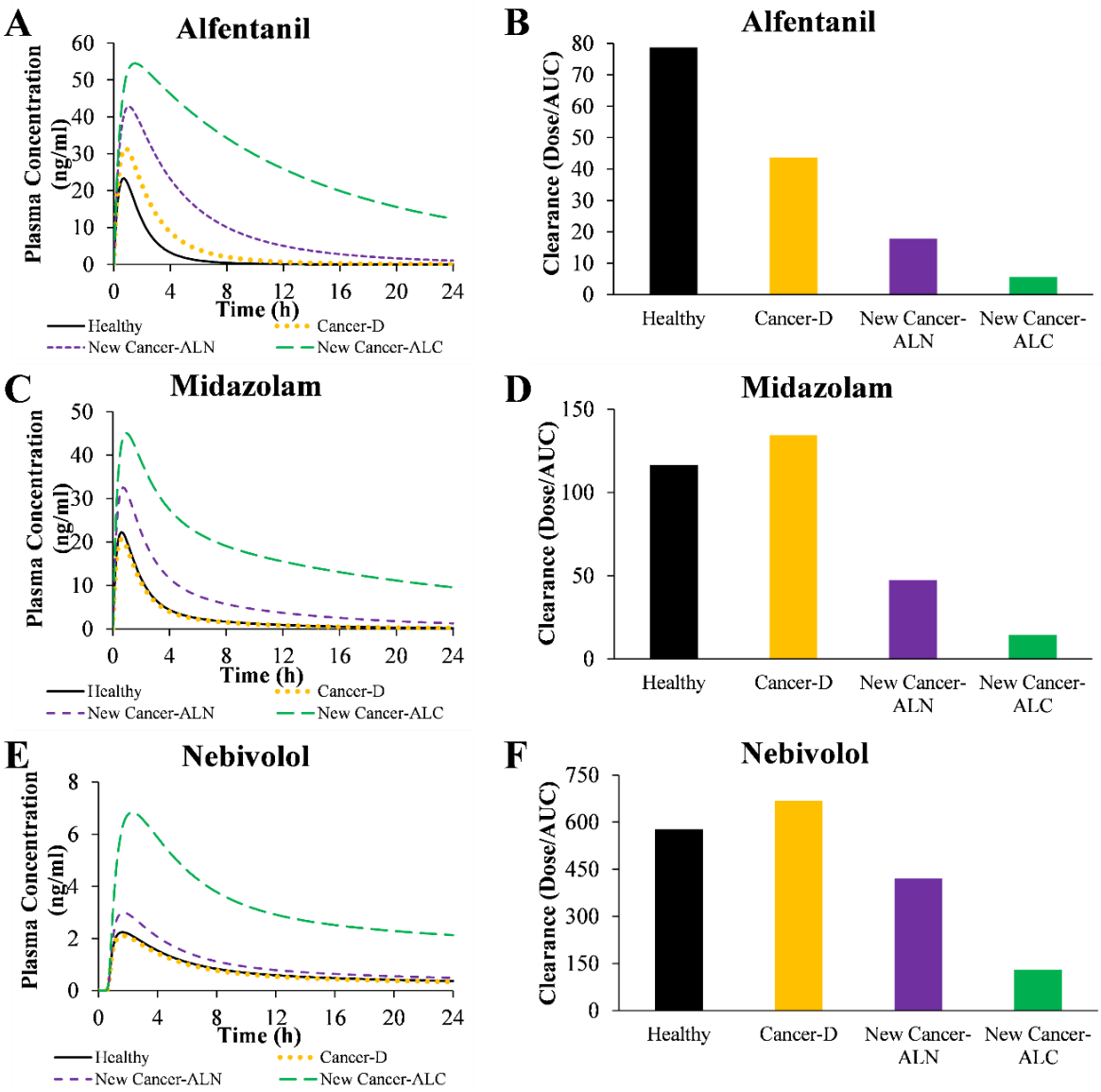

Figure 5-7 Mean predicted systemic concentration over time (24 hours) after oral administration of alfentanil (**A**), midazolam (**C**), and nebivolol (**E**), and clearance (Dose/AUC) of alfentanil (**B**), midazolam (**D**), and nebivolol (**E**). For each drug, four different models were used. Healthy: default MPPGL and abundances of CYPs and UGTs (Simcyp) with a healthy population. Cancer-D: default MPPGL and abundances of CYPs and UGTs (Simcyp) with a cancer population. New Cancer-ALN: MPPGL (Vasilogianni et al., 2021) and abundance of CYPs and UGTs measured in this study for histologically normal tissue with a cancer population. New Cancer-ALC: MPPGL (Vasilogianni et al., 2021) and abundances of CYPs and UGTs measured in this study for cancer tissue with a cancer population.

5.5 Discussion

For the first time, this study applied targeted and global LC-MS/MS-based proteomics to quantify DMEs, transporters and PD targets (including RTKs, inflammatory markers, metastatic markers) in healthy, histologically normal and cancerous livers from CRLM patients. For the proteins investigated here, no quantitative data have been reported previously in CRLM. Our experimental data were used to optimise PBPK models in cancer population (Simcyp) in order to assess the impact of the changes in abundance on PK.

Of relevance to drug metabolism, CYPs and UGTs were significantly downregulated in cancer tissue highlighting that the clearance of CYP-substrates may be significantly lower in patients with late-stage liver cancer. Abundance of CYPs and UGTs was also lower in histologically normal tissue, meaning that the impact of cancer is not limited to the tumour, affecting the metabolic function of the whole liver. Additional DMEs such as ADHs and FMO3 were downregulated in tumorous tissue, suggesting impaired capacity in almost all drug clearance pathways. Expression of anti-oxidant enzymes was decreased in tumours and normal tissue, suggesting impaired detoxification in CRLM. In agreement with our findings, data from HCC patients showed a significant impact of cancer on CYPs, UGTs, ADHs, FMO3, and SULTs (Hu et al., 2014; Yan, Gao, et al., 2015; Yan, Lu, et al., 2015; Xie et al., 2017). Our data suggest that the severity of disease (amount of liver being cancerous) and the change in abundance of enzymes are important in predicting the disease effect on metabolism and detoxification.

Transporters are important for the disposition of drugs and the trafficking of nutrients and metabolites. Abundance data on transporters showed significant changes in expression in CRLM, suggesting impaired disposition. The majority of SLC transporters were downregulated in cancerous tissue. Efflux transporters, MRP2 and MRP3, which are involved in drug resistance, were downregulated in histologically normal and tumorous tissue, while other efflux transporters involved in drug resistance, such P-gp and MRP4, were increased in cancer tissue. The lower expression of OATPs and OCT1 is consistent with data from HCC patients, whereas changes in BCRP, MRPs, and P-gp were not consistent (Billington et al., 2018). Such differences are not surprising considering differences in the type of cancer, and further analysis of individual samples is required to assess expression of proteins involved in drug resistance.

The protein expression levels of RTKs is reported for the first time in this study. Our approach employed a novel QconCAT, the KinCAT, which was used for the first time in human tissue in this study. In histologically normal tissue, expression of VGFR1/3, FGFR2, INSR, and

NTRK2 was downregulated, and that of KIT and VGFR2 upregulated. Tumour suppressant marker (RET) was exclusively expressed in histologically normal tissue. In tumour tissue, expression of markers such as TIE2, EGFR, FGFR2, and INSR was downregulated, while that of KIT, VGFR2 and EPHA2 was upregulated. Platelet-derived growth factor receptor (PGFRB) was highly and exclusively expressed in tumorous tissue, consistent with literature suggesting PGFRB is a metastasis marker (Steller et al., 2013). Desmoplasia markers were upregulated in CRLM patients, indicating more extensive growth of fibrous tissue. Consistent with previous findings (van Huizen et al., 2019), expression of collagen chains was significantly higher in CRLM. The observed perturbations of kinases and cancer-related proteins in CRLM suggests a potential effect on cancer-related pathways, such as cell survival/proliferation, angiogenesis, differentiation and metastasis (Troiani et al., 2013). In the current study, these markers (such as PI3K, mTOR, Ras, Raf, ERK, SRC and RAC1) were affected in CRLM. As pathophysiological changes can affect protein expression, these proteins can be used as potential markers for monitoring disease prognosis and as therapeutic targets.

Global proteomic data revealed reduced expression of liver function markers and upregulation of inflammatory markers in cancer. LOX5 and NFKB1, were exclusively expressed in cancer tissue, and these constitute important targets for anti-inflammatory drugs (Zappavigna et al., 2020). The severity of inflammation in cancer affects the production of cytokines and increases oxidative stress, which leads to perturbations in proteins involved in drug metabolism and disposition and can subsequently alter drug PK in cancer patients (Schwenger et al., 2018).

To assess the impact of the observed changes in expression of CYPs on drug PK, we performed PBPK simulations on CYP-substrates at different hepatic extraction levels (alfentanil, midazolam, and nebivolol). Decreased clearance of anti-cancer drugs in cancer patients has been reported previously (Piotrovsky et al., 1998; Houk et al., 2009; Hudachek and Gustafson, 2013). In our previous study (Vasilogianni et al., 2021), we assessed the effect of experimentally-derived MPPGL values in CRLM on PK by optimising and updating an existing cancer population in Simcyp. In the current study, we further updated the cancer population with abundance data for CYPs and UGTs. The changes in abundance levels affected drug exposure for all the drugs. With the assumption that the whole liver is tumorous (New Cancer-ALC model), higher drug exposure was predicted compared with a histologically normal liver (New Cancer-ALN model). The PBPK simulations show that appropriate abundance data in combination with appropriate MPPGL scalar values can significantly improve PK predictions, particularly when used with the percentage of cancerous liver tissue. Clinical data for the simulated drugs in CRLM were not available and we only assessed the

impact of change in abundance of CYPs on PK. Further simulations could verify these updated PBPK cancer models, when clinical data become available.

In conclusion, our data adds significant findings towards addressing key gaps in knowledge about human protein abundance in cancer. DMEs were significantly downregulated and transporters were perturbed in CRLM. In addition, RTKs were altered in CRLM, leading to perturbations in biological pathways relevant to cancer development and progression. These data may be valuable for proposing diagnostic and therapeutic markers. Liver function was also impaired and inflammation markers were upregulated in CRLM. Desmoplasia and metastasis markers were highly expressed in cancer samples. PBPK simulations on CYP-substrates revealed higher drug exposure (up to 13-fold) when using cancer population-specific abundance of CYPs. Our study suggests that appropriate abundance values for CRLM are critical for accurate PK prediction.

5.6 References

Adeyinka A, Nui Y, Cherlet T, Snell L, Watson PH, and Murphy LC (2002) Activated mitogen-activated protein kinase expression during human breast tumorigenesis and breast cancer progression. *Clin Cancer Res* **8**:1747–53.

Al-Majdoub ZM, Achour B, Couto N, Howard M, Elmorsi Y, Scotcher D, Alrubia S, El-Khateeb E, Vasilogianni AM, Alohali N, Neuhoff S, Schmitt L, Rostami-Hodjegan A, and Barber J (2020) Mass spectrometry-based abundance atlas of ABC transporters in human liver, gut, kidney, brain and skin. *FEBS Lett* **594**:4134–4150.

Al-Majdoub ZM, Al Feteisi H, Achour B, Warwood S, Neuhoff S, Rostami-Hodjegan A, and Barber J (2019) Proteomic quantification of human blood–brain barrier SLC and ABC transporters in healthy individuals and dementia patients. *Mol Pharm* **16**:1220–1233.

Al-Majdoub ZM, Carroll KM, Gaskell SJ, and Barber J (2014) Quantification of the proteins of the bacterial ribosome using QconCAT technology. *J Proteome Res* **13**:1211–1222.

Al-Majdoub ZM, Couto N, Achour B, Harwood MD, Carlson G, Warhurst G, Barber J, and Rostami-Hodjegan A (2020) Quantification of Proteins Involved in Intestinal Epithelial Handling of Xenobiotics. *Clin Pharmacol Ther* **0**:1–11.

Billington S, Ray AS, Salphati L, Xiao G, Chu X, Humphreys WG, Liao M, Lee CA, Mathias A, Hop CECA, Rowbottom C, Evers R, Lai Y, Kelly EJ, Prasad B, and Unadkat JD (2018) Transporter Expression in Noncancerous and Cancerous Liver Tissue from Donors with Hepatocellular Carcinoma and Chronic Hepatitis C Infection Quantified by LC-MS/MS Proteomics. *Drug Metab Dispos* **46**:189–196.

Bray F, Ferlay J, Soerjomataram I, Siegel RL, Torre LA, and Jemal A (2018) Global cancer statistics 2018: GLOBOCAN estimates of incidence and mortality worldwide for 36 cancers in 185 countries. *CA Cancer J Clin* **68**:394–424.

Cheeti S, Budha NR, Rajan S, Dresser MJ, and Jin JY (2013) A physiologically based pharmacokinetic (PBPK) approach to evaluate pharmacokinetics in patients with cancer. *Biopharm Drug Dispos* **34**:141–154.

Couto N, Al-Majdoub ZM, Achour B, Wright PC, Rostami-Hodjegan A, and Barber J (2019) Quantification of Proteins Involved in Drug Metabolism and Disposition in the Human Liver Using Label-Free Global Proteomics. *Mol Pharm* **16**:632–647.

Couto N, Al-Majdoub ZM, Gibson S, Davies PJ, Achour B, Harwood MD, Carlson G, Barber J, Rostami-Hodjegan A, and Warhurst G (2020) Quantitative Proteomics of Clinically Relevant Drug-Metabolizing Enzymes and Drug Transporters and Their Intercorrelations in the Human Small Intestine. *Drug Metab Dispos* **48**:245–254.

García-Aranda M, and Redondo M (2019) Targeting Receptor Kinases in Colorectal Cancer. *Cancers* **11**:433.

Harwood MD, Achour B, Russell MR, Carlson GL, Warhurst G, and Rostami-Hodjegan A (2015) Application of an LC–MS/MS method for the simultaneous quantification of human intestinal transporter proteins absolute abundance using a QconCAT technique. *J Pharm Biomed Anal* **110**:27–33.

Houk BE, Bello CL, Kang D, and Amantea M (2009) A population pharmacokinetic meta-analysis of sunitinib malate (SU11248) and its primary metabolite (SU12662) in healthy volunteers and oncology patients. *Clin Cancer Res* **15**:2497–2506.

Hu H, Ding X, Yang Y, Zhang H, Li H, Tong S, An X, Zhong Q, Liu X, Ma L, Liu Q, Liu B, Lu Z, Zhang D, Hu P, and Ren H (2014) Changes in glucose-6-phosphate dehydrogenase expression results in altered behavior of HBV-associated liver cancer cells. *Am J Physiol Liver Physiol* **307**:G611–G622.

Hudachek SF, and Gustafson DL (2013) Physiologically based pharmacokinetic model of lapatinib developed in mice and scaled to humans. *J Pharmacokinet Pharmacodyn* **40**:157–176.

Kao H-W, Chen H-C, Wu C-W, and Lin W-C (2003) Tyrosine-kinase expression profiles in human gastric cancer cell lines and their modulations with retinoic acids. *Br J Cancer* **88**:1058–1064.

Kim H-J, Lin D, Lee H-J, Li M, and Liebler DC (2016) Quantitative Profiling of Protein Tyrosine Kinases in Human Cancer Cell Lines by Multiplexed Parallel Reaction Monitoring Assays. *Mol Cell Proteomics* **15**:682–691.

Koivunen J, Aaltonen V, and Peltonen J (2006) Protein kinase C (PKC) family in cancer progression. *Cancer Lett* **235**:1–10.

Kurzawski M, Szeląg-Pieniek S, Łapczuk-Romańska J, Wrzesiński M, Sieńko J, Oswald S, and Droździk M (2019) The reference liver – ABC and SLC drug transporters in healthy

donor and metastatic livers. *Pharmacol Reports* **71**:738–745.

Lane CS, Nisar S, Griffiths WJ, Fuller BJ, Davidson BR, Hewes J, Welham KJ, and Patterson LH (2004) Identification of cytochrome P450 enzymes in human colorectal metastases and the surrounding liver: a proteomic approach. *Eur J Cancer* **40**:2127–2134.

Lee S, and Oh SC (2016) Advances of Targeted Therapy in Treatment of Unresectable Metastatic Colorectal Cancer. *Biomed Res Int* **2016**:1–14.

Ljuslinder I, Malmer B, Isaksson-Mettävainio M, Oberg A, Henriksson R, Stenling R, and Palmqvist R (2009) ErbB 1-4 expression alterations in primary colorectal cancers and their corresponding metastases. *Anticancer Res* **29**:1489–94.

Maher B, Ryan E, Little M, Boardman P, and Stedman B (2017) The management of colorectal liver metastases. *Clin Radiol* **72**:617–625.

Mitchell D, Puckett Y, and Nguyen QN (2019) Literature Review of Current Management of Colorectal Liver Metastasis. *Cureus* **11**:e3940.

Piotrovsky VK, Huang ML, Van Peer A, and Langenaecken C (1998) Effects of demographic variables on vorozole pharmacokinetics in healthy volunteers and in breast cancer patients. *Cancer Chemother Pharmacol* **42**:221–228.

Potratz J, Tillmanns A, Berning P, Korsching E, Schaefer C, Lechtape B, Schleithoff C, Unland R, Schäfer K-L, Müller-Tidow C, Jürgens H, and Dirksen U (2016) Receptor tyrosine kinase gene expression profiles of Ewing sarcomas reveal ROR1 as a potential therapeutic target in metastatic disease. *Mol Oncol* **10**:677–692.

Prasad B, Vrana M, Mehrotra A, Johnson K, and Bhatt DK (2017) The Promises of Quantitative Proteomics in Precision Medicine. *J Pharm Sci* **106**:738–744.

Rostami-Hodjegan A (2012) Physiologically Based Pharmacokinetics Joined With In Vitro–In Vivo Extrapolation of ADME: A Marriage Under the Arch of Systems Pharmacology. *Clin Pharmacol Ther* **92**:50–61.

Russell MR, Achour B, McKenzie EA, Lopez R, Harwood MD, Rostami-Hodjegan A, and Barber J (2013) Alternative fusion protein strategies to express recalcitrant QconCAT proteins for quantitative proteomics of human drug metabolizing enzymes and transporters. *J Proteome Res* **12**:5934–5942.

Saito T, Masuda N, Miyazaki T, Kanoh K, Suzuki H, Shimura T, Asao T, and Kuwano H (2004) Expression of EphA2 and E-cadherin in colorectal cancer: correlation with cancer metastasis. *Oncol Rep* **11**:605–11.

Schwenger E, Reddy VP, Moorthy G, Sharma P, Tomkinson H, Masson E, and Vishwanathan K (2018) Harnessing Meta-analysis to Refine an Oncology Patient Population for Physiology-Based Pharmacokinetic Modeling of Drugs. *Clin Pharmacol Ther* **103**:271–280.

Shinko D, Diakos CI, Clarke SJ, and Charles KA (2017) Cancer-Related Systemic Inflammation: The Challenges and Therapeutic Opportunities for Personalized Medicine. *Clin Pharmacol Ther* **102**:599–610.

Steller EJA, Raats DA, Koster J, Rutten B, Govaert KM, Emmink BL, Snoeren N, van Hooff SR, Holstege FCP, Maas C, Borel RIHM, and Kranenburg O (2013) PDGFRB Promotes Liver Metastasis Formation of Mesenchymal-Like Colorectal Tumor Cells. *Neoplasia* **15**:204-IN30.

Troiani T, Martinelli E, Morgillo F, Capasso A, Nappi A, Sforza V, and Ciardiello F (2013) Targeted approach to metastatic colorectal cancer: what comes beyond epidermal growth factor receptor antibodies and bevacizumab? *Ther Adv Med Oncol* **5**:51–72.

van Huizen NA, Coebergh van den Braak RRJ, Doukas M, Dekker LJM, IJzermans JNM, and Luider TM (2019) Up-regulation of collagen proteins in colorectal liver metastasis compared with normal liver tissue. *J Biol Chem* **294**:281–289.

Wlcek K, Svoboda M, Riha J, Zakaria S, Olszewski U, Dvorak Z, Sellner F, Ellinger I, Jäger W, and Thalhammer T (2011) The analysis of organic anion transporting polypeptide (OATP) mRNA and protein patterns in primary and metastatic liver cancer. *Cancer Biol Ther* **11**:801–11.

Xie C, Yan T, Chen J, Li X, Zou J, Zhu L, Lu L, Wang Y, Zhou F, Liu Z, and Hu M (2017) LC-MS/MS quantification of sulfotransferases is better than conventional immunogenic methods in determining human liver SULT activities: implication in precision medicine. *Sci Rep* **7**:3858.

Yan T, Gao S, Peng X, Shi J, Xie C, Li Q, Lu L, Wang Y, Zhou F, Liu Z, and Hu M (2015) Significantly Decreased and More Variable Expression of Major CYPs and UGTs in Liver

Microsomes Prepared from HBV-Positive Human Hepatocellular Carcinoma and Matched Pericarcinomatous Tissues Determined Using an Isotope Label-free UPLC-MS/MS Method. *Pharm Res* **32**:1141–1157.

Yan T, Lu L, Xie C, Chen J, Peng X, Zhu L, Wang Y, Li Q, Shi J, Zhou F, Hu M, and Liu Z (2015) Severely Impaired and Dysregulated Cytochrome P450 Expression and Activities in Hepatocellular Carcinoma: Implications for Personalized Treatment in Patients. *Mol Cancer Ther* **14**:2874–2886.

Yao Y-L, Shao J, Zhang C, Wu J-H, Zhang Q-H, Wang J-J, and Zhu W (2013) Proliferation of Colorectal Cancer Is Promoted by Two Signaling Transduction Expression Patterns: ErbB2/ErbB3/AKT and MET/ErbB3/MAPK. *PLoS One* **8**:e78086.

Zappavigna S, Cossu AM, Grimaldi A, Bocchetti M, Ferraro GA, Nicoletti GF, Filosa R, and Caraglia M (2020) Anti-Inflammatory Drugs as Anticancer Agents. *Int J Mol Sci* **21**:2605.

5.7 Supplementary Information

5.7.1 Supplementary Methods

Materials and chemicals

All chemicals and solvents (HPLC-grade) were purchased from Sigma-Aldrich (Poole, Dorset, UK) unless otherwise stated. EDTA-free protease inhibitor cocktail and trypsin (sequencing grade) were obtained from Roche Applied Sciences (Mannheim, Germany). Lysyl endopeptidase (Lys-C) was purchased from Wako (Osaka, Japan). All the QconCATs (MetCAT, TransCAT and KinCAT) were purchased from PolyQuant GmbH (http://www.polyquant.com/) (Germany). Non-naturally occurring peptides (NNOPs) (light standard peptides) used for the quantification of QconCATs (MetCAT, TransCAT, KinCAT) were purchased from Cambridge Peptides (Cambridge, UK). Bio-Rad based on the Coomassie Brilliant Blue G-250 dye (ThermoFisher Scientific, Hemel Hempstead, UK) and bovine serum albumin (calibration standard) were used.

Preparation of human liver microsomal fractions

Samples provided by Pfizer were supplied as microsomal fractions from healthy liver samples. Histologically normal and matched tumour liver samples provided by the MFT Biobank as tissue, which needed to be fractionated to microsomes by differential centrifugation, as previously described (Achour et al., 2017). Each liver tissue was homogenized by a Fisherbrand 150 Handheld Homogenizer (Thermo Fisher Scientific, UK) in homogenization buffer (150 mM KCl, 2 mM EDTA, 50 mM Tris, 1 mM dithiothreitol, and EDTA-free protease inhibitor cocktail, pH 7.4) at 10 ml for each gram of liver tissue. Each homogenate sample was centrifuged at 10,000 *g* for 20 min at 4°C using an Optima^{TM} L-100 ultracentrifuge (Beckman Coulter, Fullerton, CA), and the supernatant was further centrifuged at 100,000 *g* for 75 min at 4°C. The cytosol (the supernatant) of each individual sample was stored at -80°C for future use, and the pellet (microsomes) from each individual sample was re-suspended in 1 ml of storage buffer (0.25 M potassium dihydrogen phosphate, 0.25 M dipotassium phosphate, pH 7.25) and stored at -80°C. Equal volumes from each of 15 healthy microsomal samples from healthy donors were pooled together. Similar pools were made out of 16 histologically normal microsomal samples from CRLM patients and 16 matched cancerous liver microsomal samples

from CRLM patients. 70 µg of microsomal protein from each pooled sample was used for further sample preparation.

QconCATs (MetCAT and TransCAT) standards

Two QconCAT standards were used in this study, as previously described (Russell et al., 2013). The MetCAT consists of peptides for the quantification of 15 CYPs and 10 UGTs. To quantify the MetCAT, a [Glu^1]-Fibrinopeptide B analogue (GVNNEEGFFSAR), omitting the N-terminal glutamate residue, was included in the MetCAT sequence. The TransCAT is used for the quantification of transporters as previously described (Russell et al., 2013), and a modified version of it is used in the present study. The peptides incorporated into the TransCAT (Supplementary Table 5-3) belong to ABC transporters (P-gp, BSEP, MDR2, MRP2, MRP3, MRP4, MRP6, BCRP), SLC transporters (OST-α, OST-β, OCT1, OCT3, OCTN2, OAT2, OAT4, MATE1, OATP1A2, OATP1B1, OATP1B3, OATP2B1 OATP4C1, NTCP, PEPT1, ASBT, MCT1, OATP4A1), on plasma membrane marker, sodium/potassium-transporting ATPase subunit alpha-1 (ATP1A1), and two cell junction proteins, cadherin-17 (CDH17) and cadherin-23 (CDH23). To quantify the TransCAT, [Glu^1]-Fibrinopeptide B peptide (EGVNDNEEGFFSAR) and another peptide (VGFLPDGVIK) were included in the TransCAT sequence. A bacterial ribosome core was fused upstream of both QconCATs for efficient expression of the constructs (Al-Majdoub et al., 2014).

The KinCAT standard

Design of KinCAT

A QconCAT (KinCAT) for the quantification of 21 human receptor tyrosine kinases (RTKs) was designed and used for the first time, by concatenation of peptides representing: CSF-1R, EGFR, EPHA2, ERBB2, FGFR1, FGFR2, FGFR3, FLT3, IGF-1R, INSR, KIT, MET, NTRK2, PGFRa, PGFRb, RET, TIE2, UFO (AXL), VGFR1, VGFR2 and VGFR3. In addition to these proteins, peptides for the quantification of BCRP, intestinal-type alkaline phosphatase (ALPI), and alkaline phosphatase tissue-nonspecific isozyme (ALPL) were incorporated in the KinCAT. A bacterial ribosome core was fused upstream of the QconCAT sequence for efficient expression of the construct (Al-Majdoub et al., 2014). Finally, the sequences of two NNOPs (SEGVNDNEEGFFSAR, GEGVNDNEEGFFSAR) were included in the KinCAT construct and the light versions of these peptides were used for the quantification of the KinCAT.

Supplementary Table 5-4 provides the peptide sequences and corresponding proteins quantifiable by the modified KinCAT, as well as some characterization information.

For the design of KinCAT, we started with theoretical digestion of each protein target using Protein Prospector (MS Digest) (http://prospector.ucsf.edu/prospector/mshome.htm) to select of the most suitable peptides. The selection of the peptides was based on the following criteria, most of which have already been described (Achour et al., 2015):

- **Uniqueness** of the peptide sequence for the target protein. Peptide uniqueness checker (https://www.nextprot.org/tools/peptide-uniqueness-checker) was used to check the uniqueness of the peptides.
- **Peptide length** from 6 to 20 amino acids to be detectable by LC-MS.
- **No dibasic-tribasic forms** of K (lysine) and R (arginine) (e.g. KK, RR, KR, RK), which tend to be miscleaved.
- **No C- and N-terminal peptides** that are prone to exoproteolytic degradation
- **No M** (methionine-prone to oxidation) **and C** (cysteine-prone to alkylation).
- Exclude peptides with NG, NQ that are prone to deamidation, and DP that is prone to hydrolysis.
- Avoid post-translational modifications using PeptideMass – ExPASy (https://web.expasy.org/peptide_mass/).
- **No transmembrane peptides.** Phobius (http://phobius.sbc.su.se/) and Uniprot (https://www.uniprot.org/) were used to map transmembrane peptides.
- D or E residues near a cleavage site were considered as disadvantage (prone to missed cleavages).
- Isoelectric point (pI) less than 7. Protein isoelectric point calculator (http://isoelectric.org/calculate.php) was used to find the pI and MW of each peptide.

Uniprot human database was used to find the accession number of the protein, and their cellular location. The Human Protein Atlas (Version 18.1) (Uhlen et al., 2015; Thul et al., 2017) was used to confirm liver expression of the proteins.

Expression of KinCAT

The synthesis and purification of KinCAT was performed by PolyQuant GmbH (http://www.polyquant.com/) (Germany), based on the selected peptides after theoretical digestion. The expression was achieved as previously described (Pratt et al., 2006), by cloning the gene of the QconCAT construct into pET21 vector with optimized codons for improved

expression and low levels of mRNA secondary structure formation. This construct was subsequently transfected into *E. coli* and expressed in media depleted of Lysine (K) and Arginine (R), but enriched with R and K labelled with ^{13}C, resulting in a heavy construct. Lastly, the KinCAT was purified with Ni-NTA (Nickel NTA) - His-tag purification.

Characterization of KinCAT

The characterization of KinCAT was performed by PolyQuant and in-house to confirm the quality of the construct.

SDS-PAGE

SDS-PAGE was used to confirm the molecular weight and assess the purity of the KinCAT. 6 µl of KinCAT were diluted in 4 µl of water and then mixed with 10 µl of loading buffer (2 µl DTT 500 mM, 5 µl NuPAGE, 3 µl water), and analysed with SDS-PAGE. The sample was loaded onto a 5% stacking gel (3.4 ml water, 0.83 ml of 30% acryl-bisacrylamide mix, 0.63 ml of 1.5 M Tris pH 6.8, 0.05 ml of 10% SDS, 0.05 ml of 10% ammonium persulfate, and 0.005 ml TEMED) overlaid on a 12% resolving gel (6.6 ml water, 8 ml of 30% acryl-bisacrylamide mix, 5 ml of 1.5 M Tris pH 8.8, 0.2 ml of 10% SDS, 0.2 ml of 10% ammonium persulfate, and 0.008 ml TEMED), and visualized by staining with Coomassie Brilliant Blue dye (Sigma-Aldrich).

Digestion

25 µg of KinCAT was digested using filter-aided sample preparation (FASP), and desalted using a C18 column (Nest group, USA), as described below ('***Digestion and preparation of samples***'). The peptide sample (KinCAT) was dried using a vacuum concentrator and stored at −80 °C until mass spectrometric analysis. Before LC-MS, we added 15.6 µl of 3% acetonitrile-0.1% formic acid and NNOPs (1 nmol/µl stock concentration) at 2.2 µl of 1:250 diluted NNOPs for KinCAT.

Liquid chromatography and tandem mass spectrometry (LC-MS/MS)

Digested KinCAT was analysed by LC-MS/MS using an UltiMate® 3000 Rapid Separation LC (RSLC, Dionex Corporation, Sunnyvale, CA) coupled to a QE HF (Thermo Fisher Scientific,

Waltham, MA) mass spectrometer, as described below ('***Liquid chromatography and tandem mass spectrometry (LC-MS/MS)***').

Measurement of total protein content in pooled microsomal samples

The protein content of each pooled microsomal sample was determined with the Bradford assay (Bradford, 1976) in triplicate, following the manufacturer's protocol.

Digestion and preparation of samples

For each pooled microsomal sample, 70 µg of protein was digested. Each sample was mixed with known amounts of ^{13}C-labelled QconCATs (MetCAT, TransCAT and KinCAT). The pilot study was repeated twice to validate the data:

- For the main study: 7 µl of undiluted MetCAT (0.028 ug/ul), 2 µl of 1:10 diluted TransCAT (1.12 ug/ul), and 3.6 µl of 1:5 diluted KinCAT (0.1954 ug/ul).
- For the replicate study: 1.5 µl of undiluted MetCAT (0.27 ug/ul), 2 µl of 1:10 diluted TransCAT (1.12 ug/ul), and 2.6 µl of 1:5 diluted KinCAT (0.1954 ug/ul).

The protein mixtures were solubilized by sodium deoxycholate at a final concentration of 10% (w/v). The mixture was then incubated at room temperature for 10 min. Dithiothreitol (DTT) was then added at a final concentration of 0.1 M to reduce disulphide bonds; the mixture was incubated at 56^{o} C for 30 min. Filter-aided sample preparation (FASP) was used for protein sample preparation, as previously described (Al-Majdoub et al., 2019; Couto et al., 2019, 2020), with minor modifications. Before the addition of the samples, Amicon Ultra 0.5 mL centrifugal filters, 10 kDa molecular weight cut-off (Merck Millipore, Nottingham, UK), were conditioned by centrifugation of 200 µl of 0.1 M Tris buffer, pH 8.5, at 14,000 rpm at room temperature for 10 min; this step was repeated twice. The reduced protein samples were added to the filters and centrifuged at 13,000 rpm for 20 min. 200 µl of 8M urea in 0.1 M Tris buffer, pH 8.5, was added and the solution was centrifuged at 14,000 rpm for 20 min at room temperature (this step was repeated twice). The samples were subsequently alkylated with 100 µl of 50 mM iodoacetamide (IAA) in the dark for 30 min at room temperature, and then centrifuged at 14,000 rpm for 10 min. The alkylating reagent was washed twice by adding 200 µl of 8 M Urea in 0.1 M Tris pH 8.5, followed centrifugation at 14,000 rpm for 20 min at room temperature. The concentration of urea was reduced with two washes with 1 M urea in 50 mM ammonium

bicarbonate (AmBic), pH 8.0, followed centrifugation at 13,000 rpm for 20 min. To avoid the evaporation of the samples, 80 µl of 1 M urea in 50 mM AmBic, pH 8.0, was added to each filter unit. Lysyl endopeptidase was added to each sample (enzyme:protein ratio 1:50 w/w) for two hours at 30°C, and the same step was repeated for an extra two hours. Trypsin was added (enzyme/protein ratio 1:25 w/w), followed by incubation for 12 hours at 37°C, and the same step was repeated for an extra four hours. The peptide samples were recovered by centrifugation at 14,000 rpm for 20 min. 100 µl of 0.5 M NaCl was added to the filter, centrifuged at 14,000 rpm for 20 min, followed by an additional 50 µl of 0.5 M NaCl, and centrifugation at 14,000 rpm for 10 min. After this step, each sample was split into two equal volumes, and each was mixed with sample buffer (3 parts of sample:1 part of sample buffer 2% v/v trifluoroacetic acid in 20% v/v acetonitrile in water). Each sample was then desalted using a C18 column (Nest group, USA). Finally, the peptide samples were dried using a vacuum concentrator and stored at −80 °C until mass spectrometric analysis.

Before the LC-MS, samples were mixed with 9.3 µl of 3% acetonitrile-0.1% formic acid and NNOPs (stock concentration of each NNOP was 1 nmol/µl) using the following volumes/dilutions:

- For the main study: 3.5 µl of 1:10000 diluted NNOP for MetCAT, 2.5 µl of 1:20000 diluted NNOPs for TransCAT, and 6.1 µl of 1:25000 diluted NNOPs for KinCAT.
- For the replicate study (addition of unlabelled standards): 2.6 µl of 1:20000 diluted NNOP for MetCAT, 2.5 µl of 1:10000 diluted NNOPs for TransCAT, and 4.4 µl of 1:25000 diluted NNOPs for KinCAT.

Liquid chromatography and tandem mass spectrometry (LC-MS/MS)

Digested samples were analysed by LC-MS/MS using an UltiMate® 3000 Rapid Separation LC (RSLC, Dionex Corporation, Sunnyvale, CA) coupled to a QE HF (Thermo Fisher Scientific, Waltham, MA) mass spectrometer. Mobile phase A was 0.1% formic acid in water and mobile phase B was 0.1% formic acid in acetonitrile, and the column used was a 75 mm x 250 µm i.d., 1.7 µM particle size, CSH C18 analytical column (Waters, UK.) 1 µl aliquot of the sample was transferred to a 5 µl loop and loaded onto the column at a flow of 300 nl/min for 5 min at 5% B. The loop was then taken out of line and the flow was reduced from 300 nl/min to 200 nl/min in 0.5 min. Peptides were separated using a gradient from 5% to 18% B in 63.5 min, then from 18% to 27% B in 8 min and finally from 27% B to 60% B in 1 min. The

column was washed by 60% B for 3 min before re-equilibration to 5% B in 1 min. At 85 min, the flow is increased back to 300 nl/min until the end of the run at 90 min. Mass spectrometry data was acquired in a data-dependent manner for 90 min in positive mode. Peptides were selected for fragmentation automatically by data-dependant analysis of the top 12 peptides, at m/z between 300 to 1750 Th and a charge state of 2, 3 or 4, with dynamic exclusion set at 15 sec. The MS resolution was set at 120,000 with an AGC target of 3e6 and a maximum fill time set at 20 ms. The MS2 resolution was set to 30,000, with an AGC target of 2e5, a maximum fill time of 45 ms, isolation window of 1.3 Th and a collision energy of 28 eV.

5.7.2 Supplementary Results

Ratios of NP/HP and TP/HP in replicate analyses

The experiments were repeated in the replicate study to confirm the data. Using targeted analysis, we compared NP/HP and TP/HP ratios between the data presented here (main study) and the data from a replicate experiment (replicate study) for CYPs and UGTs. Supplementary Table 5-9 shows that the NP relative to HP ratio values measured in main study and replicate study were within 2 fold, except for CYP2J2 (3 fold difference between the two experiments). Similarly, the ratios of TP/HP were within 2 fold for most enzymes measured in the two experiments, with the exception of UGT1A6 (2.2 fold) and UGT1A9 (2.5 fold). Consistent with the main study, the ratios of the vast majority of enzymes measured in the replicate study were less abundant in TP than in HP (Supplementary Table 5-9). Overall, the two experiments were consistent.

5.7.3 Supplementary Tables

Supplementary Table 5-1 Demographic and clinical details of CRLM patients provided by the MFT Biobank.

Sample ID	Age at surgery (years)	Race	Sex	Body mass index, BMI (kg/m^2)	Smoking/ Alcohol use	Liver lobe	Diagnosis	Medical history	Treatment
389	52	Caucasian	Female	30.86	No/ Occasionally	Left	Metastatic moderately well differentiated adenocarcinoma	Deep vein thrombosis, asthma, duodenal ulcer, thyroid problem, liver lesions	Fragmin, levothyroxine, betamethasone, ventolin, ferrous fumarate
590	72	Caucasian	Male	32	Pipe/ 22 units per week	-	Metastatic moderate to Well differentiated adenocarcinoma (dirty necrosis)	Asthma, polypectomy, tonsillectomy, Hemicolectomy Dukes B	Salbutamol, tiotropium, lansaprozole, nasonex
633	67	Caucasian	Male	26.85	Ex-stopped/ -	Right	Metastatic adenocarcinoma & fatty liver disease	Peripheral neuropathy secondary to oxaliplatin, type 2 diabetes, hypercholesterolemia, valvular heart disease, prostate cancer with bone metastasis, colonic cancer T3N0, colorectal liver metastasis	Metformin, zoladex, oxaplatin and 5FU, irinotecan and 5FU with cetuximab
674	68	Caucasian	Female	26.67	No/ -	Right	Metastatic moderately differentiated adenocarcinoma	Rectosigmoid cancer 10/10 Dukes B	-
734	64	Caucasian	Female	23.84	No/ Occasionally	Right	Moderately to focally poorly differentiated metastatic adenocarcinoma	Primary colorectal	Dalteparin, short course of radiotherapy, adjuvant OXmdG and 5FU
746	85	Caucasian	Male	23.67	Ex (40 years)/ Moderately	Right	Metastatic papillary carcinoma	Laparoscopic R hemicolectomy T2M0,	Irbesartan, levothyroxine,

								Squamous cell carcinoma (scalp), hypothyroidism, hypertension, Chronic obstructive pulmonary disease	bisoprolol, aspirin, omeprazole, budesamide, formoterol
794	71	Caucasian	Female	22.41	No/ No	-	Metastatic adenocarcinoma with extensive intra-acinar necrosis	R hemicolectomy, pT3N2, high blood pressure, depression	Tomudex chemotherapy
818	58	Caucasian	Male	21.78	Ex (25 years)/ 18 units per week	-	Moderately differentiated metastatic adenocarcinoma	Sigmoid adenocarcinoma pT3pN2	Loperamide, carboplatin/5FU and modified de Gramont and radiotherapy
1492	34	-	Female	32.53	Ex-stopped/ Approximately 20 units per week	Right	Metastatic moderate and poorly differentiated adenocarcinoma	Bowel resection, pilonodal abcess x2, grometts (as a child), tonsillectomy (as a child), egg collection, occasional palpitations, asthma (as a child), reflux, joint problems in knees, treated for Irritable bowel syndrome	Omeprazole, amitryptyline, microgynon, glucosamine sulphate, ibuprofen, peppermint oil
1493	75	-	Male	-	No/ No	Right	Metastatic moderately differentiated adenocarcinoma	Sigmoid tumour, sleep apnoea, asthma	Cod liver oil, salbutamol inhaler, seretide inhaler, movicol
1498	63	Caucasian	Male	-	No/ Rarely	Right	Metastatic adenocarcinoma	Previous gout, anaemia, cataract operation	Doxycycline regime completed, Nil regular
1795	63		Male	36.32	Ex - stopped (previously 30cpd)/ Approximately 75 units per week	Left	Metastatic well differentiated adenocarcinoma	Adenocarcinoma, hypertension, intermittent claudication of left leg	Omeprazole, irbesartan, simvastatin, clopidogrel

1957	68	-	Male	32.16	No/ -	Left	Metastatic moderately differentiated adenocarcinoma	Primary rectal cancer, pneumonia post-operative, liver cancer, late lung metastasis	Nil regular
2036	43	-	Female	-	-/ -	Right	Metastatic moderate to poorly differentiated adenocarcinoma	Primary colorectal	Omeprazole, paracetamol
2058	79	Caucasian	Female	21.6	-/ -	Left	Metastatic adenocarcinoma	Below the knee amputation, primary colorectal, lung metastasis	Lansoprazole, ferrous sulphate, alendronic acid, paracetamol, codeine phosphate, senna, natecal D3
2095	55	Caucasian	Male	28.1	-/ -	Right	Metastatic moderately differentiated adenocarcinoma	Primary colorectal	Nil regular

Supplementary Table 5-2 Demographic and clinical details of healthy subjects provided by Pfizer.

Sample ID	Age at surgery (years)	Race	Sex	Body mass index, BMI (kg/m^2)	Smoking/ Alcohol use	Cause of death	Medical history	Treatment
HH83	18	Caucasian	Female	20.19	No/ No	Head trauma	Healthy	None
HH84	53	Caucasian	Male	19.94	No/ Social	Intracranial haemorrhage	None	None
HH87	54	Caucasian	Female	29.79	No/ No	Head trauma	Healthy	None
HH93	34	Caucasian	Male	20.62	No/ No	Cerebellar haemorrhagic injury	Healthy	Healthy
HH98	64	Caucasian	Male	37.47	No/ No	Head Injury	Healthy	None
HH99	45	Caucasian	Male	31.62	No/ No	Head trauma	Healthy	None
HH101	54	Caucasian	Female	21.95	No/ No	Motor vehicle accident	Healthy	None
HH102	52	Caucasian	Female	32.26	No/ No	Cerebral Aneurysm	Healthy	None
HH104	35	African American	Female	25.25	No/ No	Cerebral Aneurysm	Healthy	None
HH105	50	Caucasian	Male	33.47	No/ No	Cerebral Aneurysm	Healthy	None
HH106	43	Hispanic	Male	24.48	No/ No	Cerebral Vascular Aneurysm	Healthy	None
HH107	45	Caucasian	Female	24.96	No/ No	Cerebral Vascular Aneurysm	Healthy	None
HH110	54	Caucasian	Female	26.29	No/ Social	Cerebral Vascular Aneurysm	Healthy	None
HH111	43	Caucasian	Female	28.43	No/ No	Intracranial bleeding	Healthy	None
HH118	32	Caucasian	Male	26.69	No/ Social	Gunshot Wound to head	Healthy, Skin Graft on right arm in the past	Pepcid AC, Tagamet, Steroids in HS and Marines

Supplementary Table 5-3 Re-designed TransCAT; target proteins, peptides and incorporation efficiency.

Target protein	Peptide	Percent of label incorporation
P-gp	AGAVAEEVLAAIR	96.3
P-gp	AGAVAEEVLAAVR	95.1
P-gp	FYDPLAGK	98.7
BSEP	AADTIIGFEHGTAVER	93.5
BSEP	STALQLIQR	96.6
MDR3	GAAYVIFDIIDNNPK	98.6
MDR3	IATEAIENIR	
MRP2	AFEHQQR	93.6
MRP2	LTIIPQDPILFSGSLR	96.3
MRP2	YLGGDDLDTSAIR	95.2
MRP3	AEGEISDPFR	
MRP3	IDGLNVADIGLHDLR	96.7
MRP4	AEAAALTETAK	98.7
MRP4	APVLFFDR	96.0
MRP6	APETEPFLR	95.3
MRP6	SSLASGLLR	96.4
MRP6	SSLPSALLGELSK	98.7
BCRP	ENLQFSAALR	95.4
BCRP	SSLLDVLAAR	93.7
BCRP	VIQELGLDK	98.7
ASBT	IAGLPWYR	95.4
ASBT	LWIIGTIFPVAGYSLGFLLAR	
ATP1A1	IVEIPFNSTNK	98.7
ATP1A1	SPDFTNENPLETR	95.3
Cadherin-17	AENPEPLVFGVK	98.6
Cadherin-17	QNSRPGK	
Cadherin-23	ATDADEGEFGR	96.2
Cadherin-23	DAYVGALR	
MCT1	DLHDANTDLIGR	95.9
MCT1	SITVFFK	98.8
OATP4A1	ILGGIPGPIAFGWVIDK	98.6
OATP4A1	YEVELDAGVR	
OST-α	VGYETFSSPDLDLNLK	98.7
OST-α	YTADLLEVLK	98.5
OST-β	DHNSLNNLR	96.0
OST-β	ETPEVLHLDEAK	98.6
PEPT1	GNEVQIK	
PEPT1	HTLLVWAPNHYQVVK	98.7
PEPT1	TLPVFPK	
NTCP	AHLWKPK	98.1
NTCP	GIYDGDLK	98.6
OCT1	ENTIYLK	98.5

OCT1	GVALPETMK	98.8
OCT1	MLSLEEDVTEK	98.6
OCT3	FLQGVFGK	98.8
OCT3	GIALPETVDDVEK	98.7
OCTN2	DYDEVTAFLGEWGPFQR	95.4
OCTN2	TWNIR	
OAT2	NVALLALPR	96.3
OAT2	WLLTQGHVK	98.7
OAT7	DTLTLEILK	98.6
OAT7	ISLLSFTR	96.4
MATE1	DHVGYIFTTDR	96.0
MATE1	GGPEATLEVR	95.6
OATP1A2	EGLETNADIIK	98.6
OATP1A2	IYDSTTFR	95.4
OATP1B1	MFLAALSLSFIAK	
OATP1B1	LNTVGIAK	98.7
OATP1B1	YVEQQYGQPSSK	98.8
OATP1B3	IYNSVFFGR	96.5
OATP1B3	NVTGFFQSLK	98.6
OATP2B1	SSPAVEQQLLVSGPGK	98.2
OATP2B1	VLLQTLR	95.0
OATP4C1	DFPAALK	
OATP4C1	HLPGTAEIQAGK	

Supplementary Table 5-4 KinCAT; target proteins, peptides and incorporation efficiency.

Target protein	Peptide	Percent of label incorporation
ALPI	GFYLFVEGGR	98.0
ALPI	NLILFLGDGLGVPTVTATR	97.9
ALPL	LDGLDLVDTWK	98.9
ALPL	ANEGTVGVSAATER	98.1
BCRP	LFDSLTLLASGR	97.1
CSF-1R	ALTFELTLR	97.7
CSF-1R	VVEATAFGLGK	98.9
EGFR	IPLENLQIIR	98.0
EGFR	NYDLSFLK	98.8
EPHA2	TVSEWLESIK	98.9
EPHA2	AINDGFR	98.0
ERBB2	LLDIDETEYHADGGK	98.9
ERBB2	GIWIPDGENVK	98.9
FGFR1	DGVQLAESNR	97.9
FGFR1	IGPDNLPYVQILK	98.9
FGFR2	YGPDGLPYLK	98.7
FGFR2	EIEVLYIR	97.9
FGFR3	DGTGLVPSER	97.9
FGFR3	TAGANTTDK	
FGFR3	VGPDGTPYVTVLK	98.9
FLT3	TWTEIFK	98.9
FLT3	EYEYDLK	98.9
IGF-1R	ASFDER	97.9
IGF-1R	TTINNEYNYR	98.0
INSR	ESLVISGLR	98.0
INSR	TIDSVTSAQELR	98.0
KIT	LVVQSSIDSSAFK	98.9
KIT	VVEATAYGLIK	98.7
MET	LNSELNIEWK	98.9
MET	ETSIFSYR	98.2
NTRK2	NSNLQHINFTR	98.1
NTRK2	SNEIPSTDVTDK	98.9
NTRK2	ITNISSDDSGK	98.8
PGFRA	VEETIAVR	98.0
PGFRA	VVEGTAYGLSR	98.0
PGFRB	EVDSDAYYVYR	97.9
PGFRB	GFSGIFEDR	97.8
RET	LLEGEGLPFR	97.7
RET	DAPEEVPSFR	97.9
TIE2	NILVGENYVAK	98.9
TIE2	VPGNLTSVLLNNLHPR	97.9
UFO(AXL)	APLQGTLLGYR	97.9

UFO(AXL)	YGEVFEPTVER	98.1
VGFR1	DQEAPYLLR	97.7
VGFR1	FNSGSSDDVR	97.6
VGFR2	AASVGLPSVSLDLPR	98.0
VGFR2	VEAFFIIEGAQEK	98.9
VGFR3	NILLSESDVVK	98.9
VGFR3	DSEDTGVVR	97.7

Supplementary Table 5-5 Input parameters for PBPK modelling using Simcyp v20 R1 for alfentanil (predominantly metabolized by CYP3A4), midazolam (predominantly metabolized by CYP3A4 and CYP3A5), and nebivolol (predominantly metabolized by CYP3A4 and CYP2D6).

Input Parameters			
Compound Name	**SV-Alfentanil**	**Sim-Midazolam**	**SV-Nebivolol**
Mol Weight (g/mol)	416.52	325.8	405.44
log P	2.16	3.53	4.18
Compound Type	Monoprotic Base	Monoprotic Base	Monoprotic Base
pKa 1	6.5	6	8.9
pKa 2	n/a	n/a	n/a
B/P	0.63	0.603	0.626
Haematocrit	45	45	45
fu	0.104	0.032	0.02
GI Absorption Model	1st order	1st order	1st order
GI Permeability Assay	n/a	n/a	n/a
GI Peff,man	Regional	Regional	Regional
Distribution Model	Minimal PBPK Model	Minimal PBPK Model	Full PBPK Model
Vss (L/kg)	0.37	0.88	Predicted
Prediction Method	Entered	Entered	Method 1
Clearance Type	Enzyme Kinetics	Enzyme Kinetics	Enzyme Kinetics
Trial Design			
Population Name	Sim-Healthy Volunteers/Cancer	Sim-Healthy Volunteers/Cancer	Sim-Healthy Volunteers/Cancer
Use Pop Representative	No	No	No
Population Size	100	100	100
Number of Trials	10	10	10
No. of Subjects per Trial	10	10	10
Start Day/Time	Day 1, 09:00	Day 1, 09:00	Day 1, 09:00
End Day/Time	Day 2, 09:00	Day 2, 09:00	Day 2, 09:00
Study Duration (h)	24	24	24
Sampling Time	Pre-defined Uniform	Pre-defined Uniform	Pre-defined Uniform
Sampling Site Selection	Off	Off	Off
Prandial State	Fasted	Fasted	Fasted
Route	Oral	Oral	Oral
Dose Units	Dose (mg/kg)	Dose (mg)	Dose (mg)
Dose	0.043	5	4.6
Start Day/Time	Day 1, 09:00	Day 1, 09:00	Day 1, 09:00
Dosing Regimen	Single Dose	Single Dose	Single Dose

Supplementary Table 5-6 Quantification of twelve CYP and eight UGT enzymes in human HP, NP and TP liver samples.

		HP	NP	TP
Protein target	**Peptides**	**Absolute abundance (pmol mg^{-1})**		
CYP1A2	YLPNPALQR	10.1	20.9	2.0
CYP2A6	GTGGANIDPTFFLSR	15.8	36.1	4.3
CYP2B6	GYGVIFANGNR	6.9	4.8	0.2
CYP2C19	GHFPLAER	1.6	3.3	0.2
CYP2C8	SFTNFSK	24.2	29.7	4.8
CYP2C9	GIFPLAER	76.1	113.5	17.4
CYP2D6	AFLTQLDELLTEHR		116.2	7.2
CYP2E1	FITLVPSNLPHEATR	79.4	50.2	9.5
CYP2J2	VIGQGQQPSTAAR	0.2	0.0	-0.1
CYP3A4	LSLGGLLQPEK	90.2	65.9	9.0
CYP3A5	YWTEPEEFRPER	11.7		
CYP4F2	HVTQDIVLPDGR	7.7	7.8	3.3
UGT1A1	TYPVPFQR	17.0	6.3	1.5
UGT1A3	HVLGHTQLYFETEHFLK		3.3	
UGT1A4/1A5	GTQCPNPSSYIPK	27.4	23.5	1.8
UGT1A6	VSVWLLR	7.7	5.0	0.7
UGT1A9	AFAHAQWK	25.7	13.7	1.4
UGT2B15	SVINDPVYK	33.4	35.9	3.6
UGT2B4	FSPGYAIEK	29.3	26.4	3.0
UGT2B7	ADVWLIR	60.7	80.9	9.1

Supplementary Table 5-7 Quantification of transporters in human HP, NP and TP liver samples.

		HP	NP	TP
Protein target	**Peptides**	**Absolute abundance (pmol mg^{-1})**		
BCRP	VIQELGLDK	0.18		
BSEP	AADTIIGFEHGTAVER	0.55	0.51	
MDR3	GAAYVIFDIIDNNPK	0.52	0.76	0.14
MRP2	LTIIPQDPILFSGSLR	0.85	0.63	0.18
MRP3	IDGLNVADIGLHDLR	0.70	0.39	0.47
MRP6	SSLASGLLR	1.34	1.10	
P-gp	FYDPLAGK	0.46	0.60	0.71
ASBT	IAGLPWYR	0.01		
MCT1	SITVFFK	2.25	1.77	3.75
NTCP	GIYDGDLK		5.22	0.56
OAT2	NVALLALPR	1.47	1.57	0.16
OAT7	DTLTLEILK	3.33	2.08	0.25
OATP1A2	EGLETNADIIK	5.32	3.84	6.94
OATP1B1	YVEQQYGQPSSK	2.00	1.41	0.54
OATP1B3	NVTGFFQSLK	2.35	2.31	0.36
OATP2B1	SSPAVEQQLLVSGPGK	2.38	2.91	0.69
OCT1	MLSLEEDVTEK	5.36	2.93	
OST-α	YTADLLEVLK	0.03		
PEPT1	HTLLVWAPNHYQVVK		0.11	
ATP1A1	SPDFTNENPLETR	7.33	4.64	16.34
Cadherin-17	AENPEPLVFGVK		0.18	6.43

Supplementary Table 5-8 Quantification of nineteen RTKs in human HP, NP and TP liver samples.

		HP	NP	TP
Protein target	**Peptides**	**Absolute abundance (pmol mg^{-1})**		
EGFR	IPLENLQIIR	0.317	0.419	0.121
EPHA2	AINDGFR	0.052		0.051
ERBB2	LLDIDETEYHADGGK	0.033	0.080	0.145
FGFR1	IGPDNLPYVQILK			0.011
FGFR2	EIEVLYIR			0.042
FGFR3	VGPDGTPYVTVLK	0.033	0.093	
IGF-1R	TTINNEYNYR	0.008	0.125	0.141
INSR	ESLVISGLR	0.348	0.284	0.130
KIT	VVEATAYGLIK		0.057	0.011
MET	ETSIFSYR	0.185		
NTRK2	NSNLQHINFTR	0.043		0.097
PGFRA	VVEGTAYGLSR	0.038	0.054	
PGFRB	GFSGIFEDR			3.793
RET	DAPEEVPSFR		0.045	
TIE2	NILVGENYVAK	0.084	0.320	
UFO(AXL)	APLQGTLLGYR	0.094	0.052	0.033
VGFR1	DQEAPYLLR	0.097	0.161	
VGFR2	AASVGLPSVSLDLPR			0.024
VGFR3	NILLSESDVVK	0.064	0.002	

Supplementary Table 5-9 Comparison of histologically normal and tumour to healthy ratios (absolute abundance of CYPs and UGTs) between pilot study 1, and 2 (replicate study).

		Main Pilot Study (1)		Repetition Pilot Study (2)		Ratio (1)/(2)	
Protein target	**Surrogate Peptides**	**NP/HP**	**TP/HP**	**NP/HP**	**TP/HP**	**NP/HP**	**TP/HP**
CYP1A2	YLPNPALQR	2.1	0.2	1.5	0.3	1.4	0.7
CYP2A6	GTGGANIDPTFFLSR	2.3	0.3	1.3	0.3	1.7	0.9
CYP2B6	GYGVIFANGNR	0.7	0.02	0.4		1.7	
CYP2C18	SLTNFSK			0.5			
CYP2C19	GHFPLAER	2.1	0.1	1.8	0.1	1.1	1.2
CYP2C8	SFTNFSK	1.2	0.2	0.9	0.3	1.3	0.6
CYP2C9	GIFPLAER	1.5	0.2	1.1	0.4	1.4	0.6
CYP2D6	AFLTQLDELLTEHR			0.9	0.1		
CYP2E1	FITLVPSNLPHEATR	0.6	0.1	0.6	0.2	1.1	0.5
CYP2J2	VIGQGQQPSTAAR	0.3		0.9		0.3	
CYP3A4	LSLGGLLQPEK	0.7	0.1	0.4	0.1	1.8	0.7
CYP3A5	YWTEPEEFRPER			0.2			
CYP3A7	FNPLDPFVLSIK			0.9	1.6		
CYP4F2	HVTQDIVLPDGR	1.0	0.4	0.9	0.3	1.1	1.3
UGT1A1	TYPVPFQR	0.4	0.1				
UGT1A3	HVLGHTQLYFETEHFLK			0.7	0.2		
UGT1A4/1A5	GTQCPNPSSYIPK	0.9	0.1	0.4		2.2	
UGT1A6	VSVWLLR	0.7	0.1	0.6	0.2	1.1	0.5
UGT1A9	AFAHAQWK	0.5	0.1	0.4	0.1	1.5	0.4
UGT2B15	SVINDPVYK	1.1	0.1	0.8	0.2	1.4	0.6
UGT2B4	FSPGYAIEK	0.9	0.1	0.7		1.4	
UGT2B7	ADVWLIR	1.3	0.2	0.9	0.2	1.5	0.8

5.7.4 References

Achour B, Al-Majdoub ZM, Al Feteisi H, Elmorsi Y, Rostami-Hodjegan A, and Barber J (2015) Ten years of QconCATs: Application of multiplexed quantification to small medically relevant proteomes. *Int J Mass Spectrom* **391**:93–104.

Achour B, Al Feteisi H, Lanucara F, Rostami-Hodjegan A, and Barber J (2017) Global proteomic analysis of human liver microsomes: Rapid characterization and quantification of hepatic drug-metabolizing enzymes. *Drug Metab Dispos* **45**:666-675.

Al-Majdoub ZM, Al Feteisi H, Achour B, Warwood S, Neuhoff S, Rostami-Hodjegan A, and Barber J (2019) Proteomic quantification of human blood–brain barrier SLC and ABC transporters in healthy individuals and dementia patients. *Mol Pharm* **16**:1220–1233.

Al-Majdoub ZM, Carroll KM, Gaskell SJ, and Barber J (2014) Quantification of the proteins of the bacterial ribosome using QconCAT technology. *J Proteome Res* **13**:1211–1222.

Bradford M (1976) A Rapid and Sensitive Method for the Quantitation of Microgram Quantities of Protein Utilizing the Principle of Protein-Dye Binding. *Anal Biochem* **72**:248–254.

Couto N, Al-Majdoub ZM, Achour B, Wright PC, Rostami-Hodjegan A, and Barber J (2019) Quantification of Proteins Involved in Drug Metabolism and Disposition in the Human Liver Using Label-Free Global Proteomics. *Mol Pharm* **16**:632–647.

Couto N, Al-Majdoub ZM, Gibson S, Davies PJ, Achour B, Harwood MD, Carlson G, Barber J, Rostami-Hodjegan A, and Warhurst G (2020) Quantitative Proteomics of Clinically Relevant Drug-Metabolizing Enzymes and Drug Transporters and Their Intercorrelations in the Human Small Intestine. *Drug Metab Dispos* **48**:245–254.

Pratt JM, Simpson DM, Doherty MK, Rivers J, Gaskell SJ, and Beynon RJ (2006) Multiplexed absolute quantification for proteomics using concatenated signature peptides encoded by QconCAT genes. *Nat Protoc* **1**:1029–1043.

Russell MR, Achour B, McKenzie EA, Lopez R, Harwood MD, Rostami-Hodjegan A, and Barber J (2013) Alternative fusion protein strategies to express recalcitrant QconCAT proteins for quantitative proteomics of human drug metabolizing enzymes and transporters. *J Proteome Res* **12**:5934–5942.

Thul PJ, Åkesson L, Wiking M, Mahdessian D, Geladaki A, Ait Blal H, Alm T, Asplund A,

Björk L, Breckels LM, Bäckström A, Danielsson F, Fagerberg L, Fall J, Gatto L, Gnann C, Hober S, Hjelmare M, Johansson F, Lee S, Lindskog C, Mulder J, Mulvey CM, Nilsson P, Oksvold P, Rockberg J, Schutten R, Schwenk JM, Sivertsson Å, Sjöstedt E, Skogs M, Stadler C, Sullivan DP, Tegel H, Winsnes C, Zhang C, Zwahlen M, Mardinoglu A, Pontén F, von Feilitzen K, Lilley KS, Uhlén M, and Lundberg E (2017) A subcellular map of the human proteome. *Science* **356**:eaal3321.

Uhlen M, Fagerberg L, Hallstrom BM, Lindskog C, Oksvold P, Mardinoglu A, Sivertsson A, Kampf C, Sjostedt E, Asplund A, Olsson I, Edlund K, Lundberg E, Navani S, Szigyarto CA-K, Odeberg J, Djureinovic D, Takanen JO, Hober S, Alm T, Edqvist P-H, Berling H, Tegel H, Mulder J, Rockberg J, Nilsson P, Schwenk JM, Hamsten M, von Feilitzen K, Forsberg M, Persson L, Johansson F, Zwahlen M, von Heijne G, Nielsen J, and Ponten F (2015) Tissue-based map of the human proteome. *Science* **347**:1260419.

Vasilogianni AM, Achour B, Scotcher D, Peters SA, Al-Majdoub ZM, Barber J, and Rostami-Hodjegan A (2021) Hepatic Scaling Factors for In Vitro-In Vivo Extrapolation (IVIVE) of Metabolic Drug Clearance in Patients with Colorectal Cancer with Liver Metastasis. *Drug Metab Dispos* (in press).

Chapter Six: Quantitative Proteomics of Drug-Metabolizing Enzymes and Drug Transporters in Human Colorectal Cancer Metastasis and the Surrounding Liver

Declaration

Areti-Maria Vasilogianni, Zubida M. Al-Majdoub, Brahim Achour, Sheila Annie Peters, Jill Barber and Amin Rostami-Hodjegan

I carried out the literature search, generation and analysis of data, contributed to the study design and wrote the manuscript. Dr Zubida M. Al-Majdoub and Dr Brahim Achour were consulted on experimental methodology and analysis of data, and suggested edits to the manuscript. Dr Sheila Annie Peters, Dr Jill Barber and Prof. Amin Rostami-Hodjegan contributed to the study design and provided guidance. I retained editorial control.

6.1 Abstract

The objectives of this study were to comprehensively assess for first time protein expression of 22 drug metabolizing enzymes (DMEs) and 25 transporters in 15 human healthy livers, 18 cancer (2 primary and 16 colorectal cancer liver metastasis (CRLM)), and 18 paired normal liver tissues and investigate the cancer impact on their expression. LC–MS/MS (AMRT) targeted quantitative proteomics was used to quantify enzymes and transporters in human liver microsomes. We found significantly decreased levels of CYP2B6/2D6/2E1/3A4/3A5 (<6.6-fold) and UGT1A1/1A6/1A9/2B15/2B4/2B7 (<6.1-fold) in normal liver from cancer patients relative to healthy controls. CYPs (CYP3A4/3A5/2D6 etc.) were strongly decreased in tumour compared with normal (<10.9-fold) and healthy controls (<21.3-fold). Most of UGTs were downregulated in tumours compared with control (<58.1-fold) and normal livers (<19-fold). BSEP, MRPs, and P-gp were significantly decreased in normal (<3.1-fold) and tumour (<6.3-fold) versus healthy, and in tumour versus normal livers (<3.7-fold). Expression of OCT3, OAT2/7 and OATPs followed similar significant trends (<2.9-fold in normal, and <16.4-fold in tumour relative to healthy). NTCP and OCT1 were significantly lower (<9-fold), and MCT1 increased (3.3-fold) in tumour compared with normal livers. The inter-individual variability in protein expression was substantially high in cancer. The experimentally generated abundance data were integrated into PBPK models for CYP substrates (alprazolam, crizotinib, ibrutinib). We found substantial increase of drug exposure (AUC) (<9.5-fold) when using cancer-related abundance values. In conclusion, our study reveals decrease of DMEs and most transporters, with high variability in cancer, and highlights the importance of population-specific abundance data in PBPK modelling.

6.2 Introduction

Colorectal cancer (CRC) is the second most lethal type of cancer (Bray et al., 2018), being metastasized to liver in half of the patients (Maher et al., 2017), which is the main cause of mortality (Siegel et al., 2018). CRC is caused by multiple factors with many genetic and epigenetic alterations contributing to its manifestation (Nikolouzakis et al., 2018). Primary liver cancer is also leading cause of cancer death mortality, with main types being hepatocellular carcinoma (HCC) and intrahepatic cholangiocarcinoma (ICC) (Bray et al., 2018).

Liver cancer is ideally treated by surgical resection, but this is not possible for most of the patients, and chemotherapy is used to decrease the tumour growth (Chen et al., 2014; Mitchell et al., 2019). The liver is the main organ of drug metabolism, and the presence of tumour could potentially affect the pharmacokinetics (PK) and pharmacodynamics (PD) of drugs in cancer patients. Not only histologically normal liver, but also tumorous part of the liver may be important for drug metabolism and disposition in cancer patients, as drug metabolizing enzymes (DMEs), especially cytochrome P450 enzymes (CYP) and uridine 5′-diphospho-glucuronosyltransferases (UGT), in tumour are responsible for activation of anti-cancer prodrugs and disposition of them to the tissue (Michael and Doherty, 2005). Drug transporters are also very critical for drug disposition and anti-cancer drug resistance, which is achieved in cases of an increase of efflux transporters (P-gp, MRPs etc.), and decrease of influx transporters (OATPs etc.) (Akhdar et al., 2012).

Physiologically based pharmacokinetic (PBPK) models are gaining wider acceptance in regulatory decision making in the area of oncology, where recruitment and ethical/safety issues are of high importance in clinical studies (Yoshida et al., 2017). These models require the incorporation of system-specific and drug data for accurate prediction of PK of drugs (Rostami-Hodjegan, 2012). Cancer population is very heterogeneous and the PK profile of drugs (clearance, exposure, absorption etc.) may differ between cancer and healthy subjects due to a wide range of systems parameters, such as blood protein levels, comorbidities (Cheeti et al., 2013), renal impairment (Suri et al., 2015), microsomal protein per garm of liver (MPPGL) (Vasilogianni et al., 2021), abundance of drug-metabolising enzymes (DMEs) (Yan, Gao, et al., 2015), and transporters (Billington et al., 2018), and increased levels of inflammation in cancer patients (Shinko et al., 2017). Interestingly, a decrease in the abundance of several CYPs in a cancer population gave better PK predictions (Schwenger et al., 2018).

Quantitative measurements of CYPs and UGTs in HCC patients using LC-MS proteomics are available and highlight perturbations in cancerous tissues (Yan, Gao, et al., 2015; Yan, Lu, et al., 2015). LC-MS proteomics have also been used to quantify drug transporters in HCC (Billington et al., 2018). Absolute quantification data are limited and most studies report immunohistochemistry or mRNA data. Regarding CRLM, despite its high incidence, there is a scarcity of quantitative data in human tissues from CRLM patients. Starting with DMEs, the impact of CRLM on the qualitative expression profile of CYPs (Lane et al., 2004), and the expression of other DMEs in histologically normal and cancerous tissues from CRLM patients has been assessed (van Huizen et al., 2019), highlighting a potential impact of cancer on drug metabolism. Studies on transport proteins are more scarce in CRLM, focused to mRNA measurements of OATPs (Wlcek et al., 2011) or comparing the abundance between healthy livers from healthy donors and histologically normal livers from CRLM patients, with no measurements in tumorous livers (Kurzawski et al., 2019). Preliminary experiment was performed by measuring the abundance of DMEs and transporters in CRLM pooled samples (Vasilogianni et al., unpublished).

Based on the above data, the investigation of parameters defining the PK of drugs in cancer is necessary. Our study applies targeted accurate mass and retention time (AMRT) proteomics with the aim to quantify of DMEs and transporters in healthy donors, histologically normal and matched cancerous liver tissues from cancer patients. Cancer patients of the current study are mainly CRLM patients, and to our knowledge, this is the most comprehensive report to provide absolute and quantitative measurements of DMEs and transporters in CRLM. In addition, we were able to scale our abundance data for each individual sample to liver tissue for the first time in CRLM using our previously experimentally-derived microsomal protein per gram of liver (MPPGL) (Vasilogianni et al., 2021). The proteomics abundance values were also applied in PBPK simulations to predict the PK of CYP substrates of different extraction ratios. Our data highlight the implication of the abundance of DMEs in CRLM patients on the PK profiles of drugs.

6.3 Materials and Methods

6.3.1 Materials and chemicals

All chemicals and solvents (HPLC-grade) were purchased from Sigma-Aldrich (Poole, Dorset, UK) unless otherwise stated. EDTA-free protease inhibitor cocktail and Trypsin (sequencing grade) were obtained from Roche Applied Sciences (Mannheim, Germany). Lysyl endopeptidase (Lys-C) was purchased from Wako (Osaka, Japan). All the QconCATs were purchased from PolyQuant GmbH (http://www.polyquant.com/) (Germany).Non-naturally occurring peptides (NNOPs) (light peptides) used for the quantification of QconCATs were purchased from Cambridge Peptides (Cambridge, UK).

6.3.2 Human liver samples

Matched cancerous and histologically normal liver tissues from adult cancer patients (n = 18; HCC primary cancer (n=1), ICC primary cancer (n = 1), CRLM (n =16)) were purchased from the Manchester University NHS Foundation Trust (MFT) Biobank, Manchester, UK, following hepatectomy. The ethics was covered under the MFT Biobank generic ethics approval (NRES 14/NW/1260 and 19/NW/0644). The age of the donors varied from 34 to 85 years, whereas their body mass index varied from 21.6 to 36.3 kg/m^2. The gender of the patients was mixed; 7 female and 11 male. Supplementary Table 6-1 presents demographic and clinical details of the CRLM patients, provided by the MFT Biobank. Healthy human liver microsomal samples (tumour-free) from 15 healthy subjects were provided by Pfizer as microsomes (Groton, CT, USA). These samples were supplied by Vitron (Tucson, AZ, USA) and BD Gentest (San Jose, CA, USA). Ethical approval was obtained by the suppliers. Among the 15 donors, 8 were female and 7 were male, and their ages ranged from 18 to 64 years. The body mass index of the patients ranged from 19.9 to 37.5 kg/m^2. Supplementary Table 6-2 presents demographic and clinical details of the healthy subjects, provided by Pfizer.

6.3.3 Preparation of human liver microsomal fractions

Liver tissue was prepared as microsomes as previously described (Achour *et al.*, 2017). Briefly, liver tissue was homogenized using a Fisherbrand 150 Handheld Homogenizer, (Thermo Fisher Scientific, UK) in homogenization buffer (150 mM KCl, 2 mM EDTA, 50 mM Tris, 1 mM dithiothreitol, and EDTA-free protease inhibitor cocktail, pH 7.4) at 10 ml for each gram of liver tissue. Each homogenate sample was centrifuged at 10,000 *g* for 20 min at 4°C using an

Optima^{TM} L-100 ultracentrifuge (Beckman Coulter, Fullerton, CA), and the supernatant was further centrifuged at 100,000 *g* for 75 min at 4 °C. The cytosol (the supernatant) of each individual sample was stored at -80°C for future use, and the pellet (microsomes) of each individual sample was re-suspended in 1 ml of storage buffer (0.25 M potassium dihydrogen phosphate, 0.25 M dipotassium phosphate, pH 7.25) and stored at -80°C.

6.3.4 Measurement of total protein content in microsomal samples

The protein content of liver microsomes was measured using bicinchoninic acid (BCA) protein assay (Pierce® Microplate BCA Protein Assay Kit – Reducing Agent Compatible) in triplicate. Absorbance was measured at 562 nm using a SpectraMax 190 platereader (Molecular Devices, Sunnyvale, CA) with bovine serum albumin used as calibration standard.

6.3.5 QconCATs (MetCAT and TransCAT) standards

Two QconCAT standards were used in this study, the MetCAT as previously described (Russell et al., 2013), concatenated with peptides for the quantification of 15 CYPs and 10 UGTs. For MetCAT quantification, a [Glu^{1}]-Fibrinopeptide B analog (GVNNEEGFFSAR) omitting the N-terminal glutamate residue was included in the MetCAT. This is a non-naturally occurring peptide (NNOP) and a light (not labelled) peptide with the same sequence (GVNNEEGFFSAR) is used for the quantification of the MetCAT. The TransCAT has previously been described (Russell et al., 2013) and a modified version of it is used for the present study, as previously described (Vasilogianni et al., unpublished). For the accurate quantification of the TransCAT, the sequence of the [Glu^{1}]-Fibrinopeptide B peptide (EGVNDNEEGFFSAR) and another peptide (VGFLPDGVIK) were also involved in the TransCAT. Light versions of these two peptides were used for the quantification of the TransCAT. A bacterial ribosome core has been incorporated in both QconCATs for the efficient expression of the peptides incorporated in QconCATs (Al-Majdoub et al., 2014).

6.3.6 Digestion and preparation of samples

For each microsomal sample, 70 μg of protein were digested. Each sample was firstly mixed with known amounts of isotope-labelled QconCATs; 1.5 μl of undiluted MetCAT (0.27 ug/ul), and 2 μl of 1:10 diluted TransCAT (initial concentration 1.12 μg/μl). The protein mixtures were mixed sodium deoxycholate of a final concentration of 10% (w/v). The mixture was then incubated at room temperature for 10 minutes. Then, dithiothreitol (DTT) of a final

concentration of 0.1 M was added for the reduction of disulphide bonds and the mixture was incubated at 56° C for 30 minutes. For the protein digestion, the filter-aided sample preparation (FASP) was used, as previously described (Al-Majdoub et al., 2019; Couto et al., 2019) with minor modifications. Amicon Ultra 0.5 mL centrifugal filters at 10 kDa molecular weight cut-off (Merck Millipore, Nottingham, U.K.) were conditioned with 200 µl of 0.1 M Tris pH 8.5, centrifuging at 14,000 rpm at room temperature for 10 minutes, this step was repeated twice. The reduced samples were added to the filters and centrifuged at 13,000 rpm for 20 minutes. 8M urea in 0.1 M Tris pH 8.5 was used as solubilizing solution. This solution should extract the aggregated protein efficiently. Centrifugation at 14,000 rpm for 20 minutes at room temperature was followed (twice). The samples were subsequently alkylated with 100 µl 50 mM iodoacetamide (IAA) in the dark for 30 minutes at room temperature, then centrifuged at 14,000 rpm for 10 minutes. The buffer exchanged was repeated with two washes with 8 M Urea in 0.1 M Tris pH 8.5, and centrifugation at 14,000 rpm for 20 minutes at room temperature. The concentration of urea was reduced with two washes of 1 M urea in 50 mM ammonium bicarbonate (AmBic) pH 8.0 and centrifuged at 13,000 rpm for 20 minutes. To avoid the evaporation of the samples, 80 µl of 1 M Urea in 50 mm AmBic pH 8.0 was added to each filter unit. Then, lysyl endopeptidase was added to each sample (enzyme/ protein ratio 1:50) for two hours at 30° C, and the same step was repeated for extra two hours. After 4 hours of incubation with lysyl endopeptidase, trypsin was added (enzyme/ protein ratio 1:25) for 12 hours at 37° C, and the same step was repeated for extra four hours. The samples were recovered after centrifugation at 14,000 rpm for 20 minutes, 100 µl of 0.5 M sodium chloride was added to the filter, centrifuged at 14,000 rpm for 20 minutes, addition of 50 µl of 0.5 M sodium chloride to the filters, then centrifuged at 14,000 rpm for 10 minutes. After this step, each sample was split into two equal samples, and each one of them was mixed with sample buffer (3 parts of sample: 1 part of sample buffer 2% v/v trifluoroacetic acid in 20% v/v acetonitrile in water). Each sample was then desalted using a C18 column (Nest group, USA). Finally, the peptide samples were dried using a vacuum concentrator and stored at −80 °C until mass spectrometric analysis. Before the LC-MS, we added reconstitution buffer (3% acetonitrile-0.1% formic acid) and unlabelled peptides GVNDNEEGFFSAR (0.13 pmol), EGVNDNEEGFFSAR (0.25 pmol), VGFLPDGVIK (0.25 pmol) in a final volume of 60 µl.

6.3.7 Liquid chromatography and tandem mass spectrometry (LC-MS/MS)

Digested samples were analysed by LC-MS/MS using an UltiMate® 3000 Rapid Separation LC (RSLC, Dionex Corporation, Sunnyvale, CA) coupled to a QE HF (Thermo Fisher Scientific, Waltham, MA) mass spectrometer. Mobile phase A was 0.1% formic acid in water and mobile phase B was 0.1% formic acid in acetonitrile and the column used was a 75 mm x 250 µm i.d. 1.7 µM CSH C18, analytical column (Waters, UK). 1 µl aliquot of the sample was transferred to a 5ul loop and loaded on to the column at a flow of 300nl/min for 5 minutes at 5% B. The loop was then taken out of line and the flow was reduced from 300nl/min to 200nl/min in 0.5 minute. Peptides were separated using a gradient that went from 5% to 18% B in 63.5 minutes, then from 18% to 27% B in 8 minutes and finally from 27% B to 60% B in 1 minute. The column is washed at 60% B for 3 minutes before re-equilibration to 5% B in 1 minute. At 85 minutes the flow is increased to 300 nl/min until the end of the run at 90min. Mass spectrometry data was acquired in a data directed manner for 90 minutes in positive mode. Peptides were selected for fragmentation automatically by data dependant analysis on a basis of the top 12 peptides with m/z between 300 to 1750Th and a charge state of 2, 3 or 4 with a dynamic exclusion set at 15 sec. The MS Resolution was set at 120,000 with an AGC target of 3e6 and a maximum fill time set at 20ms. The MS2 Resolution was set to 30,000, with an AGC target of 2e5, a maximum fill time of 45 ms, isolation window of 1.3Th and a collision energy of 28.

6.3.8 Analysis and annotation of proteomic data

Proteomic data were processed using MaxQuant 1.6.7.0 (Max Planck Institute, Martinsried, Germany), and searched against a customized database, comprising human UniprotKB database (74,788 sequences) and QconCAT sequences. For targeted AMRT analysis, light-to-heavy intensity ratios were used with QconCAT concentrations to calculate protein amounts based on accurate mass measurement and retention time for each peptide (Al-Majdoub *et al.*, 2019, 2020). Peptides selected for quantification of CYPs, UGTs, and transporters are presented in Supplementary Tables 6-3 - 6-8.

6.3.9 Statistical data analysis

Statistical data analysis was performed using GraphPad Prism 8.1.2 (La Jolla, California USA), Microsoft Excel 2016 and R v3.6.3. Nonparametric statistics were used since data did not follow normal distribution. Differences in absolute abundances between healthy and

histologically normal, healthy and tumorous, and histologically normal and tumorous livers were assessed using Mann−Whitney U-test. The p-value cut-off for statistical significance was set at 0.05. Principal components analysis (PCA) was performed using proteome similarity data based on percentage identical peptide (PIP) and percentage identical protein (PIPr).

6.3.10 Physiologically based pharmacokinetic (PBPK) simulations

The effect of using the experimentally determined abundance of CYPs and UGTs in this study in combination with scaling factors previously determined (Vasilogianni et al., 2021) in a cancer population was assessed using PBPK modelling on Simcyp V20 Release 1 (Certara, Sheffield, UK) in healthy and cancer populations. Three CYP substrates with different hepatic extraction ratios (E_H) were used: alprazolam (predominantly metabolized by CYP3A4, and CYP3A5, low E_H), crizotinib (predominantly metabolized by CYP3A4, intermediate E_H), and ibrutinib (predominantly metabolized by CYP3A4, high E_H). The compound files were same as those provided within the Simcyp simulator, and PBPK simulations were performed using system parameters already available on the simulator for healthy ("Sim-Healthy Volunteers") and cancer ("Sim-Cancer") virtual populations, without or with changing MPPGL values (measured in Vasilogianni et al., 2021) and abundance of CYPs and UGTs measured in this study. For the abundance data, relative changes of CYPs, and UGTs between healthy and histologically normal or cancerous samples were incorporated. Similarly, relative changes of coefficient of variation (CV) percentages between healthy and histologically normal or cancerous samples were used. The effects of abundance changes on drug exposure following oral administration were assessed using previously described models (Vasilogianni et al., 2021):

Model 1 (Healthy): default MPPGL and abundance for healthy population (Simcyp).

Model 2 (Cancer-D): default MPPGL and abundance for cancer population (Simcyp).

MPPGL model 3 (New Cancer-ALN): MPPGL in histologically normal tissue (Vasilogianni et al., 2021) and abundance of CYPs (relative difference between NP and HP) were used for the cancer population, assuming the whole liver histologically normal.

MPPGL model 4 (New Cancer-ALC): MPPGL in cancerous tissue (Vasilogianni et al., 2021) and abundance of CYPs (relative difference between TP and HP) were used for the cancer population, assuming the whole liver cancerous, and the liver mass unchangeable.

For each model and drug, the trial design had the following parameters: 10 trials with 10 virtual individuals each, females to males: 0.5, age range: 20-50 years, duration of study: 24 h. The mean (for all 100 virtual subjects) systemic concentration (C_{sys})-time profiles were plotted and the area under the curve (AUC) from time 0 to 24 hours and Clearance (Dose/AUC) values were compared. Supplementary Table 6-9 provides the parameters in PBPK simulations.

6.4 Results

6.4.1 Comparison of hepatic CYP and UGT absolute abundance in healthy controls, and histologically normal and tumour HLM from cancer patients

The absolute abundance values for CYPs and UGTs were measured with LC-MS/MS proteomics, using a QconCAT standard (MetCAT). These values were expressed as pmol of protein per mg of microsomal protein and compared among three groups (healthy and cancer paired with normal liver tissues) of human liver microsomes (HLM). We found that the expression of CYP2B6, CYP2D6, CYP2E1, CYP3A4 and CYP3A5 (Figure 6-1A) in histologically normal samples were significantly lower than in healthy tissues (Mann−Whitney test, $p < 0.05$), while the rest of CYPs were similarly expressed between these two groups.

We also found that the protein expression of CYP1A2, CYP2A6, CYP2C18, CYP2C19, CYP2C8, CYP2C9, CYP2D6, CYP2E1, CYP2J2, CYP3A4, CYP3A5, CYP4F2) in tumour tissues were statistically lower than in healthy ($p<0.05$) and lower (with the exception of CYP2C18) than in histologically normal tissues ($p<0.05$). Similar expression of CYP3A7 was observed among the samples.

Subsequently, we analysed UGT enzymes in the three different groups. The expression of UGT1A1, UGT1A6, UGT1A9, UGT2B15, UGT2B4 and UGT2B7 were significantly decreased (Figure 6-1B) in histologically normal tissues compared with healthy controls ($p < 0.05$), with the rest of UGTs being expressed at similar levels in the two groups. Another finding was that UGT1A1, UGT1A3, UGT1A6, UGT1A9, UGT2B15, UGT2B4 and UGT2B7 were significantly decreased in tumour compared with healthy livers (Mann-Whitney, $p < 0.05$). Additionally, UGT1A1, UGT1A3, UGT1A6, UGT1A9, UGT2B11, UGT2B15, UGT2B4, and UGT2B7 were significantly decreased in tumour compared with histologically normal livers from cancer patients ($p < 0.05$).

The absolute values of the abundance of CYPs and UGTs for individual samples are provided in Supplementary Tables 6-3, 6-4, and 6-5 respectively.

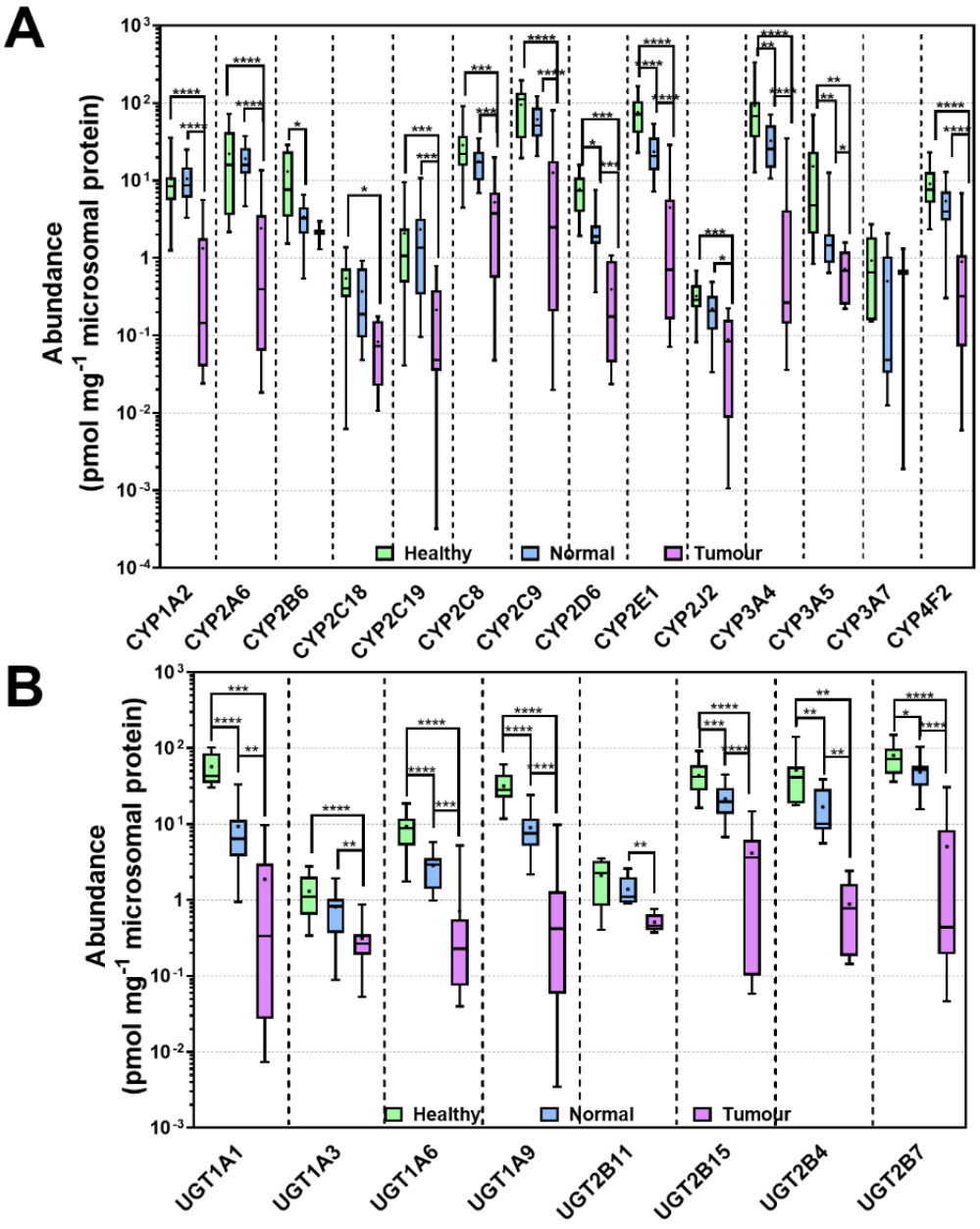

Figure 6-1 Absolute abundance of cytochrome P450 enzymes (CYPs) (**A**) and UDP-glucuronosyltransferases (UGTs) (**B**) in healthy, histologically normal and tumorous HLM. Abundances are represented as box and whiskers plots with the whiskers showing the minimum and maximum values, the boxes showing the 25th and 75th percentiles, the lines showing the medians, and the + signs showing the means. Mann−Whitney test was used to assess statistically significant differences between healthy and histologically normal, between healthy and tumorous livers and between histologically normal and tumorous livers for each protein. The asterisk (*) represents statistical difference (*$p < 0.05$; ** $p < 0.01$; ***$p < 0.001$; **** $p < 0.0001$).

6.4.2 Differences in protein expression levels of ABC and SLC transporters between tumour, normal and healthy microsomal fractions

The absolute abundance for ABC and SLC transporters was measured with the aid of TransCAT. Figure 6-2A shows that ABC transporters generally tend to decrease in livers from cancer patients. Among these, P-gp, BSEP, MRP2, MRP3 and MRP6 expressions were downregulated at a very high level of significance ($p < 0.05$) in tumour and histologically normal versus healthy controls. Significant decrease in the abundance of BSEP, and MRP2 was also observed in tumour compared with matched histologically normal livers ($p < 0.05$). BCRP and MRP4 were expressed at similar levels in healthy, histologically normal and cancer livers. Similarly, the abundance of most SLC transporters was decreased in livers from cancer patients. More specifically, Organic cation transporter (OCT) 1, Organic anion transporter (OAT) 2, OAT7, Organic anion transporter polypeptide-related protein (OATP) 1B1, and OATP2B1 were significantly decreased in histologically normal and tumour livers compared with healthy controls ($p < 0.05$), and in tumour relative to histologically normal livers from cancer patients ($p < 0.05$). The expression levels of OCT3 and OATP1B3 were significantly downregulated in normal and tumour compared with healthy livers ($p < 0.05$). The expression of Monocarboxylate transporter 1 MCT1 was significantly lower in normal compared with healthy, and higher in tumour than in normal ($p < 0.05$), while Na(+)/taurocholate transport protein NTCP was significantly decreased in normal compared with healthy and in tumour compared with normal livers ($p < 0.05$). However, no differences were observed in the abundance of OST-α, OST-β, ASBT, PEPT1, and OATP1A2 in the compared microsomal samples.

The absolute values of the abundance of ABC and SLC transporters for individual livers are provided in Supplementary Tables 6-6, 6-7, and 6-8 respectively.

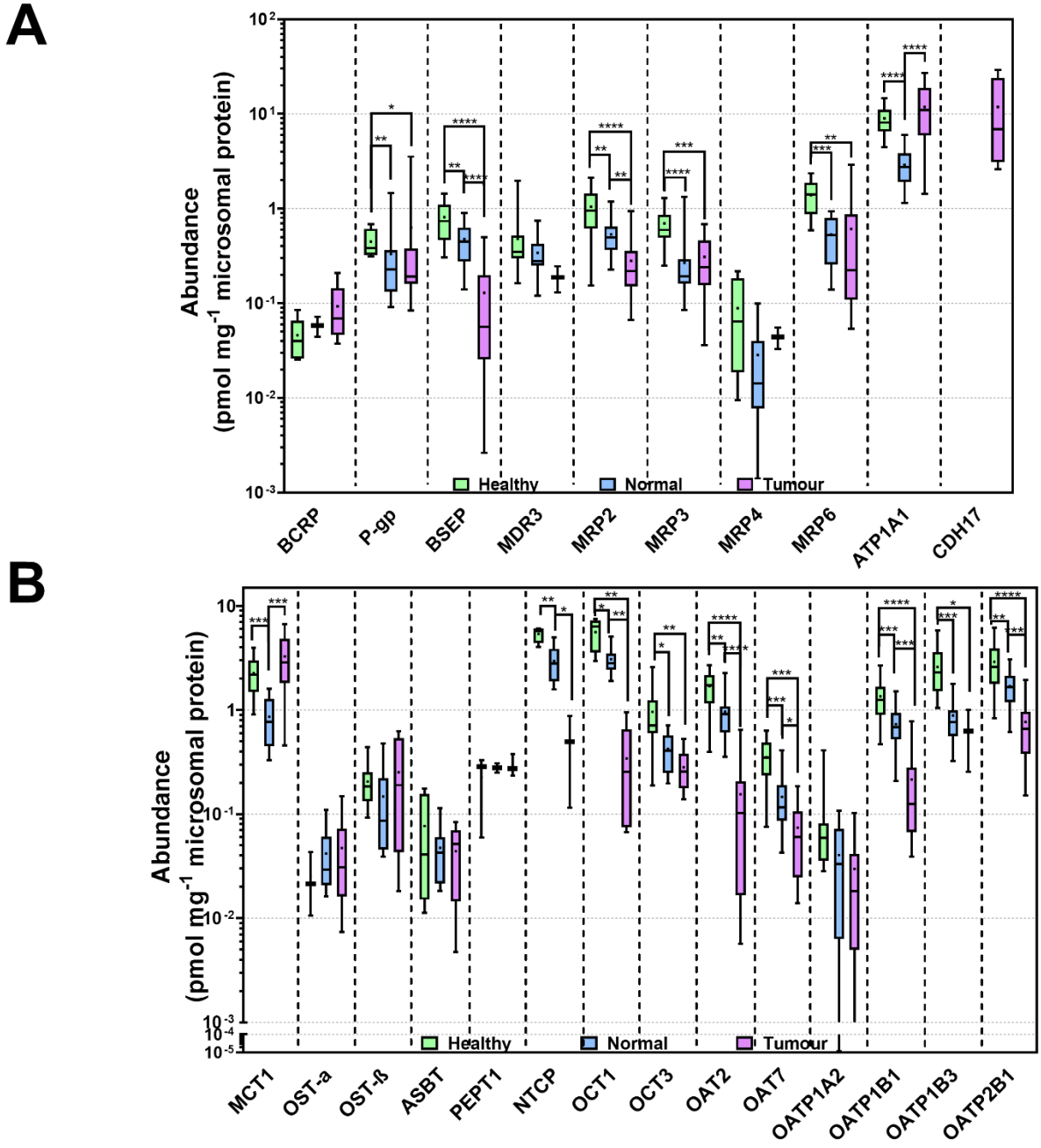

Figure 6-2 Absolute abundance of ATP-binding cassette transporters (ABCs), ATP1A1 and Cadherin-17 (CDH17) (**A**) and solute carrier transporters (SLCs) (**B**) in healthy, histologically normal and tumorous HLM. Absolute abundance is expressed in pmol of protein per mg of liver microsomal protein. Abundances are represented as box and whiskers showing the minimum and maximum values, the boxes showing the 25th and 75th percentiles, the lines showing the medians, and the + signs showing the means. Mann−Whitney test was used to assess statistically significant differences between healthy and histologically normal, between healthy and tumorous livers and between histologically normal and tumorous livers for each protein. The asterisk (*) represents statistical difference (*p < 0.05; ** p < 0.01; ***p < 0.001; **** p < 0.0001).

6.4.3 Relative expression of CYPs and UGTs in the three sets of HLM

The pie charts represent the relative abundance distribution of CYPs (Figure 6-3A, B, C) and UGTs (Figure 6-3D, E, F) in the healthy, histologically normal and tumour HLM. Among the quantified CYPs, CYP2C9 was the most abundant of all P450 isoforms in all groups (29% of quantified CYPs in healthy, 34% in histologically normal, and 35% in tumour). CYP3A4 was the second most abundant, followed by CYP2E1 and CYP2C8, in healthy and histologically normal. However, CYP2C8 was the second most abundant CYPs (15%) in tumour, followed by CYPE1 (13%), and then CYP3A4 (12%). The least abundant CYPs were CYP2J2 and CYP2C18 in all groups. Among UGTs, UGT2B7 was found to be the most abundant in all groups (29% in healthy, 44% in histologically normal, and 34% in tumour). The second most abundant UGT was UGT1A1 (21%) in healthy, and UGT2B15 in histologically normal (19%) and tumour (28%). UGT2B4 was the third most abundant UGT in healthy (19%) and histologically normal (15%), and UGT1A1 in tumour (13%). The least abundant UGT was UGT1A3 in all groups.

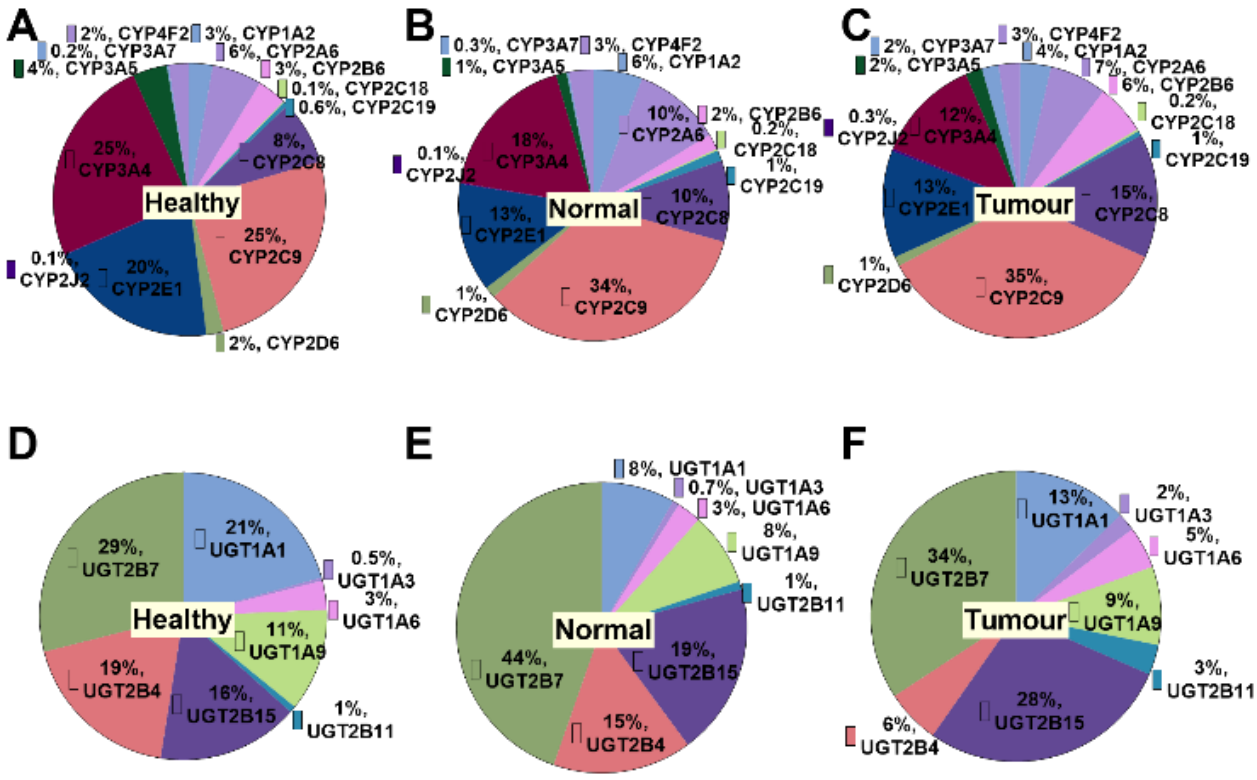

Figure 6-3 Pie charts representing the relative abundance distribution of CYPs (**A, B, C**), and UGTs (**D, E, F**) in healthy, histologically normal and tumorous HLM.

6.4.4 Relative abundance distribution of ABC and SLC transporters in healthy controls, and histologically normal and tumour HLM from cancer patients

The pie charts represent the relative abundance distribution of ABC (Figure 6-4A, B, C) and SLC (Figure 6-4D, E, F) transporters in healthy controls, and histologically normal and tumour HLM from cancer patients. The most abundant ABC transporters quantified with the TransCAT in healthy controls and histologically normal livers were MRP6 (28% in healthy, 21% in normal), followed by MRP2 (21% in healthy and normal), and BSEP (16% in healthy, 19% in normal). However, the most abundant ABC transporter in tumour livers was P-gp (28%), followed by MRP6 (27%), and MRP3 (14%). BCRP and MRP4 were the least abundant ABC transporters quantified in all groups.

The most abundant SLC transporters quantified were the same in healthy and histologically normal livers; OCT1 (24% in healthy, 25% in normal), NTCP (23% in healthy, 24% in normal), and OATP2B1 (12% in healthy, 14% in normal). The distribution differs in tumour, with MCT1 being 47% of SLC transporters, OATP2B1 14%, and OATP1B2 9%. ASBT, OST-α, OATP1A2 were the least abundant SLC transporters in all groups.

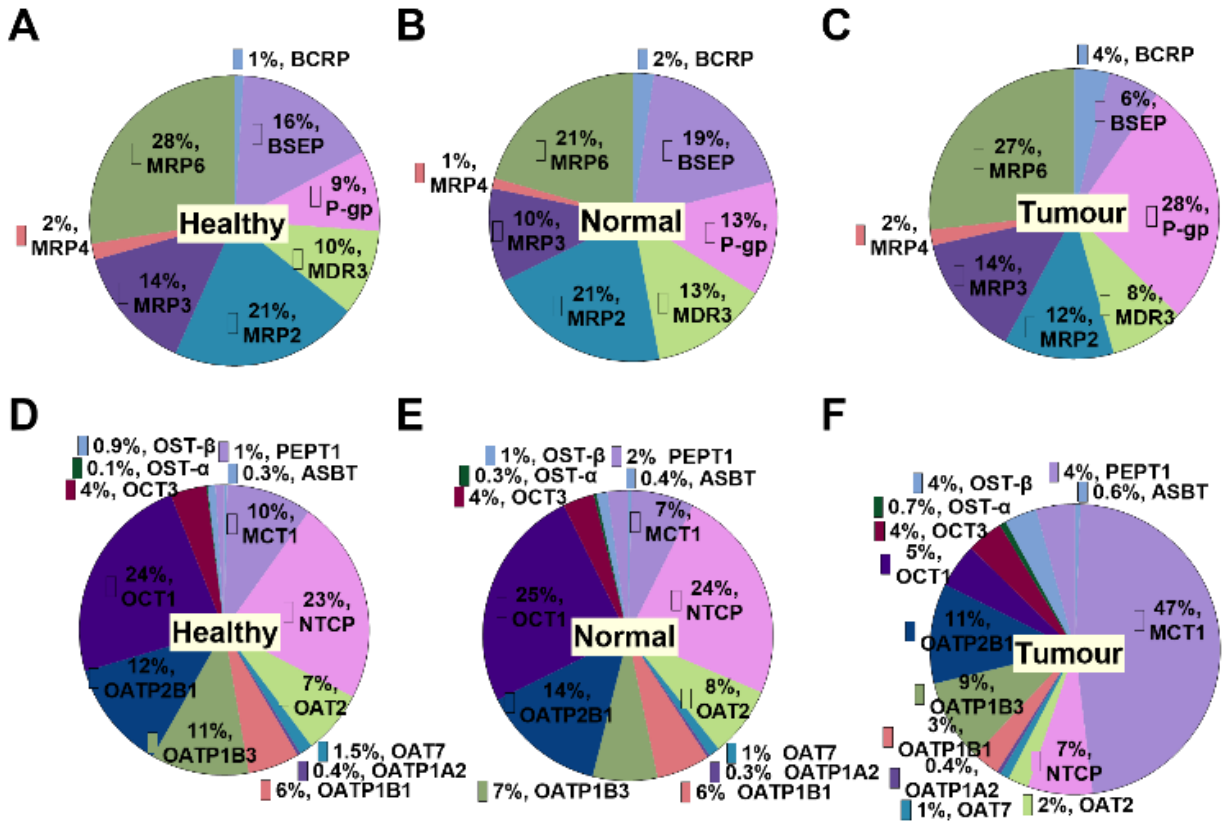

Figure 6-4 Relative abundance distribution of ABCs (**A, B, C**), and SLCs (**D, E, F**) in healthy, histologically normal and tumorous HLM.

6.4.5 Relative abundance of CYPs and UGTs among healthy controls, and histologically normal and tumour HLM from cancer patients

Figures 6-5A depicts the relative abundance of CYPs expressed as ratio of healthy to histologically normal (fold changes). The dotted line is set to 1 meaning no difference between healthy and normal. For each target, the average abundance in all the healthy livers was divided by the average abundance in all normal livers. CYP2B6, CYP2D6, CYP2E1, CYP3A4, CYP3A5 were more than 2 fold (range 2.9 - 6.6 fold) higher in healthy controls compare to histologically normal livers, showing a decrease of CYPs in histologically normal livers from cancer patients compared with healthy controls. Figure 6-5B shows that the ratio of the abundance of CYPs in healthy to tumour livers was more than 2 fold, with the exception of CYP3A7 (1.4 fold). CYPs were decreased in tumour compared with healthy controls, with a decrease ranging from 3.6 fold (CYP2J2) to 21.3 fold (CYP3A4). Figure 6-5C provides the ratio of the abundance of CYPs in histologically normal to matched tumour livers, which was higher than 2 fold with the exception of CYP2B6 and CYP3A7. This ratio ranges from 2.5 (CYP2J2) to 10.9 fold (CYP2C19), showing a decrease of CYPs in the tumorous parts of liver compared with the adjacent histologically normal parts.

Figure 6-5D shows a ratio of UGTs in healthy to normal higher than 1. More specifically, UGT1A3, UGT2B11 and UGT2B7 were slightly decreased in normal compared with healthy (< 2 fold), and the rest UGTs were decreased by 2 fold (UGT2B15) up to 6.1 fold (UGT1A1). Ratios of healthy to tumour (Figure 6-5E) range from 4.1 (UGT1A3) to 58.1 (UGT2B4) fold showing a significant decrease of UGTs in normal livers from cancer patients compared with controls. Ratios of histologically normal to tumour (Figure 6-5F) range from 2.6 (UGT1A3) to 19 (UGT2B4) fold showing decrease of UGTs in tumour.

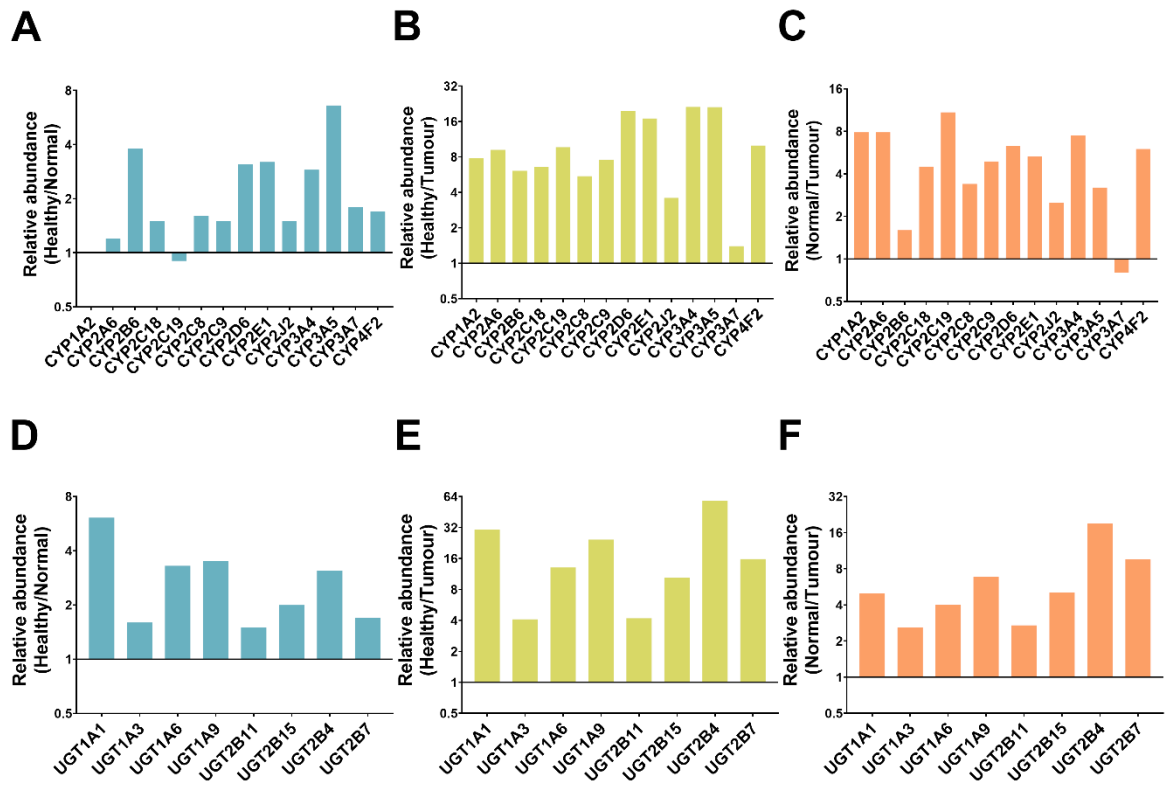

Figure 6-5 Relative abundances of CYPs, and UGTs in HLM. Panels **A, B, C** represent the abundance ratios of CYPs in healthy to histologically normal (**A**), healthy to tumour (**B**), and histologically normal to tumour livers (**C**). Panels **D, E, F** represent the abundance ratios of UGTs in healthy to histologically normal (**D**), healthy to tumour (**E**), and histologically normal to tumour livers (**F**). The dotted line is set to 1 (no change).

6.4.6 Relative abundance of ABC and SLC transporters on healthy controls, histologically normal and tumour tissues

Figure 6-6A depicts the ratios of the abundance of ABC transporters in healthy to histologically normal livers, which were higher than 2 fold (up to 3.1) for MRP2, MRP3, MRP4, and MRP6 showing a decrease of them in normal. Figure 6-6B represents the ratios of ABCs in healthy to tumour, and we observe ratios of BSEP, MRPs and MDR3 ranging from 2-6.3 fold showing that these transporters were decreased in tumour compared with healthy controls. Conversely, ratio of BCRP in healthy to tumour was 0.5, showing 2 fold increase in tumour. Figure 6-6C shows that the ratio of P-gp in histologically normal to tumour was 0.5 meaning 2 fold increase in tumour, and the ratio of BSEP in histologically normal to tumour was 3.7 fold (decrease in tumour).

Ratios of SLC transporters in healthy to normal (Figure 6-6D) exceed 2 (up to 2.9) for MCT1, OAT7, OATP1A2, OATP1B3, and OCT3, showing a decrease of them in normal compared

with healthy. Ratios of NTCP, OATs, OATPs and OCTs in healthy to tumour were higher than 2 (ranging from 3.2 to 16.4) showing a decrease of them in tumour compared with healthy, and the ratio for OST-α was 0.5 (2 fold increase in tumour). Lastly, ratios of NTCP, OATs, OCT1, OATP1B1 and OATP2B1 in normal to tumour were higher than 2 (up to 9) showing a decrease of them in tumour compared with normal, and the ratio for MCT1 was 0.3 (3.3 fold increase in tumour).

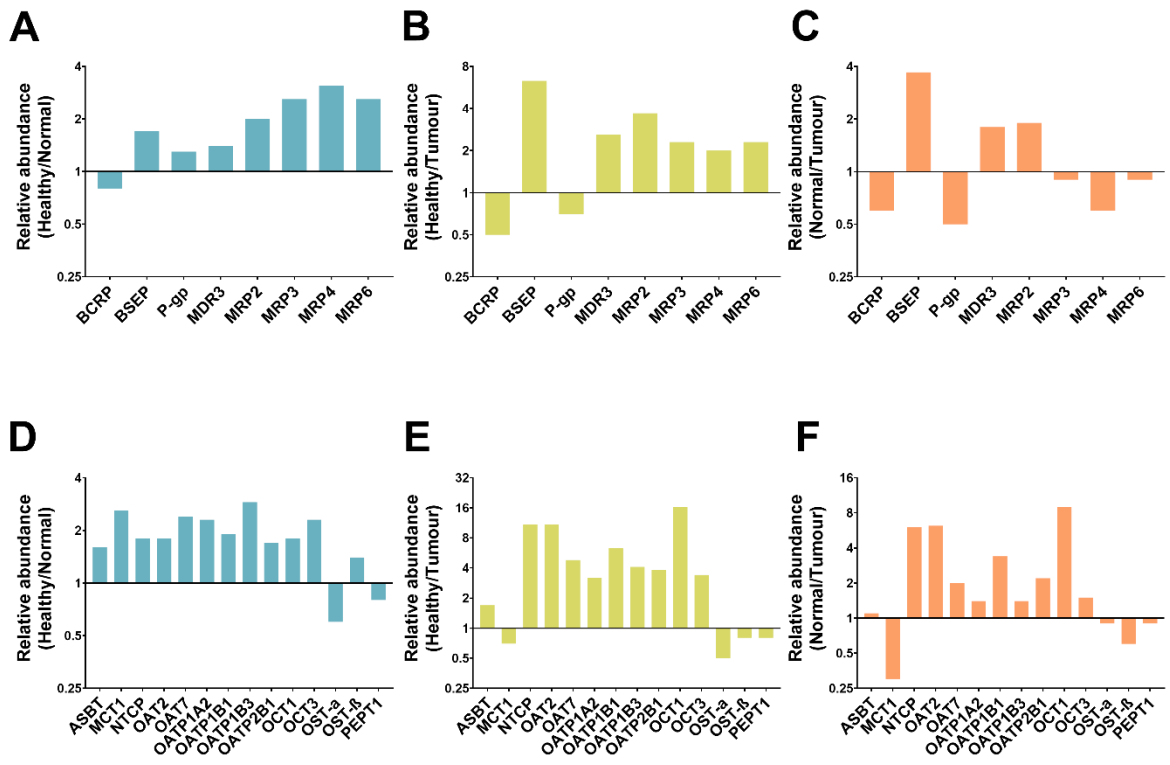

Figure 6-6 Relative abundances of ABC and SLC transporters in HLM. Panels **A, B, C** represent the abundance ratios of ABCs in healthy to histologically normal (**A**), healthy to tumour (**B**), and histologically normal to tumour livers. Panels **D, E, F** represent the abundance ratios of SLCs in healthy to histologically normal (**D**), healthy to tumour (**F**), and histologically normal to tumour livers. The dotted line is set to 1 (no change).

6.4.7 Relative abundance of CYPs, UGTs and transporters in paired tumour and normal tissues

Figure 6-7 represents the ratio of abundance in histologically normal to matched tumour livers for each individual for CYPs (A), UGTs (B), ABC (C), and SLC (D) transporters. The absence of a dot means the absence of the ratio due to the absence of the target in this specific sample. The graphs show that there was no consistency in individual ratios normal to tumour (same donors) across the liver samples for the quantified targets. The changes of the abundance of each target in tumour compared with histologically normal were not consistent across samples, showing no trend.

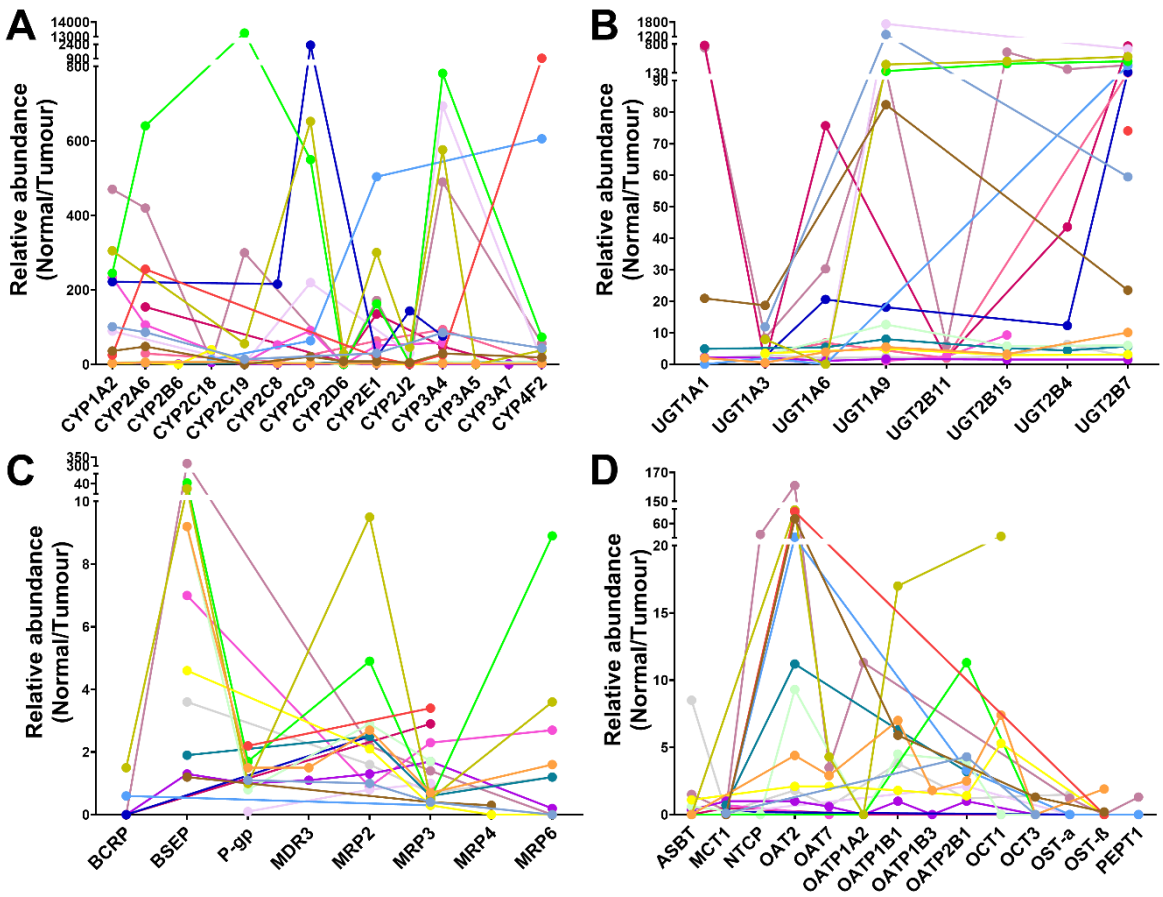

Figure 6-7 Relative abundance of CYPs (**A**), UGTs (**B**), ABCs (**C**), and SLCs (**D**). Relative abundances are expressed as ratios of abundance in histologically normal to matched tumour HLM for each 18 individual (n = 18).

6.4.8 Normalization of the abundance of CYPs, UGTs and transporters (pmol/mg) to gram of liver

According to the contents of MPPGL determined in our previous work (Vasilogianni et al., 2021), individual abundance data per pmol/mg microsomal protein in normal and tumour livers of CRLM were scaled to gram tissue levels by multiplying the MPPGL with the individual abundance values, representing the enzyme and transporter abundance of liver (Figure 6-8). However, when calculating the enzyme abundance based on liver tissue (per gram of tissue), there was no clear trend between the abundance in microsomal protein level and liver tissue level in individual liver samples. For this analysis, we only included 11 cancerous livers, because for the rest of the samples the MPPGL values were not available.

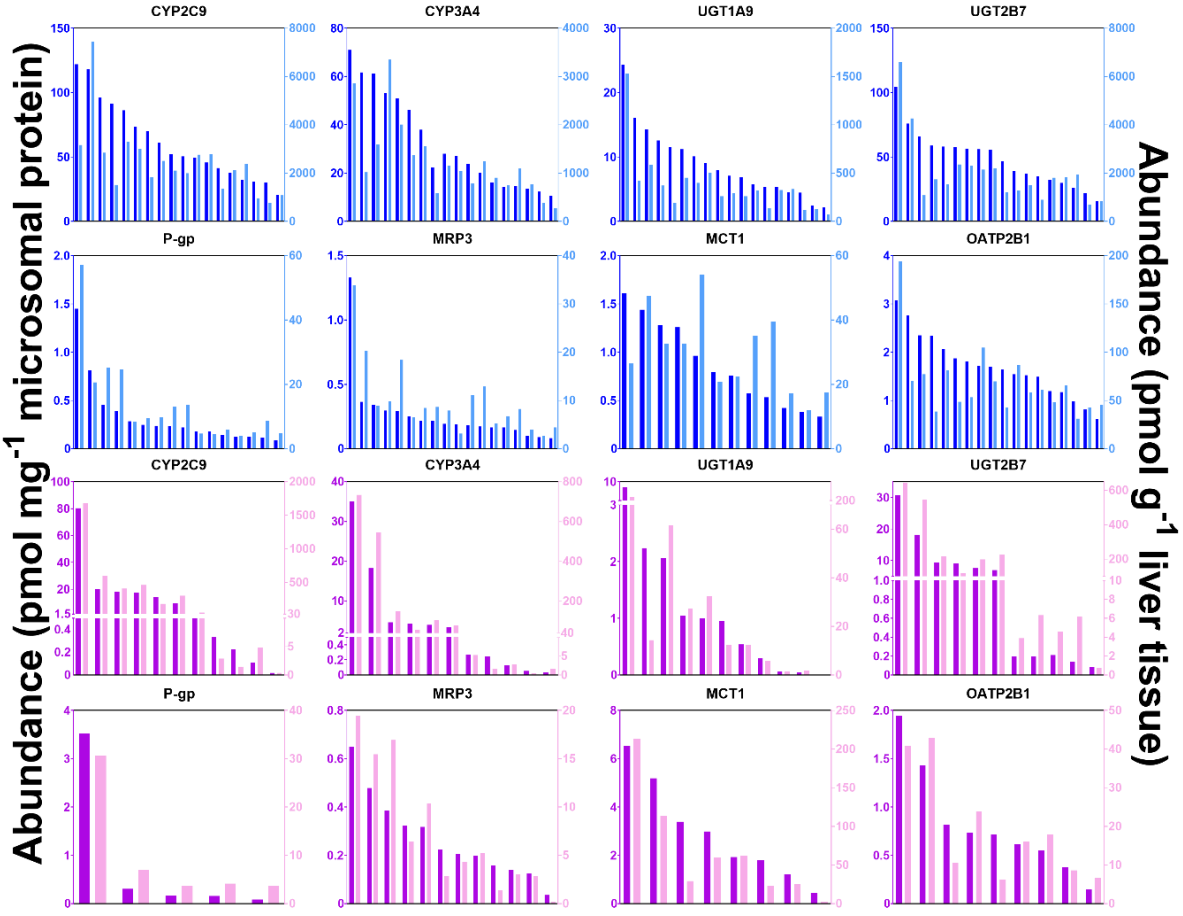

Figure 6-8 Abundance of CYP2C9, CYP3A4, UGT1A9, UGT2B7, P-gp, MRP3, MCT1, and OATP2B1 in histologically normal (graphs on the top, blue bars) and tumour (graphs at the bottom, pink bars). Abundance is expressed as pmol of protein per mg of microsomal protein in the left y axis (dark blue bars for histologically normal and dark pink for tumour), and as pmol of protein per g of liver in the right y axis (light blue bars for histologically normal and light pink for tumour).

6.4.9 Principal component analysis (PCA)

Percentage identical peptides (PIP) and percentage identical proteins (PIPr) were calculated between samples as previously described (Al Feteisi et al., 2018; Al-Majdoub et al., 2019), and the results were analysed by principal components analysis (PCA) (Figure 6-9). The healthy and the normal liver samples form two distinct clusters, indicating a high homogeneity of each one of these groups. However, little clustering was observed for the cancer liver samples reflecting the nature of cancer as a disease (a phenotypic range rather than one phenotype). PC1 explains the difference between healthy and cancer livers at 62% and 67% of the variance for PIP and PIPr. PC2 explains the difference between healthy and histologically normal livers at 12% and 15% of the variance for PIP and PIPr. It shows that normal and healthy livers were very similar but different from cancer livers. Cancer livers were also different from one another. The total explained variance by disease and histology was 74% and 82% for PIP and PIPr, which means we can explain most of the variability in phenotype based on only these two factors.

Interestingly, sample T32 clusters with the normal livers in PIP and was between the clusters of normal and tumour livers in PIPr. T32 was actually enclosed in the 95% confidence interval for normal livers, which means it was most likely normal than cancer. Although sample T32 was characterised as tumour by the biobank, its colour and texture resembles to be between normal and tumour. Samples T46 and T48 were distant from the rest tumour samples, which is expected as these were the only primary cancer samples. Samples H57, H61, H62, and H63 were pooled healthy samples (analytical replicates). Samples N58 and T59 constitute pooled histologically normal and pooled tumour samples, respectively.

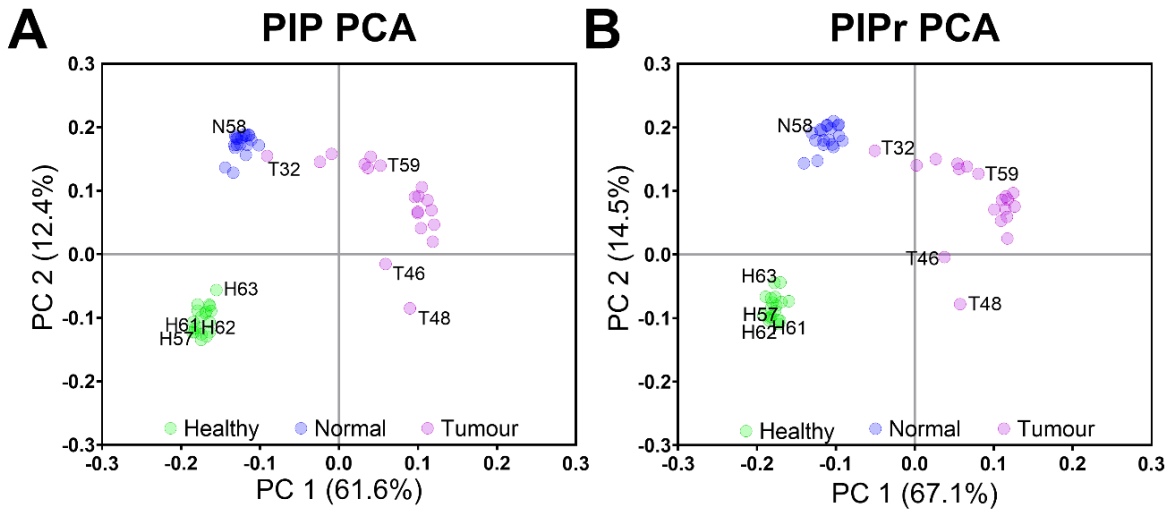

Figure 6-9 Principal components analysis (PCA) of peptide (**A**) and protein (**B**) similarity data, using percentage identical peptide (PIP) and percentage identical protein (PIPr) values, respectively.

6.4.10 Physiologically-based pharmacokinetic (PBPK) simulations

Simulations for three CYP substrates with different hepatic extraction ratios (E_H); alprazolam (low E_H = 0.04 in Healthy, CYP3A4, and CYP3A5 substrate), crizotinib (intermediate E_H = 0.44 in Healthy, CYP3A4 substrate), and ibrutinib (high E_H = 0.91 in Healthy, CYP3A4 substrate), were performed. We used four different models (Figure 6-10); Model 1 (Healthy) used default MPPGL and abundance of CYPs and UGTs (Simcyp) with a healthy population, Model 2 (Cancer-D) used default MPPGL and abundance of CYPs and UGTs (Simcyp) with a cancer population, Model 3 (New Cancer-ALN) used MPPGL (Vasilogianni et al., 2021) and abundance of CYPs and UGTs measured in this study for histologically normal tissue with a cancer population, and Model 4 (New Cancer-ALC) used MPPGL (Vasilogianni et al., 2021) and abundance of CYPs and UGTs measured in this study in cancer tissue with a cancer population.

New Cancer-ALN assumes that the whole liver is histologically normal, with maximum metabolic capacity of microsomal enzymes, whereas New Cancer-ALC assumes that the whole liver is cancerous with minimum metabolic capacity of microsomal enzymes. For alprazolam, crizotinib, and ibrutinib AUC predicted using model New Cancer-ALC was 1.8, 2.1, and 9.5-fold higher of that obtained using model Healthy, showing an increase in the exposure of CYP substrates in case of advanced cancer, where most liver is cancerous.

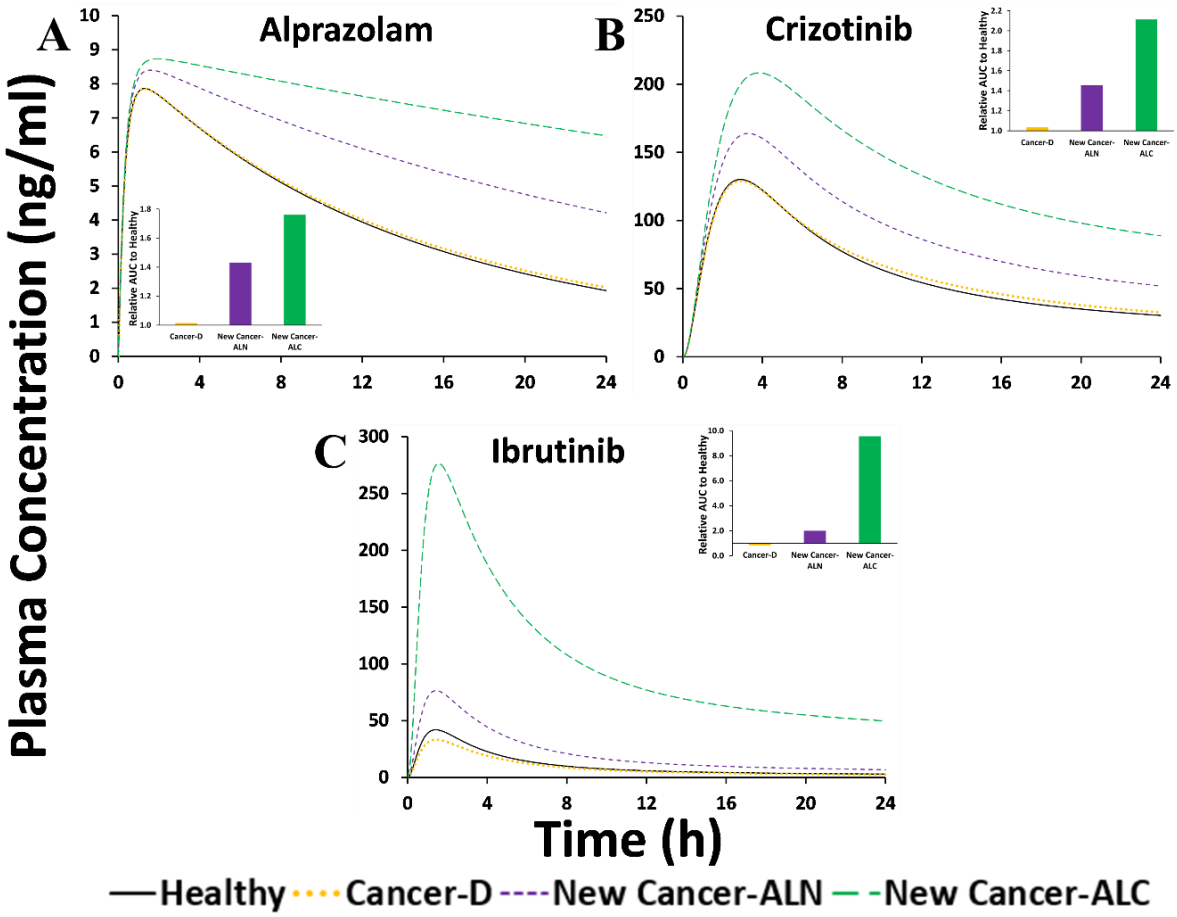

Figure 6-10 Mean predicted systemic concentration over time after oral administration of alprazolam (**A**), crizotinib (**B**), and ibrutinib (**C**). For each drug, four different methods of scaling were used. Healthy: default MPPGL (Simcyp) with a healthy population. Cancer-D: default MPPGL with a cancer population. New Cancer-ALN: MPPGL measured in this study for histologically normal tissue with a cancer population. New Cancer-ALC: MPPGL measured in this study for cancer tissue with a cancer population. Inset graphs show the Relative AUC ratios of Cancer-D, New Cancer-ALN, and New Cancer-ALC to Healthy.

6.5 Discussion

Quantitative proteomics is useful for PBPK models in cancer and other diseases (Sharma et al., 2020). However, protein abundance is not always available. To our knowledge, this is the first comprehensive study of DMEs and transporters levels in healthy and tumour human liver. Our previous pilot study (Vasilogianni et al., unpublished) provided quantitative measurements in pooled liver samples. Here, we quantified DMEs and transporters in individual healthy controls, histologically normal and matched cancerous liver tissues from cancer patients (mainly CRLM), using LC-MS/MS. For these targets, no human liver expression data have previously been reported in CRLM, and the abundances of these proteins are reported for the first time. The current analysis confirmed our previous findings and quantified proteins in

individual liver samples, providing a more comprehensive picture of protein expression and inter-individual variability in healthy, cancer and matched normal liver tissues.

CYPs and UGTs are involved in the clearance of more than 90% of drugs (Rowland et al., 2013), with CYPs being responsible for the metabolism of 80% of clinically used drugs (Zanger and Schwab, 2013). In CRLM treatment, Irinotecan is metabolized by CYP3A4/5, and UGT1A1/9 (Ma and McLeod, 2003; de Man et al., 2018), and Regorafenib by CYP3A4, and UGT1A9 (Rey et al., 2015). It has been documented in HCC, that most CYPs and UGTs are significantly decreased in cancerous compared with peri-carcinomateous tissues (Yan, Gao, et al., 2015; Yan, Lu, et al., 2015). Our pilot study (Vasilogianni et al., unpublished) showed decrease of DMEs in a cancerous pooled liver sample from CRLM patients compared with healthy and histologically normal, in agreement with the current study in individual samples. The absolute quantification measurements clearly highlight that CYPs and UGTs are either decreased or similarly expressed in histologically normal and significantly decreased in cancerous compared with histologically normal and healthy livers. The multiple CYP enzymes quantified include most of the major CYPs involved in drug metabolism. Interestingly, DMEs levels increased by up to 58.1-fold in cancerous compared with healthy livers implying that drug metabolism may be severely affected in patients with a cancerous liver leading to higher exposure of CYP and UGT substrates and therefore, high toxicity.

Drug transport proteins have an important role in drug disposition and drug-drug interactions (DDIs) (Liang et al., 2020), and may be involved in resistance to chemotherapeutic drugs (Akhdar et al., 2012). Transporters involved in drug disposition in CRLM include OATP1B1, Pgp, BCRP, MRP1, and MRP2 for Irinotecan (Ma and McLeod, 2003; de Man et al., 2018) and MRP2 and OATP1B1 (Ohya et al., 2015) for Regorafenib. Our data revealed altered abundance of a wide range of transporters in cancer, with a decreasing trend of SLCs in histologically normal versus healthy, and a more significant decrease in cancerous livers. These findings are in agreement with our measurements in pooled samples (Vasilogianni et al., unpublished).

The majority of the studied ABCs (BSEP, MRP2, MRP3, MRP6, P-gp) were downregulated in cancer patients, or unchanged (such as BCRP, MDR3 and MRP4) in this study. Our data comply with our previous pilot report with regard to the downregulation of MRP2 and MRP3 as well as the unchangeable expression of BCRP in tumours (Vasilogianni et al., unpublished). In contrast to the data of the current study, the pilot study showed an increase of MRP4 in

cancer. Transporters are low abundance proteins and thus, more sensitive to technical differentiations. Our data are in agreement with a study in HCC, where OATPs, OCT1, and ABC transporters decreased in cancerous tissues (Billington et al., 2018). There are no absolute quantitative data of the protein levels of transporters in the literature for CRLM to compare with. Transporters were decreased by up to 16.4-fold, in cancerous relative to healthy livers. These data could be useful for predictions of hepatic drug disposition in cancer patients.

The relative distribution of DMEs and transporters was also assessed. The most abundant CYPs in all liver samples were CYP2C9, CYP3A4, CYP2E1, and CYP2C8, with varying percentage of expression across different groups. Moreover, UGT2B7 was the most abundant in all groups. Our results were consistent with the literature (Ohtsuki et al., 2011; Achour et al., 2014; Zhang et al., 2016; Couto et al., 2019). The most abundant ABC transporters were MRP6, MRP2, and BSEP in healthy and normal livers, in agreement with other studies (Vildhede et al., 2015; Couto et al., 2019), but P-gp and MRP6 in cancerous livers. OCT1 and NTCP were the most abundant SLCs in healthy and normal, while MCT1 in cancerous livers. The increase of MCT1 in cancer is supported by the literature suggesting that MCT1 is involved in tumour progression and could be a useful therapeutic target in oncology (Payen et al., 2020).

The range of protein abundance levels for DMEs was wider in cancerous samples, indicating high heterogeneity in cancer. The maximum inter-individual variation across CYPs, UGTs, ABCs and SLCs in healthy samples was 231 (CYP2C19), 11 (UGT1A6), 23 (MRP4), and 16-fold (ASBT), which is smaller compared with a previous study that used label-free quantification method (Couto et al., 2019). On the contrary, the maximum inter-individual variation across CYPs, UGTs, ABCs and SLCs in cancer samples was 4063 (CYP2C9), 2784 (UGT1A9), 190 (BSEP), and 179-fold (OATP1A2), respectively. The PCA indicates that healthy, normal and cancerous samples constitute 3 distinct groups, but the cancerous group is not homogeneous. Figure 6-7 indicates that the ratio of abundance for each protein target in histologically normal to matched tumour livers for each individual is not consistent across the samples. Considering that normal livers belong to a homogeneous group (PCA), the lack of a specific trend for the expression of each protein target for each individual could be attributed to the heterogeneity in cancerous livers. This heterogeneity could be explained by the fact that individuals differ in the cancer cell differentiation, severity, type of cancer, previous treatment and other characteristics.

The absolute abundance values were expressed in units of pmol of protein per mg of microsomal protein. It has been suggested that varying abundance of highly abundant proteins (not DMEs/transporters) can impact on the abundance of DMEs and transporters, and correction factors (e.g. MPPGL) could normalize the abundance and express it as pmol of protein per g of liver tissue (Achour et al., 2017). In our study, we multiplied pmol of protein per mg of microsomal protein by MPPGL measured in our previous study (Vasilogianni et al., 2021) to define abundance in pmol of protein per g of liver tissue, and we did not observe any trends between them for each protein target across the samples. This is in line with another study (Billington et al., 2018) demonstrating that normalization from mg of membrane protein to g of liver altered the pattern of expression of drug transporters in some cases. Scaling to tissue level may be more appropriate for PK predictions in PBPK models, and thus in our simulations we used MPPGL in addition to protein abundance to normalize to tissue level.

Based on the abundance data from the current study, and in addition to MPPGL values specific for cancer (Vasilogianni et al., 2021), we assessed the contribution of the abundance of CYPs to drug exposure by PBPK simulations of three CYP substrates available in Simcyp simulator (alprazolam, and anti-cancer tyrosine kinase inhibitors crizotinib and ibrutinib). Our simulations showed a substantial difference in drug exposure (AUC), when using typical parameters from healthy population instead of cancer-specific parameters. This difference in AUC increases with increasing E_H; 1.8, 2.1 and 9.5-fold higher AUC for alprazolam (low E_H), crizotinib (intermediate E_H), and ibrutinib (high E_H) when assume that the whole liver is cancerous (New Cancer-ALC). Therefore, abundance data may have a substantial impact on PK profiles, especially when high amount of liver is cancerous (advanced cancer). Abundance data specific for a cancer population in addition to the amount of liver being cancerous are necessary for PBPK models. There are no clinical data for the simulated drugs in CRLM patients. Further work could verify our updated models for cancer populations once clinical data are available. The aim of the current study is only to assess the impact of the abundance of CYPs on PK in cancer. Overall, we show that population specific abundance data for DMEs are important in PBPK for cancer and progress of disease.

To conclude, our study provides for the first time protein abundance data for hepatic DMEs and transporters in individual cancer patients with a focus on CRLM. CYPs and UGTs were substantially decreased and transporters were altered in cancer. Inter-individual variability was high for DMEs and transporters, with higher amounts in cancer. Abundance data were normalized to tissue level, highlighting the importance of relating our values to liver by using

MPPGL. Lastly, our PBPK simulations on CYP substrates demonstrated higher drug exposure in healthy population relative to population-specific abundance of CYPs. Appropriate abundance values specific for cancer population may contribute to more accurate predictions of PK in cancer. The quantitative data generated in this report will be used to address data gaps in cancer PBPK models.

6.6 References

Achour B, Al Feteisi H, Lanucara F, Rostami-Hodjegan A, and Barber J (2017) Global proteomic analysis of human liver microsomes: Rapid characterization and quantification of hepatic drug-metabolizing enzymes. *Drug Metab Dispos*, **45**:666–675.

Achour B, Russell MMR, Barber J, and Rostami-Hodjegan A (2014) Simultaneous quantification of the abundance of several cytochrome p450 and uridine 5′-diphospho-glucuronosyltransferase enzymes in human liver microsomes. *Drug Metab Dispos*, **42**:500–510.

Akhdar H, Legendre C, Aninat C, and More F (2012) Anticancer Drug Metabolism: Chemotherapy Resistance and New Therapeutic Approaches, in *Topics on Drug Metabolism* p 6, InTech.

Al-Majdoub ZM, Al Feteisi H, Achour B, Warwood S, Neuhoff S, Rostami-Hodjegan A, and Barber J (2019) Proteomic Quantification of Human Blood-Brain Barrier SLC and ABC Transporters in Healthy Individuals and Dementia Patients. *Mol Pharm* **16**:1220–1233.

Al-Majdoub ZM, Carroll KM, Gaskell SJ, and Barber J (2014) Quantification of the proteins of the bacterial ribosome using QconCAT technology. *J Proteome Res* **13**:1211–1222.

Al-Majdoub ZM, Couto N, Achour B, Harwood MD, Carlson G, Warhurst G, Barber J, and Rostami-Hodjegan A (2020) Quantification of Proteins Involved in Intestinal Epithelial Handling of Xenobiotics. *Clin Pharmacol Ther* **0**:1–11.

Al Feteisi H, Al-Majdoub ZM, Achour B, Couto N, Rostami-Hodjegan A, and Barber J (2018) Identification and quantification of blood–brain barrier transporters in isolated rat brain microvessels. *J Neurochem* **146**:670-685.

Billington S, Ray AS, Salphati L, Xiao G, Chu X, Humphreys WG, Liao M, Lee CA, Mathias A, Hop CECA, Rowbottom C, Evers R, Lai Y, Kelly EJ, Prasad B, and Unadkat JD (2018) Transporter Expression in Noncancerous and Cancerous Liver Tissue from Donors with Hepatocellular Carcinoma and Chronic Hepatitis C Infection Quantified by LC-MS/MS Proteomics. *Drug Metab Dispos* **46**:189–196.

Bray F, Ferlay J, Soerjomataram I, Siegel RL, Torre LA, and Jemal A (2018) Global cancer statistics 2018: GLOBOCAN estimates of incidence and mortality worldwide for 36 cancers in 185 countries. *CA Cancer J Clin* **68**:394–424.

Cheeti S, Budha NR, Rajan S, Dresser MJ, and Jin JY (2013) A physiologically based pharmacokinetic (PBPK) approach to evaluate pharmacokinetics in patients with cancer. *Biopharm Drug Dispos* **34**:141–154.

Chen X, Liu H-PL, Li M, and Qiao L (2014) Advances in non-surgical management of primary liver cancer. *World J Gastroenterol* **20**:16630.

Couto N, Al-Majdoub ZM, Achour B, Wright PC, Rostami-Hodjegan A, and Barber J (2019) Quantification of Proteins Involved in Drug Metabolism and Disposition in the Human Liver Using Label-Free Global Proteomics. *Mol Pharm* **16**:632–647.

de Man FM, Goey AKL, van Schaik RHN, Mathijssen RHJ, and Bins S (2018) Individualization of Irinotecan Treatment: A Review of Pharmacokinetics, Pharmacodynamics, and Pharmacogenetics. *Clin Pharmacokinet* **57**:1229–1254.

Kurzawski M, Szeląg-Pieniek S, Łapczuk-Romańska J, Wrzesiński M, Sieńko J, Oswald S, and Droździk M (2019) The reference liver – ABC and SLC drug transporters in healthy donor and metastatic livers. *Pharmacol Reports* **71**:738–745.

Lane CS, Nisar S, Griffiths WJ, Fuller BJ, Davidson BR, Hewes J, Welham KJ, and Patterson LH (2004) Identification of cytochrome P450 enzymes in human colorectal metastases and the surrounding liver: a proteomic approach. *Eur J Cancer* **40**:2127–2134.

Liang X, Staiger KM, Riddle E, Hao J, and Lai Y (2020) Role of transporters in drug disposition and drug-drug interactions, in *Identification and Quantification of Drugs, Metabolites, Drug Metabolizing Enzymes, and Transporters* pp 311-337.

Ma M, and McLeod H (2003) Lessons Learned from the Irinotecan Metabolic Pathway. *Curr Med Chem* **10**:41–49.

Maher B, Ryan E, Little M, Boardman P, and Stedman B (2017) The management of colorectal liver metastases. *Clin Radiol* **72**:617–625.

Michael M, and Doherty MM (2005) Tumoral drug metabolism: Overview and its implications for cancer therapy. *J Clin Oncol* **23**:205–229.

Mitchell D, Puckett Y, and Nguyen QN (2019) Literature Review of Current Management of Colorectal Liver Metastasis. *Cureus*, *Cureus* **11**:e3940.

Nikolouzakis T, Vassilopoulou L, Fragkiadaki P, Mariolis Sapsakos T, Papadakis G,

Spandidos D, Tsatsakis A, and Tsiaoussis J (2018) Improving diagnosis, prognosis and prediction by using biomarkers in CRC patients (Review). *Oncol Rep* **39**: 2455-2472.

Ohtsuki S, Schaefer O, Kawakami H, Inoue T, Liehner S, Sato A, Ishiguro N, Kishimoto W, Ludwig-Schwellinger E, Ebner T, and Terasaki T (2011) Simultaneous Absolute Protein Quantification of Transporters, Cytochrome P450s and UDP-glucuronosyltransferases as a Novel Approach for the Characterization of Individual Human Liver: Comparison with mRNA Levels and Activities. *Drug Metab Dispos* **40**:83–92.

Ohya H, Shibayama Y, Ogura J, Narumi K, Kobayashi M, and Iseki K (2015) Regorafenib Is Transported by the Organic Anion Transporter 1B1 and the Multidrug Resistance Protein 2. *Biol Pharm Bull* **38**:582–586.

Payen VL, Mina E, Van Hée VF, Porporato PE, and Sonveaux P (2020) Monocarboxylate transporters in cancer. *Mol Metab* **33**:48–66.

Rey JB, Launay-Vacher V, and Tournigand C (2015) Regorafenib as a single-agent in the treatment of patients with gastrointestinal tumors: an overview for pharmacists. *Target Oncol* **10**:199–213.

Rostami-Hodjegan A (2012) Physiologically Based Pharmacokinetics Joined With In Vitro–In Vivo Extrapolation of ADME: A Marriage Under the Arch of Systems Pharmacology. *Clin Pharmacol Ther* **92**:50–61.

Rowland A, Miners JO, and Mackenzie PI (2013) The UDP-glucuronosyltransferases: Their role in drug metabolism and detoxification. *Int J Biochem Cell Biol* **45**:1121–1132.

Russell MR, Achour B, McKenzie EA, Lopez R, Harwood MD, Rostami-Hodjegan A, and Barber J (2013) Alternative fusion protein strategies to express recalcitrant QconCAT proteins for quantitative proteomics of human drug metabolizing enzymes and transporters. *J Proteome Res* **12**:5934–5942.

Schwenger E, Reddy VP, Moorthy G, Sharma P, Tomkinson H, Masson E, and Vishwanathan K (2018) Harnessing Meta-analysis to Refine an Oncology Patient Population for Physiology-Based Pharmacokinetic Modeling of Drugs. *Clin Pharmacol Ther* **103**:271–280.

Sharma S, Suresh Ahire D, and Prasad B (2020) Utility of Quantitative Proteomics for Enhancing the Predictive Ability of Physiologically Based Pharmacokinetic Models

Across Disease States. *J Clin Pharmacol* **60**:S17–S35.

Shinko D, Diakos CI, Clarke SJ, and Charles KA (2017) Cancer-Related Systemic Inflammation: The Challenges and Therapeutic Opportunities for Personalized Medicine. *Clin Pharmacol Ther* **102**:599–610.

Siegel RL, Miller KD, and Jemal A (2018) Cancer statistics, 2018. *CA Cancer J Clin* **68**:7–30.

Suri A, Chapel S, Lu C, and Venkatakrishnan K (2015) Physiologically based and population PK modeling in optimizing drug development: A predict-learn-confirm analysis. *Clin Pharmacol Ther* **98**:336–344.

van Huizen NA, Coebergh van den Braak RRJ, Doukas M, Dekker LJM, IJzermans JNM, and Luider TM (2019) Up-regulation of collagen proteins in colorectal liver metastasis compared with normal liver tissue. *J Biol Chem* **294**:281–289.

Vasilogianni AM, Achour B, Scotcher D, Peters SA, Al-Majdoub ZM, Barber J, and Rostami-Hodjegan A (2021) Hepatic Scaling Factors for In Vitro-In Vivo Extrapolation (IVIVE) of Metabolic Drug Clearance in Patients with Colorectal Cancer with Liver Metastasis. *Drug Metab Dispos* (in press).

Vildhede A, Wiśniewski JR, Norén A, Karlgren M, and Artursson P (2015) Comparative Proteomic Analysis of Human Liver Tissue and Isolated Hepatocytes with a Focus on Proteins Determining Drug Exposure. *J Proteome Res* **14**:3305–3314.

Wlcek K, Svoboda M, Riha J, Zakaria S, Olszewski U, Dvorak Z, Sellner F, Ellinger I, Jäger W, and Thalhammer T (2011) The analysis of organic anion transporting polypeptide (OATP) mRNA and protein patterns in primary and metastatic liver cancer. *Cancer Biol Ther* **11**:801–11.

Yan T, Gao S, Peng X, Shi J, Xie C, Li Q, Lu L, Wang Y, Zhou F, Liu Z, and Hu M (2015) Significantly Decreased and More Variable Expression of Major CYPs and UGTs in Liver Microsomes Prepared from HBV-Positive Human Hepatocellular Carcinoma and Matched Pericarcinomatous Tissues Determined Using an Isotope Label-free UPLC-MS/MS Method. *Pharm Res* **32**:1141–1157.

Yan T, Lu L, Xie C, Chen J, Peng X, Zhu L, Wang Y, Li Q, Shi J, Zhou F, Hu M, and Liu Z (2015) Severely Impaired and Dysregulated Cytochrome P450 Expression and Activities in Hepatocellular Carcinoma: Implications for Personalized Treatment in Patients. *Mol*

Cancer Ther **14**:2874–2886.

Yoshida K, Budha N, and Jin JY (2017) Impact of physiologically based pharmacokinetic models on regulatory reviews and product labels: Frequent utilization in the field of oncology. *Clin Pharmacol Ther* **101**:597–602.

Zanger UM, and Schwab M (2013) Cytochrome P450 enzymes in drug metabolism: Regulation of gene expression, enzyme activities, and impact of genetic variation. *Pharmacol Ther* **138**:103–141.

Zhang H-F, Li Z-H, Liu J-Y, Liu T-T, Wang P, Fang Y, Zhou J, Cui M-Z, Gao N, Tian X, Gao J, Wen Q, Jia L-J, and Qiao H-L (2016) Correlation of Cytochrome P450 Oxidoreductase Expression with the Expression of 10 Isoforms of Cytochrome P450 in Human Liver. *Drug Metab Dispos* **44**:1193–1200.

6.7 Supplementary Information

Supplementary Table 6-1 Demographic and clinical details of cancer patients provided by the MFT Biobank.

Sample ID	Age at surgery (years)	Race	Sex	Body mass index, BMI (kg/m^2)	Smoking/ Alcohol use	Liver lobe	Diagnosis	Medical history	Treatment
389	52	Caucasian	Female	30.86	No/ Occasionally	Left	Metastatic moderately well differentiated adenocarcinoma	Deep vein thrombosis, asthma, duodenal ulcer, thyroid problem, liver lesions	Fragmin, levothyroxine, betamethasone, ventolin, ferrous fumarate
590	72	Caucasian	Male	32	Pipe/ 22 units per week	-	Metastatic moderate to Well differentiated adenocarcinoma (dirty necrosis)	Asthma, polypectomy, tonsillectomy, Hemicolectomy Dukes B	Salbutamol, tiotropium, lansaprozole, nasonex
633	67	Caucasian	Male	26.85	Ex-stopped/ -	Right	Metastatic adenocarcinoma & fatty liver disease	Peripheral neuropathy secondary to oxaliplatin, type 2 diabetes, hypercholesterolemia, valvular heart disease, prostate cancer with bone metastasis, colonic cancer T3N0, colorectal liver metastasis	Metformin, zoladex, oxaplatin and 5FU, irinotecan and 5FU with cetuximab
674	68	Caucasian	Female	26.67	No/ -	Right	Metastatic moderately differentiated adenocarcinoma	Rectosigmoid cancer 10/10 Dukes B	-

734	64	Caucasian	Female	23.84	No/ Occasionally	Right	Moderately to focally poorly differentiated metastatic adenocarcinoma	Primary colorectal	Dalteparin, short course of radiotherapy, adjuvant OXmdG and 5FU
746	85	Caucasian	Male	23.67	Ex (40 years)/ Moderately	Right	Metastatic papillary carcinoma	Laparoscopic R hemicolectomy T2M0, Squamous cell carcinoma (scalp), hypothyroidism, hypertension, Chronic obstructive pulmonary disease	Irbesartan, levothyroxine, bisoprolol, aspirin, omeprazole, budesamide, formoterol
794	71	Caucasian	Female	22.41	No/ No	-	Metastatic adenocarcinoma with extensive intra-acinar necrosis	R hemicolectomy, pT3N2, high blood pressure, depression	Tomudex chemotherapy
818	58	Caucasian	Male	21.78	Ex (25 years)/ 18 units per week	-	Moderately differentiated metastatic adenocarcinoma	Sigmoid adenocarcinoma pT3pN2	Loperamide, carboplatin/5FU and modified de Gramont and radiotherapy
1492	34	-	Female	32.53	Ex-stopped/ Approximately 20 units per week	Right	Metastatic moderate and poorly differentiated adenocarcinoma	Bowel resection, pilonodal abcess x2, grometts (as a child), tonsillectomy (as a child), egg collection, occasional palpitations, asthma (as a child), reflux, joint problems in knees, treated for Irritable bowel syndrome	Omeprazole, amitryptyline, microgynon, glucosamine sulphate, ibuprofen, peppermint oil

1493	75	-	Male	-	No/ No	Right	Metastatic moderately differentiated adenocarcinoma	Sigmoid tumour, sleep apnoea, asthma	Cod liver oil, salbutamol inhaler, seretide inhaler, movicol
1498	63	Caucasian	Male	-	No/ Rarely	Right	Metastatic adenocarcinoma	Previous gout, anaemia, cataract operation	Doxycycline regime completed, Nil regular
1795	63		Male	36.32	Ex - stopped (previously 30cpd)/ Approximately 75 units per week	Left	Metastatic well differentiated adenocarcinoma	Adenocarcinoma, hypertension, intermittent claudication of left leg	Omeprazole, irbesartan, simvastatin, clopidogrel
1957	68	-	Male	32.16	No/ -	Left	Metastatic moderately differentiated adenocarcinoma	Primary rectal cancer, pneumonia post-operative, liver cancer, late lung metastasis	Nil regular
2036	43	-	Female	-	-/ -	Right	Metastatic moderate to poorly differentiated adenocarcinoma	Primary colorectal	Omeprazole, paracetamol
2058	79	Caucasian	Female	21.6	-/ -	Left	Metastatic adenocarcinoma	Below the knee amputation, primary colorectal, lung metastasis	Lansoprazole, ferrous sulphate, alendronic acid, paracetamol, codeine phosphate, senna, natecal D3
2095	55	Caucasian	Male	28.1	-/ -	Right	Metastatic moderately differentiated adenocarcinoma	Primary colorectal	Nil regular

1063	77	Caucasian	Male	26.6	Ex - stopped 20 years ago/ 15 units per week	Right	Moderate to poorly differentiated hepatocellular carcinoma	Primary hepatocellular carcinoma, prostate cancer	-
1359	68	Caucasian	Male	33.4	No/ Whiskey (frequency unknown)	Left	Poorly differentiated intrahepatic cholangiocarcinoma pT2a, pN1	Primary liver tumour, right elbow surgery, patient would have a cholecystectomy for gallstones but surgery was abandoned when the liver tumour was discovered, hiatus hernia, reflux	Lumigan eye drops, brinzolamide, timolol, omeprazole, bimatoprost

Supplementary Table 6-2 Demographic and clinical details of healthy subjects provided by Pfizer.

Sample ID	Age at surgery (years)	Race	Sex	Body mass index, BMI (kg/m^2)	Smoking/ Alcohol use	Cause of death	Medical history	Treatment
HH83	18	Caucasian	Female	20.19	No/ No	Head trauma	Healthy	None
HH84	53	Caucasian	Male	19.94	No/ Social	Intracranial haemorrhage	None	None
HH87	54	Caucasian	Female	29.79	No/ No	Head trauma	Healthy	None
HH93	34	Caucasian	Male	20.62	No/ No	Cerebellar haemorrhagic injury	Healthy	Healthy
HH98	64	Caucasian	Male	37.47	No/ No	Head Injury	Healthy	None
HH99	45	Caucasian	Male	31.62	No/ No	Head trauma	Healthy	None
HH101	54	Caucasian	Female	21.95	No/ No	Motor vehicle accident	Healthy	None
HH102	52	Caucasian	Female	32.26	No/ No	Cerebral Aneurysm	Healthy	None
HH104	35	African American	Female	25.25	No/ No	Cerebral Aneurysm	Healthy	None
HH105	50	Caucasian	Male	33.47	No/ No	Cerebral Aneurysm	Healthy	None
HH106	43	Hispanic	Male	24.48	No/ No	Cerebral Vascular Aneurysm	Healthy	None
HH107	45	Caucasian	Female	24.96	No/ No	Cerebral Vascular Aneurysm	Healthy	None
HH110	54	Caucasian	Female	26.29	No/ Social	Cerebral Vascular Aneurysm	Healthy	None

HH111	43	Caucasian	Female	28.43	No/ No	Intracranial bleeding	Healthy	None
HH118	32	Caucasian	Male	26.69	No/ Social	Gunshot Wound to head	Healthy, Skin Graft on right arm in the past	Pepcid AC, Tagamet, Steroids in HS and Marines

Supplementary Table 6-3 Expression levels (pmol mg^{-1}) of 14 CYP and 8 UGT enzymes quantified in human healthy liver controls.

Sample ID by the provider		HH83	HH84	HH87	HH93	HH98	HH99	HH101	HH102	HH104	HH105	HH106	HH107	HH110	HH111	HH118	Pooled healthy			
Sample name		H3	H6	H9	H12	H51	H18	H21	H53	H27	H30	H33	H36	H39	H42	H56	H57	H61	H62	H63
Protein target	Peptides	Absolute abundance (pmol mg-1)																		
CYP1A2	YLPNPALQR	35.73	16.10	11.00	10.30	8.38	8.10	7.92	5.54	10.22	5.22	7.80	1.26	3.22	14.49	10.90	6.05	5.96	5.86	5.83
CYP2A6	GTGGANIDPTFFLSR	44.99	2.17	7.60	3.56	15.75	2.57	10.20	12.26	20.32	72.00	42.38	3.15	22.31	42.21	30.25	12.05	11.99	12.05	12.71
CYP2B6	GYGVIFANGNR	6.98	1.53	7.60	3.07	3.42			5.59	15.15	26.14			21.53	23.77	28.66	3.35	5.75	5.84	5.03
CYP2C18	SLTNFSK	0.98	0.73		0.32	0.25		0.31	1.38		0.71	0.74	0.35	0.01	0.33	0.46	0.22	0.18	0.21	0.33
CYP2C19	GHFPLAER	9.43	2.42	0.86	0.65	2.00	0.12	0.61	4.58	0.04	1.51	6.20	1.07	0.48	1.14	0.20	1.03	0.98	0.96	1.14
CYP2C8	SFTNFSK	50.75	9.08	19.83	4.46	29.90	16.42	15.52	21.99	30.87	37.90	91.35	6.25	19.57	48.48	26.57	16.60	16.59	16.92	17.09
CYP2C9	GIFPLAER	195.67	92.38	52.39	27.43	136.05	127.65	34.98	114.94	19.43	145.48	160.22	29.24	57.62	125.04	111.74	46.81	48.05	47.66	47.37
CYP2D6	DIEVQGFR		7.35		10.93		15.81		5.03				1.93	3.90		9.27	3.06	3.34	3.80	
CYP2E1	FITLVPSNLPHEATR	106.10	112.78	31.46	81.91	67.74	164.17	22.94	93.17	41.00	99.57	52.48	24.65	57.26	71.86	115.26	32.05	32.95	33.06	31.93
CYP2J2	VIGQGQQPSTAAR	0.18	0.43		0.32	0.25	0.69	0.25	0.48	0.12	0.26	0.29	0.08	0.28	0.39	0.51	0.21	0.20	0.13	0.19
CYP3A4	LSLGGLLQPEK	67.63	35.60	53.80	12.85	103.86	12.65	67.53	50.87	166.71	69.59	332.37	17.81	97.37	224.29	81.98	54.94	54.88	57.40	61.40
CYP3A5	DTINFLSK		3.51	1.82	2.13	3.23		0.84	20.58	69.59		6.10	31.94	13.48			7.01	7.87	7.53	
CYP3A7	FNPLDPFVLSIK						0.73			0.65	0.16	1.85	0.15	2.72	0.23		0.28	0.37	0.39	0.26
CYP4F2	HVTQDIVLPDGR	23.03	9.88	8.16	7.60	6.00	6.28	5.11	15.57	3.11	17.26	10.39	2.86	2.33	12.80	5.40	4.64	4.56	4.66	4.98
UGT1A1	DGAFYTLK	101.51	32.86		87.06					30.34	41.95			43.92	80.54	39.57	26.49	27.01	27.08	25.50
UGT1A3	HVLGHTQLYFETEHFLK	2.23	1.79	0.62	1.58	1.10	0.83	0.44	0.70	2.36	2.03	2.77	0.34	0.69	0.64	1.39	0.94	0.81	0.85	1.07
UGT1A6	VSVWLLR	8.81	5.24	6.38	6.86	11.12	15.38	3.88	11.82	5.08	17.85	18.80	1.77	6.97	11.21	9.07	4.85	4.87	4.99	4.73
UGT1A9	AFAHAQWK	53.64	19.93	28.19	23.81	23.37	25.27	11.78	44.89	28.22	50.55	60.39	11.76	22.22	36.37	35.46	16.21	16.69	16.50	17.93
UGT2B11	DSFWLYFSQEQEILWELYDIFR												0.40	2.16	3.54	2.39			1.31	
UGT2B15	SVINDPVYK	91.26	27.46	27.93	29.08	48.67	41.61		46.51	31.53	68.80	62.71	16.52	16.31	42.44	58.76	22.18	22.02	22.57	22.72
UGT2B4	FSPGYAIEK	57.07			18.68						45.43	140.72		17.72	38.98	41.35		19.95	19.21	18.33
UGT2B7	ADVWLIR	147.24	45.93	52.77	57.47	92.46	97.85	37.79	69.20	71.34	148.98	97.69	35.84	37.65	94.73	115.57	38.09	39.84	40.41	42.41

Supplementary Table 6-4 Expression levels (pmol mg^{-1}) of 14 CYP and 8 UGT enzymes quantified in human histologically normal livers.

Sample ID by the provider		2095	2058	2036	389	590	746	818	1492	674	1957	1493	1498	633	734	794	1795	1063	1359	Pooled normal
Sample name		N1	N4	N7	N10	N13	N49	N19	N22	N25	N34	N28	N31	N37	N40	N43	N54	N45	N47	N58
Protein target	Peptides	Absolute abundance (pmol mg-1)																		
CYP1A2	YLPNPALQR	14.70	10.11	3.34	5.46	24.91	15.38	6.89	8.46	16.56	7.48	6.10	14.15	11.55	18.81	8.23	3.30	5.59	8.88	8.63
CYP2A6	GTGGANIDPTFFLSR	25.86	23.61	4.67	25.26	15.68	30.43	25.16	12.98	33.63	14.21	14.09	37.11	15.98	27.20	13.10	8.91	10.01	6.48	17.03
CYP2B6	GYGVIFANGNR		6.56					4.07		3.47	3.06	2.01	3.99	5.78		0.55		2.44	2.07	1.99
CYP2C18	SLTNFSK				0.10	0.92	0.42		0.20	0.74	0.18	0.12	0.92	0.54	0.74	0.12	0.05	0.07	0.05	0.18
CYP2C19	GHFPLAER	0.58		1.73	5.04	1.57	1.25	4.24	2.15	7.59	1.37	0.89	0.35	0.10	10.70	1.60	0.14	0.24	0.33	2.10
CYP2C8	SFTNFSK	22.59	16.27	8.21	12.94	19.98	26.61	18.69	21.12	28.92	11.17	10.32	33.13	18.16	34.67	7.61	6.90	8.98	11.65	16.04
CYP2C9	GIFPLAER	70.18	52.22	38.05	49.30	118.00	50.64	61.08	86.27	96.06	41.39	45.81	121.91	73.34	91.57	30.80	30.01	20.54	32.14	50.00
CYP2D6	DIEVQGFR		1.49	1.61	2.79	7.58					1.74	2.26				2.04	0.36			
CYP2E1	FITLVPSNLPHEATR	21.17	16.61	14.37	11.51	53.91	40.73	19.98	21.32	35.78	22.68	9.44	41.10	33.17	35.76	7.17	17.47	7.26	15.79	18.16
CYP2J2	VIGQGQQPSTAAR	0.14	0.22	0.10	0.11	0.27	0.19	0.34	0.49	0.25	0.03	0.15	0.07	0.35	0.42	0.17	0.23			0.16
CYP3A4	LSLGGLLQPEK	22.27	70.97	16.23	13.70	53.10	50.96	28.06	27.15	46.18	23.82	20.31	61.31	38.02	61.69	12.38	10.66	14.20	14.75	24.87
CYP3A5	DTINFLSK	1.46	1.60	0.65	1.29		1.98	0.73	1.12	2.32		2.05		1.45		0.78			12.57	2.55
CYP3A7	FNPLDPFVLSIK				0.05		1.84				0.04	0.12	2.08	0.79	0.05	0.04		0.02	0.01	0.23
CYP4F2	HVTQDIVLPDGR	6.44	2.51	5.67	3.15	12.02	4.43	5.32	3.54	12.83	6.41	0.37	9.60	3.57	12.15	3.36	3.47	2.70	0.31	4.54
UGT1A1	DGAFYTLK	2.80	4.37	3.58	0.94	33.39	9.73	3.51	6.74		4.66	10.03	21.37	11.91	17.96	6.71	5.69		6.11	6.89
UGT1A3	HVLGHTQLYFETEHFLK	1.00	0.99	0.22	0.40	1.03	1.03		1.04	0.65	0.76	0.59	1.86	0.33	1.91	0.82	0.09	0.19	0.93	0.72
UGT1A6	VSVWLLR	2.93	3.49	3.61	2.16			2.26			3.10	1.52	5.78		5.54	0.98	2.99	1.26	1.30	2.77
UGT1A9	AFAHAQWK	4.47	11.20	9.09	5.73	24.32	10.13	7.11	6.84	12.57	7.95	5.33	16.07	14.29	11.56	2.18	5.35	2.50	4.53	6.61
UGT2B11	DSFWLYFSQEQEILWELYDIFR														2.57	1.44	0.89	0.95	1.10	
UGT2B15	SVINDPVYK	29.33	14.16	6.88	15.39	45.13	24.04	24.85	31.34	23.15	17.33	14.85	21.99	35.47	35.86	10.39	16.83	6.70	11.99	17.60
UGT2B4	FSPGYAIEK					38.47					10.59	9.61	21.09		31.35	5.55	9.65		8.08	12.21
UGT2B7	ADVWLIR	58.16	37.21	32.45	76.07	104.67	55.91	56.51	56.00	58.75	39.21	29.80	46.81	57.80	65.99	21.99	35.26	15.79	26.04	37.10

Supplementary Table 6-5 Expression levels (pmol mg^{-1}) of 14 CYP and 8 UGT enzymes quantified in human tumour livers.

Sample ID by the provider		2095	2058	2036	389	590	746	818	1492	674	1957	1493	1498	633	734	794	1795	1063	1359	Pooled tumour
Sample name		T2	T5	T8	T11	T14	T50	T52	T23	T26	T35	T29	T32	T38	T41	T44	T55	T46	T48	T59
Protein target	Peptides	Absolute abundance (pmol mg-1)																		
CYP1A2	YLPNPALQR	0.15	0.28	0.13	1.51	0.08	5.62	0.03	1.73		1.80	0.03	5.46	0.13	0.04	2.98		0.02		1.64
CYP2A6	GTGGANIDPTFFLSR	0.30	0.49	0.02	4.32		6.46	0.04	1.95		3.31		13.45		0.06	2.98	0.06	0.09	0.22	3.75
CYP2B6	GYGVIFANGNR						1.29						2.98							
CYP2C18	SLTNFSK						0.01			0.06			0.18		0.09					
CYP2C19	GHFPLAER	0.04	0.03		0.78	0.03	0.29	0.00	0.25		0.46		0.45	0.04	0.04	0.32		0.05		0.12
CYP2C8	SFTNFSK				4.08		7.77		4.64			0.05	19.94			3.41		0.17	1.71	5.86
CYP2C9	GIFPLAER		2.49		17.52	0.18	19.98	0.11	17.94	1.51	9.27	0.02	80.29	0.33		13.97		0.23		18.26
CYP2D6	DIEVQGFR		0.18		1.08	0.26		0.04	0.76						0.08	1.07	0.05	0.02		0.53
CYP2E1	FITLVPSNLPHEATR	0.71	1.99	0.72	4.75	0.18	19.09	0.12	5.84	0.07	5.54	0.47	28.62		0.21	7.49	0.13	0.14	0.25	7.29
CYP2J2	VIGQGQQPSTAAR		0.05	0.16		0.01	0.22	0.08				0.00	0.16	0.01	0.11					
CYP3A4	LSLGGLLQPEK	0.26	2.42	0.62	3.98	0.09	18.28	0.04	3.47		4.64	0.27	35.01	0.05	0.13	4.30	0.22	0.24	0.16	8.29
CYP3A5	DTINFLSK				0.69	0.28	0.86		0.22				1.57							
CYP3A7	FNPLDPFVLSIK												1.31				0.002			0.41
CYP4F2	HVTQDIVLPDGR	0.15	0.13	0.01	1.08	0.32	1.73	0.07	0.56	0.02	0.96		6.79	0.32	0.22	1.10			0.05	1.62
UGT1A1	DGAFYTLK		0.21		0.46					0.03	0.95		9.66		0.03	3.70	0.01			2.37
UGT1A3	HVLGHTQLYFETEHFLK	0.08	0.05		0.75	0.13	0.30		0.36	0.35		0.24	0.87	0.21	0.23	0.29	0.24		0.29	0.24
UGT1A6	VSVWLLR				0.56	0.23				0.06	0.58	0.07	5.20	0.27	0.18	0.48	0.04		0.19	1.00
UGT1A9	AFAHAQWK	0.00	0.14		1.05	0.07	2.06	0.04	0.54		1.00	0.30	9.72	0.01	0.06	0.95		2.24		2.33
UGT2B11	DSFWLYFSQEQEILWELYDIFR														0.43	0.76	0.45	0.37	0.54	
UGT2B15	SVINDPVYK				4.82	0.11	8.42	0.07	5.44		3.37		14.79		0.06	3.88		0.72		4.31
UGT2B4	FSPGYAIEK										2.39	0.78			0.14	0.88	0.22			
UGT2B7	ADVWLIR	0.98	1.58	0.44	7.56	0.20	18.19	0.14	9.37	0.19	6.90	0.20	30.72	0.08	0.21	9.11	0.05		0.19	8.48

Supplementary Table 6-6 Expression levels (pmol mg^{-1}) of 9 ABC, 14 SLC transporters, ATP1, and CDH17 quantified in human healthy liver controls.

Sample ID by the provider		HH83	HH84	HH87	HH93	HH98	HH99	HH101	HH102	HH104	HH105	HH106	HH107	HH110	HH111	HH118	Pooled healthy			
Sample name		H3	H6	H9	H12	H51	H18	H21	H53	H27	H30	H33	H36	H39	H42	H56	H57	H61	H62	H63
Protein target	Peptides	Absolute abundance (pmol mg-1)																		
P-gp	FYDPLAGK	0.32	0.35		0.32	0.61		0.39	0.59	0.31	0.61	0.38		0.69	0.34		0.27	0.25	0.24	0.21
BSEP	AADTIIGFEHGTAVER	0.74	0.58	1.44	0.30	0.46	0.72	0.63	1.15	0.44	0.84	0.42	1.07	1.10	0.88	1.40	0.39	0.38	0.38	0.35
MDR3	GAAYVIFDIIDNNPK	0.39	0.32	0.53	0.16	0.24	0.55	0.27	0.48	0.30	0.35	1.97	0.47	0.35	0.30	0.52	0.19		0.35	0.45
MRP2	LTIIPQDPILFSGSLR	0.94	0.50	0.95	0.15	1.44	1.21	0.67	1.95	0.61	1.09	0.31	0.92	1.38	1.44	2.11	0.66	0.61	0.66	0.66
MRP3	IDGLNVADIGLHDLR	0.59	0.38	0.86	0.38	0.55	0.76	0.78	1.24	0.49	0.86	0.54	0.25	0.54	0.95	1.29	0.30	0.36	0.37	0.46
MRP4	APVLFFDR			0.01	0.08		0.05							0.22						
MRP6	APETEPFLR	0.93	0.91	1.51	0.82	0.88	1.32	2.06	2.35	0.59	1.65		2.16	1.56	0.83	1.80	0.71	0.53	0.66	0.71
BCRP	SSLLDVLAAR			0.04	0.04	0.06			0.03				0.08	0.03				0.03	0.01	
ASBT	IAGLPWYR		0.14		0.04	0.01	0.01	0.18	0.09	0.04			0.02	0.17			0.02		0.07	
ATP1A1	SPDFTNENPLETR	6.35	5.88	10.35	9.96	6.72	8.01	12.61	11.06	4.45	12.08	6.60	8.10	11.10	6.52	14.55	4.17	3.97	3.77	5.02
CDH17	AENPEPLVFGVK																			
MCT1	SITVFFK	1.63	2.40	3.53	1.91	1.05			2.50	0.91				2.82	1.97	3.97	0.92	1.03	1.10	1.30
OST-α	YTADLLEVLK					0.01		0.02							0.04		0.02	0.01	0.01	
OST-β	ETPEVLHLDEAK		0.09	0.20	0.13		0.14		0.18			0.25				0.44	0.03	0.06	0.06	
PEPT1	HTLLVWAPNHYQVVK				0.06				0.33					0.29			0.13	0.10	0.08	0.11
NTCP	GIYDGDLK			5.52					6.10		5.96		4.04				2.07	1.97	2.05	1.89
OCT1	GVALPETMK	7.51	4.18	6.37		2.95									7.02		3.61	3.70	3.51	3.90
OCT3	GIALPETVDDVEK	0.71	0.19	1.07	0.28	0.53	1.18		1.31	0.68	1.79		0.67	0.80	0.72	2.59	0.43	0.40	0.42	0.36
OAT2	NVALLALPR	1.73	0.56	1.89	0.40	1.59	1.13	2.71	2.58	1.15	2.17	1.45	2.01	2.21	1.69	2.11	0.81	0.98	0.84	0.91
OAT7	ISLLSFTR	0.23	0.17	0.53	0.20	0.34	0.49	0.63	0.55	0.08	0.40	0.31	0.35	0.36	0.24	0.44	0.12	0.15	0.11	0.06
MATE1	DHVGYIFTTDR																			
OATP1A2	IYDSTTFR	0.06	0.07	0.04				0.06		0.06		0.03	0.03	0.10	0.41		0.03	0.02	0.02	
OATP1B1	LNTVGIAK	1.26	0.47	1.22	0.90	1.43	1.47	2.67	0.82	1.07	1.35	0.83	1.23	2.10	1.68	1.89	0.64	0.69	0.64	0.81
OATP1B3	NVTGFFQSLK	1.25	1.05	2.64	1.66	2.52	2.30	5.83	3.61			1.51	4.11	2.16			1.51	1.51	1.73	
OATP2B1	SSPAVEQQLLVSGPGK	2.63	1.73	2.58	0.84	1.97	2.87	3.72	6.19	1.65	5.13	2.76		1.80	2.28	4.49	1.24	1.25	1.21	1.16

Supplementary Table 6-7 Expression levels (pmol mg^{-1}) of 9 ABC, 14 SLC transporters, ATP1, and CDH17 quantified in human histologically normal livers.

Sample ID by the provider		2095	2058	2036	389	590	746	818	1492	674	1957	1493	1498	633	734	794	1795	1063	1359	Pooled normal
Sample name		N1	N4	N7	N10	N13	N49	N19	N22	N25	N34	N28	N31	N37	N40	N43	N54	N45	N47	N58
Protein target	Peptides	Absolute abundance (pmol mg-1)																		
P-gp	FYDPLAGK	0.18	0.13	0.45	0.24	0.39	1.45	0.14	0.25	0.29		0.22	0.18	0.24		0.13	0.81	0.09	0.12	
BSEP	AADTIIGFEHGTAVER	0.23	0.41	0.62	0.42	0.90	0.55	0.39	0.52	0.53	0.38	0.28	0.64	0.47	0.82	0.28	0.74	0.22	0.14	0.49
MDR3	GAAYVIFDIIDNNPK	0.32			0.20	0.23	0.27	0.41	0.27			0.12	0.27	0.54	0.44	0.28	0.74	0.36		0.34
MRP2	LTIIPQDPILFSGSLR	0.41	0.23	0.91	0.43	0.63	0.54	0.34	0.62	0.53	0.38	0.37	0.59	0.76	0.69	0.28	1.18	0.27	0.46	0.59
MRP3	IDGLNVADIGLHDLR	0.25	0.10	0.36	0.15	0.29	0.22	0.19	0.22	0.09	0.30	0.18	0.34	0.17	0.19	0.17	1.33	0.08	0.17	0.36
MRP4	APVLFFDR		0.01	0.01		0.10					0.01		0.01	0.04	0.03		0.04	0.00		
MRP6	APETEPFLR				0.52	0.88		0.79		0.77	0.20	0.72	0.14	0.93		0.26		0.31	0.32	0.56
BCRP	SSLLDVLAAR					0.07				0.04										
ASBT	IAGLPWYR	0.02		0.06			0.03		0.04			0.11	0.02		0.05	0.04				
ATP1A1	SPDFTNENPLETR	2.62	1.39	4.02	2.70	3.89	2.75	1.38	2.95	2.05	3.74	3.81	3.15	2.71	4.01	1.14	5.99	1.44	2.22	3.42
CDH17	AENPEPLVFGVK																			
MCT1	SITVFFK	0.79			0.96					0.76	1.44	0.57	1.26	0.42	1.61	0.38	1.28	0.33	0.53	1.13
OST-α	YTADLLEVLK				0.02				0.11		0.02				0.03	0.03		0.04		
OST-β	ETPEVLHLDEAK		0.06		0.10			0.04	0.25			0.14		0.48		0.08		0.04		0.18
PEPT1	HTLLVWAPNHYQVVK														0.31		0.25			0.16
NTCP	GIYDGDLK	2.80	1.87	4.98	3.42	3.22				2.59	2.81	2.04	3.75		4.30	1.58	4.62	1.89	1.61	3.09
OCT1	GVALPETMK		2.71		1.90	2.74	5.07	3.52		3.46		2.36		2.89						
OCT3	GIALPETVDDVEK		0.36			0.48	0.41			0.25		0.71		0.57		0.20				
OAT2	NVALLALPR	0.96	0.51	1.62	0.92	1.47	0.75	0.76	0.95	0.93	1.45	0.57	0.62	0.96	0.91	0.36	2.28	0.79	0.58	1.08
OAT7	ISLLSFTR		0.10	0.41	0.17	0.11	0.23		0.12	0.09	0.23	0.06	0.11		0.14	0.05	0.18		0.04	0.16
MATE1	DHVGYIFTTDR															0.05				
OATP1A2	IYDSTTFR		0.04				0.03			0.00		0.11			0.06	0.01				
OATP1B1	LNTVGIAK	0.69	0.61	1.15	0.91	0.67	0.58	0.81	0.54	0.70	1.08	0.46	0.80	0.68	1.03	0.21	1.52	0.30	0.49	0.66
OATP1B3	NVTGFFQSLK		0.96	1.79	0.46		1.64	0.61	0.99	0.95		0.56		0.76		0.32		0.73		
OATP2B1	SSPAVEQQLLVSGPGK	1.64	1.19	1.18	1.55	3.08	2.06	1.70	1.52	1.80	2.35	1.71	1.87	1.49	2.34	0.99	2.76	0.81	0.61	1.58

Supplementary Table 6-8 Expression levels (pmol mg^{-1}) of 9 ABC, 14 SLC transporters, ATP1, and CDH17 quantified in human tumour livers.

Sample ID by the provider		2095	2058	2036	389	590	746	818	1492	674	1957	1493	1498	633	734	794	1795	1063	1359	Pooled tumour
Sample name		T2	T5	T8	T11	T14	T50	T52	T23	T26	T35	T29	T32	T38	T41	T44	T55	T46	T48	T59
Protein target	Peptides	Absolute abundance (pmol mg-1)																		
P-gp	FYDPLAGK	0.17		0.21	0.16	0.40		0.08	0.30				0.17	3.53						
BSEP	AADTIIGFEHGTAVER		0.35		0.05	0.03	0.12	0.01	0.06		0.20		0.50		0.00	0.08		0.03		0.04
MDR3	GAAYVIFDIIDNNPK				0.13								0.25							
MRP2	LTIIPQDPILFSGSLR	0.40			0.16	0.07	0.26	0.07	0.22		0.15	0.15	0.44	0.94	0.32	0.17		0.31		0.11
MRP3	IDGLNVADIGLHDLR	0.69	0.25	0.11	0.20	0.61	0.65	0.39	0.13	0.32	0.48	0.32	0.21	0.16	0.14	0.22	0.46	0.04	0.19	0.38
MRP4	APVLFFDR		0.03				0.06													
MRP6	APETEPFLR	1.21			0.33	0.24	2.91	0.09			0.17		0.76		0.05	0.21		0.11		0.21
BCRP	SSLLDVLAAR					0.05				0.07		0.07	0.04		0.12		0.21			
ASBT	IAGLPWYR				0.05	0.08	0.02	0.06	0.08				0.05		0.04	0.00	0.01			
ATP1A1	SPDFTNENPLETR	17.27	10.63	10.98	5.25	18.61	11.08	9.94	4.25	26.91	10.87	11.55	6.13	19.85	20.08	6.34	19.41	2.50	1.43	16.05
CDH17	AENPEPLVFGVK	22.23		3.25				2.61				5.52		29.11	8.19					
MCT1	SITVFFK	6.70	2.77	3.86						6.53	1.92	2.99	1.21	3.39	5.19	1.79	2.56	0.46		3.99
OST-α	YTADLLEVLK									0.01		0.05		0.15	0.02	0.02			0.04	
OST-β	ETPEVLHLDEAK		0.29	0.62	0.05		0.04						0.18		0.63		0.20		0.02	
PEPT1	HTLLVWAPNHYQVVK									0.27					0.23				0.38	0.18
NTCP	GIYDGDLK								0.88						0.12					
OCT1	GVALPETMK				0.26	0.08	0.95		0.36										0.07	
OCT3	GIALPETVDDVEK	0.38	0.27		0.14			0.18	0.26				0.53						0.22	0.25
OAT2	NVALLALPR		0.01	0.02	0.21	0.02	0.35		0.10	0.03	0.13		0.64		0.01	0.20				0.23
OAT7	ISLLSFTR				0.06	0.02	0.11						0.19		0.04	0.09		0.01		
MATE1	DHVGYIFTTDR								0.10							3.32				
OATP1A2	IYDSTTFR					0.04		0.04	0.00				0.10		0.01		0.005	0.02		
OATP1B1	LNTVGIAK		0.10		0.13	0.04	0.32		0.12		0.17		0.78			0.05				
OATP1B3	NVTGFFQSLK				0.26								1.00							
OATP2B1	SSPAVEQQLLVSGPGK	0.38			0.61		1.43	0.15	0.38	0.55	0.74		1.94	0.72		0.82				0.96

Supplementary Table 6-9 Input parameters for PBPK modelling using Simcyp v20 R1 for alprazolam (predominantly metabolized by CYP3A4, and CYP3A5, low extraction ratio), crizotinib (predominantly metabolized by CYP3A4, intermediate extraction ratio), and ibrutinib (predominantly metabolized by CYP3A4, high extraction ratio).

Input Parameters			
Compound Name	**SV-Alprazolam**	**SV-Crizotinib**	**SV-Ibrutinib**
Mol Weight (g/mol)	308.8	450.34	440.5
log P	2.12	4.28	3.97
Compound Type	Monoprotic Base	Diprotic Base	Monoprotic Base
pKa 1	2.4	9.4	3.78
pKa 2	n/a	5.6	n/a
B/P	0.825	1.1	0.73
Haematocrit	45	45	45
fu	0.29	0.093	0.025
GI Absorption Model	1st order	ADAM	ADAM
GI Permeability Assay	Physicochemical	Physicochemical	PCaco-2
GI Peff,man	n/a	Global	Global
Distribution Model	Minimal PBPK Model	Full PBPK Model	Minimal PBPK Model
Vss (L/kg)	0.76	Predicted	User
Prediction Method	User	Method 2	10
Clearance Type	Enzyme Kinetics	Enzyme Kinetics	Enzyme Kinetics
Trial Design			
Population Name	Sim-Healthy Volunteers/Cancer	Sim-Healthy Volunteers/Cancer	Sim-Healthy Volunteers/Cancer
Use Pop Representative	No	No	No
Population Size	100	100	100
Number of Trials	10	10	10
No. of Subjects per Trial	10	10	10
Start Day/Time	Day 1, 09:00	Day 1, 09:00	Day 1, 09:00
End Day/Time	Day 2, 09:00	Day 2, 09:00	Day 2, 09:00
Study Duration (h)	24	24	24
Sampling Time	Pre-defined Uniform	Pre-defined Uniform	Pre-defined Uniform

Sampling Site Selection	Off	Off	Off
Prandial State	Fasted	Fasted	Fasted
Route	Oral	Oral	Oral
Dose Units	Dose (mg)	Dose (mg)	Dose (mg)
Dose	0.5	250	560
Start Day/Time	Day 1, 09:00	Day 1, 09:00	Day 1, 09:00
Dosing Regimen	Single Dose	Single Dose	Single Dose

Chapter Seven: Quantitative Proteomics of Receptor Tyrosine Kinases in Patients with Colorectal Cancer Liver Metastasis

Declaration

Areti-Maria Vasilogianni, Zubida M. Al-Majdoub, Brahim Achour, Sheila Annie Peters, Amin Rostami-Hodjegan, and Jill Barber

I carried out the literature search, generation and analysis of data, contributed to the study design and wrote the manuscript. Dr Zubida M. Al-Majdoub and Dr Brahim Achour were consulted on experimental methodology and analysis of data, and suggested edits to the manuscript. Dr Sheila Annie Peters, Dr Jill Barber and Prof. Amin Rostami-Hodjegan contributed to the study design and provided guidance. I retained editorial control.

7.1 Abstract

Defects in human receptor tyrosine kinases (RTKs) expression can have a negative impact on the clinical course of tumors and the drug response. Since liver metastases are of increasing clinical significance, 21 RTKs expression levels were assessed in 15 human healthy livers, 18 liver cancer samples (2 primary and 16 colorectal cancer liver metastasis (CRLM)) matched with histologically normal tissue, by QconCAT-targeted method. Our study showed, for the first time, lower expression of EGFR, INSR, VGFR2, and AXL in cancer, and increased IGF1R expression in tumour relative to normal livers. EPHA2 and PGFRB were significantly upregulated in tumours. Expression of VGFR1/2, PGFRA, KIT, CSF1R, FLT3, FGFR1/3, ERBB2, NTRK2, TIE2, RET, and MET was comparable among healthy, normal and tumour livers or not detected in some cases. Strong and significant correlations were observed ($Rs > 0.50$, $p < 0.05$) for EGFR with INSR and KIT, while FGFR2 correlated with PGFRA, and VGFR1 with NTRK2 in healthy livers. In histologically normal tissue, there were correlations between TIE2 and FGFR1, EPHA2 and VGFR3, FGFR3 and PGFRA. EGFR correlated with INSR, ERBB2, KIT and PGFRA, and KIT with AXL and FGFR2. In tumours, CSF1R correlated with AXL, EPHA2 with PGFRA, and NTRK2 with PGFRB and AXL. RTKs abundance distribution was also assesed. RET was the most abundant in normal and healthy livers (~35%), while PGFRB was highest in tumours (~46%). Our study demonstrated perturbed expression of several RTKs in cancer and this is of high value for uncovering important biomarkers for patients with liver cancer.

7.2 Introduction

Cancer is a leading cause of death globally with increasing incidence (Sung et al., 2021). Colorectal cancer (CRC) is the third most common and the second most lethal type of cancer (Bray et al., 2018). It mainly metastasizes to the liver followed by the lungs, distant lymph nodes, and peritoneum (Holch et al., 2017), with approximately one fourth of the patients having liver metastasis at the initial diagnosis of primary cancer, and half of the patients having liver metastasis during the course of their disease (Maher et al., 2017). Primary cancer has also high rates of mortality, and its main types are hepatocellular carcinoma (HCC) and intrahepatic cholangiocarcinoma (ICC) (Bray et al., 2018). Although surgical resection of liver cancer (primary or secondary) is the ideal solution for treatment and long-term survival, this is not always possible and other methods are used, including chemotherapy, biologic therapy, radio-embolization, and radiofrequency ablation with the aim to reduce the tumour (Chen et al., 2014; Mitchell et al., 2019).

Protein kinases are important regulators of cell signalling and almost half of the human kinases can be mapped to known disease including cancer. Kinases may be mutated or dysregulated leading to perturbed signalling pathways, which renders kinases important disease biomarkers and pharmacology targets for cancer treatment (Smyth and Collins, 2009; Bhullar et al., 2018). Kinase inhibitors are widely used in oncology, with most of the FDA approved anti-cancer new molecular entities in years 2011-2017 being small molecule kinase inhibitors (Faucette et al., 2017). Receptor tyrosine kinases (RTKs) are important regulators of various cellular processes and pathways, and many anti-cancer drugs act as Receptor tyrosine kinase inhibitors (RTKIs) for the treatment of colorectal cancer liver metastasis (CRLM) (Lee and Oh, 2016; Goel, 2018) and hepatocellular carcinoma (HCC) (Chen et al., 2019). Examples of FDA approved multi-kinase inhibitors include Regorafenib for the treatment of CRLM, and Cabozantinib and Sorafenib for the treatment of HCC by blocking the activity of multiple protein kinases that participate in oncogenesis, tumour angiogenesis, and tumour microenvironment formation (Wilhelm et al., 2011; García-Aranda and Redondo, 2019). Although RTKIs are promising therapeutic tools, high heterogeneity and mutations in kinases cause resistance to RTKIs, which is a big challenge for effective treatment. This raises the need for understanding the underlying mechanisms better and investigating suitable predictive biomarkers to facilitate personalised medicine (Chen et al., 2019; García-Aranda and Redondo, 2019).

RTKs are cell surface receptors involved in the regulation of important biological pathways and include receptors involved in vascularization (vascular endothelial growth factor receptors;

VEGFRs), epidermal growth factor receptors (EGFRs), fibroblast growth factor receptors (FGFRs), insulin growth factor receptor (IGFR), platelet-derived growth factor receptors (PDGFRs), proto-oncogene c-KIT and others (Regad, 2015). RTKs demonstrate an aberrant expression in several cancer types that is usually related to poor prognosis in cancer patients (Ghosh et al., 2020). The expression levels of kinases vary depending on the stage of cancer (primary or metastatic) (Adeyinka et al., 2002) and the cancer type (Koivunen et al., 2006), indicating the necessity of investigating thoroughly different disease stages and types.

Despite the important roles of RTKs in cancer, it is surprising that there is scarcity of quantitative measurements in human cancer tissues. RTKs protein quantification data are limited to cell lines using multiplexed parallel reaction monitoring assays (Kim et al., 2016), whereas gene expression profiles are studied in human gastric cancer cell lines (Kao et al., 2003), and Ewing sarcoma (Potratz et al., 2016). EGFR and ErbB2 expression data are mainly measured by immunohistochemistry methods in primary tumours and metastases of CRC patients (Ljuslinder et al., 2009), whereas, ErbB2, and Met expression was measured in colorectal cancer cells in the same population (Yao et al., 2013). The EPHA2 expression and its correlation with cancer progression and metastasis in CRC tissue was also established (Saito et al., 2004). In additions, PGFRB gene expression, and its role in epithelial-to-mesenchymal transition (EMT), and metastasis in human CRC cohorts was studied (Steller et al., 2013). However, it is important to mention that immunohistochemistry provides semi-quantitative protein data, and mRNA data may not correlate well with protein levels. LC-MS proteomics is widely used for providing quantitative measurements of proteins and identifying important biomarkers in disease states (El-Khateeb et al., 2019) and therefore, it would be useful to utilize it for further understanding of the expression of RTKs in cancer. In our previous pilot study (Vasilogianni et al, unpublished), we quantified RTKs in pooled healthy and cancer livers using LC-MS, but measurements on individual samples were not performed. Studying RTKs and provide quantification comparisons, especially for individual patients, will help understand these targets better and improve personalized treatment for these patients.

The aim of the current study was to quantify RTKs that constitute significant targets in cancer treatment, and assess the impact of cancer on their expression levels. For this purpose, accurate mass and retention time (AMRT) proteomic approach was utilized to provide absolute quantification measurements of RTKs in individual healthy human liver microsomes (HLM) from healthy donors (controls), and histologically normal and matched cancerous HLM from cancer patients. Cancer patients in the current study were mainly CRLM patients, and two of

them had primary hepatic cancer. To our knowledge, this is the first time in which RTKs were quantified in HLM from individual healthy and CRLM subjects and aimed to assess the disease impact and identify biomarkers to contribute to the cancer therapy. In addition, we were able to clarify the relative distribution of RTKs and we highlighted significant correlations between various RTKs in each group of samples.

7.3 Materials and Methods

7.3.1 Materials and chemicals

All chemicals and solvents (HPLC-grade) were purchased from Sigma-Aldrich (Poole, Dorset, UK) unless otherwise stated. EDTA-free protease inhibitor cocktail and Trypsin (sequencing grade) were obtained from Roche Applied Sciences (Mannheim, Germany). Lysyl endopeptidase (Lys-C) was purchased from Wako (Osaka, Japan). All the QconCATs were purchased from PolyQuant GmbH (http://www.polyquant.com/) (Germany).Non-naturally occurring peptides (NNOPs) (light peptides) used for the quantification of QconCATs were purchased from Cambridge Peptides (Cambridge, UK).

7.3.2 Liver samples

Matched cancerous and histologically normal liver tissues from adult cancer patients (n = 18; HCC primary cancer (n=1), ICC primary cancer (n = 1), CRLM (n =16)) were purchased from the Manchester University NHS Foundation Trust (MFT) Biobank, Manchester, UK, following hepatectomy. The ethics was covered under the MFT Biobank generic ethics approval (NRES 14/NW/1260 and 19/NW/0644). The age of the donors varied from 34 to 85 years, whereas their body mass index varied from 21.6 to 36.3 kg/m^2. The gender of the patients was mixed; 7 female and 11 male. Supplementary Table 7-1 presents demographic and clinical details of the CRLM patients, provided by the MFT Biobank. Healthy human liver microsomal samples (tumour-free) from 15 healthy subjects were provided by Pfizer as microsomes (Groton, CT, USA). These samples were supplied by Vitron (Tucson, AZ, USA) and BD Gentest (San Jose, CA, USA). Ethical approval was obtained by the suppliers. Among the 15 donors, 8 were female and 7 were male, and their ages ranged from 18 to 64 years. The body mass index of the patients ranged from 19.9 to 37.5 kg/m^2. Supplementary Table 7-2 presents demographic and clinical details of the healthy subjects, provided by Pfizer.

7.3.3 Preparation of human liver microsomal fractions

Liver tissue was prepared as microsomes as previously described (Achour *et al.*, 2017). Briefly, liver tissue was homogenized using a Fisherbrand 150 Handheld Homogenizer (Thermo Fisher Scientific, UK) in homogenization buffer (150 mM KCl, 2 mM EDTA, 50 mM Tris, 1 mM dithiothreitol, and EDTA-free protease inhibitor cocktail, pH 7.4) at 10 ml for each gram of liver tissue. Each homogenate sample was centrifuged at 10,000 *g* for 20 min at 4°C using an Optima^{TM} L-100 ultracentrifuge (Beckman Coulter, Fullerton, CA), and the supernatant was further centrifuged at 100,000 *g* for 75 min at 4 °C. The cytosol (the supernatant) of each individual sample was stored at -80°C for future use, and the pellet (microsomes) of each individual sample was re-suspended in 1 ml of storage buffer (0.25 M potassium dihydrogen phosphate, 0.25 M dipotassium phosphate, pH 7.25) and stored at -80°C.

7.3.4 Measurement of total protein content in individual microsomal samples

The protein content of liver microsomes was measured using bicinchoninic acid (BCA) protein assay (Pierce® Microplate BCA Protein Assay Kit – Reducing Agent Compatible) in triplicate. Absorbance was measured at 562 nm using a SpectraMax 190 platereader (Molecular Devices, Sunnyvale, CA) with bovine serum albumin used as calibration standard.

7.3.5 QconCAT (KinCAT) standard

A novel QconCAT standard was used in this study, the KinCAT as described in our previous pilot study (Vasilogianni et al, unpublished) and consists of peptides for the quantification of 21 Receptor tyrosine kinases (RTKs). For the quantification of the KinCAT, two [Glu^{1}]-Fibrinopeptide B analogs (SEGVNNEEGFFSAR and GEGVNNEEGFFSAR) were included in the construct of the QconCAT. These are non-naturally occurring peptide (NNOP) and light (not labelled) peptides with the same sequences (SEGVNNEEGFFSAR and GEGVNNEEGFFSAR) are used for the quantification of the KinCAT. The peptides incorporated into the KinCAT belong to the following RTKs: Macrophage colony-stimulating factor 1 receptor CSF1R, Epidermal growth factor receptor EGFR, Ephrin type-A receptor 2 EPH2A, Erythroblastic oncogene B2 ERBB2, Fibroblast growth factor receptors FGFR1/2/3, fms like tyrosine kinase FLT3, Insulin-like growth factor 1 receptor IGF1R, Insulin receptor INSR, Mast/stem cell growth factor receptor KIT, Hepatocyte growth factor receptor MET, Neurotrophic tyrosine kinase receptor type 2 NTRK2, Platelet-derived growth factor receptors PGFRA/B, Proto-oncogene tyrosine-protein kinase receptor RET, Angiopoietin-1 receptor

TIE2, Tyrosine-protein kinase receptor UFO AXL, and Vascular endothelial growth factor receptors VGFR1/2/3). A bacterial ribosome core has been incorporated in both KinCAT for the efficient expression of the incorporated peptides (Al-Majdoub et al., 2014).

7.3.6 Digestion and preparation of samples

For each microsomal sample, 70 µg of protein were digested. Each sample was firstly mixed with known amounts of isotope-labelled KinCAT; 2.6 µl of 1:5 diluted KinCAT (initial concentration 0.1954 ug/ul). The protein mixtures were mixed sodium deoxycholate of a final concentration of 10% (w/v). The mixture was then incubated at room temperature for 10 minutes. Then, dithiothreitol (DTT) of a final concentration of 0.1 M was added for the reduction of disulphide bonds and the mixture was incubated at 56^{o} C for 30 minutes. For the protein digestion, the filter-aided sample preparation (FASP) was used, as previously described (Couto et al., 2019; Al-Majdoub et al., 2019) with minor modifications. Amicon Ultra 0.5 mL centrifugal filters at 10 kDa molecular weight cut-off (Merck Millipore, Nottingham, U.K.) were conditioned with 200 µl of 0.1 M Tris pH 8.5, centrifuging at 14,000 rpm at room temperature for 10 minutes, this step was repeated twice. The reduced samples were added to the filters and centrifuged at 13,000 rpm for 20 minutes. 8M urea in 0.1 M Tris pH 8.5 was used as solubilizing solution. This solution should extract the aggregated protein efficiently. Centrifugation at 14,000 rpm for 20 minutes at room temperature was followed (twice). The samples were subsequently alkylated with 100 µl 50 mM iodoacetamide (IAA) in the dark for 30 minutes at room temperature, then centrifuged at 14,000 rpm for 10 minutes. The buffer exchanged was repeated with two washes with 8 M Urea in 0.1 M Tris pH 8.5, and centrifugation at 14,000 rpm for 20 minutes at room temperature. The concentration of urea was reduced with two washes of 1 M urea in 50 mM ammonium bicarbonate (AmBic) pH 8.0 and centrifuged at 13,000 rpm for 20 minutes. To avoid the evaporation of the samples, 80 µl of 1 M Urea in 50 mm AmBic pH 8.0 was added to each filter unit. Then, lysyl endopeptidase was added to each sample (enzyme/ protein ratio 1:50) for two hours at 30^{o} C, and the same step was repeated for extra two hours. After 4 hours of incubation with lysyl endopeptidase, trypsin was added (enzyme/ protein ratio 1:25) for 12 hours at 37^{o} C, and the same step was repeated for extra four hours. The samples were recovered after centrifugation at 14,000 rpm for 20 minutes, 100 µl of 0.5 M sodium chloride was added to the filter, centrifuged at 14,000 rpm for 20 minutes, addition of 50 µl of 0.5 M sodium chloride to the filters, then centrifuged at 14,000 rpm for 10 minutes. After this step, each sample was split into two equal samples, and each one of them was mixed with sample buffer (3 parts of sample: 1 part of sample buffer

2% v/v trifluoroacetic acid in 20% v/v acetonitrile in water). Each sample was then desalted using a C18 column (Nest group, USA). Finally, the peptide samples were dried using a vacuum concentrator and stored at −80 °C until mass spectrometric analysis. Before the LC-MS, we added reconstitution buffer (3% acetonitrile-0.1% formic acid) and unlabelled peptides SEGVNNEEGFFSAR (0.176 pmol) and GEGVNNEEGFFSAR (0.176 pmol) in a final volume of 60 µl.

7.3.7 Liquid chromatography and tandem mass spectrometry (LC-MS/MS)

Digested samples were analysed by LC-MS/MS using an UltiMate® 3000 Rapid Separation LC (RSLC, Dionex Corporation, Sunnyvale, CA) coupled to a QE HF (Thermo Fisher Scientific, Waltham, MA) mass spectrometer. Mobile phase A was 0.1% formic acid in water and mobile phase B was 0.1% formic acid in acetonitrile and the column used was a 75 mm x 250 µm i.d. 1.7 µM CSH C18, analytical column (Waters, UK). 1 µl aliquot of the sample was transferred to a 5ul loop and loaded on to the column at a flow of 300nl/min for 5 minutes at 5% B. The loop was then taken out of line and the flow was reduced from 300nl/min to 200nl/min in 0.5 minute. Peptides were separated using a gradient that went from 5% to 18% B in 63.5 minutes, then from 18% to 27% B in 8 minutes and finally from 27% B to 60% B in 1 minute. The column is washed at 60% B for 3 minutes before re-equilibration to 5% B in 1 minute. At 85 minutes the flow is increased to 300 nl/min until the end of the run at 90min. Mass spectrometry data was acquired in a data directed manner for 90 minutes in positive mode. Peptides were selected for fragmentation automatically by data dependant analysis on a basis of the top 12 peptides with m/z between 300 to 1750Th and a charge state of 2, 3 or 4 with a dynamic exclusion set at 15 sec. The MS Resolution was set at 120,000 with an AGC target of 3e6 and a maximum fill time set at 20ms. The MS2 Resolution was set to 30,000, with an AGC target of 2e5, a maximum fill time of 45 ms, isolation window of 1.3Th and a collision energy of 28.

7.3.8 Analysis and annotation of proteomic data

Proteomic data were processed using MaxQuant 1.6.7.0 (Max Planck Institute, Martinsried, Germany), and searched against a customized database, comprising human UniprotKB database (74,788 sequences) and QconCAT sequences. For targeted AMRT analysis, light-to-heavy intensity ratios were used with QconCAT concentrations to calculate protein amounts

based on accurate mass measurement and retention time for each peptide (Al-Majdoub et al., 2019, 2020). Peptides selected for quantification of RTKs are presented in Supplementary Tables 7-3 – 7-5.

7.3.9 Statistical data analysis

Statistical data analysis was performed using GraphPad Prism 8.1.2 (La Jolla, California USA). Nonparametric statistics were used since the data did not follow normal distribution. Differences in absolute abundances between healthy and histologically normal livers, between healthy and tumorous livers, and between histologically normal and tumorous livers were assessed using Mann−Whitney U-test. Histologically normal and tumour samples are matched but abundance data were not available for all targets in each sample, with some values being only available for normal samples and not their matched tumour or the reverse. In this instance, Mann−Whitney U-test was used to assess any statistical differences. In additions, differences in absolute abundances between histologically normal and matched tumorous livers for individuals (same donors) were assessed using Wilcoxon test. In this case, the comparisons included abundance data that were available for both normal and paired tissues and the rest of the samples were excluded from this comparison. For the assessment of correlations between RTKs, Spearman correlation and linear regression analysis were used. In each of the above cases, the probability cut-off value for statistical significance was set at $p < 0.05$.

7.4 Results

The main objective of this study was to measure the expression of RTKs that play important biological roles in CRLM and could be used as biomarkers to improve therapy. The absolute abundance of 21 pharmacologically important RTKs was measured for the first time with LC-MS/MS proteomics using a QconCAT standard (KinCAT), which we previously designed and utilized (Vasilogianni et al, unpublished). The abundance of RTKs was expressed as pmol of protein per mg of microsomal protein and the expression levels of each RTK protein target was compared among human liver microsomes (HLM) generated from healthy livers, histologically normal (peri-carcinomatous) livers from cancer patients, and matched (same donors) tumour livers from cancer patients.

7.4.1 Differential expression of RTKs in HLMs from healthy subjects, and paired histologically normal and tumour HLMs

Figure 7-1 shows that several RTKs were expressed at significantly different levels among healthy, histologically normal and tumorous livers. EGFR was significantly lower in histologically normal (0.22 ± 0.12 pmol mg^{-1} microsomal protein) and tumour (0.09 ± 0.06 pmol mg^{-1} microsomal protein) compared with healthy controls (0.34 ± 0.15 pmol mg^{-1} microsomal protein) (Mann-Whitney test, $p < 0.01$ and $p < 0.0001$, respectively), and in tumour relative to histologically normal ($p < 0.0001$) livers. INSR was expressed at significantly lower levels in histologically normal (0.14 ± 0.09 pmol mg^{-1} microsomal protein) and tumour livers (0.13 ± 0.06 pmol mg^{-1} microsomal protein) relative to healthy controls (0.39 ± 0.11 pmol mg^{-1} microsomal protein) ($p < 0.0001$). VGFR3 was significantly downregulated in tumour (0.05 ± 0.08 pmol mg^{-1} microsomal protein) compared with healthy livers (0.07 ± 0.03 pmol mg^{-1} microsomal protein) ($p < 0.01$). Similarly, we observed a reduction of AXL in tumour (0.06 ± 0.04 pmol mg^{-1} microsomal protein) compared with healthy samples (0.03 ± 0.03 pmol mg^{-1} microsomal protein) ($p < 0.05$). Comparing the abundance of FGFR2 in healthy (0.12 ± 0.07 pmol mg^{-1} microsomal protein) and histologically normal microsomes (0.05 ± 0.03 pmol mg^{-1} microsomal protein), we found a significant decrease in normal livers ($p < 0.01$), with no significant changes in tumour (0.09 ± 0.08 pmol mg^{-1} microsomal protein). On the contrary, IGF1R significantly increased in tumour (0.08 ± 0.04 pmol mg^{-1} microsomal protein) compared with histologically normal (0.04 ± 0.03 pmol mg^{-1} microsomal protein) livers ($p < 0.05$). Similarly, EPHA2 was expressed in significantly higher levels in tumour (0.09 ± 0.09 pmol mg^{-1} microsomal protein) compared with histologically normal (0.04 ± 0.03 pmol mg^{-1} microsomal protein) livers ($p < 0.05$). Lastly, PGFRB was significantly upregulated in tumour (2.2 ± 1.85 pmol mg^{-1} microsomal protein) compared with healthy (0.11 ± 0.04 pmol mg^{-1} microsomal protein) ($p < 0.001$) and histologically normal livers (0.13 ± 0.06 pmol mg^{-1} microsomal protein) ($p < 0.01$).

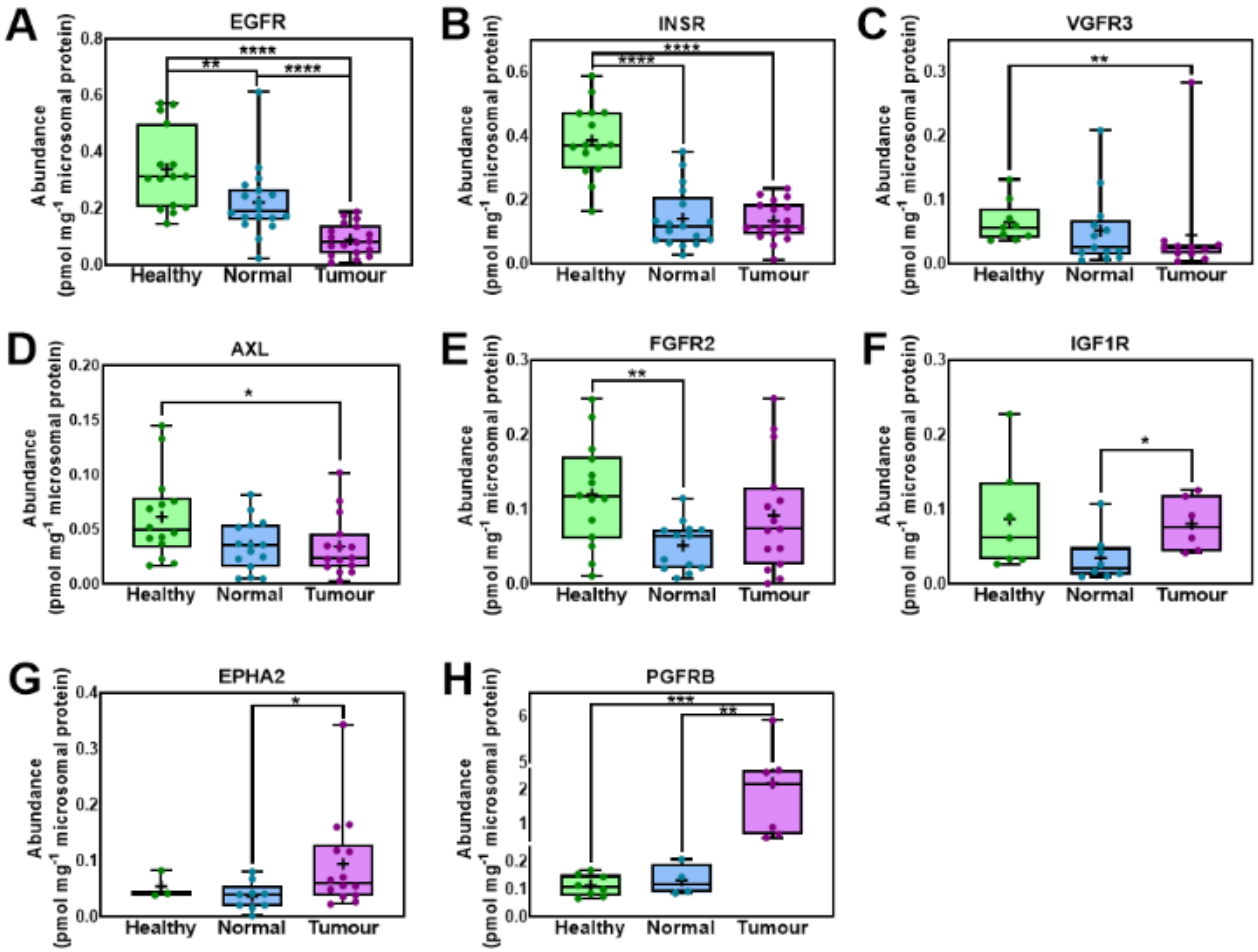

Figure 7-1 Absolute abundance of receptor tyrosine kinases (RTKs) with different levels of expression in healthy, histologically normal and tumorous HLM. Abundances are represented as box and whiskers plots with the whiskers showing the minimum and maximum values, the boxes showing the 25th and 75th percentiles, the lines showing the medians, the + signs showing the means, and the dots representing individual values. Mann−Whitney test was used to assess statistically significant differences between healthy and histologically normal, between healthy and tumorous samples for each protein, and between histologically normal and tumorous samples for each protein. The asterisk (*) represents statistical difference (*p < 0.05; ** p < 0.01; ***p < 0.001; **** p < 0.0001).

Figure 7-2 depicts the individual RTK abundance values that were collected (detected) from paired normal and tumour samples. Each line connects abundance from normal and tumour sample from same donor. Figures 7-2A and 7-2G show a significant decrease of EGFR (Wilcoxon, $p < 0.0001$) and a significant increase of EPHA2 ($p < 0.05$) in the group of tumour livers compared with matched histologically normal livers. This is consistent with the data in Figure 7-1 when considering all the abundance data for all donors. However, the low number of samples did not allow to uncover statistically significant trends for IGFR1 (n = 3) and PGFRB (n = 3) as in Figure 7-1.

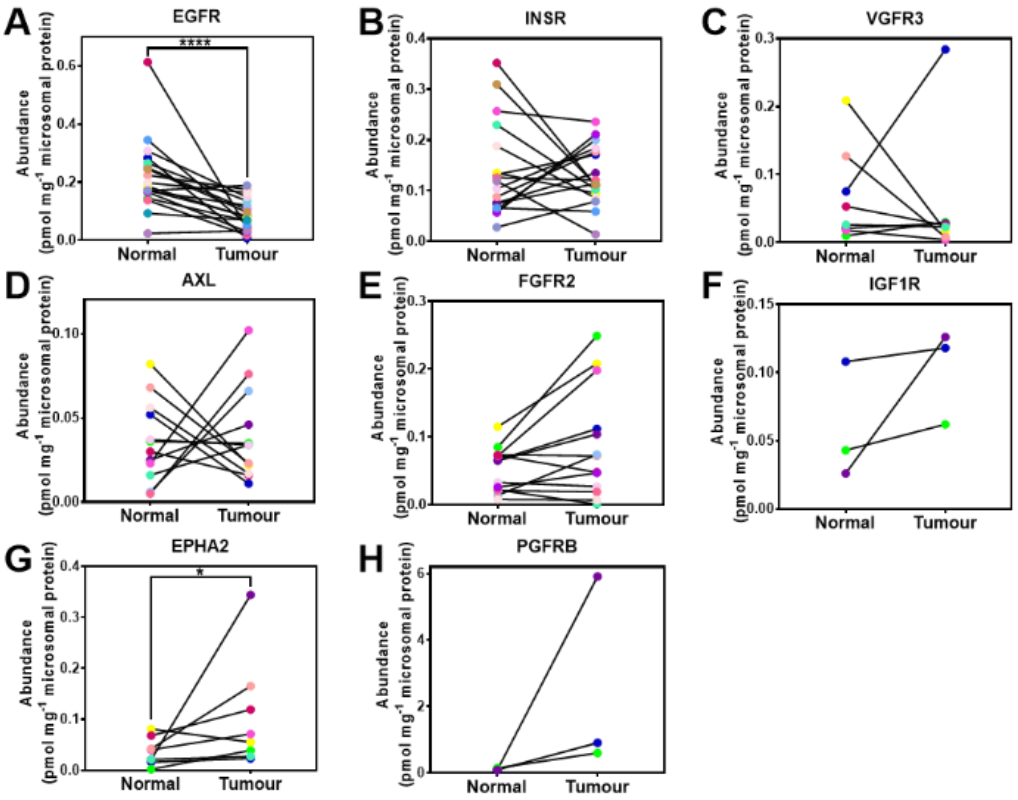

Figure 7-2 Absolute abundance of EGFR (**A**), INSR (**B**), VGFR3 (**C**), AXL (**D**), FGFR2 (**E**), IGF1R (**F**), EPHA2 (**G**), and PGFRB (**H**) in paired (same donor) histologically normal and tumorous HLM. Each line connects abundance values from matched HLM samples. Wilcoxon test was used to assess statistically significant differences between histologically normal and matched tumorous samples for each protein. The asterisk (*) represents statistical difference (*$p < 0.05$; **** $p < 0.0001$).

7.4.2 Receptor tyrosine kinase absolute expression in healthy and CRLM

Figure 7-3 provides abundance values for RTK class III (PGFRA, KIT, CSF1R, FLT3) and IV (VGFR1, VGFR2) in healthy, histologically normal and tumorous HLM. No statistical difference in the expression of VGFR1 was observed between histologically normal (0.11 ± 0.17 pmol mg^{-1} microsomal protein) and healthy samples (0.07 ± 0.05 pmol mg^{-1} microsomal protein) but this may be due to the low number of histologically normal liver samples (n = 3) where VGFR1 was quantified. VGFR2 was similarly expressed in histologically normal (0.02 ± 0.02 pmol mg^{-1} microsomal protein) and tumour (0.02 ± 0.01 pmol mg^{-1} microsomal protein) samples, and quantified in a small number of healthy samples (n = 3). Similar abundance for PGFRA was observed between healthy, histologically normal, and tumour livers. CSF1R was quantified in only 2 histologically normal samples, and its abundance levels were similar between healthy (0.22 ± 0.11 pmol mg^{-1} microsomal protein) and tumour (0.18 ± 0.19 pmol mg^{-1} microsomal protein) samples. The abundance of KIT was similar between healthy (0.19

± 0.11 pmol mg^{-1} microsomal protein) and histologically normal (0.23 ± 0.23 pmol mg^{-1} microsomal protein) livers.

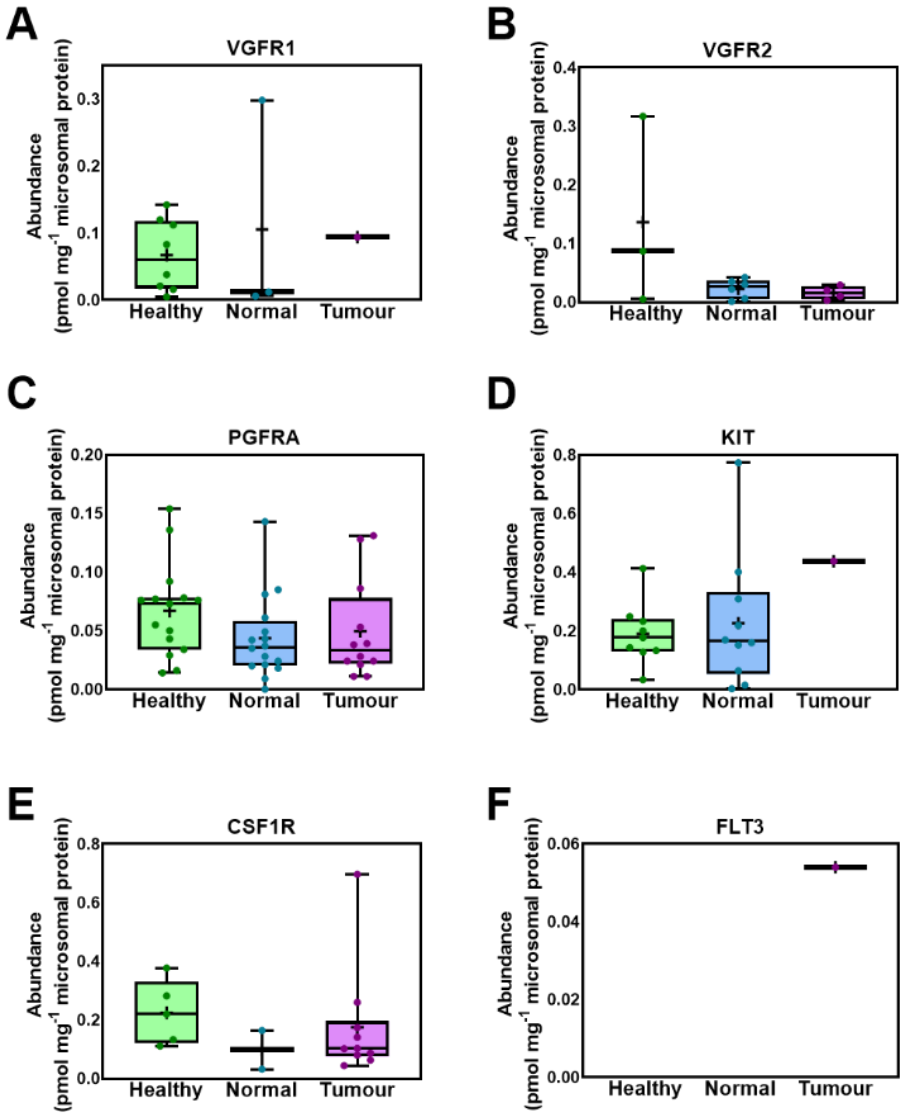

Figure 7-3 Absolute abundance of VGFR1 (**A**), VGFR2 (**B**), PGFRA (**C**), KIT (**D**), CSF1R (**E**), and FLT3 (**F**) in healthy, histologically normal and tumorous HLM. Abundances are represented as box and whiskers plots with the whiskers showing the minimum and maximum values, the boxes showing the 25th and 75th percentiles, the lines showing the medians, the + signs showing the means, and the dots representing individual values. Mann−Whitney test was used to assess statistically significant differences between healthy and histologically normal, between healthy and tumorous samples for each protein, and between histologically normal and tumorous samples for each protein, where the number of samples was enough. No significant differences were observed ($p > 0.05$).

Various RTKs were also quantified in healthy and paired samples of normal and cancer HLM and are depicted in Figure 7-4. FGFR1 was only quantifiable in two tumour samples and similarly expressed in healthy (0.58 ± 0.59 pmol mg^{-1} microsomal protein) and histologically normal (0.36 ± 0.51 pmol mg^{-1} microsomal protein) livers. The expression values of FGFR3 (0.03 ± 0.01, 0.03 ± 0.03, and 0.04 ± 0.03 pmol mg^{-1} microsomal protein), ERBB2 (0.05 ± 0.03, 0.05 ± 0.03, and 0.06 ± 0.04 pmol mg^{-1} microsomal protein), NTRK2 (0.1 ± 0.15, 0.06 ± 0.06, and 0.05 ± 0.04 pmol mg^{-1} microsomal protein), and TIE2 (0.13 ± 0.06, 0.12 ± 0.06, and 0.24 ± 0.19 pmol mg^{-1} microsomal protein) were overall similar in the healthy and the paired samples of healthy and tumour. However, RET was similarly expressed between healthy (1.48 ± 0.92 pmol mg^{-1} microsomal protein) and histologically normal (0.98 ± 0.61 pmol mg^{-1} microsomal protein) samples, and only detected in two tumour samples. MET was only quantified in two tumour samples and no comparison was possible.

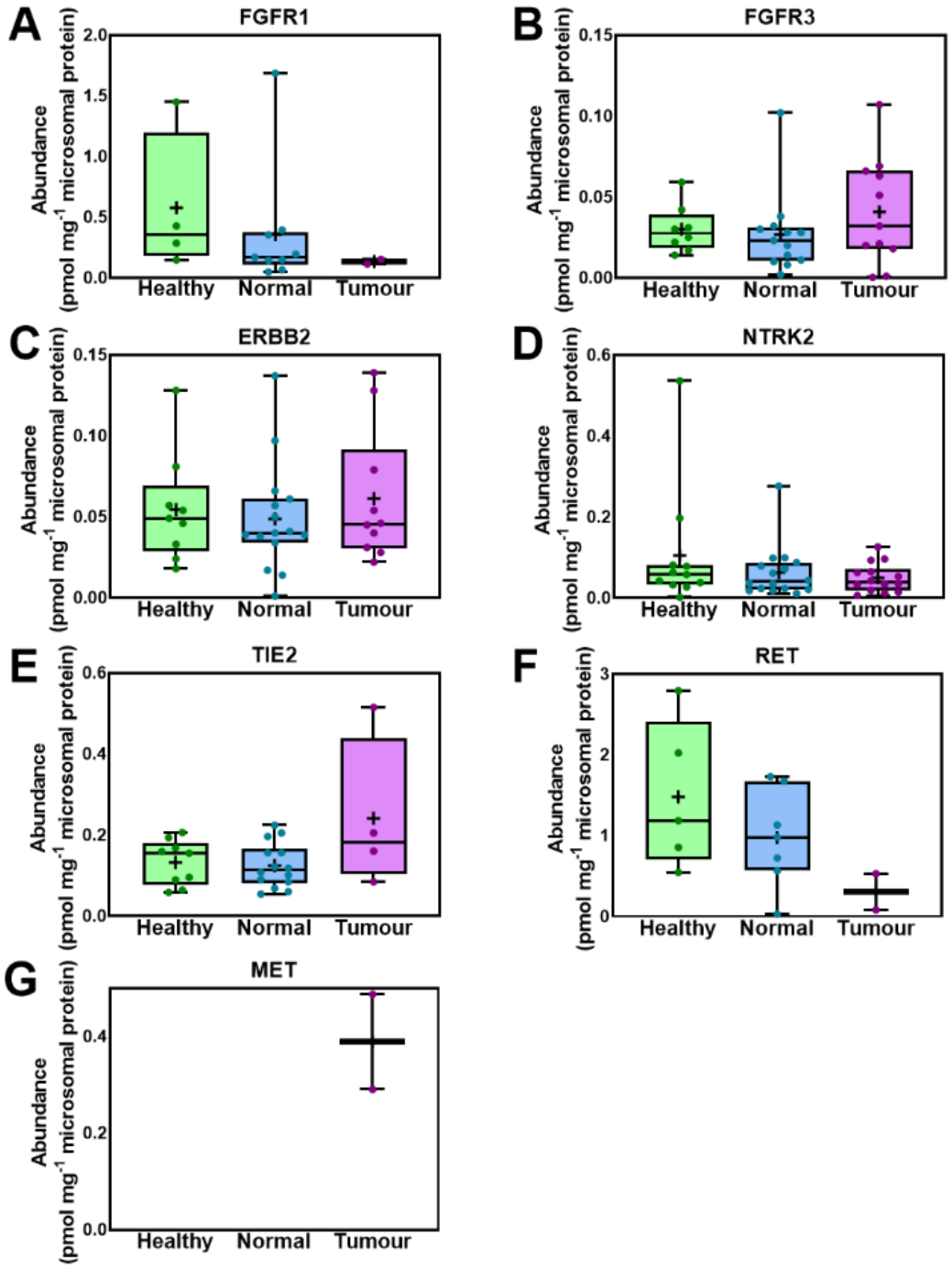

Figure 7-4 Absolute abundance of FGFR1 (**A**), FGFR3 (**B**), ERBB2 (**C**), NTRK2 (**D**), TIE2 (**E**), RET (**F**) and MET (**G**). Abundances are represented as box and whiskers plots with the whiskers showing the minimum and maximum values, the boxes showing the 25th and 75th percentiles, the lines showing the medians, the + signs showing the means, and the dots representing individual values. Mann−Whitney test was used to assess statistically significant differences between healthy and histologically normal, between healthy and tumorous samples for each protein, and between histologically normal and tumorous samples for each protein, where the number of samples was enough. No significant differences were observed ($p > 0.05$).

Figure 7-5 presents the individual abundance values of RTKs (PGFRA, FGFR3, ERBB2, NTRK2, and TIE2) that were detectable in both normal and tumour samples from same donor. These proteins were quantified in more than three pairs of samples. Each line connects abundance from normal and tumour sample from same donor. There were no significant differences for none of the targets between histologically normal and matched tumour samples, showing similar abundance values in the two groups. This is in agreement with the data in Figures 7-3 and 7-4.

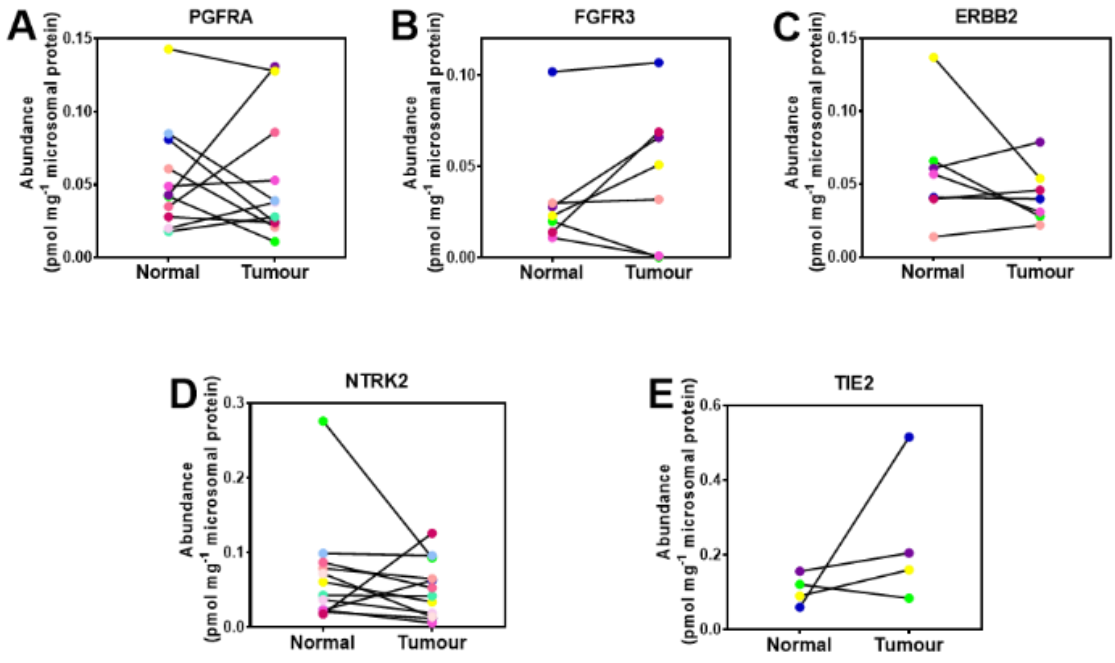

Figure 7-5 Absolute abundance of RTKs similarly expressed in paired histologically normal and tumorous HLM. Each line connects abundance values from matched HLM samples. Wilcoxon test was used to assess statistically significant differences between histologically normal and matched tumorous samples for each protein. No significant differences were observed ($p > 0.05$).

Table 7-1 provides the expression levels of 21 RTKs in healthy, histologically normal and tumour livers represented by the median, the mean and standard deviation of the mean (SD), the coefficient of variation (CV), and the range (minimum to maximum value). The absolute values of the abundance of RTKs for individual healthy, histologically normal and tumour livers samples and surrogate peptides used for quantification are provided in Supplementary Tables 7-3 – 7-5.

Table 7-1 Expression levels of 21 RTKs in healthy, histologically normal and tumour livers represented by the median, the mean and standard deviation of the mean (SD), the coefficient of variation (CV), and the range (minimum to maximum value).

RTK	Median (pmol mg^{-1})			Mean ± SD (pmol mg^{-1})			CV (%)			Range (pmol mg^{-1})			n		
	H	N	T	H	N	T	H	N	T	H	N	T	H	N	T
AXL	0.05	0.04	0.02	0.06 ± 0.04	0.04 ± 0.02	0.03 ± 0.03	63.67	66.09	79.18	0.02 - 0.15	0.01 - 0.08	0.003 - 0.1	14	15	15
CSF1R	0.22	0.10	0.10	0.22 ± 0.11	0.1 ± 0.09	0.18 ± 0.19	48.69	95.24	110.7	0.11 - 0.38	0.03 - 0.16	0.04 - 0.7	5	2	10
EGFR	0.31	0.19	0.08	0.34 ± 0.15	0.22 ± 0.12	0.09 ± 0.06	42.97	56.13	61.58	0.15 - 0.57	0.02 - 0.61	0.01 - 0.19	15	18	18
EPHA2	0.04	0.04	0.06	0.05 ± 0.02	0.04 ± 0.03	0.09 ± 0.09	44.97	68.61	90.31	0.04 - 0.08	0.002 - 0.08	0.02 - 0.34	3	9	14
ERBB2	0.05	0.04	0.05	0.05 ± 0.03	0.05 ± 0.03	0.06 ± 0.04	61.39	68.91	67.54	0.02 - 0.13	0.001 - 0.14	0.02 - 0.14	9	15	10
FGFR1	0.36	0.17	0.13	0.58 ± 0.59	0.36 ± 0.51	0.13 ± 0.03	102.9	144.3	20.36	0.15 - 1.45	0.05 - 1.69	0.11 - 0.15	4	9	2
FGFR2	0.12	0.07	0.07	0.12 ± 0.07	0.05 ± 0.03	0.09 ± 0.08	58.12	63.55	82.68	0.01 - 0.25	0.01 - 0.12	0.001 - 0.25	14	13	15
FGFR3	0.03	0.02	0.03	0.03 ± 0.01	0.03 ± 0.03	0.04 ± 0.03	48.8	94.21	81.59	0.01 - 0.06	0.002 - 0.1	0.0003 - 0.11	8	13	11
FLT3	-	-	0.05	-	-	-	-	-	-	-	-	-	-	-	1
IGF1R	0.06	0.02	0.08	0.09 ± 0.07	0.04 ± 0.03	0.08 ± 0.04	84.11	94.6	45.26	0.03 - 0.23	0.01 - 0.11	0.04 - 0.13	7	8	6
INSR	0.37	0.12	0.12	0.39 ± 0.11	0.14 ± 0.09	0.13 ± 0.06	29.2	66.51	45.16	0.17 - 0.59	0.03 - 0.35	0.01 - 0.24	15	17	18
KIT	0.18	0.16	0.44	0.19 ± 0.11	0.23 ± 0.23	-	55.5	100.9	-	0.03 - 0.41	0.003 - 0.77	-	9	10	1
MET	-	-	0.39	-	-	0.39 ± 0.14	-	-	35.86	-	-	0.29 - 0.49	-	-	2
NTRK2	0.06	0.04	0.04	0.1 ± 0.15	0.06 ± 0.06	0.05 ± 0.04	144.6	103.1	72.42	0 - 0.54	0.01 - 0.28	0.01 - 0.13	11	16	14
PGFRA	0.07	0.04	0.03	0.07 ± 0.04	0.04 ± 0.04	0.05 ± 0.04	59.72	81.47	85.99	0.01 - 0.15	0.0004 - 0.14	0.01 - 0.13	15	16	12

PGFRB	0.11	0.12	2.18	0.11 ± 0.04	0.13 ± 0.06	2.2 ± 1.85	34.4	42.77	84.2	0.07 - 0.17	0.09 - 0.21	0.6 - 5.91	8	4	7
RET	1.19	0.98	0.30	1.48 ± 0.92	0.98 ± 0.61	0.3 ± 0.32	62.04	62.17	104.3	0.55 - 2.79	0.03 - 1.73	0.08 - 0.53	5	7	2
TIE2	0.16	0.11	0.18	0.13 ± 0.06	0.12 ± 0.06	0.24 ± 0.19	42.44	44.33	78.58	0.06 - 0.21	0.05 - 0.22	0.08 - 0.52	9	14	4
VGFR1	0.06	0.01	0.09	0.07 ± 0.05	0.11 ± 0.17	-	79.86	158.4	-	0.01 - 0.14	0.01 - 0.3	-	8	3	1
VGFR2	0.09	0.03	0.02	0.14 ± 0.16	0.02 ± 0.02	0.02 ± 0.01	118.6	71.88	73.47	0.01 - 0.32	0.001 - 0.04	0.003 - 0.03	3	6	4
VGFR3	0.06	0.03	0.03	0.07 ± 0.03	0.05 ± 0.06	0.05 ± 0.08	49.38	111.2	176.6	0.04 - 0.13	0.01 - 0.21	0.004 - 0.28	9	13	11

7.4.3 Correlations in liver RTK expression profiles

The correlation of protein abundance between different RTKs in healthy, histologically, normal and tumour samples has been assessed (Figure 7-6) and only significant correlations ($p < 0.05$) are presented. Significant correlations were considered strong when the values correlated well (Rs > 0.60) and the scatter was very limited scatter ($R^2 > 0.30$). Significant correlations were considered moderate in cases of good correlation (Rs > 0.50) and limited scatter ($R^2 > 0.25$).

In healthy HLM, strong, significant, and positive correlation was observed between INSR and EGFR, between KIT and EGFR, and between FGFR2 and PGFRA. On the contrary, there was a significant and negative correlation between VGFR1 and NTRK2. In histologically normal HLM, we found strong, significant, and positive correlations between TIE2 and FGFR1, INSR and EGFR, ERBB2 and EGFR, KIT and EGFR, KIT and AXL, EPHA2 and VGFR3, FGFR3 and PGFRA, and KIT and FGFR2. Although significant ($p < 0.05$) and good (Rs > 0.50) correlations were observed between PGFRA and EGFR, and PGFRA and INSR, the scatter was too high ($R^2 < 0.1$). In tumour HLM, there was strong, significant and positive correlation between PGFRB and NTRK2. Moderate, significant and positive correlation (Rs > 0.60, $R^2 > 0.25$) was identified between AXL and NTRK2, and CSF1R and AXL. The correlation between INSR and EPHA2 was weak, significant, and positive (Rs > 0.50, $R^2 < 0.25$). Lastly, strong, significant, and negative correlation was observed between EPHA2 and CSF1R, and moderate, significant, and negative correlation between CSF1R and PGFRA.

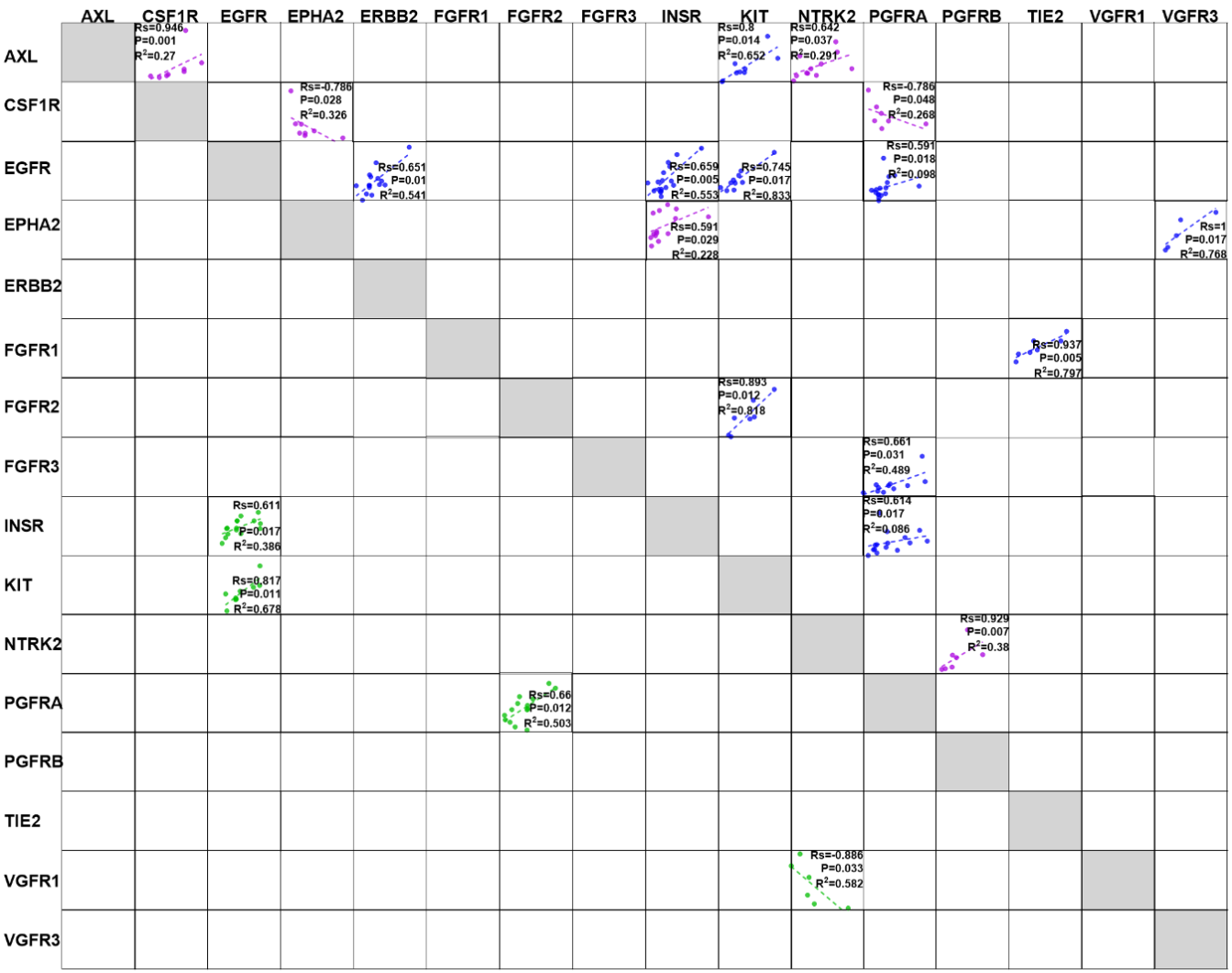

Figure 7-6 Correlation matrix of protein abundance of RTKs in healthy (green), histologically normal (blue) and tumour (purple) HLM. Abundance values are expressed in pmol of protein per mg of microsomal protein. Rs is Spearman rank order correlation coefficient. Strong (Rs>0.70, $p < 0.05$), and moderate and significant correlations (Rs>0.50, $p < 0.05$) are presented.

7.4.4 Relative abundance distribution of RTKs in healthy normal and tumour HLM

Human liver microsomes were used for protein quantification of RTKs to understand their distribution at the protein level across the three conditions. The pie charts represent the relative abundance distribution of RTKs in healthy controls (Figure 7-7A), and histologically normal (Figure 7-7B), and tumour (Figure 7-7C) HLM from cancer patients. The relative distribution of the quantified RTKs is similar in healthy and histologically normal samples, with RET being the most abundant. The second most abundant RTK in healthy and histologically normal livers is FGFR1 (13.4% and 12.7%, respectively), followed by INSR (9.1%) and EGFR (7.9%) in healthy, and KIT (8.1%) and EGFR (7.9%) in histologically normal livers. The least abundant RTKs in healthy were FGFR3 (0.7%) and EPHA2 and ERBB2 (1.3%), whereas in histologically normal VGFR2 (0.8%) and FGFR3 (1%).

However, the relative distribution of RTKs differs in tumour livers. The most abundant RTK was PGFRB, representing almost half of the quantified RTKs (45.7%), followed by KIT (9.1%), MET (8.1%), and RET (6.3%). The least abundant RTKs included VGFR2 (0.3%) and AXL (0.7%).

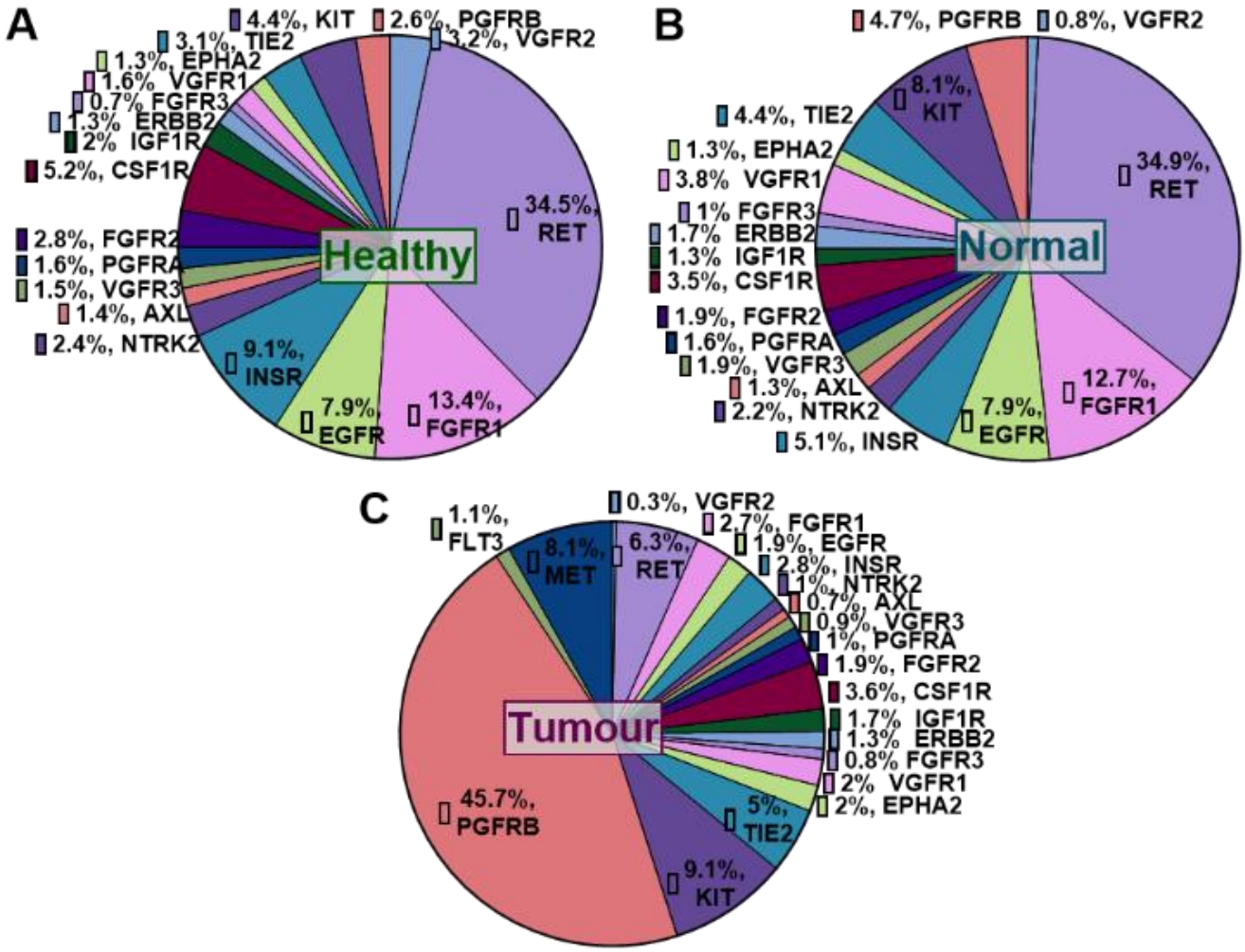

Figure 7-7 Pie charts illustrating the relative abundance distribution of RTKs in healthy (**A**), histologically normal (**B**) and tumorous (**C**) HLM.

7.5 Discussion

The current study describes, for the first time, expression levels of RTKs in healthy, histologically normal and liver metastasis. RTKs are very promising targets for treatment of cancer patients and this raises the need to learn more about them. 15 healthy, and tumour with paired normal samples from 18 cancer patients were examined for expression of 21 RTKs using LC-MS/MS proteomics and AMRT approach. The RTKs relative distribution across the 3 conditions was also assessed. Additionally, we investigated correlations of different RTKs in the 3 groups of samples.

Our data suggest low expression of EGFR in histologically normal and more significantly in tumour compared with healthy livers, and this may dictate high risks of developing cancer.

Result from previous group supports the role of EGFR in the regulation of cell proliferation, differentiation, and migration (Yarden and Sliwkowski, 2001), and its over-expression has been linked with negative prognosis for survival for CRC patients (Huang et al., 2017). This decrease was also apparent when comparing matched samples from same donors. This is in line with immunohistochemistry data showing that EGFR is lost in several metastasising primary colorectal cancer tumours (Ljuslinder et al., 2009). Study has shown that INSR and IGF1R are important for energy metabolism, cell growth, and cancer (Nakae et al., 2001) and to our knowledge, no quantitative data exist for INSR. In our study, INSR was expressed less in histologically normal and tumour livers than in healthy donors. On the contrary, IGF1R significantly increased in tumour livers. Literature data on IGF1R are contradictory; showing either low IGF1R expression correlated with increased risk of liver metastasis in CRC, or absence of correlation or mildly elevated IGF1R mRNA in CRC (Shali et al., 2016). Immunohistochemistry data showed that VGFR3 is a protein associated with vascularization and presence of hepatic metastasis in CRC patients (Martins et al., 2013). In our study, VGFR3 was significantly decreased in tumour compared with the healthy livers. Several studies have shown that the expression of AXL was enhanced in advanced CRC, which may be associated with poor survival (Uribe et al., 2017). We found that AXL was decreased in tumour compared with healthy livers. Previously, a study showed the importance of FGFR2 for cell migration, invasion, growth and cancer progression in CRC (Matsuda et al., 2012), gene amplification has been found in a primary CRC (Carter et al., 2017), and its expression has been associated with poor survival (Li et al., 2019). In our data, the abundance of FGFR2 was significantly decreased in normal relative to healthy livers. However, we showed increased abundance of EPHA2 and PGFRB in tumour compared with histologically normal livers. EPHA2 regulates tumour initiation, vascularization, tumour progression and metastasis and immunohistochemistry in colorectal tumours indicated significantly higher expression levels of EPHA2 compared with matched normal tissue (Saito et al., 2004; Dunne et al., 2016). Increase of PGFRB was in agreement with the literature, as PGFRB overexpression is associated with angiogenesis, invasion, metastasis, and poor survival in CRC and is a biomarker for diagnosis and treatment (Steller et al., 2013; Manzat Saplacan et al., 2017). Decrease in the abundance of EGFR and INSR and increase in EPHA2 and PGFRB in tumour was consistent with our previous pilot study (Vasilogianni et al, unpublished).

In addition to the above, 13 other RTKs (VGFR1, VGFR2, PGFRA, KIT, CSF1R, FLT3, FGFR1, FGFR3, ERBB2, NTRK2, TIE2, RET, and MET) were measured for first time. These

RTKs generally show an overexpression in CRC and are important regulators in metastasis, cancer progression, resistance to chemotherapy, angiogenesis, differentiation, growth, cell survival and proliferation (García-Aranda and Redondo, 2019). In our study, FGFR3, ERBB2, NTRK2, TIE2, VGFR2, and PGFRA displayed similar expression levels among healthy, histologically normal, and tumour livers. FGFR1, RET, VGFR1, and KIT were similarly expressed between healthy and histologically normal livers, while no comparison was possible with tumour samples due to the low number of tumour samples expressing these proteins. Similar expression of CSF1R in healthy livers compared with tumour livers was observed. FLT3 and MET were only identified in 1 or 2 tumour samples. RTKs are low abundance proteins and this may be the cause for not being identified in some samples.

Although several studies mentioned above show an overexpression of RTKs in primary CRC, this does not come in disagreement with our data. We measured RTKs in metastatic tumours, and it is possible that these tumours lose the expression of RTKs as described in an immunohistochemistry study showing that EGFR is lost in metastasising primary colorectal cancer tumours (Ljuslinder et al., 2009). This means that the expression of RTKs may not follow the same patterns in primary and secondary tumours. In additions, we measured absolute abundance of RTKs for the first time using a QconCAT-targeted approach where a unique peptide for each protein target was used. This technique is very sensitive. Recent studies have highlighted the mismatch between mRNA and protein abundance for several enzymes and transporters in liver and intestine. Therefore, mRNA abundances cannot be used as surrogate for protein abundances and direct measurements are required. Our suggestion for further studies would be to measure RTKs from matched primary and secondary tumours and assess if expression of RTKs is lost in metastatic tumours. For the purpose of treatments, it would be recommended to know total expression of both-primary and secondary tumours.

RTKs are regulators of various complicated pathways in cells and it is suggested to be investigated from the perspective of pathways rather than individual proteins. Therefore, it is important to elucidate their relationship in the cells and find any possible correlations between them, which could suggest important diagnosis and treatment markers. Interestingly, we found positive correlations of EGFR with KIT and INSR, FGFR2 with PGFRA, and negative correlations of VGFR1 with NTRK2 in healthy livers. Similarly, in normal livers, EGFR positively correlated with INSR and KIT. Additionally, positive correlations were observed between TIE2 and FGFR1, ERBB2 and EGFR, KIT and AXL, EPHA2 and VGFR3, FGFR3 and PGFRA, and KIT and FGFR2. In tumour livers, NTRK2 positively correlated with PGFRB

and AXL. AXL positively correlated with CSF1R, and INSR with EPHA2. CSF1R negatively correlated with EPHA2 and PGFRA. These correlations are novel and they are not previously reported. These data highlight that there is an important interplay among RTKs and these correlations may be important for suggesting a panel of diagnostic markers or a set of proteins that should be targeted by a multi-kinase inhibitor for appropriate treatment. The number of samples in this study may be a limiting factor. RTKs are low abundance proteins and thus, not quantifiable in all the samples.

To our knowledge, this is the first study that determines the relative distributions of RTKs in healthy, tumour and matched normal livers. RET was the most abundant RTK (more than one third of the quantified RTKs) in healthy and histological normal livers. This is not surprising knowing that RET is a tumour suppressor gene. It may promote colon cancer when it is hyper-methylated and inactivated but lead to apoptosis when restored (Luo et al., 2013). High expression of RET in healthy and normal tissues is indicative of no inactivation of the gene and thus, no tumour. On the contrary, relative distribution differs in tumour, with PGFRB being the most abundant RTK (45.7%). This is in line with the literature data discussed above describing PGFRB as diagnostic and therapeutic marker for CRLM patients.

Overall, our study provides for the first time absolute quantification measurements for RTKs in livers from healthy individuals, and cancer patients with a focus on CRLM. Our data showed a significant decrease of EGFR, INSR, VGFR2, and AXL in cancer, increase of IGF1R in tumour relative to normal, and increase of EPHA2 and PGFRB in cancer. Expression levels of other RTKs (VGFR1, VGFR2, PGFRA, KIT, CSF1R, FLT3, FGFR1, FGFR3, ERBB2, NTRK2, TIE2, RET, MET) were either expressed at similar levels among the three groups or comparisons were not possible due to their identification and quantification in a limited number of samples. Samples from CRC primary tumours would be useful to assess if same patterns are followed in colon. This would be important for suggesting right treatment for these patients. Several correlations among RTKs were observed in all groups of livers showing a potential interaction among them and regulation of common pathways. Low abundance of RTKs rendered them not quantifiable in several samples, and this may hide other important correlations. Therefore, higher number of samples would be useful for further studies. Lastly, our data revealed the relative distribution of RTKs in healthy, normal and tumour livers. Our data showed perturbed expression of several RTKs in cancerous liver and these results could serve as means of suggesting biomarkers for cancer patients with liver cancer, mainly CRLM.

7.6 References

Achour B, Al Feteisi H, Lanucara F, Rostami-Hodjegan A, and Barber J (2017) Global proteomic analysis of human liver microsomes: Rapid characterization and quantification of hepatic drug-metabolizing enzymes. *Drug Metab Dispos* **45**:666–675.

Adeyinka A, Nui Y, Cherlet T, Snell L, Watson PH, and Murphy LC (2002) Activated mitogen-activated protein kinase expression during human breast tumorigenesis and breast cancer progression. *Clin Cancer Res* **8**:1747–53.

Al-Majdoub ZM, Al Feteisi H, Achour B, Warwood S, Neuhoff S, Rostami-Hodjegan A, and Barber J (2019) Proteomic Quantification of Human Blood-Brain Barrier SLC and ABC Transporters in Healthy Individuals and Dementia Patients. *Mol Pharm* **16**:1220–1233.

Al-Majdoub ZM, Carroll KM, Gaskell SJ, and Barber J (2014) Quantification of the proteins of the bacterial ribosome using QconCAT technology. *J Proteome Res* **13**:1211–1222.

Al-Majdoub ZM, Couto N, Achour B, Harwood MD, Carlson G, Warhurst G, Barber J, and Rostami-Hodjegan A (2020) Quantification of Proteins Involved in Intestinal Epithelial Handling of Xenobiotics. *Clin Pharmacol Ther* **0**:1–11.

Bhullar KS, Lagarón NO, McGowan EM, Parmar I, Jha A, Hubbard BP, and Rupasinghe HPV (2018) Kinase-targeted cancer therapies: progress, challenges and future directions. *Mol Cancer* **17**:48.

Bray F, Ferlay J, Soerjomataram I, Siegel RL, Torre LA, and Jemal A (2018) Global cancer statistics 2018: GLOBOCAN estimates of incidence and mortality worldwide for 36 cancers in 185 countries. *CA Cancer J Clin* **68**:394–424.

Carter JH, Cottrell CE, McNulty SN, Vigh-Conrad KA, Lamp S, Heusel JW, and Duncavage EJ (2017) FGFR2 amplification in colorectal adenocarcinoma. *Mol Case Stud* **3**:a001495.

Chen S, Cao Q, Wen W, and Wang H (2019) Targeted therapy for hepatocellular carcinoma: Challenges and opportunities. *Cancer Lett* **460**:1–9.

Chen X, Liu H-PL, Li M, and Qiao L (2014) Advances in non-surgical management of primary liver cancer. *World J Gastroenterol* **20**:16630.

Couto N, Al-Majdoub ZM, Achour B, Wright PC, Rostami-Hodjegan A, and Barber J (2019) Quantification of Proteins Involved in Drug Metabolism and Disposition in the Human

Liver Using Label-Free Global Proteomics. *Mol Pharm* **16**:632–647.

Dunne PD, Dasgupta S, Blayney JK, McArt DG, Redmond KL, Weir J-A, Bradley CA, Sasazuki T, Shirasawa S, Wang T, Srivastava S, Ong CW, Arthur K, Salto-Tellez M, Wilson RH, Johnston PG, and Van Schaeybroeck S (2016) EphA2 Expression Is a Key Driver of Migration and Invasion and a Poor Prognostic Marker in Colorectal Cancer. *Clin Cancer Res* **22**:230–242.

El-Khateeb E, Vasilogianni A-M, Alrubia S, Al-Majdoub ZM, Couto N, Howard M, Barber J, Rostami-Hodjegan A, and Achour B (2019) Quantitative mass spectrometry-based proteomics in the era of model-informed drug development: Applications in translational pharmacology and recommendations for best practice. *Pharmacol Ther* **203**:107397.

Faucette S, Wagh S, Trivedi A, Venkatakrishnan K, and Gupta N (2017) Reverse Translation of US Food and Drug Administration Reviews of Oncology New Molecular Entities Approved in 2011-2017: Lessons Learned for Anticancer Drug Development. *Clin Transl Sci* 1–24.

García-Aranda M, and Redondo M (2019) Targeting Receptor Kinases in Colorectal Cancer. *Cancers (Basel)* **11**:433.

Ghosh S, Marrocco I, and Yarden Y (2020) Roles for receptor tyrosine kinases in tumor progression and implications for cancer treatment. *Adv Cancer Res* **147**:1–57.

Goel G (2018) Evolution of regorafenib from bench to bedside in colorectal cancer: Is it an attractive option or merely a “me too” drug? *Cancer Manag Res* **10**:425–437.

Holch JW, Demmer M, Lamersdorf C, Michl M, Schulz C, von Einem JC, Modest DP, and Heinemann V (2017) Pattern and Dynamics of Distant Metastases in Metastatic Colorectal Cancer. *Visc Med* **33**:70–75.

Huang C, Zhou Q, Hu Y, Wen Y, Qiu Z, Liang M, Mo J, Xu J, Sun C, Liu F, and Chen X (2017) Hepatocyte growth factor is a prognostic marker in patients with colorectal cancer: a meta-analysis. *Oncotarget* **8**:23459–23469.

Kao H-W, Chen H-C, Wu C-W, and Lin W-C (2003) Tyrosine-kinase expression profiles in human gastric cancer cell lines and their modulations with retinoic acids. *Br J Cancer*

88:1058–1064.

Kim H-J, Lin D, Lee H-J, Li M, and Liebler DC (2016) Quantitative Profiling of Protein Tyrosine Kinases in Human Cancer Cell Lines by Multiplexed Parallel Reaction Monitoring Assays. *Mol Cell Proteomics* **15**:682–691.

Koivunen J, Aaltonen V, and Peltonen J (2006) Protein kinase C (PKC) family in cancer progression. *Cancer Lett* **235**:1–10.

Lee S, and Oh SC (2016) Advances of Targeted Therapy in Treatment of Unresectable Metastatic Colorectal Cancer. *Biomed Res Int* **2016**:1–14.

Li P, Huang T, Zou Q, Liu D, Wang Y, Tan X, Wei Y, and Qiu H (2019) FGFR2 Promotes Expression of PD-L1 in Colorectal Cancer via the JAK/STAT3 Signaling Pathway. *J Immunol* **202**:3065–3075.

Ljuslinder I, Malmer B, Isaksson-Mettävainio M, Oberg A, Henriksson R, Stenling R, and Palmqvist R (2009) ErbB 1-4 expression alterations in primary colorectal cancers and their corresponding metastases. *Anticancer Res* **29**:1489–94.

Luo Y, Tsuchiya KD, Il Park D, Fausel R, Kanngurn S, Welcsh P, Dzieciatkowski S, Wang J, and Grady WM (2013) RET is a potential tumor suppressor gene in colorectal cancer. *Oncogene* **32**:2037–2047.

Maher B, Ryan E, Little M, Boardman P, and Stedman B (2017) The management of colorectal liver metastases. *Clin Radiol* **72**:617–625.

Manzat Saplacan RM, Balacescu L, Gherman C, Chira RI, Craiu A, Mircea PA, Lisencu C, and Balacescu O (2017) The Role of PDGFs and PDGFRs in Colorectal Cancer. *Mediators Inflamm* **2017**:1–9.

Martins SF, Garcia EA, Luz MAM, Pardal F, Rodrigues M, and Filho AL (2013) Clinicopathological correlation and prognostic significance of VEGF-A, VEGF-C, VEGFR-2 and VEGFR-3 expression in Colorectal cancer. *Cancer Genomics and Proteomics* **10**:55–68.

Matsuda Y, Ueda J, and Ishiwata T (2012) Fibroblast Growth Factor Receptor 2: Expression, Roles, and Potential As a Novel Molecular Target for Colorectal Cancer. *Patholog Res Int* **2012**:1–8.

Mitchell D, Puckett Y, and Nguyen QN (2019) Literature Review of Current Management of Colorectal Liver Metastasis. *Cureus* **11**:e3940.

Nakae J, Kido Y, and Accili D (2001) Distinct and Overlapping Functions of Insulin and IGF-I Receptors. *Endocr Rev* **22**:818–835.

Potratz J, Tillmanns A, Berning P, Korsching E, Schaefer C, Lechtape B, Schleithoff C, Unland R, Schäfer K-L, Müller-Tidow C, Jürgens H, and Dirksen U (2016) Receptor tyrosine kinase gene expression profiles of Ewing sarcomas reveal ROR1 as a potential therapeutic target in metastatic disease. *Mol Oncol* **10**:677–692.

Regad T (2015) Targeting RTK Signaling Pathways in Cancer. *Cancers* **7**:1758–1784.

Saito T, Masuda N, Miyazaki T, Kanoh K, Suzuki H, Shimura T, Asao T, and Kuwano H (2004) Expression of EphA2 and E-cadherin in colorectal cancer: correlation with cancer metastasis. *Oncol Rep* **11**:605–11.

Shali H, Ahmadi M, Kafil HS, Dorosti A, and Yousefi M (2016) IGF1R and c-met as therapeutic targets for colorectal cancer. *Biomed Pharmacother* **82**:528–536.

Smyth LA, and Collins I (2009) Measuring and interpreting the selectivity of protein kinase inhibitors. *J Chem Biol* **2**:131–151.

Steller EJA, Raats DA, Koster J, Rutten B, Govaert KM, Emmink BL, Snoeren N, van Hooff SR, Holstege FCP, Maas C, Borel RIHM, and Kranenburg O (2013) PDGFRB Promotes Liver Metastasis Formation of Mesenchymal-Like Colorectal Tumor Cells. *Neoplasia* **15**:204-IN30.

Sung H, Ferlay J, Siegel RL, Laversanne M, Soerjomataram I, Jemal A, and Bray F (2021) Global cancer statistics 2020: GLOBOCAN estimates of incidence and mortality worldwide for 36 cancers in 185 countries. *CA Cancer J Clin* caac.21660.

Uribe DJ, Mandell EK, Watson A, Martinez JD, Leighton JA, Ghosh S, and Rothlin C V. (2017) The receptor tyrosine kinase AXL promotes migration and invasion in colorectal cancer. *PLoS One* **12**:e0179979.

Wilhelm SM, Dumas J, Adnane L, Lynch M, Carter CA, Schütz G, Thierauch K-H, and Zopf D (2011) Regorafenib (BAY 73-4506): A new oral multikinase inhibitor of angiogenic, stromal and oncogenic receptor tyrosine kinases with potent preclinical antitumor activity.

Int J Cancer **129**:245–255.

Yao Y-L, Shao J, Zhang C, Wu J-H, Zhang Q-H, Wang J-J, and Zhu W (2013) Proliferation of Colorectal Cancer Is Promoted by Two Signaling Transduction Expression Patterns: ErbB2/ErbB3/AKT and MET/ErbB3/MAPK. *PLoS One* **8**:e78086.

Yarden Y, and Sliwkowski MX (2001) Untangling the ErbB signalling network. *Nat Rev Mol Cell Biol* **2**:127–137.

7.7 Supplementary Information

Supplementary Table 7-1 Demographic and clinical details of cancer patients provided by the MFT Biobank.

Sample ID	Age at surgery (years)	Race	Sex	Body mass index, BMI (kg/m^2)	Smoking/ Alcohol use	Liver lobe	Diagnosis	Medical history	Treatment
389	52	Caucasian	Female	30.86	No/ Occasionally	Left	Metastatic moderately well differentiated adenocarcinoma	Deep vein thrombosis, asthma, duodenal ulcer, thyroid problem, liver lesions	Fragmin, levothyroxine, betamethasone, ventolin, ferrous fumarate
590	72	Caucasian	Male	32	Pipe/ 22 units per week	-	Metastatic moderate to Well differentiated adenocarcinoma (dirty necrosis)	Asthma, polypectomy, tonsillectomy, Hemicolectomy Dukes B	Salbutamol, tiotropium, lansaprozole, nasonex
633	67	Caucasian	Male	26.85	Ex-stopped/ -	Right	Metastatic adenocarcinoma & fatty liver disease	Peripheral neuropathy secondary to oxaliplatin, type 2 diabetes, hypercholesterolemia, valvular heart disease, prostate cancer with bone metastasis, colonic cancer T3N0, colorectal liver metastasis	Metformin, zoladex, oxaplatin and 5FU, irinotecan and 5FU with cetuximab
674	68	Caucasian	Female	26.67	No/ -	Right	Metastatic moderately differentiated adenocarcinoma	Rectosigmoid cancer 10/10 Dukes B	-

734	64	Caucasian	Female	23.84	No/ Occasionally	Right	Moderately to focally poorly differentiated metastatic adenocarcinoma	Primary colorectal	Dalteparin, short course of radiotherapy, adjuvant OXmdG and 5FU
746	85	Caucasian	Male	23.67	Ex (40 years)/ Moderately	Right	Metastatic papillary carcinoma	Laparoscopic R hemicolectomy T2M0, Squamous cell carcinoma (scalp), hypothyroidism, hypertension, Chronic obstructive pulmonary disease	Irbesartan, levothyroxine, bisoprolol, aspirin, omeprazole, budesamide, formoterol
794	71	Caucasian	Female	22.41	No/ No	-	Metastatic adenocarcinoma with extensive intra-acinar necrosis	R hemicolectomy, pT3N2, high blood pressure, depression	Tomudex chemotherapy
818	58	Caucasian	Male	21.78	Ex (25 years)/ 18 units per week	-	Moderately differentiated metastatic adenocarcinoma	Sigmoid adenocarcinoma pT3pN2	Loperamide, carboplatin/5FU and modified de Gramont and radiotherapy
1492	34	-	Female	32.53	Ex-stopped/ Approximately 20 units per week	Right	Metastatic moderate and poorly differentiated adenocarcinoma	Bowel resection, pilonodal abcess x2, grometts (as a child), tonsillectomy (as a child), egg collection, occasional palpitations, asthma (as a child), reflux, joint problems in knees, treated for Irritable bowel syndrome	Omeprazole, amitryptyline, microgynon, glucosamine sulphate, ibuprofen, peppermint oil

1493	75	-	Male	-	No/ No	Right	Metastatic moderately differentiated adenocarcinoma	Sigmoid tumour, sleep apnoea, asthma	Cod liver oil, salbutamol inhaler, seretide inhaler, movicol
1498	63	Caucasian	Male	-	No/ Rarely	Right	Metastatic adenocarcinoma	Previous gout, anaemia, cataract operation	Doxycycline regime completed, Nil regular
1795	63		Male	36.32	Ex - stopped (previously 30cpd)/ Approximately 75 units per week	Left	Metastatic well differentiated adenocarcinoma	Adenocarcinoma, hypertension, intermittent claudication of left leg	Omeprazole, irbesartan, simvastatin, clopidogrel
1957	68	-	Male	32.16	No/ -	Left	Metastatic moderately differentiated adenocarcinoma	Primary rectal cancer, pneumonia post-operative, liver cancer, late lung metastasis	Nil regular
2036	43	-	Female	-	-/ -	Right	Metastatic moderate to poorly differentiated adenocarcinoma	Primary colorectal	Omeprazole, paracetamol
2058	79	Caucasian	Female	21.6	-/ -	Left	Metastatic adenocarcinoma	Below the knee amputation, primary colorectal, lung metastasis	Lansoprazole, ferrous sulphate, alendronic acid, paracetamol, codeine phosphate, senna, natecal D3
2095	55	Caucasian	Male	28.1	-/ -	Right	Metastatic moderately differentiated adenocarcinoma	Primary colorectal	Nil regular

1063	77	Caucasian	Male	26.6	Ex - stopped 20 years ago/ 15 units per week	Right	Moderate to poorly differentiated hepatocellular carcinoma	Primary hepatocellular carcinoma, prostate cancer	-
1359	68	Caucasian	Male	33.4	No/ Whiskey (frequency unknown)	Left	Poorly differentiated intrahepatic cholangiocarcinoma pT2a, pN1	Primary liver tumour, right elbow surgery, patient would have a cholecystectomy for gallstones but surgery was abandoned when the liver tumour was discovered, hiatus hernia, reflux	Lumigan eye drops, brinzolamide, timolol, omeprazole, bimatoprost

Supplementary Table 7-2 Demographic and clinical details of healthy subjects provided by Pfizer.

Sample ID	Age at surgery (years)	Race	Sex	Body mass index, BMI (kg/m^2)	Smoking/ Alcohol use	Cause of death	Medical history	Treatment
HH83	18	Caucasian	Female	20.19	No/ No	Head trauma	Healthy	None
HH84	53	Caucasian	Male	19.94	No/ Social	Intracranial haemorrhage	None	None
HH87	54	Caucasian	Female	29.79	No/ No	Head trauma	Healthy	None
HH93	34	Caucasian	Male	20.62	No/ No	Cerebellar haemorrhagic injury	Healthy	Healthy
HH98	64	Caucasian	Male	37.47	No/ No	Head Injury	Healthy	None
HH99	45	Caucasian	Male	31.62	No/ No	Head trauma	Healthy	None
HH101	54	Caucasian	Female	21.95	No/ No	Motor vehicle accident	Healthy	None
HH102	52	Caucasian	Female	32.26	No/ No	Cerebral Aneurysm	Healthy	None
HH104	35	African American	Female	25.25	No/ No	Cerebral Aneurysm	Healthy	None
HH105	50	Caucasian	Male	33.47	No/ No	Cerebral Aneurysm	Healthy	None
HH106	43	Hispanic	Male	24.48	No/ No	Cerebral Vascular Aneurysm	Healthy	None
HH107	45	Caucasian	Female	24.96	No/ No	Cerebral Vascular Aneurysm	Healthy	None
HH110	54	Caucasian	Female	26.29	No/ Social	Cerebral Vascular Aneurysm	Healthy	None

HH111	43	Caucasian	Female	28.43	No/ No	Intracranial bleeding	Healthy	None
HH118	32	Caucasian	Male	26.69	No/ Social	Gunshot Wound to head	Healthy, Skin Graft on right arm in the past	Pepcid AC, Tagamet, Steroids in HS and Marines

Supplementary Table 7-3 Targeted quantification of nineteen Receptor tyrosine kinases (RTKs) transporters in 15 human liver microsomes from healthy subjects.

Sample ID by the provider		HH83	HH84	HH87	HH93	HH98	HH99	HH101	HH102	HH104	HH105	HH106	HH107	HH110	HH111	HH118
Sample name		H3	H6	H9	H12	H51	H18	H21	H53	H27	H30	H33	H36	H39	H42	H56
Protein target	Peptides	Absolute abundance (pmol mg-1)														
VGFR2	AASVGLPSVSLDLPR	0.317	0.005			0.087										
RET	LLEGEGLPFR	2.023	1.185	2.793				0.545				0.854				
FGFR1	DGVQLAESNR					0.284			0.426	0.145						1.448
EGFR	IPLENLQIIR	0.211	0.197	0.307	0.314	0.204	0.573	0.569	0.306	0.147	0.502	0.185	0.356	0.549	0.314	0.356
INSR	ESLVISGLR	0.292	0.367	0.372	0.472	0.373	0.435	0.366	0.348	0.165	0.474	0.242	0.297	0.589	0.474	0.539
NTRK2	NSNLQHINFTR	0.038	0.042			0.002			0.032	0.081	0.063	0.197	0.536	0.058	0.027	0.078
AXL	APLQGTLLGYR	0.076	0.073	0.042	0.047	0.043	0.019	0.133		0.037	0.017	0.023	0.087	0.069	0.145	0.052
VGFR3	NILLSESDVVK	0.037	0.071		0.102	0.038	0.046		0.132	0.044				0.060	0.057	
PGFRA	VVEGTAYGLSR	0.078	0.076	0.092	0.014	0.055	0.154	0.050	0.077	0.043	0.076	0.016	0.034	0.136	0.029	0.073
FGFR2	EIEVLYIR	0.119	0.114	0.168	0.086	0.181	0.224	0.146	0.136	0.027	0.011	0.063	0.115	0.248	0.051	
CSF1R	VVEATAFGLGK		0.133		0.377			0.111		0.220	0.282					
IGF1R	TTINNEYNYR				0.228	0.137			0.034	0.027	0.033		0.062	0.090		
ERBB2	LLDIDETEYHADGGK	0.024	0.057	0.046		0.081		0.128	0.054	0.049			0.033	0.018		
FGFR3	VGPDGTPYVTVLK		0.025		0.022	0.031	0.014	0.042	0.030		0.017			0.059		
VGFR1	FNSGSSDDVR				0.120	0.112		0.021	0.142	0.016	0.083	0.005		0.038		
EPHA2	TVSEWLESIK							0.042			0.039			0.083		
TIE2	NILVGENYVAK		0.168	0.159	0.058	0.206	0.193			0.064	0.089	0.095	0.155			
KIT	LVVQSSIDSSAFK		0.034	0.177	0.143	0.133		0.413	0.249	0.128		0.233		0.200		
PGFRB	GFSGIFEDR				0.169	0.073	0.067	0.145		0.155		0.084	0.114	0.100		
FLT3	TWTEIFK															
MET	LNSELNIEWK															

Supplementary Table 7-4 Targeted quantification of nineteen Receptor tyrosine kinases (RTKs) transporters in 18 histologically normal (peri-carcinomateous) liver microsomes from cancer patients.

Sample ID by the provider		2095	2058	2036	389	590	746	818	1492	674	1957	1493	1498	633	734	794	1795	1063	1359
Sample name		N1	N4	N7	N10	N13	N49	N19	N22	N25	N34	N28	N31	N37	N40	N43	N54	N45	N47
Protein target	Peptides	Absolute abundance (pmol mg-1)																	
VGFR2	AASVGLPSVSLDLPR			0.022	0.042				0.006	0.035		0.030				0.001			
RET	LLEGEGLPFR		1.730		0.723				0.029	1.673		1.131		0.565				0.979	
FGFR1	DGVQLAESNR							0.354	0.168			0.393		0.149	0.193	0.047	1.686	0.064	0.143
EGFR	IPLENLQIIR	0.283	0.145	0.173	0.185	0.249	0.224	0.613	0.265	0.307	0.170	0.138	0.198	0.166	0.345	0.093	0.245	0.024	0.171
INSR	ESLVISGLR	0.132	0.075	0.076	0.135	0.257	0.088	0.352	0.230	0.104	0.063	0.126	0.188	0.057	0.310	0.066		0.119	0.028
NTRK2	NSNLQHINFTR	0.098	0.011	0.018	0.023		0.276		0.021	0.061	0.023	0.079	0.018	0.043	0.087	0.072	0.099	0.035	0.037
AXL	APLQGTLLGYR		0.052	0.036	0.025	0.082	0.023	0.068	0.030	0.054		0.036	0.016	0.037	0.056	0.005	0.005		0.006
VGFR3	NILLSESDVVK	0.075	0.010	0.061	0.021	0.209			0.009		0.018	0.127	0.044		0.053	0.026		0.006	0.020
PGFRA	VVEGTAYGLSR	0.081	0.037	0.009	0.042	0.043	0.143	0.049	0.061		0.021	0.028	0.018	0.020	0.085	0.035	0.024		0.000
FGFR2	EIEVLYIR		0.066	0.085	0.065	0.115	0.072		0.074	0.073	0.022	0.033	0.014		0.008	0.026			0.021
CSF1R	VVEATAFGLGK							0.164								0.032			
IGF1R	TTINNEYNYR		0.017			0.108		0.043	0.011	0.014		0.010		0.026		0.052			
ERBB2	LLDIDETEYHADGGK	0.041		0.066	0.061			0.137	0.057	0.050	0.034	0.017	0.014	0.039	0.040	0.001	0.097	0.038	0.039
FGFR3	VGPDGTPYVTVLK	0.102	0.032		0.020				0.028	0.008	0.023	0.011	0.030	0.014	0.038	0.028		0.002	0.010
VGFR1	FNSGSSDDVR						0.298							0.012		0.006			
EPHA2	TVSEWLESIK				0.016			0.002		0.021		0.081	0.041	0.040	0.068	0.021	0.042		
TIE2	NILVGENYVAK	0.205	0.060	0.224	0.121		0.054	0.156	0.156	0.084		0.196	0.090		0.118	0.068		0.101	0.108
KIT	LVVQSSIDSSAFK				0.152	0.401	0.309	0.773	0.169			0.160		0.219		0.003		0.064	0.015
PGFRB	GFSGIFEDR				0.208			0.092	0.144			0.086							
FLT3	TWTEIFK																		
MET	LNSELNIEWK																		

Supplementary Table 7-5 Targeted quantification of twenty-one Receptor tyrosine kinases (RTKs) transporters in 18 tumorous human liver microsomes from cancer patients.

Sample ID by the provider		2095	2058	2036	389	590	746	818	1492	674	1957	1493	1498	633	734	794	1795	1063	1359
Sample name		T2	T5	T8	T11	T14	T50	T52	T23	T26	T35	T29	T32	T38	T41	T44	T55	T46	T48
Protein target	Peptides	Absolute abundance (pmol mg-1)																	
VGFR2	AASVGLPSVSLDLPR						0.020			0.010			0.029						0.003
RET	LLEGEGLPFR				0.080								0.529						
FGFR1	DGVQLAESNR										0.151				0.113				
EGFR	IPLENLQIIR	0.008	0.067	0.084	0.080	0.108	0.175	0.044	0.136	0.149	0.120	0.018	0.164	0.030	0.054	0.070	0.097	0.033	0.189
INSR	ESLVISGLR	0.171	0.114	0.135	0.095	0.236	0.177	0.110	0.103	0.184	0.200	0.121	0.086	0.211	0.112	0.059	0.218	0.014	0.079
NTRK2	NSNLQHINFTR				0.063	0.035	0.093	0.033	0.012	0.034	0.006	0.065	0.126	0.042	0.053	0.014	0.096		0.019
AXL	APLQGTLLGYR	0.024	0.011	0.035	0.046	0.022	0.102	0.023	0.016		0.003		0.034	0.034	0.017		0.076	0.011	0.066
VGFR3	NILLSESDVVK	0.284	0.030		0.028	0.017		0.036		0.016	0.004	0.008			0.025	0.023	0.026		
PGFRA	VVEGTAYGLSR	0.024			0.011	0.131	0.128	0.053	0.021			0.024	0.028	0.038	0.039	0.086		0.011	
FGFR2	EIEVLYIR	0.085	0.112	0.249	0.104	0.208	0.198		0.072	0.048	0.001	0.027	0.074	0.130	0.007	0.047			0.019
CSF1R	VVEATAFGLGK		0.080	0.697	0.260	0.087		0.102		0.044		0.103	0.174	0.141	0.063				
IGF1R	TTINNEYNYR				0.042	0.118		0.062			0.045		0.092	0.126					
ERBB2	LLDIDETEYHADGGK	0.040	0.128	0.028	0.079	0.139	0.045	0.054	0.031				0.022		0.046				
FGFR3	VGPDGTPYVTVLK	0.107		0.063	0.0003	0.021	0.020	0.018	0.066		0.051	0.001	0.032	0.069					
VGFR1	FNSGSSDDVR								0.094										
EPHA2	TVSEWLESIK		0.056		0.023	0.117	0.161	0.039	0.049	0.344	0.036	0.055		0.071	0.119	0.027	0.165		0.066
TIE2	NILVGENYVAK		0.515		0.084			0.205					0.160						
KIT	LVVQSSIDSSAFK												0.438						
PGFRB	GFSGIFEDR							0.904	0.598	2.516		5.914		2.181			2.582		0.693
FLT3	TWTEIFK										0.054								
MET	LNSELNIEWK					0.487	0.290												

Chapter Eight: Conclusions and Future Work

8.1 Setting the Needs for Oncology Populations

Clinical trials in oncology are very challenging. Recruitment of appropriate populations is not always possible and patients constitute a heterogeneous population resulting in a substantial variability in drug pharmacokinetics (PK). Model-informed precision dosing can help to overcome these obstacles via physiologically-based pharmacokinetic (PBPK) modelling, which is gaining wider regulatory acceptance in oncology. IVIVE-PBPK strategies require population-specific systems parameters, in order to accurately predict the fate of drugs in various patient populations. Although some systems parameters have been defined in cancer, there are still many unknown areas. For instance, the abundance of drug metabolising enzymes (DMEs) and transporters has not been studied in every cancer type. DMEs and transporters have a fundamental role in drug metabolism, absorption and disposition and any perturbation in their expression could lead to altered PK profiles, and thus high toxicity or low efficacy of the drug. Liver is the main organ of metabolism and hepatic cancer is expected to affect liver function. It is therefore important to know if DMEs and transporters are affected in patients with liver cancer (primary or metastatic), to what extent, and if the perturbed abundance of DMEs and transporters could affect PK profiles. Focusing on colorectal cancer liver metastasis (CRLM), there are no quantitative data on the expression levels of liver DMEs and transporters. Therefore, the main aim of this project was to fill in this gap. Abundance data in addition to population-specific scalars are necessary for the *in vitro-in vivo* extrapolation of metabolic drug clearance. These scalars have not been studied in CRLM and this project attempted to define them. The overall aim was to incorporate scalars along with abundance data (DMEs, transporters), in order to improve PBPK models for cancer. Lastly, various pathways are affected in cancer and proteins involved in them could serve as potential pharmacodynamics (PD) markers for diagnosis and treatment. Therefore, this project aimed to quantify a wide range of PD markers for the first time in CRLM, with the characteristic example of receptor tyrosine kinases (RTKs).

8.2 What this projects adds to the previous knowledge

The first step of this project was to critically review the available literature for cancer and define which systems parameters that could affect drug exposure are already known and which

are still missing (chapter 1). Although there are some reviews covering this subject, we focused for the first time on the existing gaps for CRLM and highlighted the need for obtaining quantitative data on CYPs, UGTs, drug transporters and scalars for accurate predictions of PK via modelling in CRLM patients.

Reliable quantitative measurements of proteins can be obtained with LC-MS/MS proteomics that has already been used for the quantification of DMEs and transporters in various tissues. Chapter 2 comprehensively reviews the available quantitative proteomic methods, how they are applied in translational pharmacology and offers recommendations for the selection of proteomic techniques. Taking into consideration the available proteomic techniques, it was concluded that the QconCAT methodology is ideal for quantifying the protein targets (CYPs, UGTs, transporters, RTKs) of this project, along with the accurate mass and retention time (AMRT). The total protein approach (TPA) was used to provide relative abundance of proteins involved in biological pathways that may be affected in cancer.

Various software packages are available for the analysis of LC-MS proteomics data, and it is worth knowing if they generate data of similar quantity and quality, and if some can perform better than others. Chapter 3 compares two widely used software packages - Mascot/Progenesis LC-MS and MaxQuant, utilising proteomics data generated from human liver microsomes using global proteomics methods. The two software packages demonstrated some differences especially at peptides levels. This suggests that if they are used together, they can maximise the use of datasets when using global proteomics. However, both software packages behaved well and generated robust common peptides giving confidence that either of them can be trusted. Thus, for this PhD project the open access software MaxQuant was used for the data analysis.

Hepatic intrinsic clearance is an important parameter for the prediction of drug exposure. In vitro data relevant to metabolic drug clearance of specific pathways need to be extrapolated to clearance at liver tissue level (per gram of liver). For this extrapolation, several scaling factors are used, such as microsomal protein per gram of liver (MPPGL) in cases that the in vitro data are generated from liver microsomes. Scaling values may differ in disease states and need to be defined for different diseases. In CRLM, such values were not studied and were not available in simulators such as Simcyp. In chapter 4, scaling factors specific for CRLM patients were defined for the first time. MPPGL were significantly decreased in cancerous livers from CRLM patients compared with histologically normal livers, implying that metabolism may be

significantly decreased in cancer. Application of the experimental data on PBPK models showed differences in drug exposure when using CRLM-specific scalars instead of scalars for healthy subjects. These data are necessary for accurate PK profiles and decrease the parameters that should be tested with sensitivity and uncertainty analysis for the improvement of the model.

Limited knowledge on system-specific parameters could be an inhibitory factor for the development of models in disease populations. To overcome this obstacle, in chapter 5, the abundance of DMEs and transporters was quantified for the first time in pooled liver microsomes from cancerous and histologically normal livers from CRLM patients, and compared with healthy controls. Most CYPs and UGTs were lower in cancer livers indicating that metabolism of CYP or UGT substrates can be affected in CRLM patients. Abundance data on CYPs in addition to MPPGL defined in chapter 4 were incorporated into PBPK models for CYP substrates and this resulted in significantly higher drug exposure compared with the cases where abundance and scaling data from healthy subjects were used. This means that patients with cancerous liver may need to be dosed separately due to high risk of toxicity. Other DMEs and transporters were also impaired, indicating that drug disposition can be significantly affected. Liver markers revealed hepatic impairment in CRLM. Additionally, inflammatory markers were increased in cancer and this inflammatory environment may be responsible for perturbed expression of DMEs and transporters. Other markers that were quantified for the first time and perturbed in CRLM involved markers of desmoplasia, and metastasis. Interestingly, we designed for the first time a QconCAT standard (‘KinCAT’) for the quantification of 21 receptor tyrosine kinases (RTKs) that are widely targeted by anti-cancer agents. Many RTKs were altered in CRLM. This study sets the basis on defining systems parameters in CRLM, but further experiments are needed on individual samples to validate the data and assess the inter-individual variability for each target. This will require robust statistical analysis and reveal which targets significantly differ in cancer.

Chapter 6 provides absolute quantification data on DMEs and transporters for the first time in individual livers from cancer patients with a focus on CRLM. A substantial decrease of DMEs and most transporters was observed in cancer, indicating that the metabolic and disposition of drugs may be dramatically impaired in cancer patients. Inter-individual variability was also assessed and was higher in cancerous livers. This variability is an important parameter to be used for models. Abundance values were scaled to tissue levels with MPPGL and PBPK simulations of CYP substrates were performed to assess the impact of downregulated DMEs

on PK. Our simulations clearly showed that the decreased abundance of DMEs can significantly increase the drug exposure and the use of population-specific abundance data for pharmacokinetic predictions is required.

Chapter 7 focuses on PD protein targets and more specifically on receptor tyrosine kinases. These proteins are very important for cancer treatment as they are targeted by several FDA approved multi-kinase inhibitors. Although there are some mRNA and immunohistochemistry data on RTKs in various types of cancers, there are no absolute quantification data in livers from CRLM patients. Knowing any perturbations in the abundance of RTKs in these patients could be particularly important to elucidate why some patients do not respond well to treatment with kinase inhibitors. Therefore, chapter 7 provides quantification of 21 RTKs in paired normal and tumour livers from CRLM patients compared with healthy controls. We found a lower expression of EGFR, INSR, VGFR2, AXL, and an increase of IGF1R, EPHA2 and PGFRB in tumour livers. The relative distribution was also different in tumour livers, and several correlations among RTKs were observed. These data could be valuable towards precision medicine in CRLM patients. However, it would be interesting to have relevant measurements from primary colorectal cancer tissues, in order to have the whole profile in CRLM patients.

8.3 Future perspectives

Although a wide range of non-CYP non-UGT DMEs were measured in pooled samples, it would be useful to assess their inter-individual variability in CRLM patients and compare them with healthy controls. The data that have already been generated during this project could be further analysed using the label-free approach to provide quantification of non-CYP non-UGT DMEs in individual livers. The same approach could be used to further investigate metastasis, inflammation and other cancer markers in individual samples. In addition to the quantification of RTKs, abundance of non-receptor tyrosine kinases is equally important to be assessed, as these are also important pharmacology targets. These are cytosolic proteins and thus, not measured in our microsomal fractions used for the purpose of this project. However, during the tissue fractionation, the cytosolic fraction was stored and could be used in the future for further analysis. The cell debris containing mitochondria and nucleus was also kept as it could potentially be analysed to explore cancer markers. Another suggestion for the future would be to measure RTKs in primary colorectal cancer and assess if the expression of these markers is

being lost in metastasis. Having the whole picture of RTKs in both primary and metastatic tissues in CRLM patients is important for facilitating precision medicine, especially in cases where patients do not respond to cancer treatment. It would also be interesting to source peri-carcinomatous normal liver samples at different distances from the tumour (same donor) and assess if there is a differential expression of proteins depending on the distance from the tumour. This would be an important element to be considered when sourcing samples. Extrahepatic impact of cancer on drug exposure could also be assessed by measuring DMEs and transporters in the intestine and other tissues of CRLM patients. The application of the data generated during this project in PBPK models can improve current models by increasing confidence with the use of population-specific systems parameters. When clinical data of drugs in CRLM patients are available, our proteomics data along with the scaling factors could validate our models. Lastly, a recommendation for the future would be to perform similar studies in other cancer types that are less studied, for instance small intestine cancer. All these data collected here, in addition to future studies in the same line, could lay the foundation for precision dosing in cancer.